CHARACTERISTICS AND BEHAVIOR OF PLASMA CUT-WELDED H-SHAPED STEEL COLUMNS

By
PRAMALATHAN ARASARATNAM, B.Sc.Eng

A Thesis

Submitted to the School of Graduate Studies

in Partial Fulfillment of the Requirements

for the Degree of

Masters of Applied Science

McMaster University

MASTERS OF APPLIED SCIENCE (2005) McMaster University
(CIVIL ENGINEERING) Hamilton, Ontario

Title : Characteristics and Behavior of Plasma Cut-Welded H-Shaped Steel Columns

Author : P.Arasaratnam, *B.Sc.Eng (Hons)* (Sri Lanka)

Supervisor : K.S.Sivakumaran

Number of Pages : xiii, 7-11

ABSTRACT

Welded built-up structural steel members are widely used as columns, beams, and beam-columns in various buildings, bridges, industrial complexes, etc. Modern cutting techniques are used in the fabrication of such members. Besides traditional saw cutting and oxy-flame cutting, the modern cutting techniques include plasma cutting, laser cutting, water-jet cutting, etc. The different cutting techniques induce different degrees of Heat Affected Zones (HAZ), which subsequently creates different degrees of geometrical and mechanical imperfections (residual stresses). Therefore, it could be expected that the true behavior of structural steel columns manufactured by such cutting techniques be different.

The main objective of this investigation was to study the characteristics and behavior of plasma cut-welded H-shaped steel columns at different slenderness ratios. However, this investigation also considered similar flame cut-welded H-shaped steel columns for comparison purposes. The H-shaped column sections were fabricated from plates having specified yield strength of 350MPa. First, the initial plate was cut into plate strips and then the plate strips (flanges and web) were welded together to form the H-shaped section in this investigation. The strength of these columns were established under uni-axial compressive loading with pinned end condition, allowing for minor axis rotation. Moreover, the structural imperfections such as residual stresses and geometrical imperfections were established. The residual stresses distributions were established at various stages of fabrication processes using the "method of section" technique. That is, the residual stresses in initial plate, plate strips (cutting effects), and column sections (cutting and welding effects) were established. Similarly, the geometrical imperfections were established at various stages of fabrication processes in this investigation.

The temperature profiles were measured during the cutting and welding processes. As part of the scientific documentation, the mechanical characteristic of virgin steel plates were obtained by standard coupon tensile test.

Based on the experimental results on column strength, the general behavior of plasma cut columns and flame cut columns were similar. However, it was found that the plasma cut-welded steel columns seemed to carry higher loads than that of flame cut-welded columns for higher slenderness ratios ($\lambda \geq 1$). For lower slenderness ratios ($0.5 < \lambda < 1$), it was found that the flame cut-welded columns had higher strength than plasma cut-welded columns in this investigation. The residual stress distribution of both plasma cut column section and flame cut column section had the same general distribution. However, in general, the flame cut columns had high intensity of tensile residual stresses at their flange tips than the plasma cut columns. Moreover, the out-of-plane imperfections of column sections were within the code limitations. However, it was found that the flame cut-welded H-shaped steel columns seemed to have higher out-of-plane imperfections than the similar plasma cut-welded H-shaped steel columns in this investigation.

ACKNOWLEDGEMNTS

- The author would like to express his sincere and heartfelt appreciation to his supervisor, Prof.K.S.Sivakumaran, for his invaluable, systematic and precious guidance, and financial support, during the course of this study.
- Mr. Fuller Micah, Mr.Mourice Forget, Mr. Dave Perrett, and Mr. Peter Koudys are also to be thanked for their technical assistance for the experimental setup in the laboratory.
- Financial assistance from the Dept. of Civil Engineering, McMaster University, the CISC-Steel Structures Education Foundation, The Materials and Manufacturing Ontario (MMO), and The Walter Inc. are greatly appreciated.
- The assistance of Telco Steel Works (Steel Fabricators and Erectors), Mississauga, Ontario, in plate cutting is greatly acknowledged.
- The assistance of Walter's Inc, Hamilton, Ontario, in welding of column sections and base plates is also greatly acknowledged.
- Further, the water jet cutting by McMaster Manufacturing Research Institute (MMRI), Ancaster, Ontario, is also to be acknowledged.
- Finally, the author would also like to thank his brother Haran Arasaratnam for his assistance to review this thesis report

A.P.Lathan

TABLE OF CONTENTS

LIST OF TABLES

LIST OF FIGURES

LIST OF SYMBOLS

A	-Cross-section area
b	-Width of a rectangular section
c	-Distance form neutral axis to extreme fiber
C	-Absolute elasticity
d	-Depth of a rectangular section
e	-Load eccentricity
E	-Elastic modulus
E_t	-Tangent modulus
F	-Airy's function
F_{max}	-Maximum stress
F_{ult}	-Ultimate strength
F_y	-Yield strength
k	-Empirical factor
K	-Effective length factor
L	-Column length
P	-Axial load
P_e	-Euler buckling load
P_y	-Axial load at yielding
P_u	-Ultimate load
r	-Radius of gyration
S_y	-Longitudinal stresses in y-direction
T	-Temperature
w	-Half plate width
α	-Coefficient of linear thermal expansion
λ	-Non dimensional slenderness ratio
δ_0	-Maximum initial crookedness

Chapter 1

INTRODUCTION

1.1 The Structural Steel Members

Structural steel is one of the most widely used building materials in various structures ranging from small residential houses to complex structures such as high rise office and residential buildings, bridges, towers, advanced base structures, etc. The reason for wide use of structural steel in construction work is because steel has many favorable material properties over other constructional materials such as reinforced concrete, timber, etc. The favorable material properties of steel include high strength to weight ratio, high stiffness to weight ratio, high ductility performance, etc. The high strength to weight ratio of structural steel is highly preferred in the construction of stable structures with less weight. The high strength and high stiffness of steel also permit the use of long, clear spans with a minimum number of columns for more usual structures. Furthermore, due to the high ductile behavior, the structural steel framing members often exhibit high deformation before complete failure. Thus, steel structures allow a structural engineer and the general public to easily identify the signs of impending failure in the form of cracking of interior or exterior finishes before complete collapse. Strength and ductility of steel are customarily measured by means of a standard tension coupon test. A typical stress-strain curve for a mild-carbon structural steel is as shown in Figure 1.1.

Basically, depending on the way by which the forces are carried, the structural steel members can be categorized into columns, beams, beam-columns, braces, etc. A member subject to compressive axial load is known as column, which is often a vertical member. In general, the strength of a column is limited by its buckling behavior. A straight or slightly curved structural member, primarily supporting loads applied at right angles to the longitudinal axis, is known as a beam. Beam-Column is a member that simultaneously withstands axial load as well as significant bending moment. In beam-columns, lateral loading, applied end moments, or eccentric application of the axial load may cause bending effects.

The structural steel members can be rolled to shape or can be formed to shape by cold working or can be formed to shape by cutting and welding plates together. The rolled and welded built-up sections are mainly used in heavy steel constructions, whereas the cold-formed sections are commonly used in residential houses and low-rise commercial buildings. The structural steel members are manufactured in a wide variety of shapes and sizes. Some of the most commonly used structural steel shapes are illustrated in Figure 1.2. The mostly used structural members are the W-shape (wide-flange), the S-shape (American standard I-beam), the C-shape (channel sections), and hollow sections which include rectangular, square, and circular cross-sections. The W-, S-, and C-shape structural members are designated by their nominal depth (mm) and weight per unit length (kg/m) in accordance with the Hand Book of Steel Construction (CISC, 2004), whereas the hollow sections are designated by their outer dimensions (mm) and thickness (mm) in accordance with the same Hand Book. For example, W200x52 means the W-shape section having nominal depth of 200mm and the weight per unit length is about 52kg/m. On the other hand, for a hollow section, HSS102x76x9.5 means the rectangular section having nominal outer dimensions of 102mmx76mm and the wall thickness of 9.5mm.

I-shaped structural steel sections, which are generally referred to as W shapes, are widely used as beam members since their shape provides an efficient resistance to bending moments. They are also used as columns to transfer pure axial load, and as beam-column in the context of both axial load and bending moment effects may exist. The W-shape member has parallel inner and outer flange surfaces with a constant thickness, whereas the S-shape has a slope on the inner flange surfaces as shown in Figure 1.2. Thus, these two shapes can easily be differentiated. The C-shape/channel sections are not very efficient members as a beam or as a column when they are used alone. However, efficient built-up members can be formed from channel sections by assembling them together i.e., welding or reverting.

In this investigation, the sections referred to as I-shaped or H-shaped sections are of particular interest due to the fact that this section profile is commonly used to carry the axial loads and bending moments efficiently. The I-shaped sections considered in this research work were formed from wide rolled plates. Firstly the wide rolled plates were cut to size using different cutting techniques such as plasma cutting and flame cutting. Then the sections were formed by gas metal arc welding (GMAW) process.

1.2 The Conventional Methods for Forming of Structural Steel Members

The conventional forming operations such as cold forming and hot rolling have long been used in manufacturing various structural steel products. The manufacturing process of steel is carefully carried out through certain systematic steps. In the first step known as melting process, raw materials are charged in a blast furnace where hot air is forced into melt iron and fluxes at about 1600°C. The second step is refining process, in which molten metal from the blast furnace is taken to steel melting shop where further reduction of impurities is done in oxygen furnace. The third step is casting process where the liquid steel is cast into semi-finished products such as billets, blooms, slabs, etc. The final step is known as rolling process where the semi-finished products are reheated at about 1200°C to make metal malleable and then rolled into finished products.

Cold-Forming: Cold-Formed steel structural members are shapes commonly manufactured from steel-plate, sheet or strip material. The manufacturing process involves forming the section by either press-braking or cold roll-forming to achieve the desired shape. Some of the examples for cold-formed structural steel are corrugated steel roof, floor decks, wall panels, storage racks and wall studs. Press-braking is often used for producing small quantity of simple shapes. Cold roll forming is the most widely used method for the production of roof, floor and wall panels. It is also used for producing structural members such as cees, zees and hat sections. During cold roll-forming, sheet stock is fed longitudinally through a series of rolls, each of which works the sheet progressively until it reaches the desired shape. A simple section may require as few as six pairs of roll, but a complex shape may require as many as 24 to 30. The thickness of the cold- formed steel structural members that can be formed from steel sheets or strips generally ranges from 0.4mm (~0.0149 inches) to about 6.4mm (~0.25 inches), although the steel plates and bars of thickness around 25mm (1 inch) can be cold-formed successfully into structural shapes (Yu, 2000).

Hot-Forming: Hot forming refers to forming of structural shapes carried out at an elevated temperature (usually near 900°C). Very large deformations are possible in hot working because the recovery processes keep pace with the deformation. Therefore a greater degree of forming may be carried out with hot- forming than cold-forming. Additionally, the total energy necessary to deform a given component will be much lower for hot working than for cold working, as the strength of steel decreases with increasing temperature. Hot-forming is, therefore, appropriate to plate application where the required deformation is greater than that attainable with cold-forming. Hot-forming may also be a desirable alternative to cold-forming where press capacity is limited.

Hot-Rolling: Hot-Rolling is one of the major fabrication processes in making different types of steel shapes. From the light sections to heavy structural sections can be formed by rolling process. The rolling process is typically carried out at an elevated temperature of approximately 1200°C. In the rolling process, the material is passed through two rollers revolving at the same speed in opposite directions. The rolling operation shapes the steel, reduces the cross section, elongates it and increases its strength. Normally, ingots from the steelmaking furnace are first rolled into slabs, billets or blooms and later rolled into final form (plates, bars or shapes) in a finishing mill. In the continuous casting process, steel is directly cast as slabs or blooms by passing the ingot stage and subsequently into the final product form.

Welded Built-up Process: For built-up members, the rolled steel plates provide the basic elements which make possible any built-up shape. The welded built-up process allows a much greater flexibility than hot-rolling which gives only a limited range of shapes. Thus, the welded built-up process permits the designer to choose the most suitable member shape and size to carry the required design load effectively. Normally, in the welded built-up process, the plate pieces are first cut to size from the original rolled plates by different types of cutting techniques such as flame cutting, plasma cutting, saw cutting, etc., and then formed to desired shape by welding process. The detailed descriptions of different modern cutting techniques used in the fabrication of structural steel are given in the next section.

1.3 Modern Cutting Techniques in Fabrication of Structural Steel Members

There exist various metal cutting methods presently in use to cut metals. Besides, traditional saw cutting, flame (oxy-fuel) cutting, plasma cutting, laser cutting, and water jet cutting are used in modern structural steel fabrication. Traditionally, saw cutting and flame cutting have been in use for many decades in metal cutting process. However, with the advancements in manufacturing technologies fabricators have begun to use different cutting techniques. These modern cutting techniques have many advantages over the traditional saw cutting and flame cutting methods. These advantages include considerably faster rate of cut, superior bevel control, excellent finished product with dimensional accuracy and repeatability, elimination or reduction in supplemental machining operations, etc. However, each of the metal cutting techniques has its inherent advantages and disadvantages, when various factors such as operating cost, size of heat affected zone (HAZ), cutting speed, edge cleanliness, degree of tolerance required, and types of metal to be cut are taken into account. The pros and cons associated with each of the cutting technique are described in Table 1.1.

<u>Saw Cutting</u>: Saw cutting is a conventional method used in cutting metals. Relatively thin metals can be cut with heavy shears using this system. Cold sawing with hardened blade is performed to obtain very smooth cuts with extreme precision. This cutting method is only

applicable for linear cutting and the cutting speed is low when compared with other advanced cutting methods.

Flame (Oxy-Fuel) Cutting: The oxy-fuel or flame cutting technology is still the principal process for cutting metal plate for most metal processors. In this process acetylene and oxygen gas mix is used to produce a controlled flame at an elevated temperature. The required temperature is maintained by a flame which is obtained from the combustion of a specified fuel gas mixed with pure oxygen. This cutting technique is very useful in simultaneous multiple-cutting, high production runs at relatively slow speed. Also, this process is an excellent choice for end-users requiring inexpensive cutting through carbon steel and most alloys. Though this method is used to produce near-neat shapes, it creates a large heat affected zone (HAZ) around the cut that must be removed by additional machining. This process cannot be used to cut three dimensional cutting and sandwich structures with cavities. The cutting process is predominantly influenced by the hardness of a material to be cut. The process tolerance is approximately 0.76mm (0.03inch), and the degree of cut edges to completely parallel is fair. The common application for this process is cutting of flat sheet and plates of greater thickness.

Plasma (Arc) Cutting (PAC): Plasma cutting is a process that utilizes a highly positioned nozzle orifice to constrict a very high temperature and ionized gas. Therefore, it can be used to melt and sever sections of electrically conductive metals as shown in Figure 1.3. This process is performed by removing the molten metal with a high velocity jet of ionized gas issuing from the constricting orifice. Plasma Arc Cutting came into practice in the mid 1950's and became commercially successful shortly after its introduction to industry. The ability of the process to sever any electrically conductive materials made it especially attractive for cutting nonferrous metals that could not be cut by the flame cutting process. It was initially used for cutting stainless steel and aluminum. As the cutting process was developed, it was found that it had advantages over other cutting process for cutting carbon steel as well as nonferrous metals.

The energy density produced by a plasma torch is determined by the ratio of electrical current flow through the nozzle to the effective area of the nozzle orifice. This energy density can be measured as amps per square inch. Conventional nitrogen plasma cutting systems have an energy density in the range of about 19 to 31amps per square millimeter (12,000 to 20,000 amps per square inch). This energy density has typically been determined by economic factors. In other words, if the energy density is increased by changing the amperage to nozzle orifice ratio, the electrode and nozzle (consumables) will wear at an unacceptable rate. Because of this the cutting cost will increase. Although the higher density produces better cut edge quality, it comes at an unacceptable cost. Therefore manufacturers of plasma cutting equipment had to design their plasma systems to operate with an acceptable cut quality, combined with an acceptable level of consumable life.

In the early 1980's oxygen was introduced as a plasma gas for cutting carbon steels with greatly improved quality of cutting edge. It competed with nitrogen cutting at certain power levels. The oxygen cut edge was squarer, and the dross formation was minimal. Oxygen plasma also provides a metallurgically cleaner edge that allowed for better weldability, formability, and machineability of the cut part (see Figure 1.3(b)). Unfortunately, this advancement in technology created even shorter consumables parts life due to the reaction of the oxygen on the electrode material inside the torch. The earlier nitrogen plasma systems were capable of cutting for considerably long running before the consumable wear would seriously affect cut quality. However, the plasma operation working on oxygen systems, cutting the same material at the same speeds, required new consumables after considerably short run. Moreover, the oxygen systems produced a higher per meter cutting cost. When the better cut quality, along with lower secondary operation costs were factored in, the oxygen cutting process was an acceptable alternative to the conventional nitrogen systems. Clearly the oxygen plasma process would be well received if life span of consumable parts could be improved.

There are notable limitations to PAC when compared to the most mechanical cutting means. PAC introduces hazards such as fire, electrical shock, intense-light, fumes, gases and noise. The composition and rate of generation of fumes and gasses depend on many factors including arc current, cutting speed, material being cut and gases used. The fume and gas by-products will usually consists of the oxide of the metal being cut, ozone, and oxides of nitrogen. These fumes must be removed from the work area or eliminated at the source by using exhaust system. Codes may require that the exhaust be filtered before being vented to the atmosphere. Several alternative fume removal systems are available for mechanized cutting. One system consists of two parts, a cutting table which maintains a water bed that contacts the bottom surface of the work piece, and a water-shroud nozzle. Another system also uses a water bed, but instead of having the level of the water contact only the bottom surface of the work-piece, the water totally submerges the work-piece. This system is referred to as "*underwater plasma cutting*".

The cutting thickness capability of conventional plasma system varies depending on system manufacturer and power levels. In general terms, plasma systems are available to cut aluminium of about 150mm (~6inch) thick, stainless steel of about 125mm (~5inch) thick and carbon steels of about 32mm (~1.25inch) thick. Three dimensional metal cutting and cutting sandwich structures with cavities are not possible by this process. Also, this process can cut materials with different melting points. The quality of the cutting is highly influenced by the hardness of the material to be cut. Flat sheet and plates of greater thickness are often cut using this process.

<u>Water Jet Cutting</u>: Water jet cutting is a process used to cut materials using a jet of pressurized water of above 40MPa (60ksi) in pressure (Tesko Laser Divison, 2003). Often the water is mixed with an abrasive like garnet that enables more materials to be cut cleanly to close tolerances and squarely with good edge finish. Combining the high pressurized water with the abrasive produces stream that can be used to cut more materials than the plain water jet without the abrasive additive. Water jets are capable of cutting many industrial materials including stainless steel, inconel, titanium, aluminium, tool steel, ceramics, granite and armor plate. While three dimensional material cutting is possible to some extend, the ability of cutting sandwich structures with cavities is limited. Cutting material with impaired access is limited due to small distance between the nozzle and material to be cut. The cutting process is influenced by the hardness of the material. The abrasive water jet cuts through material ranging from 0.75mm (1/32″) to 305mm (12″) thick to high accuracy with creating virtually no heat affected zone (HAZ). Abrasive water jet is widely used for the cutting of complex shapes and fragile materials such as glass and high performance metals. The high failure rate due to breakage and chipping of corners during conventional processing is virtually

eliminated in this cutting system. Figure 1.4 shows a Water Jet cutting system in operation.

Laser Cutting: Laser cutting system uses CO_2 mixed with other gases to form a gas lasing medium. They have long had a reputation of cutting component parts with very tight tolerance. Laser cutting is the best metal cutting system for producing a precise cut with the narrowest "heat affected zone" (HAZ) (Tesko Laser Divison, 2003). In this process, three dimensional metal cutting is difficult due to rigid beam guidance and the regulation of distance. All metals (except highly reflective metals), plastics, glass and wood can be cut using this process. Materials with different melting points can barely be cut. Gas laser operations on sandwich structures with cavities are not possible in this method of cutting. Common application of this process is cutting of a flat sheet steel of medium thickness for sheet metal processing. Figure 1.5 shows a Laser cutting system in operation.

The following is the current capital costs associated with above mentioned cutting processes in increasing order: Flame cutting, Plasma cutting, Water jet cutting, and Laser cutting. Heat-Affected-Zone associated with these cutting processes in decreasing order is: Flame cutting, Plasma cutting, Laser cutting, and Water jet cutting.

1.4 The Influence of Fabrication Techniques on the Strength of Structural Steel Columns

As discussed previously, the structural steel column sections can be formed by either hot-rolling process or built-up process, where steel plates provide the basic elements for any built up shapes. Different fabrication techniques used in forming the sections cause different degree of structural and mechanical imperfections. The predominant factors that influence the strength of steel column sections are the presence of residual stresses and the presence of geometrical imperfections. Therefore, the incorporation of these imperfections in the evaluation of load bearing capacity of the most practical steel columns (intermediate range of slenderness) has derived much greater attention by steel designers. Since most of the present steel column design is primarily based on (a) hot-rolled section and (b) welded built-up section, the structural imperfections associated with these two different fabrication techniques are to be discussed in detail in this chapter.

Hot -Rolled Column Sections: In the fabrication of column sections by rolling process, the formation of residual stresses takes place as a result of differential cooling. The differential cooling always occurs during the process of cooling from the rolling temperature to ambient temperature. The magnitude and distribution of residual stresses in hot-rolled shapes depend upon the factors such as type of cross-section, rolling temperature, cooling conditions, and metal properties (Beedle and Tall, 1960). The experimental studies made on establishing residual stress distributions in the steel sections of similar shapes made of different steel grades have shown that the distributions and magnitudes of the residual stress are similar. Thus, it could be presumed that the effect of steel grade on the residual stress distribution is not as great as the effect of geometry. The typical variation of residual stresses due to hot-rolling process in most common structural steel sections are shown in Figure 1.6 (Stiemer, 2000)

Furthermore, extensive column strength analyses were made by Batterman and Johnston (1967) by interrelating the residual stresses and initial curvature of rolled columns. Also this study included the columns having different yield strength, different values of maximum compressive residual stresses with five different curvatures corresponding to initial mid-length out-of-straightness ranging from 0 to L/250, and slenderness ratios ranging from 20 to 240. The presence of compressive residual stresses at the flange tips of rolled H-shaped sections result in rapid loss of stiffness as weak axis inelastic buckling occurs. As a consequence of rapid loss in stiffness, the column buckles early creating a reduction in its capacity. In this investigation, the pioneering residual stress measurements were made in rolled H-shaped sections and the results obtained are given in Chapter 5.

Welded Built-Up Sections: Welded built-up members are frequently used in heavy steel constructions, because the members can be formed in a wide variety of sizes with desired shapes. Also these members are relatively more economical, easy to manufacture, and more accessible to work environment. However, the built-up shapes fabricated from rolled steel plates by means of cutting and welding processes have large heat affected zones (HAZ) due to different kinds of thermal treatment during the fabrication process. Subsequently, the HAZ is translated into residual stresses and geometric imperfections. As discussed earlier, the combined effect of presence of residual stresses and the initial imperfections resulting from the manufacturing process (cutting and welding) have a significant influence on the strength of welded H- or box-section column sections which are subjected to compressive loads.

Studies carried out by earlier investigators in the area of strength of welded built-up columns have primarily been concerned with shapes manufactured from universal mill plates (the normal edge produced by rolling between horizontal and vertical finishing rolls) and flame-cut plates. The H-shaped column sections manufactured from universal mill plates were found to have fairly high compressive residual stresses at the flange tips (McFalls and Tall,

1962) whereas the H-shaped columns manufactured from flame-cut plates were found to have more favorable residual stresses (tensile stresses) at the flange tips. The tensile residual stresses at the flange tips were a direct result of the flame cutting of the plates (cutting effects). Welding reduces theses to some extent, but not enough to change their favorable effect on column strength (McFalls and Tall, 1962). Because of the presence of tensile residual stresses at the flange tips of H-shaped columns, it delays the deterioration in minor axis stiffness. This delay in minor axis buckling is of great significance as it generally governs the buckling of H-shapes. Thus, the load carrying capacity of flame-cut columns was higher than that of universal mill columns when the columns were permitted to rotate about weak axis. Figure 1.7 shows the typical residual stress distribution in hot-rolled shape, welded box section, plate with rolled edges (universal mill plates), plate with flame cut edges, and I-shape section fabricated from flame cut plates (Brockenbrough and Merritt, 1999).

The strength differences between box-shape columns, on the other hand, made of universal mill and flame-cut plates are relatively small, because the high heat input from the welding on the edges overrides the residual stresses in the component plates (Bjorhovde et al, 1972). Also the early investigations on column strength were made on the rolled H-shaped columns and the universal mill plate welded built-up columns. The test results on these shapes showed that the strength of this type of welded columns was significantly less than that of corresponding rolled shapes. However, this was not true for relatively heavy shapes at low slenderness ratio (Estuar and Tall, 1963).

The influence of cutting and welding processes on the overall distribution of residual stresses in the surrounding area during fabrication process of built-up columns has extensively been investigated by researchers in the past. However, the influence of welding on the magnitude and the overall distribution of the residual stresses was found to have higher effect on small and medium size column than that for the heavy shapes (Galambos, 1998). The intensity of residual stresses in welded plates depends upon many factors such as type of cutting, type of welding (butt weld or arc weld), heat of welding, speed of welding and rate of cooling. In this investigation, the effect of cutting techniques, namely, plasma cutting and flame cutting on residual stress distributions in H-shaped columns were experimentally obtained. Eventually the strength of welded built-up columns fabricated from plasma-cut plates and flame-cut plates were compared. The investigation considered columns having different values of slenderness ratio and the associated details are described in Chapter 6.

1.5 Scope and Objectives

It has long been established from previous studies that the variables influencing column strength are numerous. However, the magnitude and distribution of residual stresses, initial out-of-straightness and accidental eccentricity of applied load are known to be the major factors influencing most practical columns (intermediate slenderness ratio). The magnitude and distribution of residual stresses and the magnitude of initial out-of-straightness depend largely on the method used to manufacture the column. Therefore, the method of manufacturing process has a direct influence on the strength of a column. In this research work the strength of welded columns manufactured by two different cutting methods, namely, plasma cutting and flame cutting will be investigated. The columns that are referred to as H-shaped sections are of particular interest in this study, due to the fact that this section profile is commonly used and is widely available. The column tests will be carried out under pinned end condition and subject to an uni-axial compressive load. In order that in future, we may develop analytical tools to predict the load carrying capacity of the columns, the test program will include tensile coupon test, residual stress measurements, stub column tests and long column tests. The temperature measurements during cutting and welding process will also be taken since this information may be used to drive analytical models for residual stress profile in structural steel in the future work.

Objective: 1 of this investigation is to measure the temperature profile during the cutting and welding operations. The measured temperature distributions are expected to be used in future studies related to prediction of various residual stress models by analytical approach.

Objective: 2 of this investigation is to establish the geometrical imperfections associated with the different fabrication techniques (plasma and flame cut column sections). The geometrical imperfections in this investigation will be established at different stages of fabrication process. Firstly, the initial out-of-plane imperfections of original plates will be established. Secondly, the surface imperfections on the plate strips after cutting will be established. Finally, after forming the section, the imperfections in terms of sweep, camber, and sectional variations will be established.

Objective: 3 of this investigation is to experimentally establish the residual stress distribution present in the initial plates, plate strips after cutting, and welded built-up H-shaped column sections fabricated from plasma cut plates and flame cut plates. For residual stress measurements, the "method of section" technique, which is a destructive method, will be used.

Objective: 4 of this investigation is to perform the column tests and thus, predict the capacity of plasma cut columns and flame cut columns. The columns having non-dimensional slenderness ratios of about 0.2, 0.3, 0.5, 0.8, 1.0, and 1.2 will be considered, as these values cover the range of ratios of most practical steel columns (intermediate column range). The effect of fabrication techniques such as plasma cut and flame cut on strength of the steel columns will be analyzed and compared. Hence, the capacity of the columns obtained through this experimental investigation will be compared with the present Canadian Code for structural steel columns in accordance with CAN/CSA-S16-01 standard (CSA, 2004) and further discussion and conclusion will be made at the end of this research work.

Moreover, as part of scientific documentation, the material behavior of the steel plates that are used in the fabrication of the steel columns will be obtained. The standard tensile coupons will be cut from each of the original steel plates and tested in the Tinius Olsen Machine with the capacity of 600kN. Then, the most important parameters such as yield strength, ultimate strength, elastic modulus, etc., will be obtained.

1.6 Thesis Outline

In this thesis report, Chapter 2 outlines the research methodology performed in this investigation. Chapter 3 includes the temperature measurements during various stages of fabrication process of welded built-up columns. Also, it reviews how the past work was done in predicting residual stresses in steel plates from the temperature measurements, thus expanding the prediction of residual stress analytical models for various structural shapes such as I-shaped sections, box shapes, etc. Moreover, the temperature profiles obtained in this research work and the detailed descriptions of observations made during cutting process as well as welding process are provided in this chapter. Chapter 4 includes a discussion on how the geometrical imperfections are associated with different types of fabrication techniques and to what extend the geometrical imperfections influence the strength of columns. This chapter describes the measurement procedures followed in this research work to establish the geometrical imperfections at various stages of fabrication process. Also, this chapter includes the presentation of various types geometrical imperfections associated with the plate and the column sections. The first part of the Chapter 5 describes the various aspects of different techniques used to establish the residual stresses in structural components. Moreover, this chapter explains the detailed measurement procedure associated with the "method of section" technique used in this investigation. This chapter also explains how this technique was further modified by doing some pilot tests in this investigation to come up with the proper measurement procedure in the subsequent work. This chapter concludes with the presentation of residual stress results obtained for plasma cut columns and flame cut columns in this investigation.

Chapter 6 provides the various aspects of experimental study of plasma cut columns and flame cut columns. In the first part of this chapter, the general behavior of structural steel columns is described. The second part of this chapter describes the various aspects of multiple column strength curves and their systematic developments by the previous researchers in this area. The third part of this chapter explains the detailed test procedures carried out in this investigation to establish the strength of columns at different slenderness ratios. Also, this chapter provides the summary of work done towards establishing mechanical chateristics of steel plates used in this investigation. This chapter concludes with the presentation of test results and associated discussions.

In Chapter 7, summary of this investigation, conclusions derived, recommendations made regarding the current column design code, and the recommendations for future study are given. Detailed results associated with the tension coupon tests are given in Appendix A.

Cutting Method	Advantages	Disadvantages
Flame Cutting	• Suitable for medium and large size thickness • Lower investment and spare parts cost • Economical application for several torches	• Not suitable for cutting of material below 5mm thickness • High heat impact and subsequent large HAZ • Low accuracy to size at repeat cuts as a result of heat impact • Low cutting speed
Plasma Cutting	• Cutting of all electrically conductive material • Excellent suitability for thin and medium thick mild steel (up to 30mm) • Cutting high-strength steels with low heat impact • High cutting speed (up to 10 times higher than flame cut) • Clean cuts without necessity of after treatment on medium and thick plates	• Limited to 160mm with dry cutting and 120mm underwater cutting • Excessive noise • Considerable HAZ
Laser Cutting	• High accuracy for thin and medium thick plates • Cutting of tiny holes, narrow webs, and nose angled geometries • Rectangular cutting edges • Very small heat impact • Very small cutting kerf (0.2~0.4mm) • High cutting speed at thin plates	• High investment and operating cost • Limited in material thickness (Mild steel 20~25mm, High alloyed steel 15mm, Aluminium 10mm) • Medium thick plates don't have an even surfaces • Exact distance control between torch and work piece necessary • Reflecting material surfaces decreases the process stability • Low efficiency
Water Jet Cutting	• Cutting of all material; wide range of thickness • No heat impact, no HAZ • Narrow cutting kerf, square cuts, high accuracy, and excellent quality	• High investment and operational expenses • Very slow at cutting "hard" materials • Wet and noisy • No manual use and limited for 3D cutting

Table 1.1: General Advantages and Disadvantages of Different Cutting Technologies

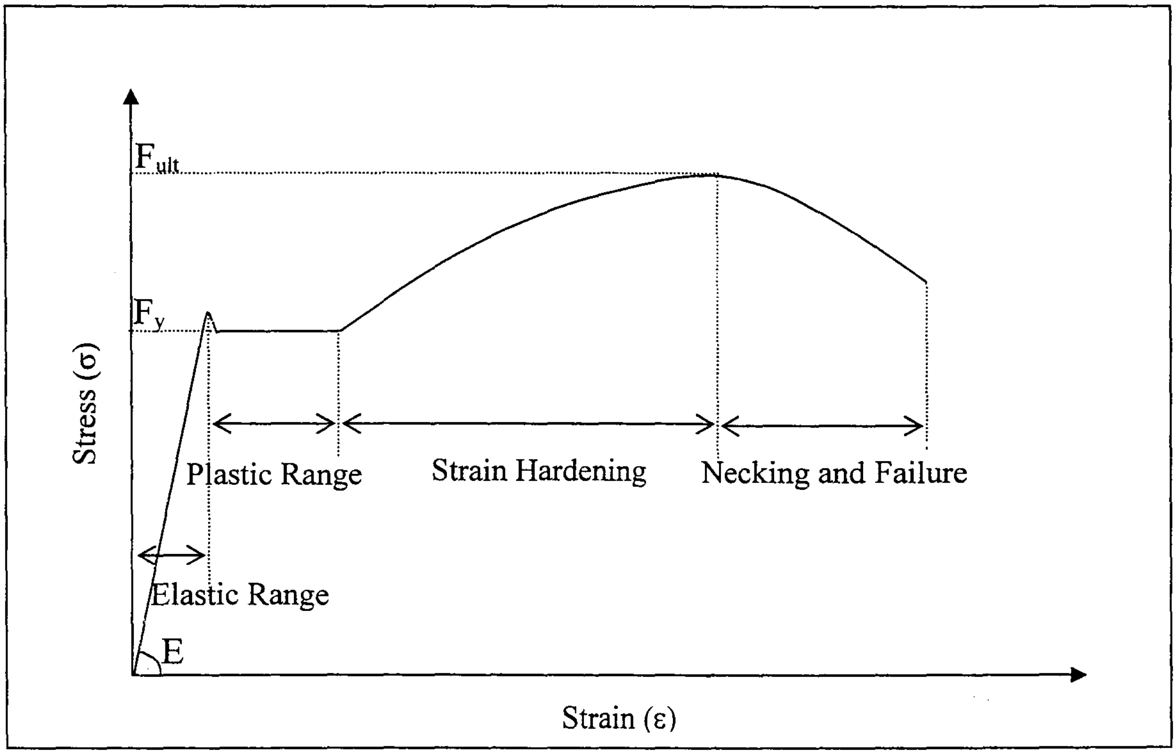

Figure 1.1: Typical Stress Strain Curve- Mild-Carbon Steel

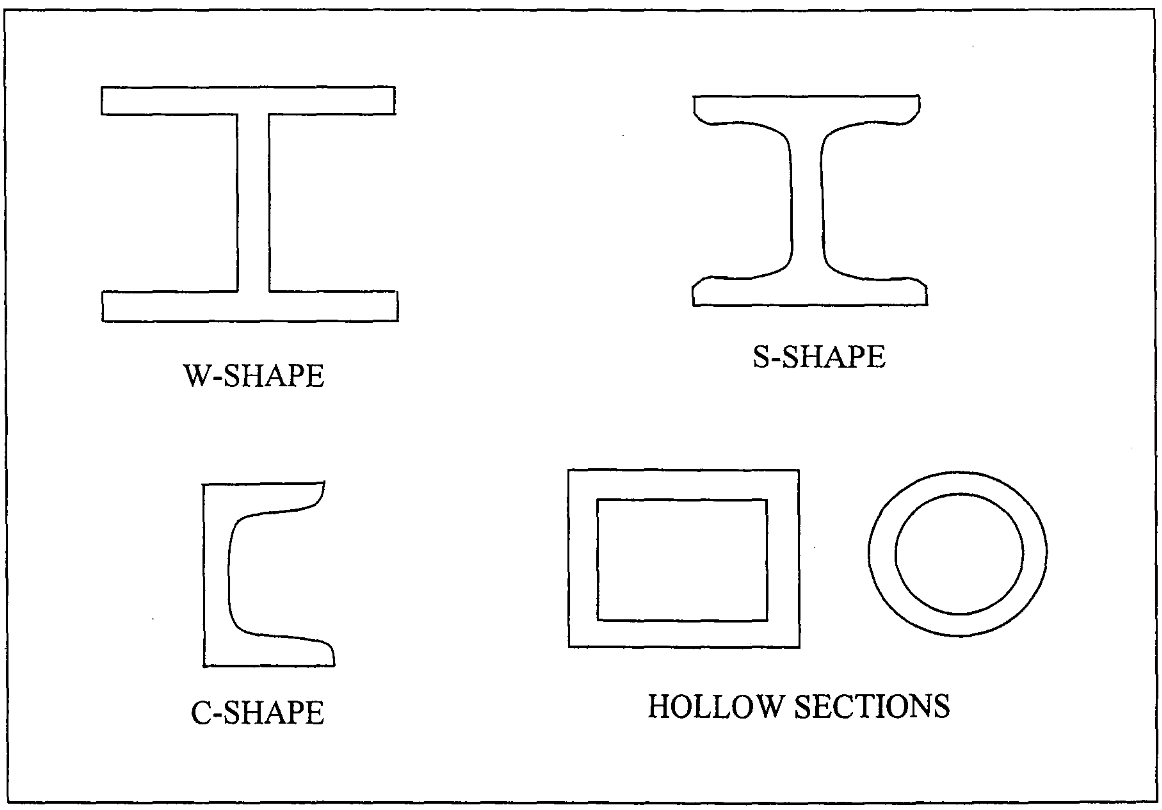

Figure 1.2: The Most Common Structural Steel Shapes

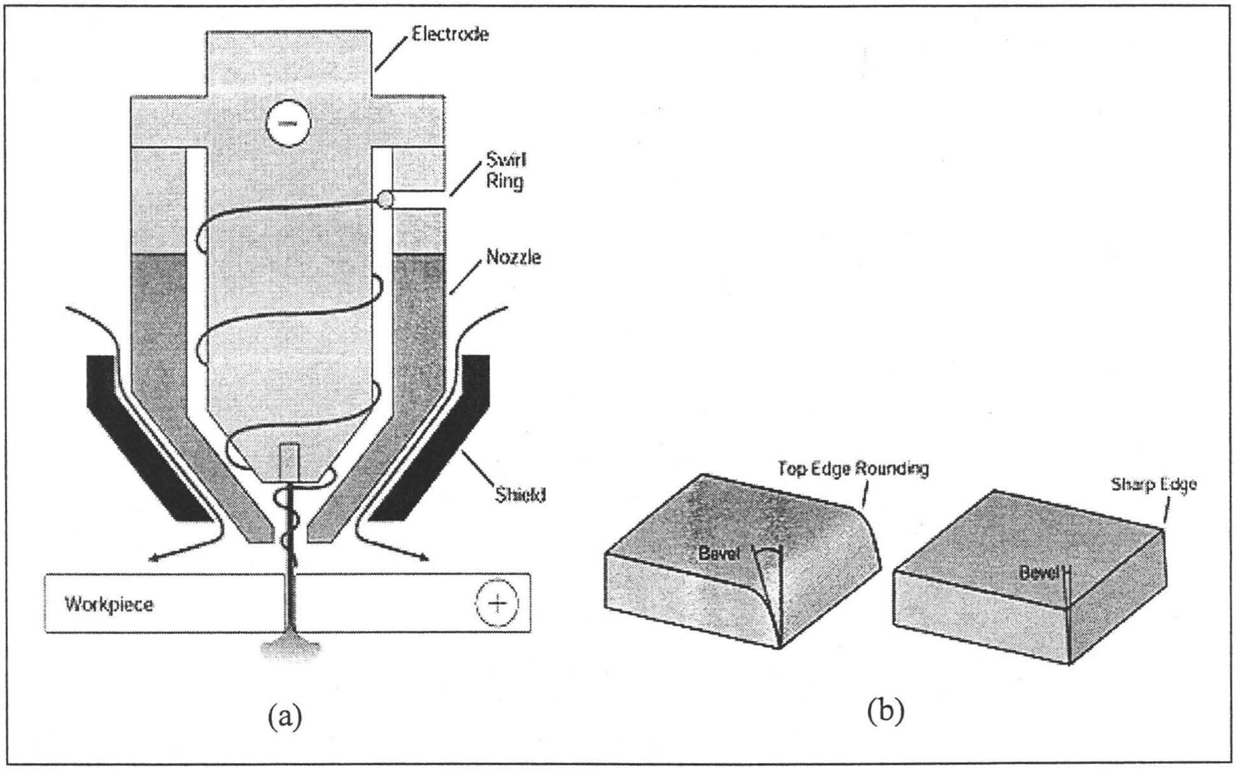

Figure 1.3: The Plasma Cutting System and the Bevel Control of Conventional Nitrogen Plasma Cut and that of Oxygen Plasma Cut
(Penton Media, Inc., www.hypertherm.com)

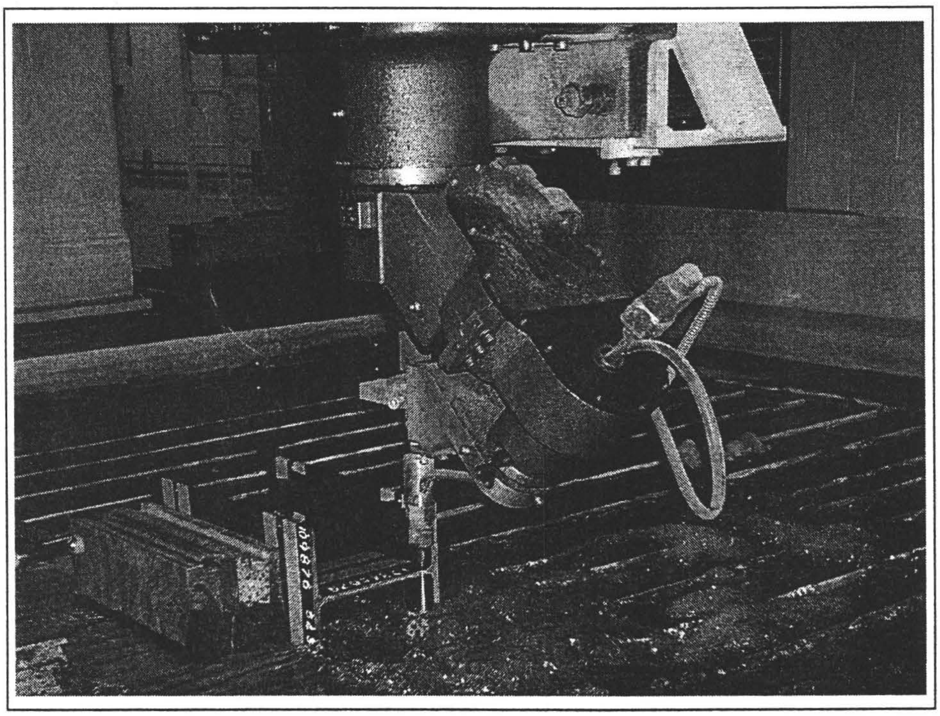

Figure 1.4: The Water Jet Cutting System

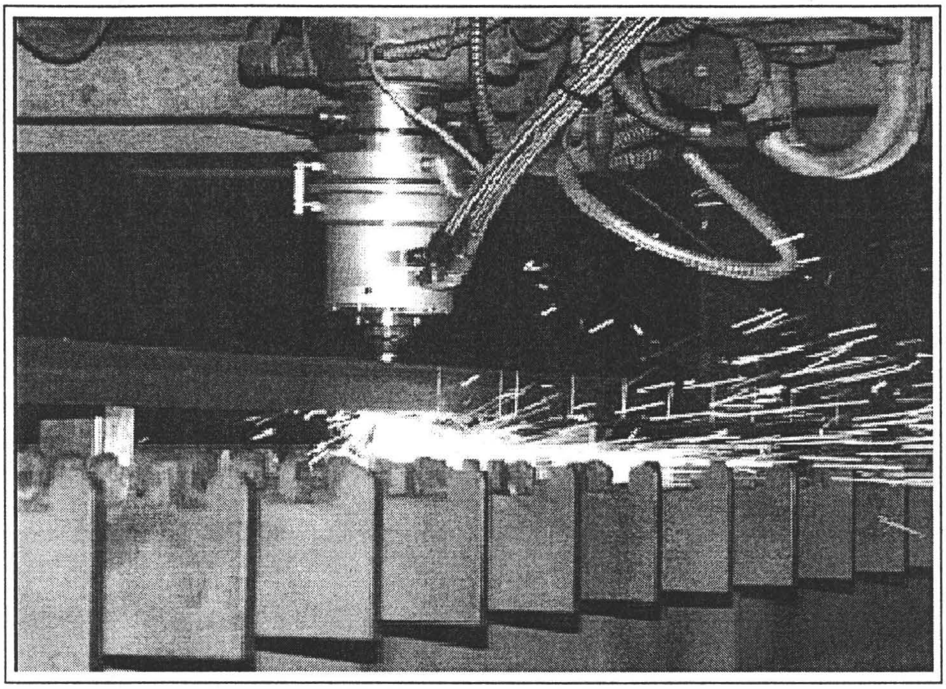

Figure 1.5: The Laser Cutting System
(Bender Ship Building and Repair Company Inc., www.bmpcoe.org)

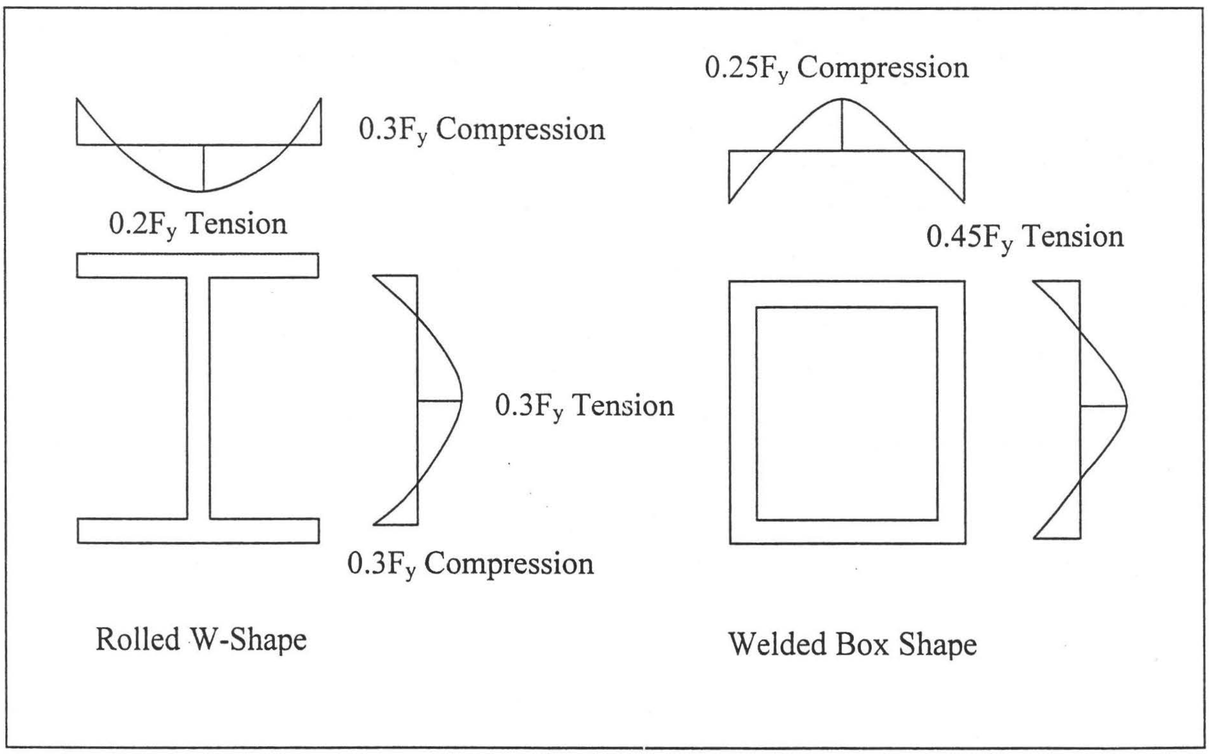

Figure 1.6: Typical Residual Stress Distributions in Rolled Shapes (Stiemer, 2000)

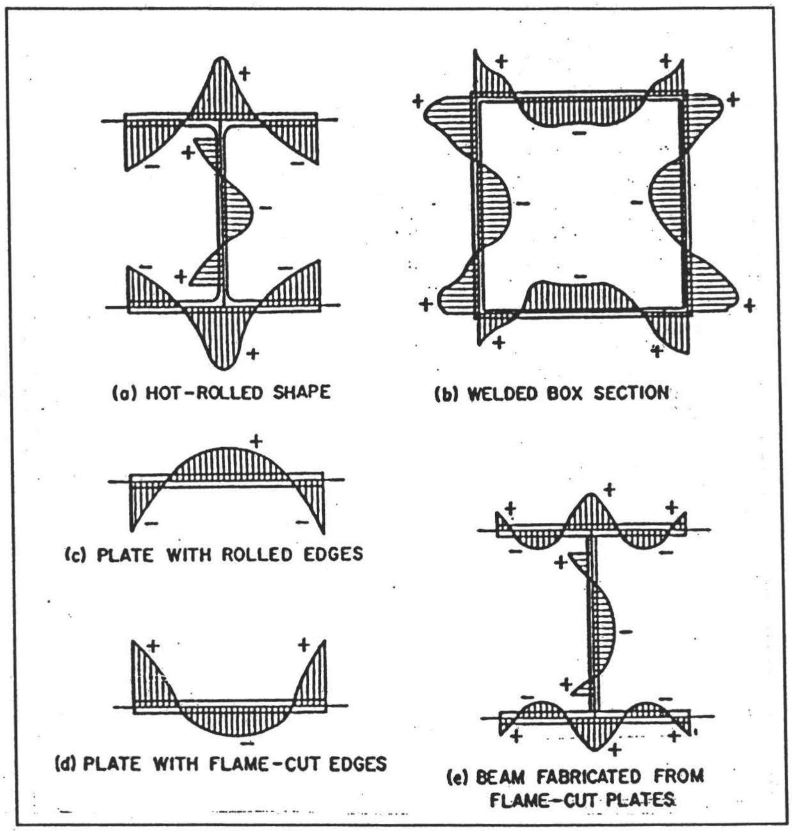

Figure 1.7: The Residual Stress Distribution in Shapes Manufactured by Different Fabrication Process (Brockenbrough and Merritt, 1999)

Chapter 2

RESEARCH METHODOLOGY

2.1 Introduction

This chapter provides a detailed description of the research methodology followed in this investigation. In order that readers may clearly understand the research work carried out in this investigation, it was decided to provide this material as a stand alone chapter. Thus, this chapter provides step by step details of this experimental investigation. A flow chart provided with this chapter (see Figure 2.1) will explain the original idea of this investigation, different stages of fabrication processes, and associated measurements taken at various stages of the fabrication processes and the testing procedures.

In brief, the primary objectives of this research work were:

(a) to establish the strength of steel columns fabricated from plasma cut plates

(b) to establish the strength of steel columns fabricated from flame cut plates

(c) to compare the strength of the plasma cut columns to that of the flame cut columns.

(d) to compare the predicted values with code equations based on the Canadian Standard CAN/CSA-S16-01 (CSA, 2004).

Therefore, it was decided to perform a number of column tests on column sections fabricated from steel plates cut by plasma cutting and traditional flame cutting. In practice, the most steel columns are considered to fall into the intermediate slenderness ratios and behave inelastically. Therefore, the column specimens tested in this investigation were selected such that the lengths of the columns were within the intermediate column range, except for a very short column ($\lambda \leq 0.5$). The description of the column sections and associated cross-sectional dimensions, lengths, and mechanical characteristics will be presented in the following chapters in detail. In addition to the column tests, this investigation includes establishment of residual stresses, establishment of mechanical characteristics, and measurements of temperature variations during fabrication process (cutting and welding). The measurements of imperfections such as gauge readings for residual stress measurements and geometrical imperfections were continuously monitored when plates went through various stages of fabrication processes

2.2 The Preparation of Steel Plates and Initial Measurements

To achieve the objectives of this research work, six identical steel plates obtained from the same production batch were used to form the column sections. The overall dimensions of the plates were chosen considering the dimensions of the column sections to be fabricated and other tests to be conducted. It was decided in this investigation that the specimens for column tests, the specimens for stub column tests, and the specimens for residual stress measurements were to be in the same column stock to ensure the consistency of the tests to be carried out. Also, the left over pieces from the same original plates were to be used to make standard tensile coupons and thus, to find out the associated mechanical characteristics of each of the plates. Thus, the chosen dimensions for each of the original steel plates were of 3960mm (156inch) long, 710mm (28inch) wide, and 9.5mm (3/8inch) thick. The specified yield strength and ultimate strength of the plates were approximately 350MPa and 500MPa, respectively. In the first stages of this research work, the following steps were carried out as preparation of plates and to establish associated initial measurements.

Step 01: In the first step, the locations of the flange and the web portions of the column sections were identified and then the grid-lines were marked in the longitudinal direction of the plate. Then the portions for intermediate column, stub column, and the portion for residual stress measurements were located as shown in Figure 2.2. The area between the column portion and the stub column portion was selected as the potential location for residual stress measurements in this research work (see the Figure 2.2). This was to eliminate the possible end effects that might affect the distributions of the residual stresses present in the column section. Also, the locations for temperature measurements were marked on the original plate as shown in the Figure 2.2

Step 02: In the second step, after identifying the location for residual stress measurements, grid lines along the strips to be sliced were marked and numbered for subsequent residual stress measurements in this research work. Pairs of gauge holes were laid out within each strip using a hand-held drilling machine attached to a drill stand. The detailed description associated with the selection of length of the specimen for residual stress measurements and the width of strips to be sliced will be provided in Chapter 5. Moreover, in this step, the initial gauge-hole readings corresponding to each strip were taken using the "*Demec*" mechanical dial gauge. Also, the detailed residual stress measurement procedure to be followed before taking the dial gauge reading will be explained in Chapter 5.

Step 03: This step was associated with the geometrical imperfections measurements on the surface of the original steel plates. The measurements were taken at 300mm (12inch) interval along the lines; 1-1, a-a, 2-2, b-b, 3-3, c-c, and 4-4 as shown in Figure 2.3.

All the measurements were taken after making sure that the plate was flat. Also, the measurements were taken at every 100mm in the transverse direction along the grid lines A-A, B-B, and C-C (see the Figure 2.3). Further details associated with geometric imperfections are given in Chapter 4.

2.3 The Cutting Process of Steel Plates

As part of the fabrication process, the flanges and the web of a column section were cut to size from the original steel plates discussed in the previous section. Three plates, designated herein as plate-01, plate-03, and plate-05, were cut by plasma cutting and the rest of the three plates, designated herein as plate-02, plate-04, and plate-06, were cut by flame cutting. The observations made during these cutting processes will be provided in Chapter 3 and Chapter 4. As a continuous work of this investigation, the following steps describe the associated work done during the cutting process and after the cutting process.

Step 04: In this step, the temperature measurements were taken at certain time intervals. In this study, it was decided to take the temperature measurement at suitable time intervals since the time interval between two successive cutting operations were different during cutting process on the plates. Hence, the measurements were taken only on the specific marks made on the original plate as shown in the Figure 2.2. The measurement procedure, details of the instruments used for measuring the temperature, and further associated detail description of this step will be explained in Chapter 3.

Step 05: In this step, the gauge hole measurements were taken on the plate pieces which are designated to be the flange and the web pieces for a column section. These measurements were taken to establish change in residual stresses due to cutting process.

Step 06: In this step, the geometrical imperfections associated with the different cutting process (plasma and flame) were taken on each of the plate pieces. The detailed measurement procedure involved in this step and the associated results will be given in Chapter 4.

Step 07: In this step, standard coupon tests were carried out as a routine test to obtain the mechanical characteristics of each of the steel plates used herein. Two coupon specimens from each plate were tested. The tensile coupon testing procedures involved provided by American Society for Testing and Material Standards A370-02 (ASTM, 2002). The detailed procedure associated with this coupon test and the graphical interpretation of the test results will be provided in Appendix 'A'.

2.4 The Welding Process

Welding was the other part of the fabrication process in this investigation. The column specimens to be tested were welded by one pass of weldment on each side of the web using a Gas Metal Arc Welding (GMAW) process. CO_2 was used as a sealing gas with flux core wire when welding operation was carried out. The welding operation herein was done by automatic equipment moving roughly at a speed of 190mm/min (7.5 inch/min). Current and voltage used during this process were approximately 330 Amps and 35 Volts, respectively.

Before welding was carried out, the cut plate pieces were assembled together to form the desired shape (I-shape) by clamping the plate pieces in position. The assembled section was then tack welded at certain locations along the column length. Thereafter, the assembled section with tack welds was placed against a supporting beam roughly at an angle of 45° as shown in Figure 2.4. At this point, the column section and the supporting beam were tack welded together at certain locations to avoid unnecessary movements during the welding operation (see the Figure 2.4). In this welding operation, the nominal leg length of the welding was about 10mm. Figure 2.5 shows the surface of the welding in the longitudinal direction of a column specimen.

Step 08: In this step, the temperature measurements were taken during welding, and after the welding process. The selected time interval between successive temperature measurements was approximately 5 minutes. The detailed description of this step and the graphical interpretation of the temperature variation will be provided in Chapter 3.

2.5 The Column Sections and the Associated Measurements

There were a total of six 'I' shaped column sections formed. Note that, at this point, the length of the column sections was the same as the length of the original plates of 3960mm (156inch). As a continuous part of this investigation, the measurements of gauge readings for residual stress measurements as well as geometrical imperfections in terms of sweep, camber, and the sectional variations were taken in the following steps.

Step 09: In this step, the gauge readings for residual stress measurements were recorded. Note that the gauge readings taken at this point would be the initial readings for the subsequent residual stress measurements. Therefore the gauge readings were taken with care, since the initial readings can not be duplicated. The detailed procedures were to be followed every time before taking the gauge-hole readings are provided in Chapter 5.

Step 10: In this step, the column sections were separated as the specimen for column test, stub column test, and the specimen for residual stress measurements. The separation was performed using cold sawing. Moreover, in this step, the gauge readings and the geometrical imperfections associated with each of column specimens and stub column specimens were recorded. Note that the gauge readings taken, at this point, herein were designated as gauge readings after "cut-01". Figure 2.6 shows the column section just after the welding, column specimen for testing, stub column specimen for testing and the specimen for residual stress measurements.

Step 11: In this step, the measurements of the geometrical imperfections in terms of sweep and camber associated with each column sections were measured. The detailed procedure for measuring these imperfections will clearly be explained in Chapter 4. Moreover, the sectional variations of each of column sections were traced to see how the welding influences the out-of-flatness of sectional elements and out-of-squareness of the whole section.

The detailed procedures associated with the residual stress measurements such as, measurements of gauge readings which were designated herein as the readings after "cut-02", after separation of web from flanges, measurements after final slicing of the specimens by water jet cut will be discussed in Chapter 5. Figure 2.7 shows the basic step associated with the residual stress measurements obtained by the "method of section" technique. Moreover, the Chapter 5 will provide presentation of the tests results, comparison and conclusion of test results obtained form plasma cut column sections and flame cut column sections. The detailed procedure associated with the column tests such as overall test set up, placement of LVDTs, alignment of columns within the test set up, presentation of tests results, etc will be provided in Chapter 6.

2.6 Testing for Axial Capacity of Columns

A total of twelve column tests were performed in this investigation. As discussed earlier, all the column tests were done under uni-axial compressive load with the pinned end condition permitting the rotation about minor-axis. Moreover, each of the column specimens was welded with a base plate having dimensions of 300x300x6.25mm on both sides of a column section. This was to ensure the uniform application of compressive loads over the cross-section. The following steps briefly describe the test procedures undertaken in this investigation.

Step 12: In this step, firstly the column specimen was aligned within the test set-up which was specially designed for this investigation as shown in Figure 2.8. After ensuring that the column specimen was aligned, LVDTs were placed at locations where the deflection at mid-height, deflections at quarter points, and rotation at both ends of the column section were to be measured. One LVDT was placed in the mid-height of the flange to make sure whether there was any transverse movement during testing. The column specimen was loaded to a certain limit (well within the proportional limit, approximately 2kN to 5kN) and unloaded to initial stage. This was done to ensure that each of the LVDTs settled itself and ready to pick up readings. The detailed procedure associated with the column tests such as overall test set up, placement of LVDTs, alignment of column specimen within the test set up, presentation of test results, etc., are provided in Chapter 6.

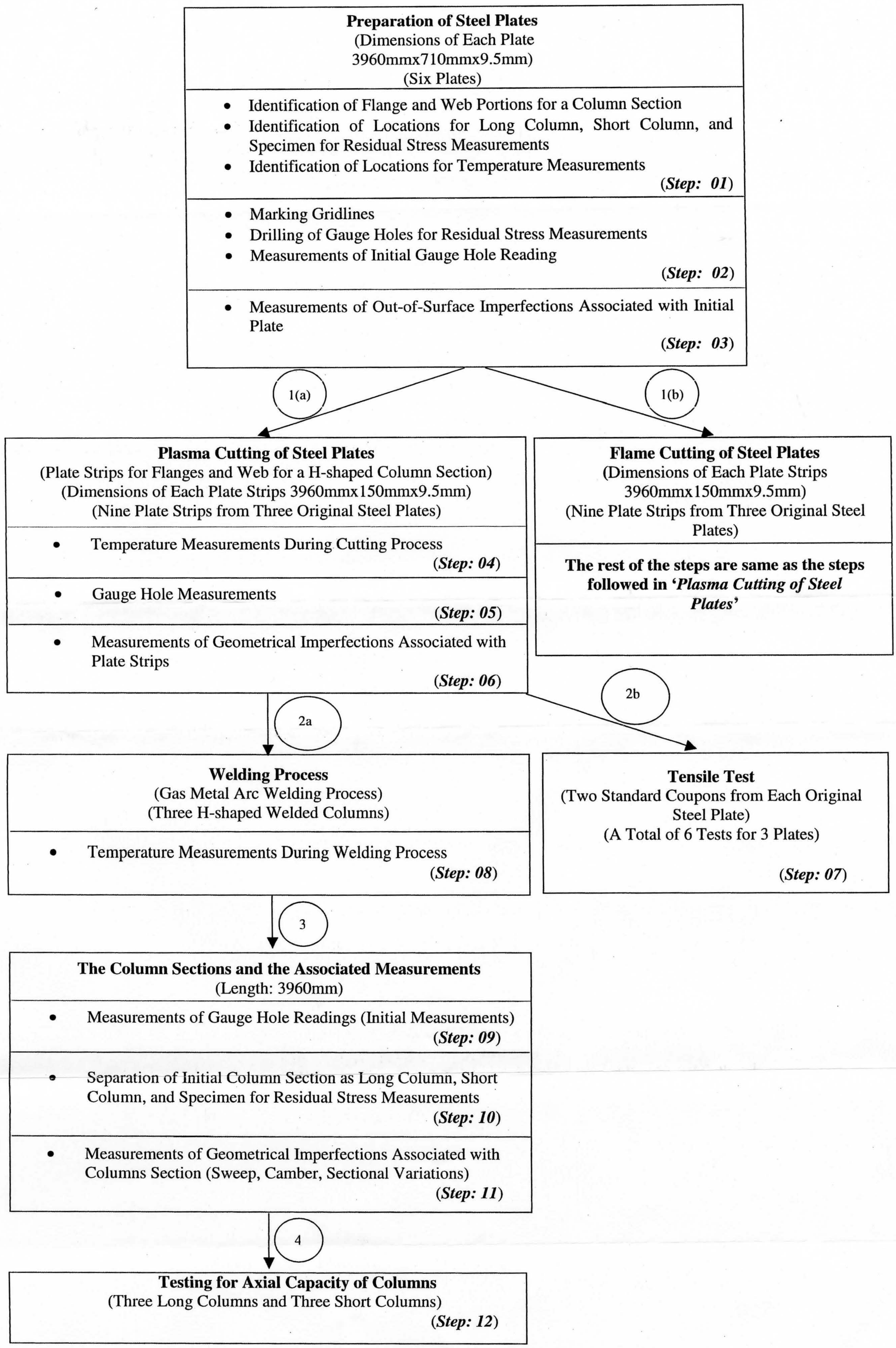

Figure 2.1: The Various Procedures Associated With This Investigation

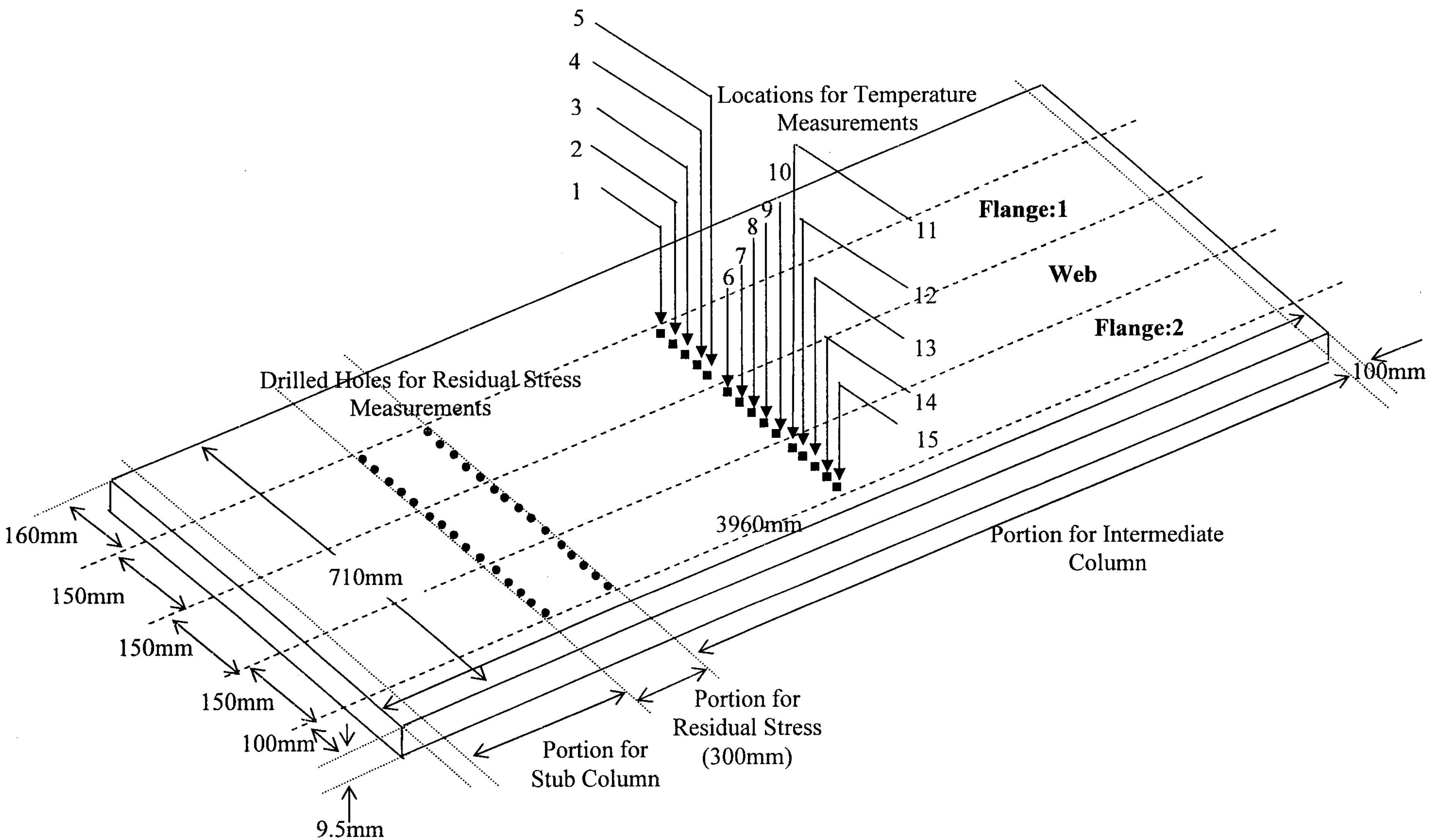

Figure 2.2: Identification of Column Locations and Measurement Locations in Steel Plate (*Step: 01*)

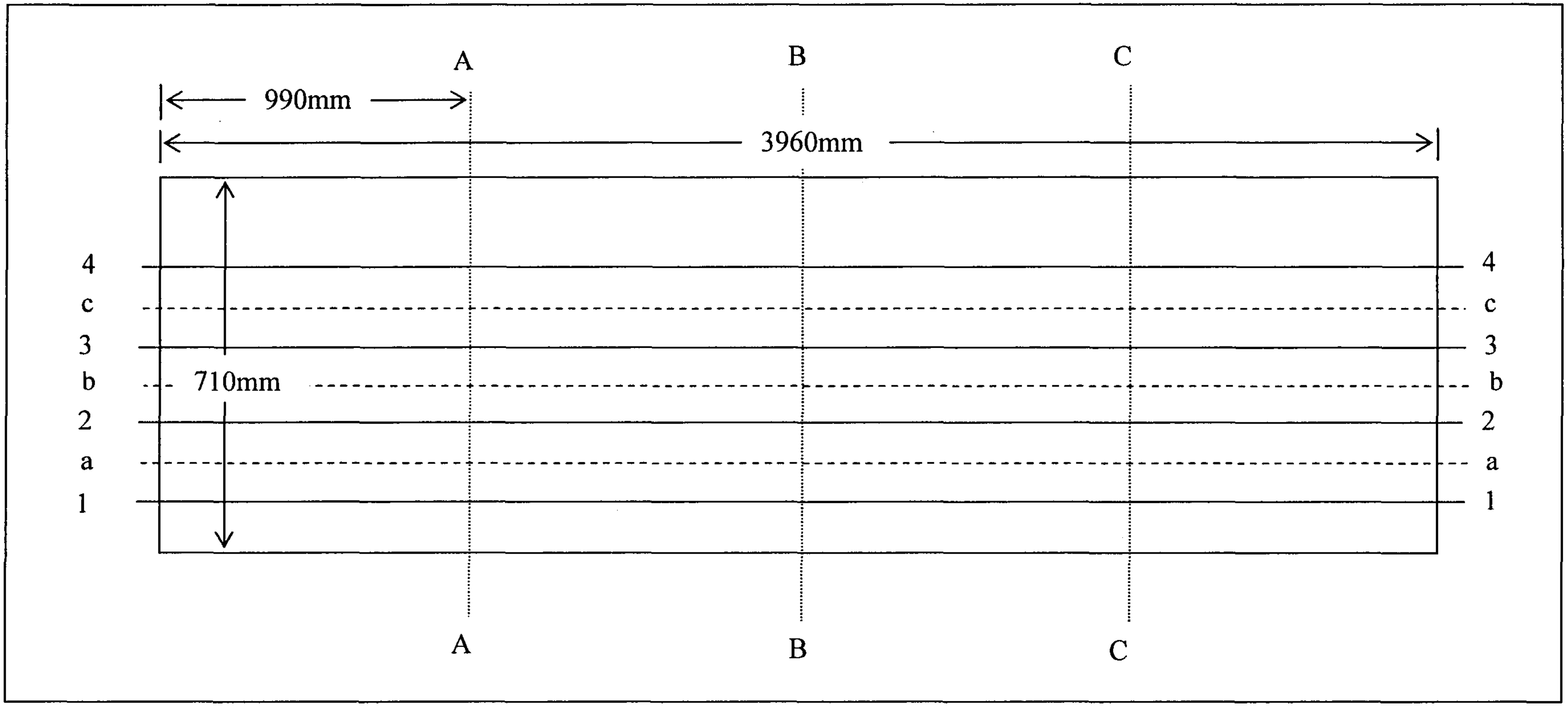

Figure 2.3: The Plan View of a Plate with Grid Lines for Measurements of Surface Imperfections

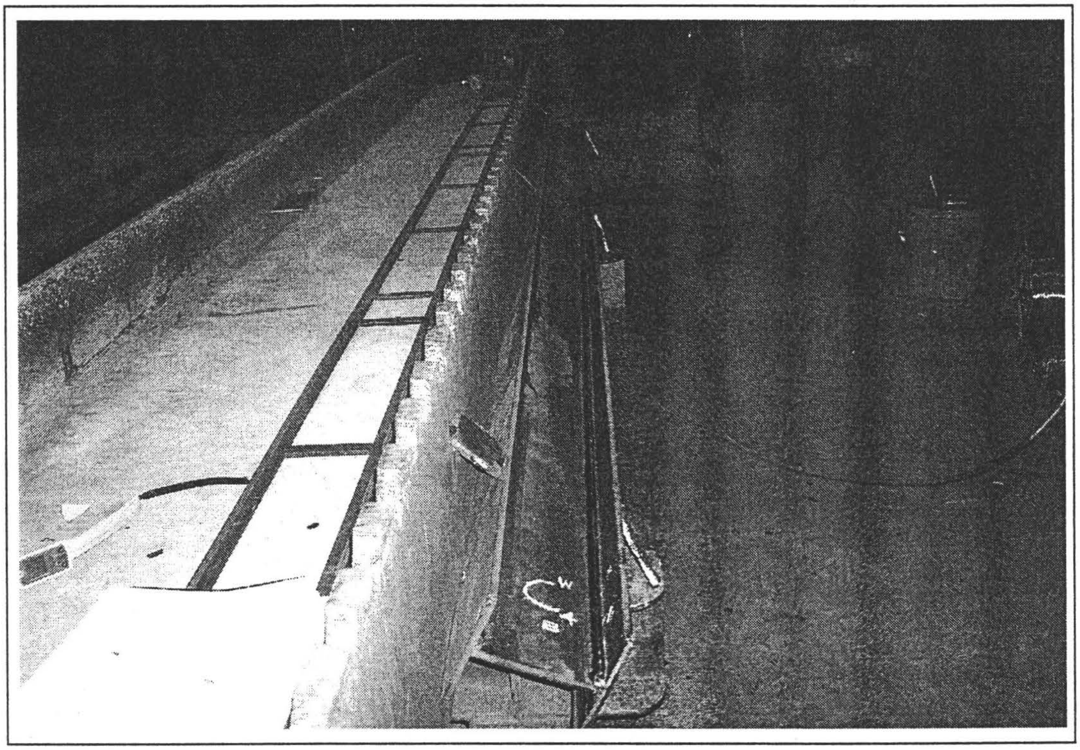

Figure 2.4: The Column Section during Welding Operation

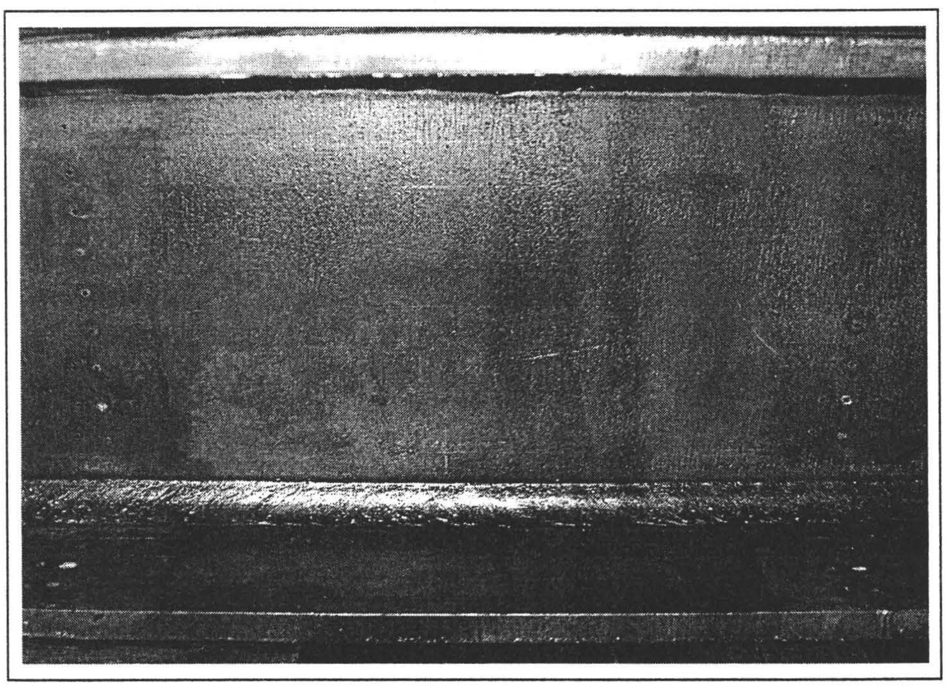

Figure 2.5: The Surface of Gas Metal Arc Welding

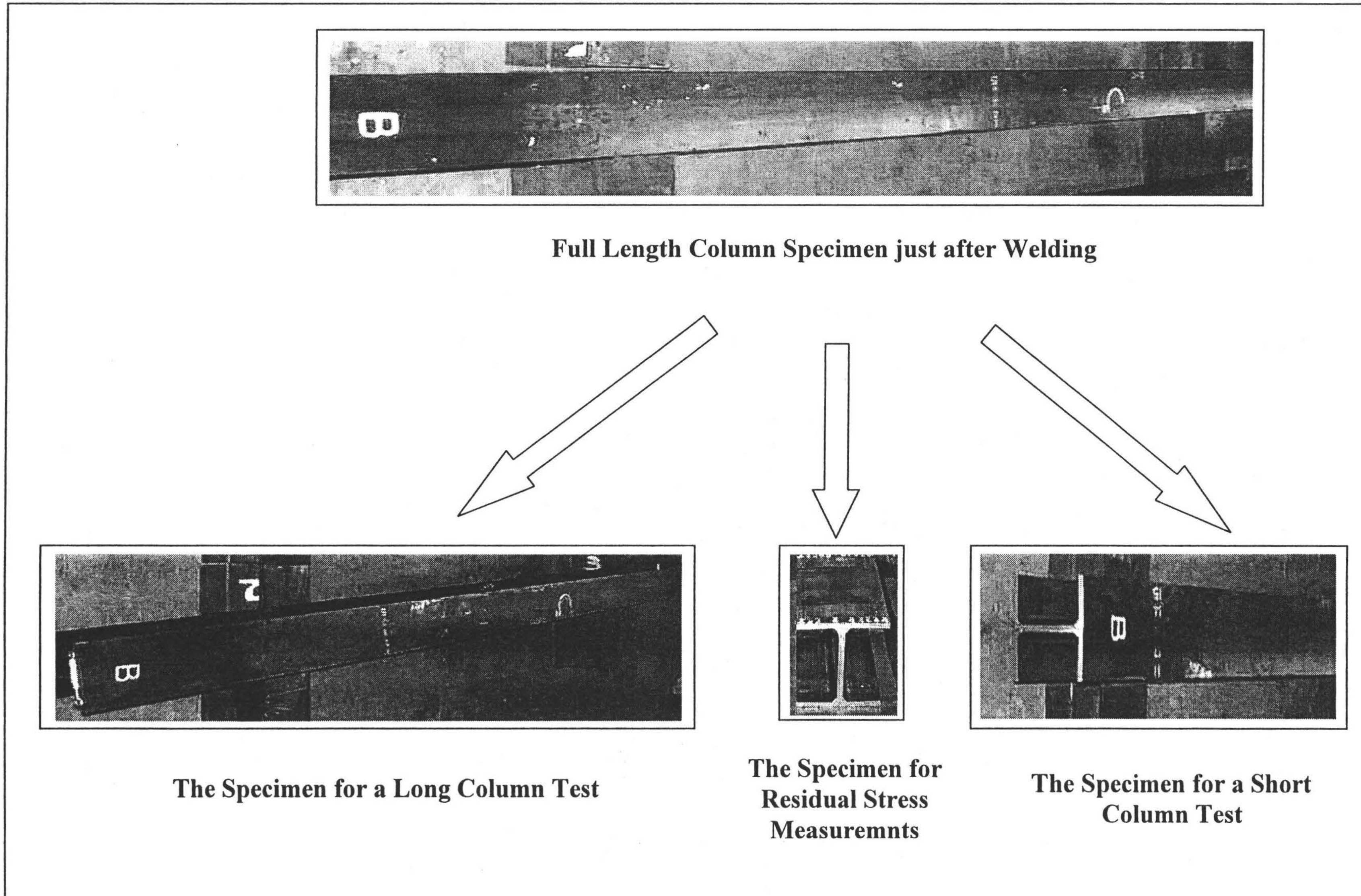

Figure 2.6: The Initial Column Section, Specimens for Column Test, Stub Column Test, and Residual Stress Measurements

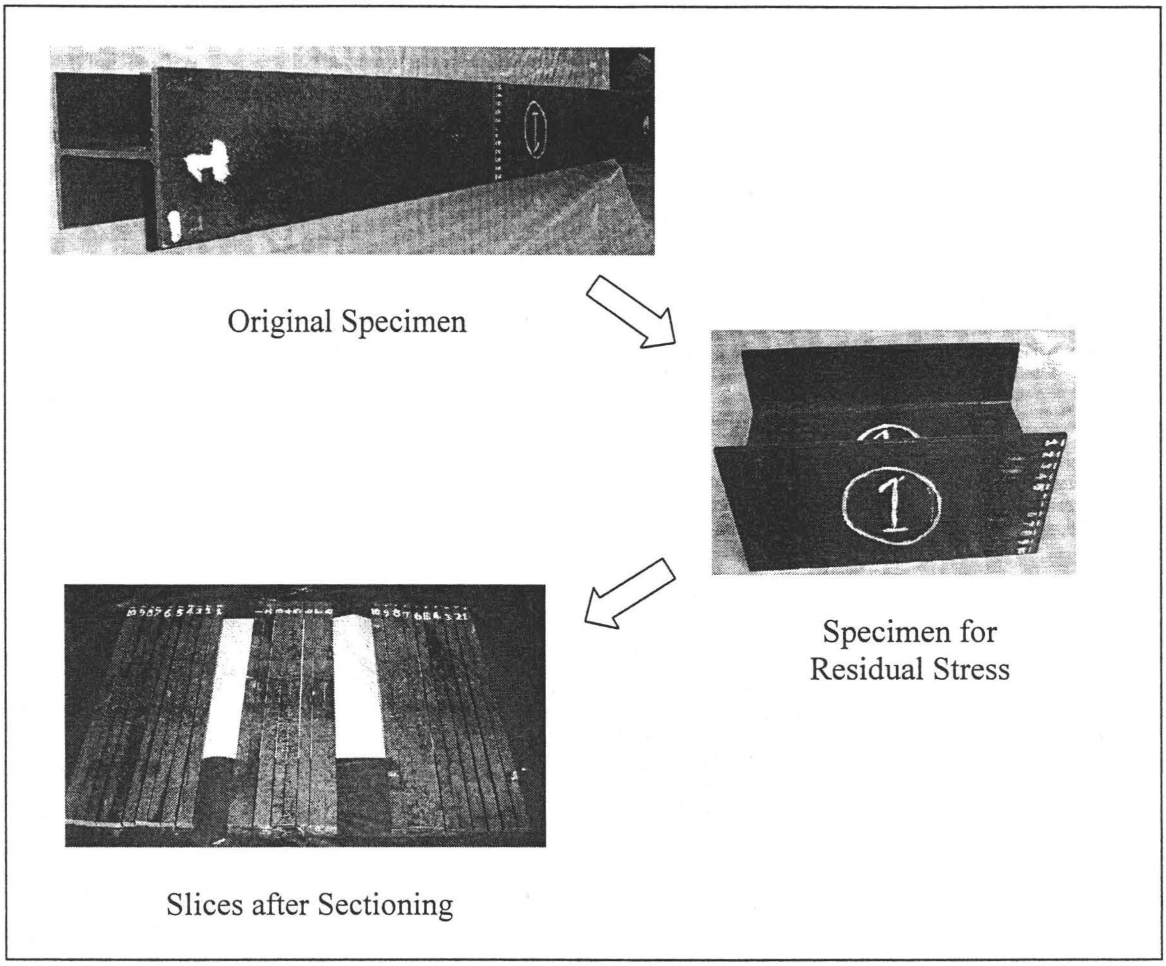

Figure 2.7: Residual Stress Measurement Procedures Using "Method of Section" Technique

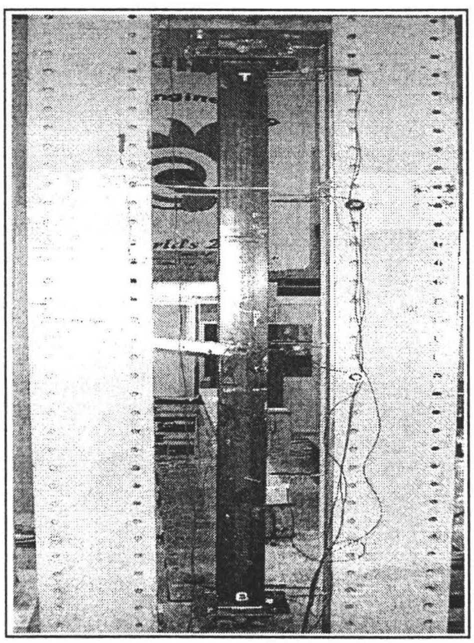

Figure 2.8: The Experimental Setup for Axially Loaded Column Tests

Chapter 3

TEMPERATURE PROFILES

3.1 Introduction

In this chapter, the work done by previous researchers on temperature measurements and the direct influence of temperatures on the strength of steel members as a result of forming residual stresses and geometrical imperfections is discussed. Also, this chapter describes in detail the temperature measurement procedures followed in this investigation. The last section of this chapter provides the temperature profiles obtained due to the cutting process and the welding process.

The steel fabrication process basically deals with a great quantity of heat, which may cause considerable thermo-elastic-plastic deformations and non-homogeneous distribution of mechanical characteristics over the cross-section. The fabrication of structural steel members by hot-rolling process involves temperatures as high as 900°C. Since the fabrication of welded built-up sections basically deals with cutting and welding operations, the fabrication process of welded built-up sections is associated with high temperatures.

In this investigation, the primary reasons for why the temperature variations with time during the fabrication process were taken are:

(a) to have general observations of temperature variations with time (i.e., temperature profiles) due to the plasma cutting and flame cutting processes.

(b) to have general observations of temperature variations with time due to the Gas Metal Arc Welding (GMAW) process.

(c) to use this information in future analytical studies related to prediction of residual stresses present in steel members.

The brief description of analysis developed for determining the residual stresses by the past researchers will be explained under the following section (section: 3.2) of this chapter.

3.2 Previous Works on Measurements of Temperature Distributions and Associated Prediction of Imperfections in Steel Members

Many researchers, in the past, have made their effort on establishing residual stresses in welded steel plates by analytical approach. Early theories in this area developed by Grüning (1934), Griffiths (1941), Rosenthal (1945), and Weiner (1956) were reviewed in a paper published by Nagaraja Rao and Tall (1961). Grüning (1934) assumed that the residual stress was equal to the thermal stress at the instant of welding and the thermal stresses were being limited by the yield strength of the material. This value of residual stress was approximately true since the thermal stresses at the instant of welding have the greatest influence on the resulting residual stress. Griffiths (1941) measured residual stresses transverse to joints along which two plate pieces were welded. He used plates of size 1200x115x16 mm (48x41/2x5/8 inch) and 915x305x16 mm (36x12x5/8 inch) and the magnitude of residual stress was observed to be 69 to 104MPa. Also he found that the greatest value in tension was at a distance of 25 to 50mm away from the line of weld. Wilson and Hao (1945) conducted tests on two sets of center-welded plates; the first set of plates had a width of 125mm (5 inch) and thickness of 22mm (7/8 inch), whereas the second set of plates had a width of 305mm (12 inch) and thickness of 16mm (5/8 inch). The residual stress at the weld in the 125 mm wide plate was 253MPa (34 ksi) tension and 138MPa (20 ksi) compression at the edges. The corresponding stresses in the 305mm wide plates were 330MPa (48 ksi) and 124MPa (18 ksi), respectively. Rosenthal (1945) made a detailed investigation of the temperature distribution resulting from welding and reported solutions for a number of cases. After that, Weiner (1956) has presented a rigorous solution to the three-dimensional plate, disregarding, however, the variation of mechanical properties with temperature.

As mentioned above, Grüning (1934) developed a solution to obtain the residual stresses in a rectangular plate with a butt weld along the center line. The development of this solution was based on the assumption that the residual stresses in such a plate were equal to the thermal stresses that would be produced by cooling the plate to room temperature from an initial temperature. The initial temperature represents the highest temperature at each point attained during welding. He limited the highest temperature to 600°C (1112°F), because it was assumed that above this temperature the steel is in a plastic state. Hence, he used an average modulus equal to three-fourths of the modulus at room temperature, since the modulus of elasticity decreases with an increase in temperature. He assumed also that the coefficient of linear thermal expansion is constant and equal to $11\mathrm{x}10^{-6}$ per degree Celsius ($61\mathrm{x}10^{-7}$ per deg. F.).

With these assumptions, the problem was resolved within the field of the theory of elasticity. The residual stresses in the plate were considered to be two-dimensional since the thickness of the plate was usually small in comparison with other dimensions. The governing equation presented by Grüning (1934) for this problem was, in the form, equation 3.1.

$$\nabla^4 F = \alpha E\left(\frac{\partial^2 T}{\partial x^2} + \frac{\partial^2 T}{\partial y^2}\right) \tag{3.1}$$

This is the 4^{th} order partial differential equation. The term 'F' in the above equation represents Airy's function, α is the coefficient of linear thermal expansion, E is the modulus of elasticity, and T is temperature. Moreover, Grüning (1934) presented solution for such plates considering four different temperature gradients.

Boulton and Lance Marin (1936) (Wilson and Hao, 1945) published a well-developed theory, which takes account of plastic deformations. The basic assumption of their theory was that, in a long plate, the longitudinal strain varies linearly with respect to transverse distance (defined herein as x-axis direction), which is measured across the whole width of the plate, except in cross-sections near its ends. This has been found to be approximately true by actual strain measurements. They considered different situations of a plate with welding. For example, they considered a plate with the weld deposits on one of its edges only, both edges, and weld deposits on the middle of a plate. Hence, in this work, the stress-strain relations in all regions were established. The temperature gradient across the section at any instant was determined by a theoretical formula.

A solution of thermal residual stresses in a plate with a weld deposit along the center line was presented by Rodgers and Fetcher (1938) (Wilson and Hao, 1945). Their basic assumption was that a plane cross section remains plane during the temperature change, and that the end effects can be neglected. Under these conditions, there will be no transverse shearing stresses, and the longitudinal stress can be expressed as

$$S_y = +E\alpha T - \frac{1}{2w}\int_{-w}^{w} E\alpha T dx \tag{3.2}$$

In which T is positive for a rising temperature, and positive S_y indicates tension. The second term on the right represents a uniform compression equal to the average value of the tension corresponding to the first term. The temperature at various points on the cross section was determined by actual measurements. In the equation (3.2), E is the modulus of elasticity, α is the coefficient of linear thermal expansion, T is temperature, and w is half width of the plate.

To consider the fact that E and α vary with the temperature, the time intervals were taken so small that E and α could be considered constant for each interval. The residual stresses were obtained by adding, successively, the stress increments thus obtained. The stress at any point is limited to the yield point corresponding to the temperature at that point. A unique feature of this method is that a complete history of stress variation during the process can be obtained. The prediction of the residual stresses in steel plates having weld deposits along the different locations such as weld deposits along the mid line of the plate, weld deposits along the both edges of the plate, and the deposits along the one of the plate's edges can easily be used to simulate conditions obtained in actual built-up shapes.

From the review of analytical studies made on establishment of residual stresses in welded plates, it can be observed that the determination of temperature distribution is an important step in calculation of residual stresses. This is because, once the temperature distribution is obtained, the thermal stresses, and thus the residual stresses, can be calculated. The prediction of residual stresses in that way is not simple and must follow a step-by-step procedure since the material properties will keep varying with temperature. Thus, the step-by-step method takes into account the complete history of cooling and the variation of material properties. At each step, the plastic deformation is considered and equilibrium accounted for, such that the complete history of stress throughout the cooling is obtained.

3.3 The Procedures Associated With Temperature Measurements

In this investigation, the temperature measurements were taken during and after cutting process, as well as during and after welding process. The interval for temperature measurements for plasma cutting was 2 minutes in the beginning and then, after finishing the whole cutting operations on the plate, the temperature measurement interval was 5 minutes. During the flame cutting, the initial temperature measurement interval was chosen depending on the speed of the cutting and the time delay between two successive cuttings. However, after finishing the whole cutting operation on the plate, the temperature measurements were taken for every 5 minutes. The temperature measurements were continuously taken until the plate pieces cooled down closer to the ambient temperature. The same procedures were followed during the welding process too. However, during the welding process, it was decided that the measurements were to be taken at 5 minute time intervals. All temperature measurements were taken only on the marks specified in the original steel plate (see Figure 3.1). Before either cutting of the plate or welding of the plate pieces, the initial temperature measurements were taken over the specified marks.

Two different types of instruments were used in this investigation to measure the temperatures. They are the Infrared Thermometer and the Infrared Pyrometer. The Infrared Thermometer was used to measure the low temperature ranges, however, the Infrared Pyrometer was used to measure high temperatures. The relevant details of these instruments are given below;

(a) The Infrared Thermometer (Model # : OS542)

Measurements Range: -20°C to 500°C

Response Time: 0.5sec

Accuracy: ± 2°C of Reading

Emmisivity: 0.98(fixed)

(b) The Infrared Pyrometer (Model #: OS3707):

Measurements Range: 250°C to 2000°C

Response Time: 0.5sec

Accuracy: ± 0.40% of Reading

Emmisivity Range: 0.1 to 1.00 in 0.01 Steps (digitally set)

3.3.1 The Observations during Cutting Process

(a) Plasma Cutting

During the plasma cutting process, first, the whole plate [3960 mm (156 inch) x710 mm (28 inch)] was placed on the cutting bed as shown in Figure 3.2. In the beginning of the cutting operation, the machine parameters were adjusted in the plasma cutting machine which controls the function of the cutting nozzle in the subsequent operation. The parameters were,

1. Torch-to-work Distance : 4mm (5/32 inch)
2. Initial Torch Piercing Height: 8mm (3/16 inch)
3. Arc Voltage Setting: 155 Volts
4. Current: 200 Amps
5. Travel Speed: 3500 mm/min (140 inch/min)
6. Approximate Motion Delay Time: 0.3sec

The values of above parameters for the plasma cutting depend upon the thickness of the plate to be cut. Therefore, the values given herein are associated with plates having thickness of 9.5mm (3/8 inch). Note that the values of the above parameters were selected by a workman in the fabrication shop based on his own experience in this cutting. The observed typical striking temperature during plasma cut was about 650°C. Moreover, the cut edge by plasma cut was smooth and thus, no additional machining was necessary. The cutting tolerance was approximately 1mm to 2mm. Water level in the cutting bed during the plasma cutting was kept at about 50mm below the bottom surface of the plate. Also, it was observed that the plasma cutting operation was noisy.

(b) Flame Cutting

The same cutting bed was used for both plasma and flame cutting with different cutting torches. However, during the flame cut operation the water was totally drained off. As done in the plasma cutting operation, the following machine parameters were adjusted in the flame-cutting machine;

1. Pressure of Oxy Heating Pilot Flame: 2.0 bar
2. Pressure of Oxy Piercing Flame: 2.0 bar
3. Pressure of Oxy Heating Cut Flame: 2.0 bar
4. Heating Height: 4mm
5. Piercing Height: 10mm
6. Working Height: 18mm
7. Piercing Delay:1.0sec
8. Warm Up Time: 25sec
9. Cutting Speed: 540 mm/min (21 inch/min)
10. Slow down Speed : 400 mm/min (16 inch/min)

The values of above parameters for flame cutting operation depend upon the thickness of the steel plate to be cut. Note that the values of the above parameters were selected by a workman in the fabrication shop based on his own experience in this cutting. The observed maximum striking temperature was about 850°C. The cut edge was not as smooth as the plasma cut. Therefore additional grinding was needed to get relatively smooth edges. The cutting tolerance was approximately 2mm to 3mm. Figure 3.3 shows the flame cutting operation while cutting the plate in this investigation.

3.3.2 The Observations during Welding Process

Automatic Gas Metal Arc (*GMAW*) welding process was used to assemble the plate pieces to a desired shape. In this process, the speed of travel was selected as 190 mm per minute (7.5 inch/min). The arc was maintained between the work-piece and a bare wire electrode, fed at constant speed selected to give the required current, and the arc length was controlled by the power source. Wire, gas, and power were fed to an automatically moving welding-gun, leaving the operator free to concentrate on correct weld deposit.

The bare wire electrode, which is consumable, was shielded by a pure CO_2 "Active" gas. The wire was fed at constant speed to control the current, within the arc length being controlled by the power source. Also the wire/flux combination used in this welding process was single-pass/single-wire with full penetration fillet weld. The current and voltage used for entire welding operation were approximately 300 to 350 Amps and 32 to 38 Volts, respectively. The selection of current, voltage, welding speed, diameter of wire, etc depend upon the thickness of the steel plates to be welded. The maximum striking temperature measured during the welding process herein was 1100°C. Figure 3.4 shows the welding of a H-shaped steel column section in this investigation.

3.4 Presentation of Temperature Profile

General Description

In this investigation, the variation of temperature with time was recorded due to cutting operations and welding processes. Three initial plates designated herein as plate-1, plate-3, and plate-5 were cut by plasma cutting (see Figure 3.2) while the other three initial plates designated herein as plate-2, plate-4, and plate-6 were cut by flame cutting (see Figure 3.3). The cut plate pieces were welded together to form H-shaped column sections by gas metal arc welding process (see Figure 3.4). As discussed previously, it was decided in this investigation that the temperature measurements were to be taken on the specific locations as shown in Figure 3.1. The locations were marked as 20x20 mm square at a spacing of about 30mm (see Figure 3.1) on the original steel plates. The size of the locations (20x20mm) was selected based on the criteria that the Infrared Pyrometer (Model: OS3707) used in this investigation had a capability of measuring temperature accurately on a target having size of 20mm (0.8 inch) from the distance of about 4m. Furthermore, the locations were colored with black paint to keep the emmisivity of those locations approximately equal to 1.00. Because the Infrared Thermometer (Model: OS542) used in this investigation had a fixed emmisivity of 1.0 and thus, it can be obtained more accurate readings by matching up the emmisivity of thermometer and targets.

3.4.1 Plasma Cutting

The General Description of Temperature Profiles Obtained Due to Plasma Cutting

Figures 3.5 through 3.7 show the variation of temperature profile with time due to plasma cutting operation. Each figure shows the temperature variation at specific locations designated herein, as 1, 2, 3..., 15 (see the Figure 3.1). The temperature at each location was first recorded before the cutting operation began, i.e., at this time the temperature might be same as the ambient temperature. As soon as the 1st cut passes the Location: 15, the first set of temperature measurements after cutting (at time is equal to zero in this investigation) were recorded. At this time the maximum temperature of about 30°C was measured at location: 15 and the measurements at the rest of the locations were generally seemed to be in the order as; $T_{15} > T_{14} > T_{13} > T_{12} > T_{11} > T_{10} > T_9 > T_8 > T_7 > T_6 > T_5 \geq T_4 \geq T_3 \geq T_2 \geq T_1$, where T_{15} means the temperature at Location: 15. Moreover, at this time it can generally be observed that the temperatures at Locations: 5, 4, 3, 2, and 1 seemed to be unaffected and were close to ambient temperature. As soon as the 2nd cut passes between Locations: 10 and 11, the second set of temperature measurements were obtained. At this time, it was generally observed that the temperatures at Locations: 10 and 11 were higher than the rest of the locations. However, in plate-01, at this time even though the temperature at Location 11 increased from previous reading, the temperatures at the rest of the locations such as Location: 14, 13, and 12 decreased. As soon as the third cut passes between Location: 5 and 6, the third set of reading were obtained. At this time, the temperatures at Locations: 5 and 6 were higher than the temperatures at the rest of the locations (see Figures 3.5 through 3.7). The fourth set of readings after cutting was obtained as soon as the cut passes besides Location: 1 (see Figure 3.4). At this time the general variation of temperature at each locations seemed to in the order of; $T_1>T_2>T_3>T_4>T_5>T_6>T_7>T_8>T_9>T_{10}\geq T_{11}\geq T_{12}\geq T_{13}\geq T_{14}\geq T_{15}$. The subsequent temperature measurements were continuously monitored at an interval of 5 minutes in this investigation until the cut pieces cooled down approximately to ambient temperature. However, due to unavoidable circumstances such as inadequate space for placing the plate strips, time restrictions, etc., the number of observations made in this investigation was different from one particular plate to another plate. Note that, no temperature measurements were taken between two successive cuttings in this investigation for safety reasons.

The Comparison of Temperature Profiles Due to Plasma Cutting

As a common observation from Figures 3.5 through 3.7, the maximum temperatures just after cutting, ranged from 29°C to 34°C. However, the typical striking temperature measured during plasma cutting operation was about 650°C for each plate. Also, it can generally be observed that the rate of cooling of plate decreases with increasing time period. The Figure 3.8 shows the comparison of temperature variation at Location: 15, 10, and 8 with time in plates designated herein as plate-01, -03, and -05 assuming these locations representing the general variations of temperature with time for every other location in each plates. From this figure, it can be observed that the overall variation of temperature profile with time was approximately the same for each cutting of plates. However, it can be seen from the figure that the there were slight temperature fluctuations at the same location of each plate as soon as the 1st cut just passes the Location: 15. The maximum temperature measured at Location: 15 in plate-01, -03, and -05 were 29°C, 26°C, and 29°C, respectively. Similarly, at Location: 10 in plate-01,-03, and -05 were 26°C, 34°C, and 33°C, respectively. At Location: 8 in plate-01, -03, and -05 were 24°C, 25°C, and 26°C, respectively. The maximum temperature at the same location in each plate seemed to occur at the same time (see Figure 3.8). Moreover, it can be seen from the figure that after attainment of the maximum temperature, the cooling rate of the same locations in each of the plates was approximately the same.

3.4.2 Flame Cutting

The General Description of Temperature Profiles Obtained Due to Flame Cutting

Figures 3.9 through 3.11 show the variation of temperature profile with time due to flame cutting operation. As used for plasma cutting, the same numbering order and the cutting sequence were followed in this cutting (see Figure 3.1). Furthermore, the same procedure as discussed in the plasma cutting to measure the temperature was followed in this cutting operation. However, the time intervals between two successive cuttings herein were different from plasma cutting due to the difference in cutting speed of these two different cutting operations (the cutting speed of plasma cutting was 3556 mm/min (140 inch/min) while that of flame cutting was 533 mm/min (21 inch/min)). Note that, no intermediate temperature readings between two successive cuttings were obtained during the flame cutting operation. Moreover, the time taken between two successive cuttings during flame cutting was different from a plate to another plate as seen in Figures 3.9 through 3.11.

The Comparison of Temperature Profiles Due to Flame Cutting

Figures 3.9 through 3.11 show the variation of temperature with time due to flame cutting. The maximum temperatures measured just after flame cutting operation, ranged from 97°C to 127°C. However, the typical striking temperature measured during flame cutting was about 850°C. Moreover, it can be observed from the Figures 3.9 through 3.11 that the rate of cooling decreased with increasing time period. Figure 3.12 shows the comparison of temperature profile for each of the plates at specific locations such as Location: 15, 10, and 8. From the Figure 3.12, it can be seen that the variation of temperature profile at Location: 15 was approximately the same for all plates. Similar variations in temperature profile can be seen at Location: 10 however, there was a slight temperature fluctuation in plate-06. The variation of temperature profile at Location: 8 was almost identical for plate-04 and plate-06. However, the variation of temperature profile in plate-02 was different from that in the other plates. Because, in plate-02 the time taken to pass the locations where the temperature measurements to be observed for the 2nd cut (10min) was less than the time taken for the 2nd cut in other two plates (plate-04 and plate-06). Therefore the temperature at Location: 8 began to drop down earlier than the temperature at the same location dropping down in other plates (see the Figure 3.9). Note that, the temperature variation at Location: 15 was greatly unaffected by 3rd cut and 4th cut since the plate strip was separated after 2nd cutting. Similarly the Location: 10 was unaffected by the 4th cut since the plate strip having this location was separated after 2nd and 3rd cut (see the Figure 3.1). The maximum temperature measured at Location: 15 in plates-01, -03, and -05 were 94°C, 83°C, and 85°C, respectively. Similarly, at Location: 10 in plates-01,-03, and -05 were 97°C, 98°C, and 104°C, respectively. At Location: 8 in plates-01, -03, and -05 were 112°C, 85°C, and 93°C, respectively. The maximum temperature at the same location in each plate seemed to occur at different time since the time interval between the 1st cut and 2nd cut, 2nd cut and 3rd cut as well as 3rd cut and 4th cut for different plate was different due to unavoidable circumstances such as operational delay due to inexperience workmanship, difficulties in control the constant distance between the nozzle and the plate surface during cutting operation, etc.

The Comparison of Plasma Cutting and Flame Cutting

Based on the observations and measurement made in this investigation, the followings can be given in points form as below;

1. The typical striking temperature measured during plasma cutting was about 650°C, whereas the typical striking temperature measured during flame cutting was about 850°C.
2. The maximum temperature measured in the plate immediately after (t = 2min, in plate-03) plasma cutting was 34°C, but just after flame cutting was 127°C (t = 30min, in plate-02).
3. The cutting speed of plasma cutting (140 inch/min) was about seven times faster than that of flame cutting (12 inch/min).
4. Both cutting methods had the same general variation of temperature profiles with time (see Figures 3.8 and 3.12).

3.4.3 Welding Process

The General Description of Temperature Profile Obtained Due to Welding

As discussed earlier, the plate strips cut from the same original steel plate were welded together to form I-shaped sections in this investigation. As part of this investigation, the temperature profile was continuously monitored during and after the welding process. The welding process associated with forming the I-section herein, was done in four-passes individually. Each pass can be described as a line of single pass welding. Thus, each line of single pass welding was done on either side of the web which was connected to the flanges along their middle portion. Figure 3.13 shows the sequence of welding and the temperature measurement locations associated with each of the column sections in this investigation. Thus, it can be observed that the column section-01, -03, and -05 had the same sequence of welding with respect to associated locations where the temperature measurements were to be taken. The section-02 and -06 had the same sequence of welding with respect to the temperature measurement locations. Figures 3.14 through 3.19 show the variation of temperature profile with time for each column section during welding process in this investigation.

The Comparison of Temperature Profile Due to Welding

A maximum temperature of 250°C was measured immediately after welding process in each column sections. As a common observation, the temperature at flange-web junction was the maximum for all the column sections. The temperature profiles obtained for column section-01, -03, and -05 had approximately the same variation (see Figure 3.20) since the sequence of welding associated with theses sections were the same. Similarly, the temperature profiles obtained for column section-02 and -06 were identical to each other (see Figure 3.21) since the sequence of welding associate with these sections are the same. A maximum temperature of 200°C was measured at one of the flange tips of column section-03. Moreover, it can be observed from all the figures that the temperature profiles obtained for the web portion of each column sections were similar to each other since the temperature variation in the web portion was independent of the sequence of welding. During the welding process, the first temperature measurements for each pass were taken as soon as the welding nozzle just passed the temperature measurements location of interest. Subsequently, as discussed earlier, the temperature measurements were continuously monitored for every 5 minute in this investigation. The number of readings taken for first three passes varied for different section. However, for the fourth pass of each section the readings were monitored until the section cooled down to ambient temperature. It was also observed that the rate of cooling decreased with increasing time period. The comparison of temperature profile obtained at Locations: 1, 3, and 8 for sections having similar welding sequence are shown in Figures 3.20 and 3.21 assuming these locations were representing the rest of the locations. From theses figures, it can be observed that the temperature variations at the same locations for the sections having similar welding sequence were approximately the same.

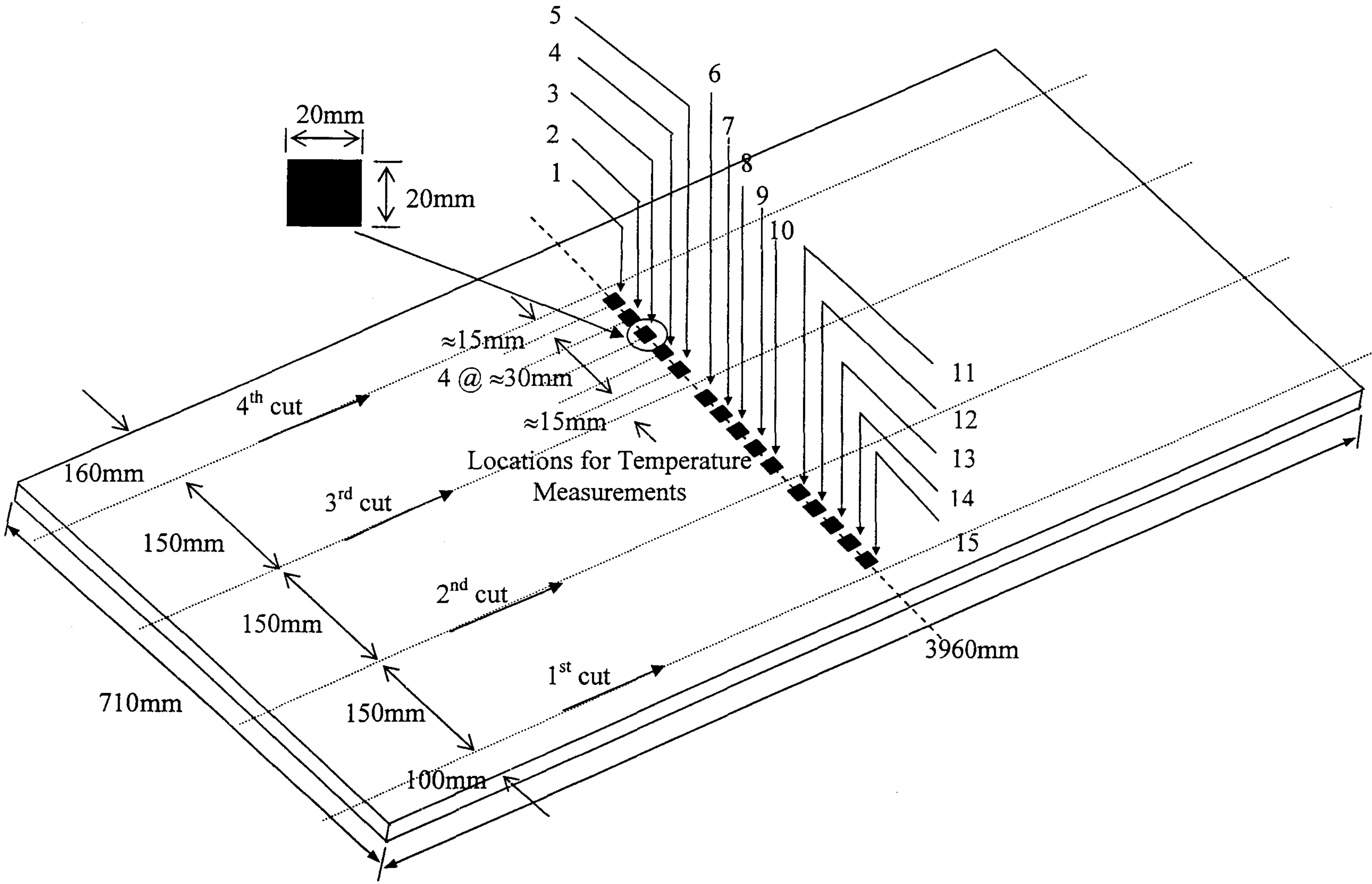

Figure 3.1: The Temperature Measurement Locations and Cutting Sequence

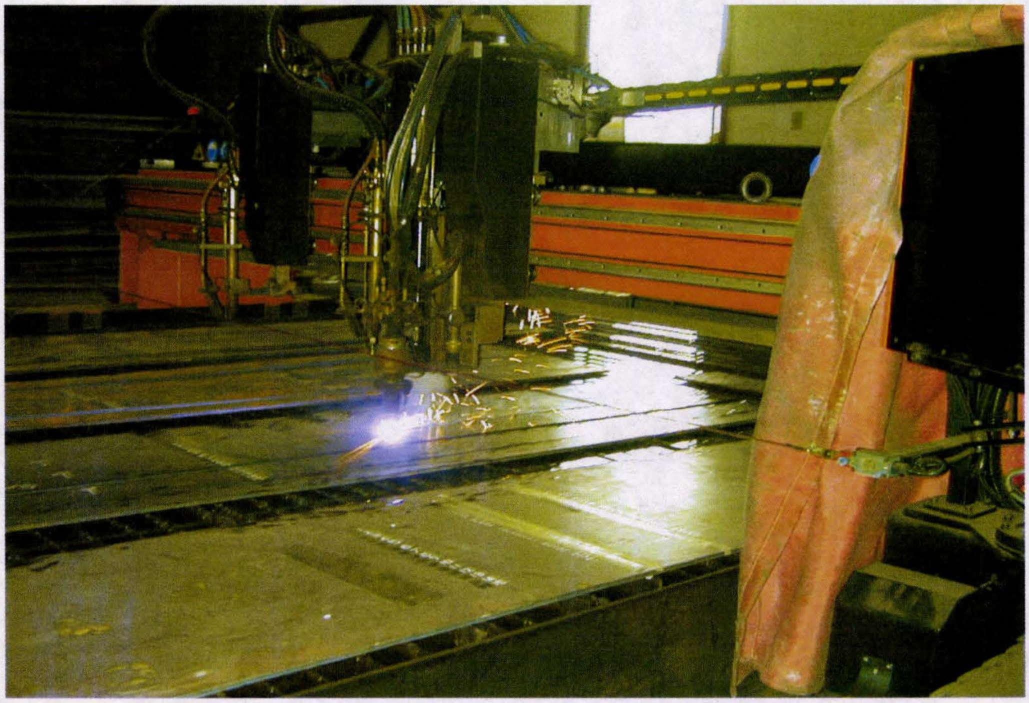

Figure 3.2: Plasma Cutting of Plate

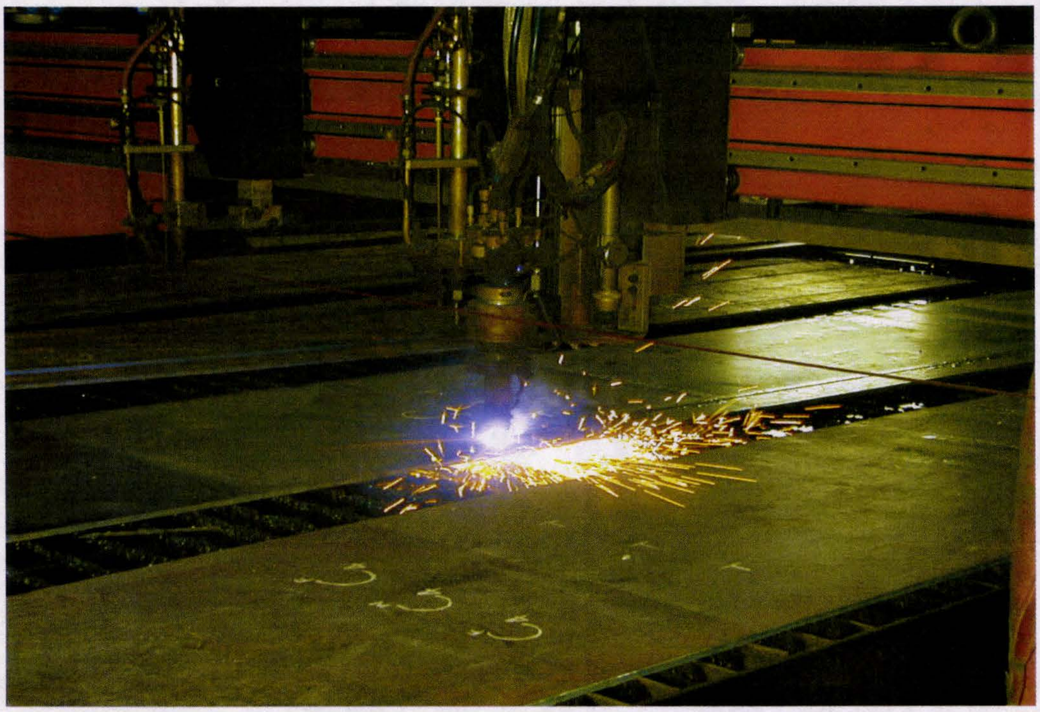

Figure 3.3: Flame Cutting of Plate

Figure 3.4: The Welding of H-Shaped Steel Column

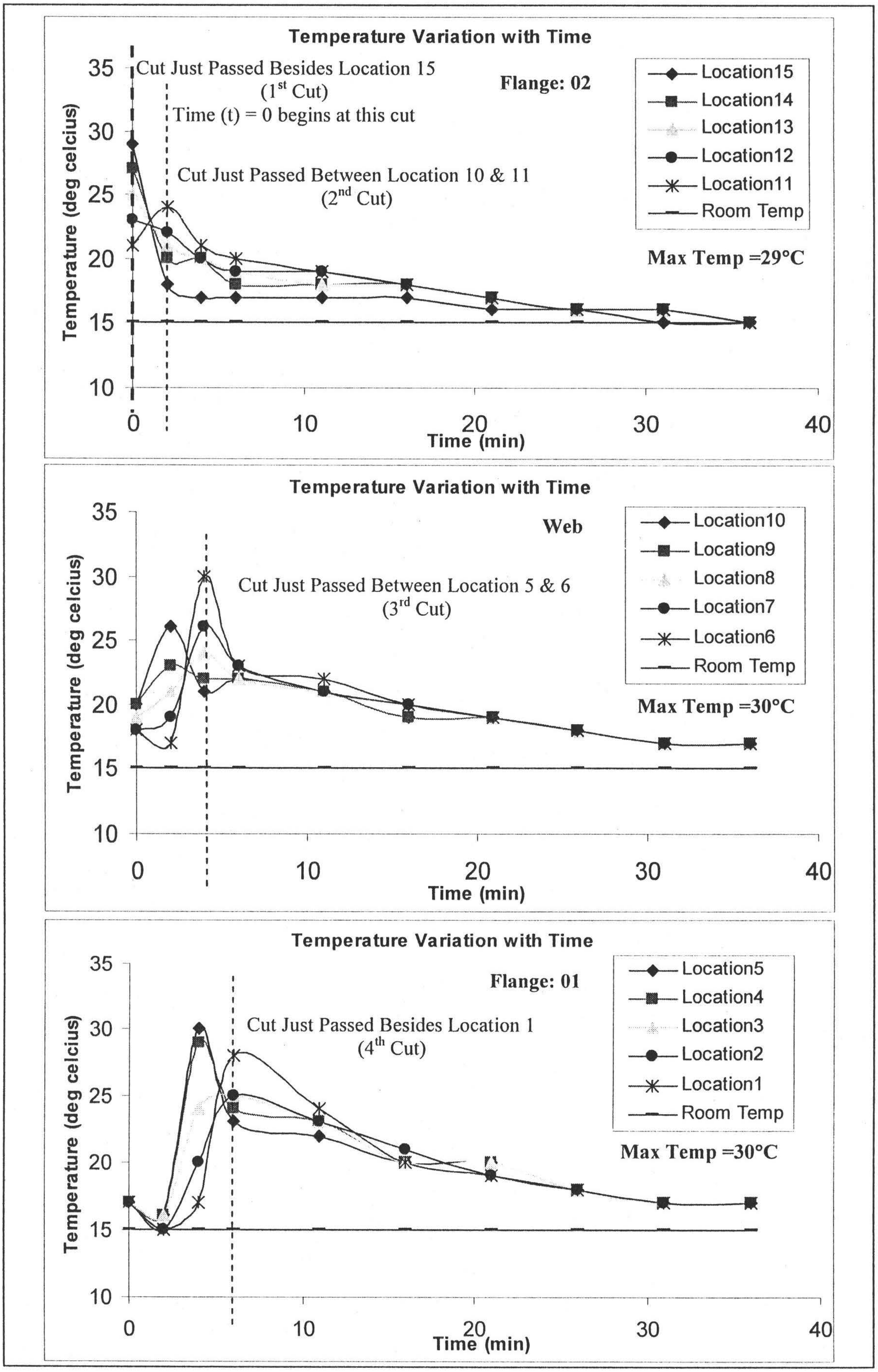

Figure 3.5: Temperature Distributions in Plate-01 (Plasma Cut)

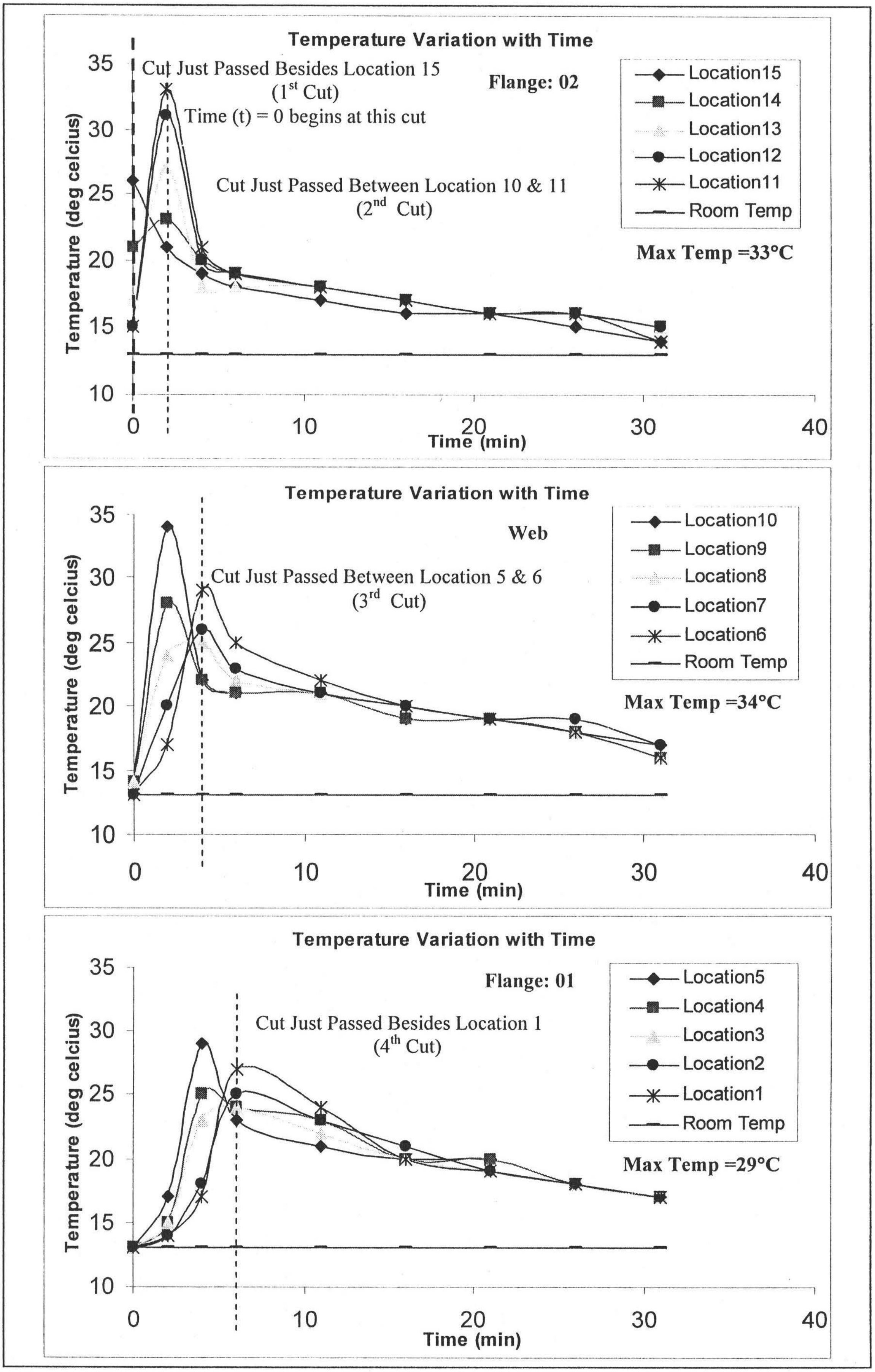

Figure 3.6: Temperature Distributions in Plate-03 (Plasma Cut)

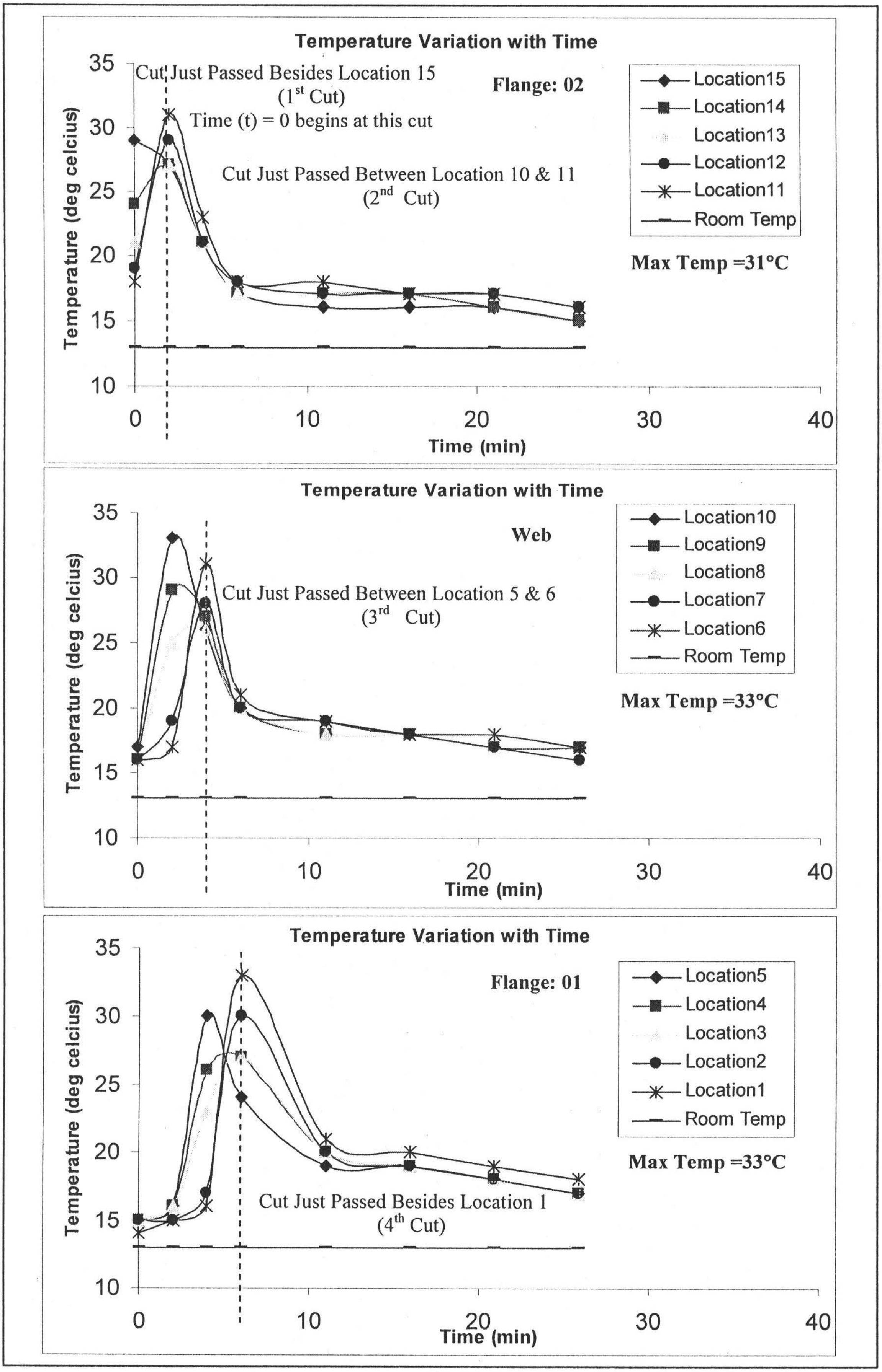

Figure 3.7: Temperature Distributions in Plate-05 (Plasma Cut)

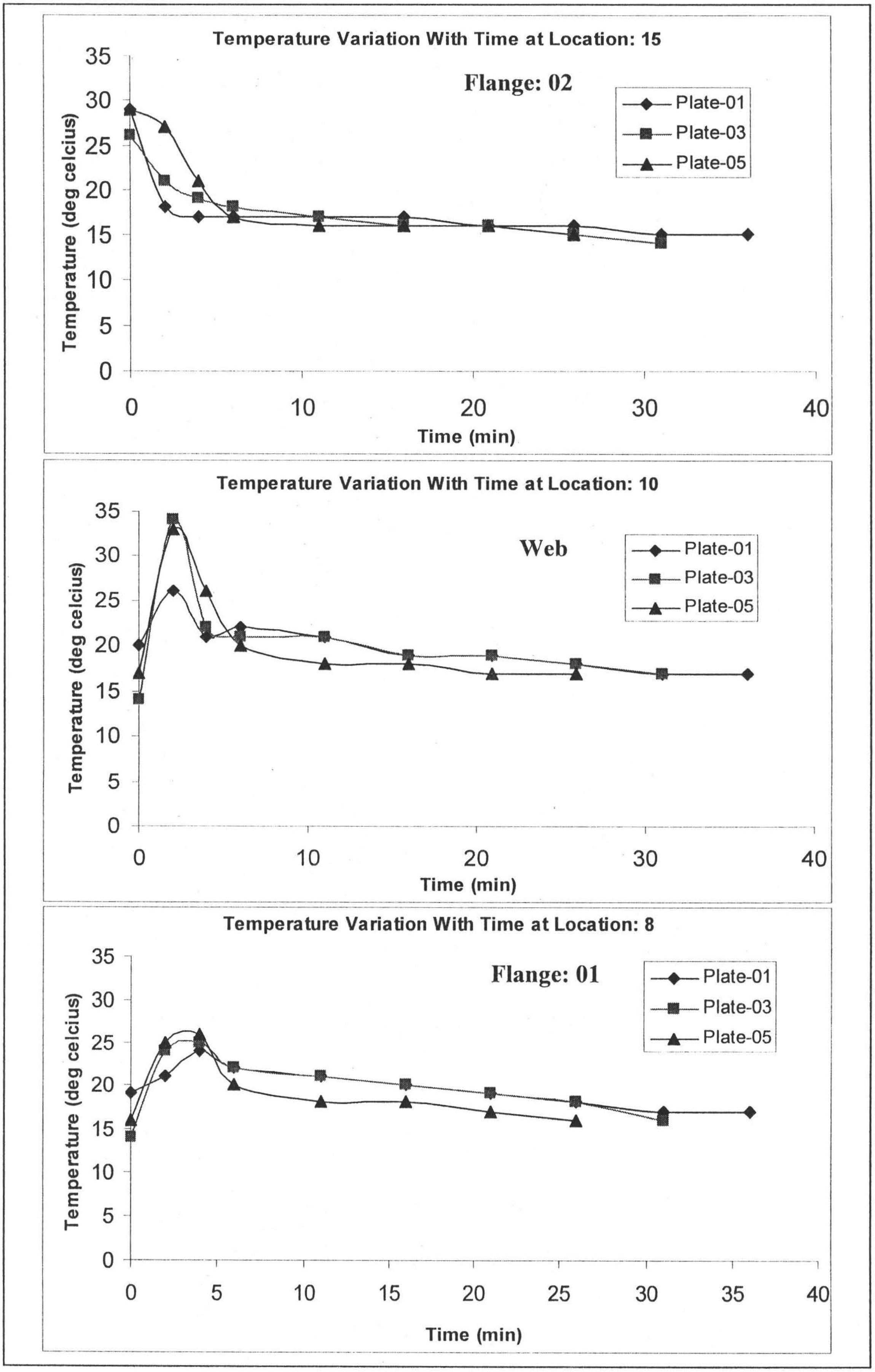

Figure 3.8: The Comparison of Temperature Profile for Plasma Cutting

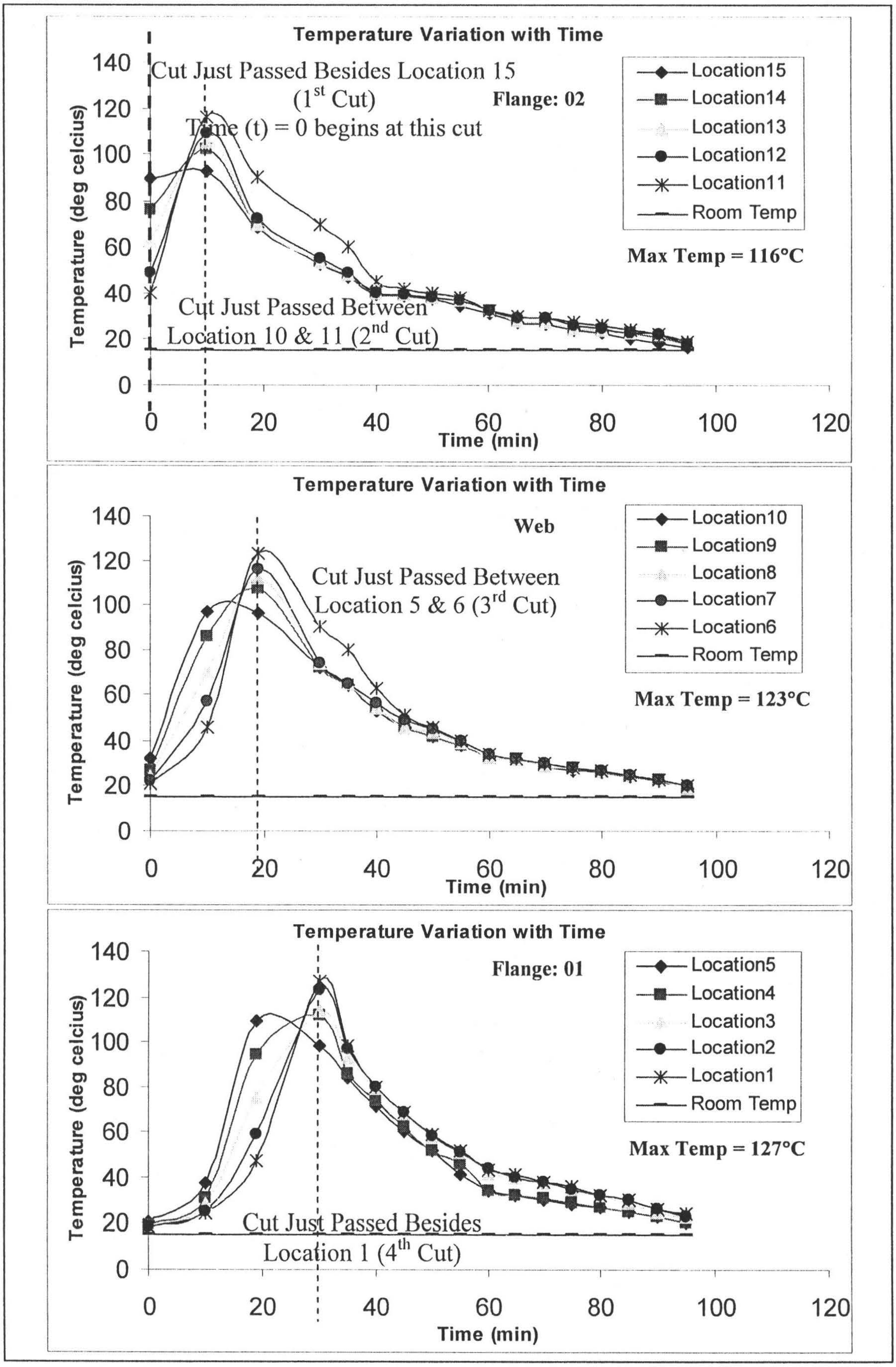

Figure 3.9: Temperature Distributions in Plate-02 (Flame Cut)

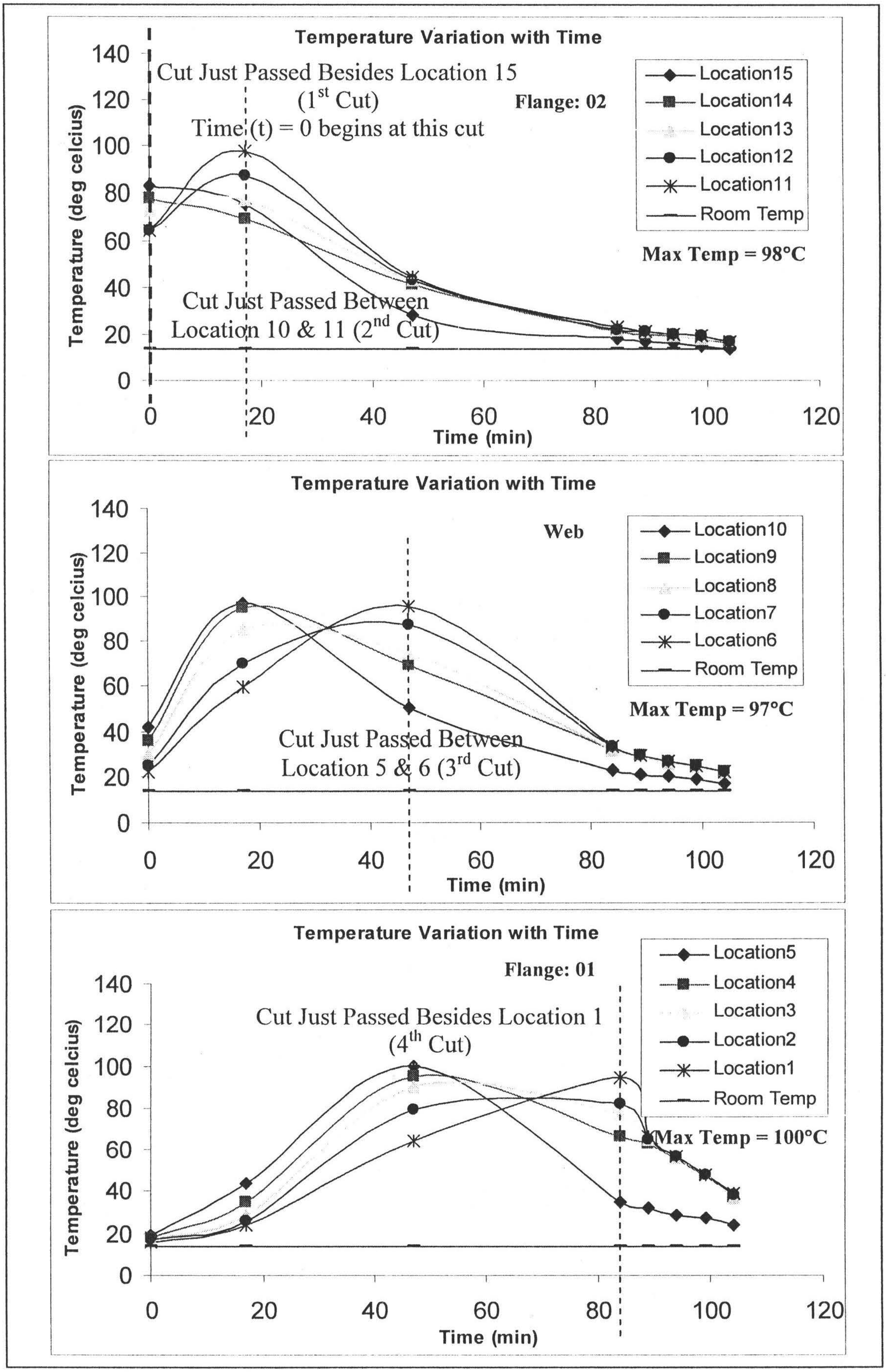

Figure 3.10: Temperature Distributions in Plate-04 (Flame Cut)

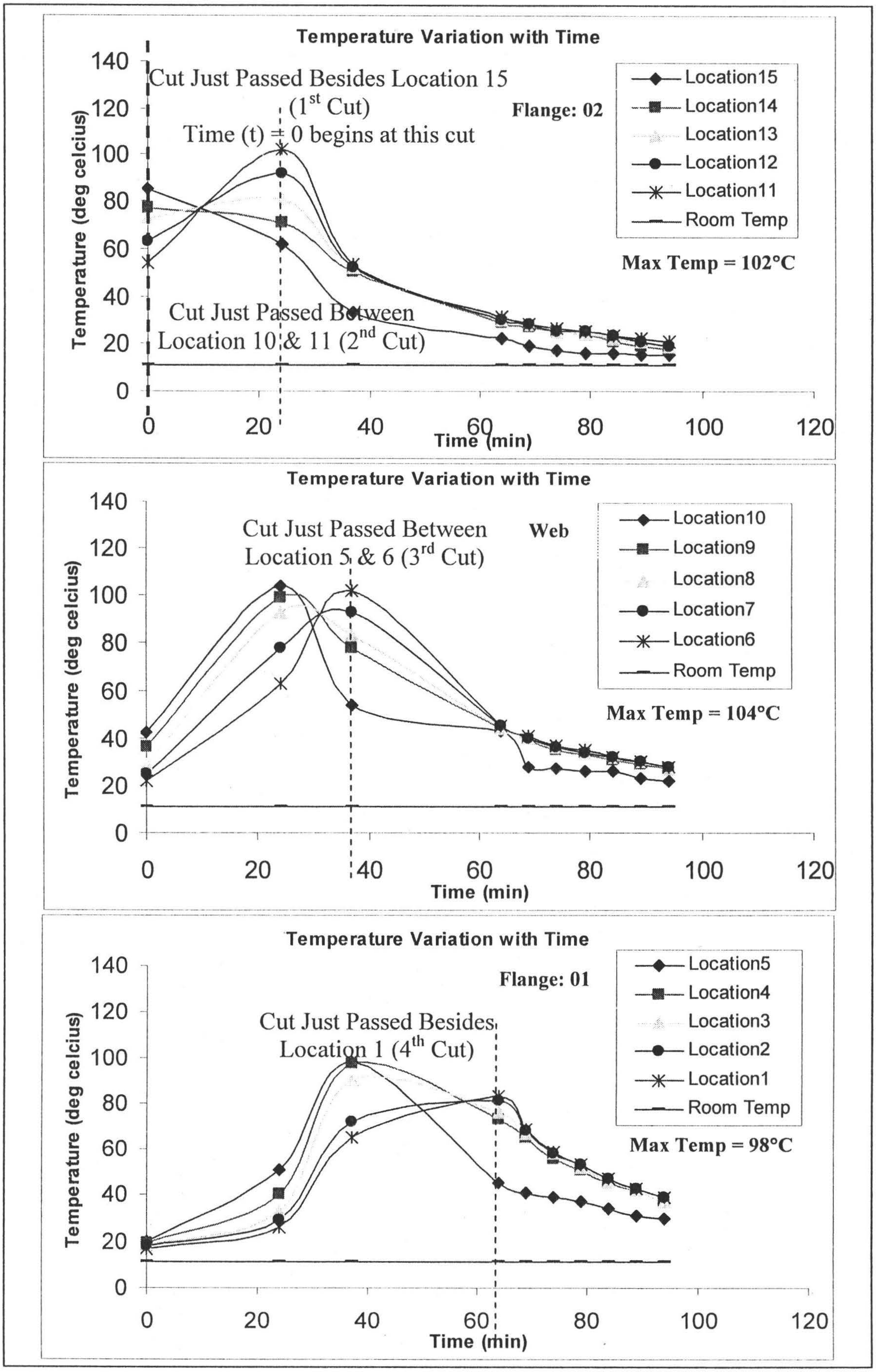

Figure 3.11: Temperature Distributions in Plate-06 (Flame Cut)

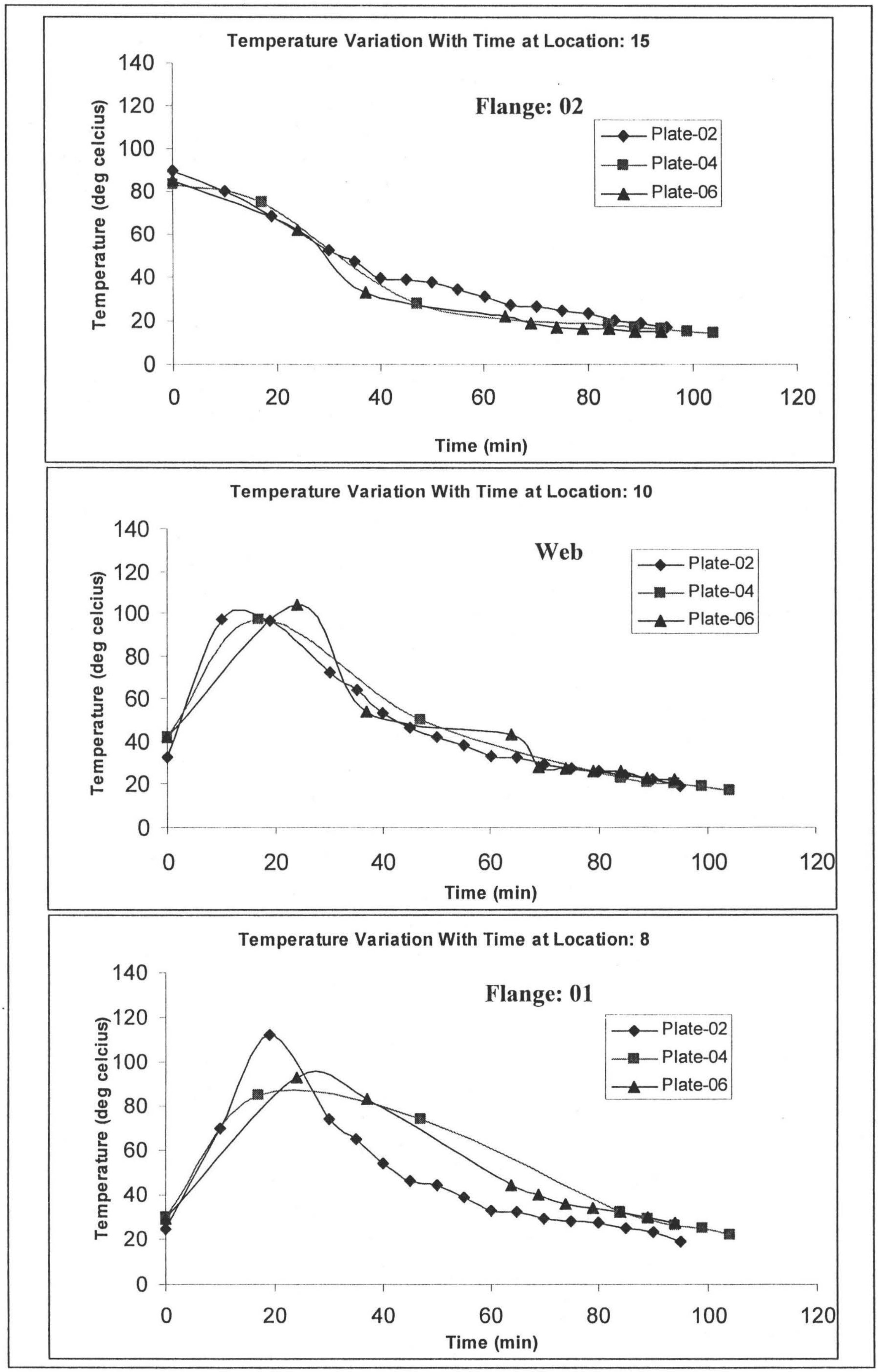

Figure 3.12: The Comparison of Temperature Profile for Flame Cutting

<table>
<tr><th>Column Designation</th><th>Welding Sequence</th></tr>
<tr><td>Column Section-01, -03, and -05</td><td>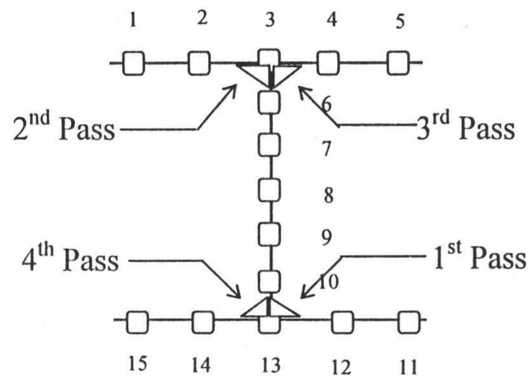
</td></tr>
<tr><td>Column Section-02 and -06</td><td>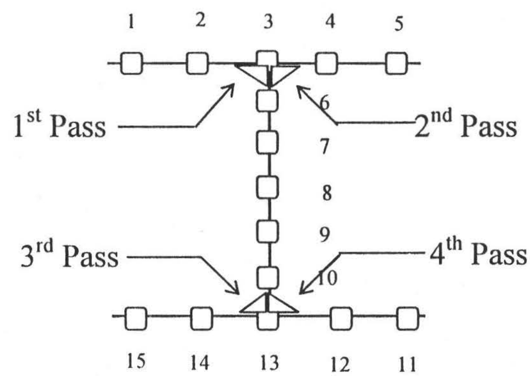
</td></tr>
<tr><td>Column Section-04</td><td>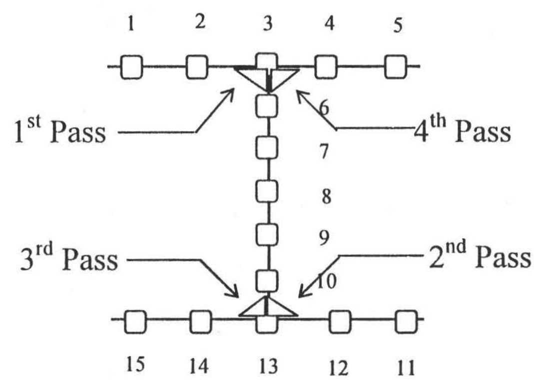
</td></tr>
</table>

Figure 3.13: The Sequence of Welding Associated With Column Sections

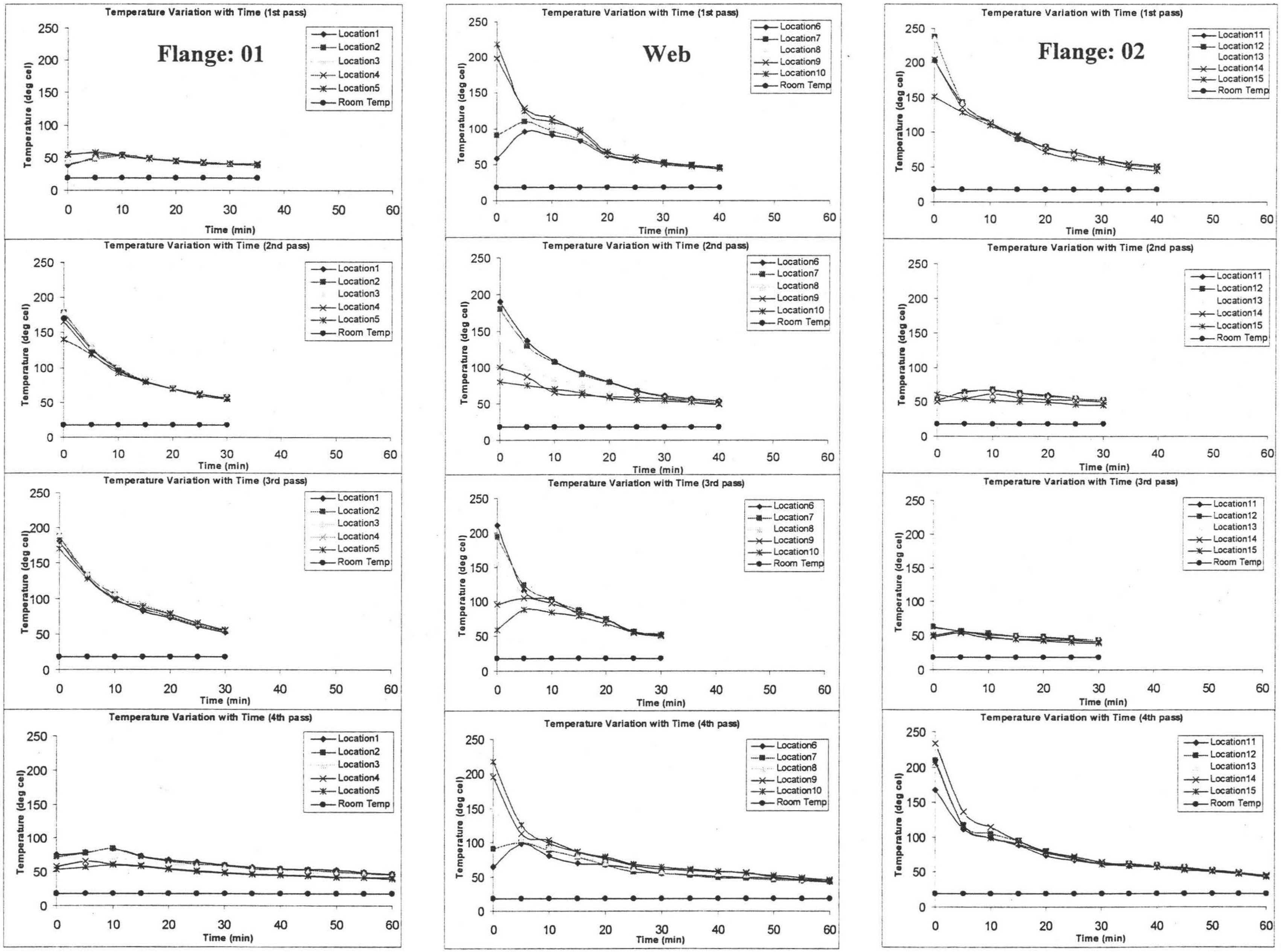

Figure 3.14: Temperature Profile Due to Welding (Column-01)

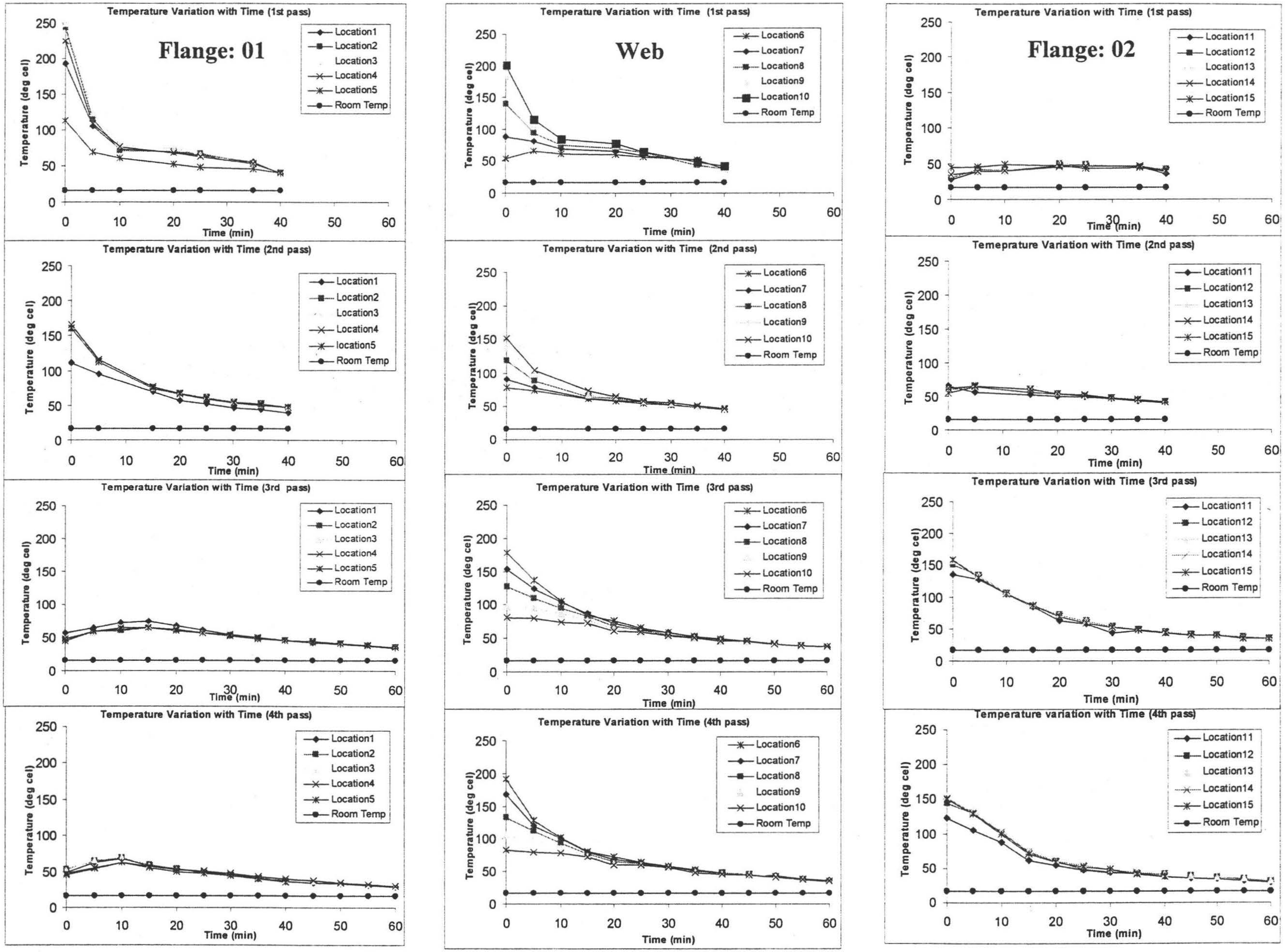

Figure 3.15: Temperature Profile Due to Welding (Column-02)

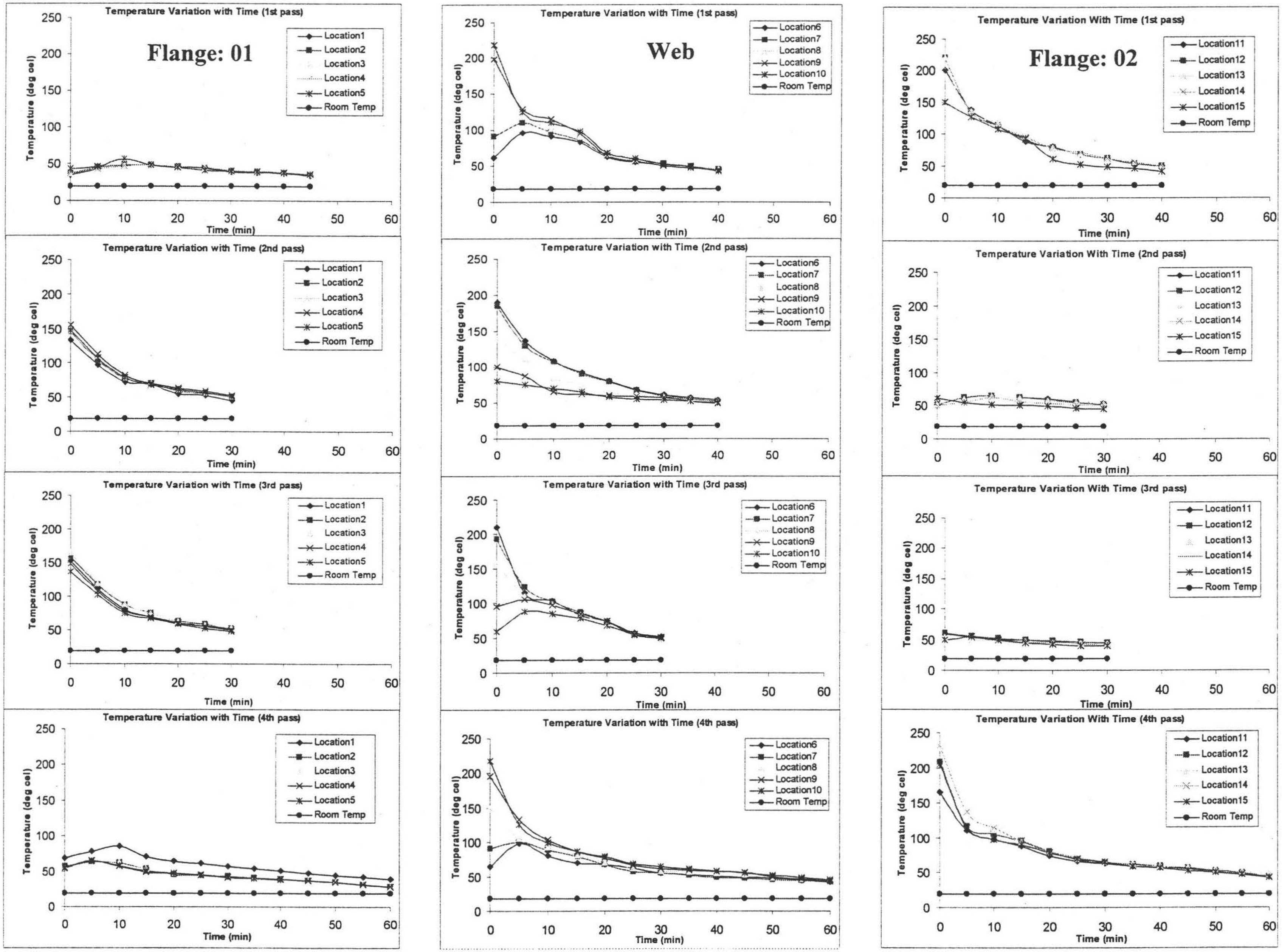

Figure 3.16: Temperature Profile Due to Welding (Column-03)

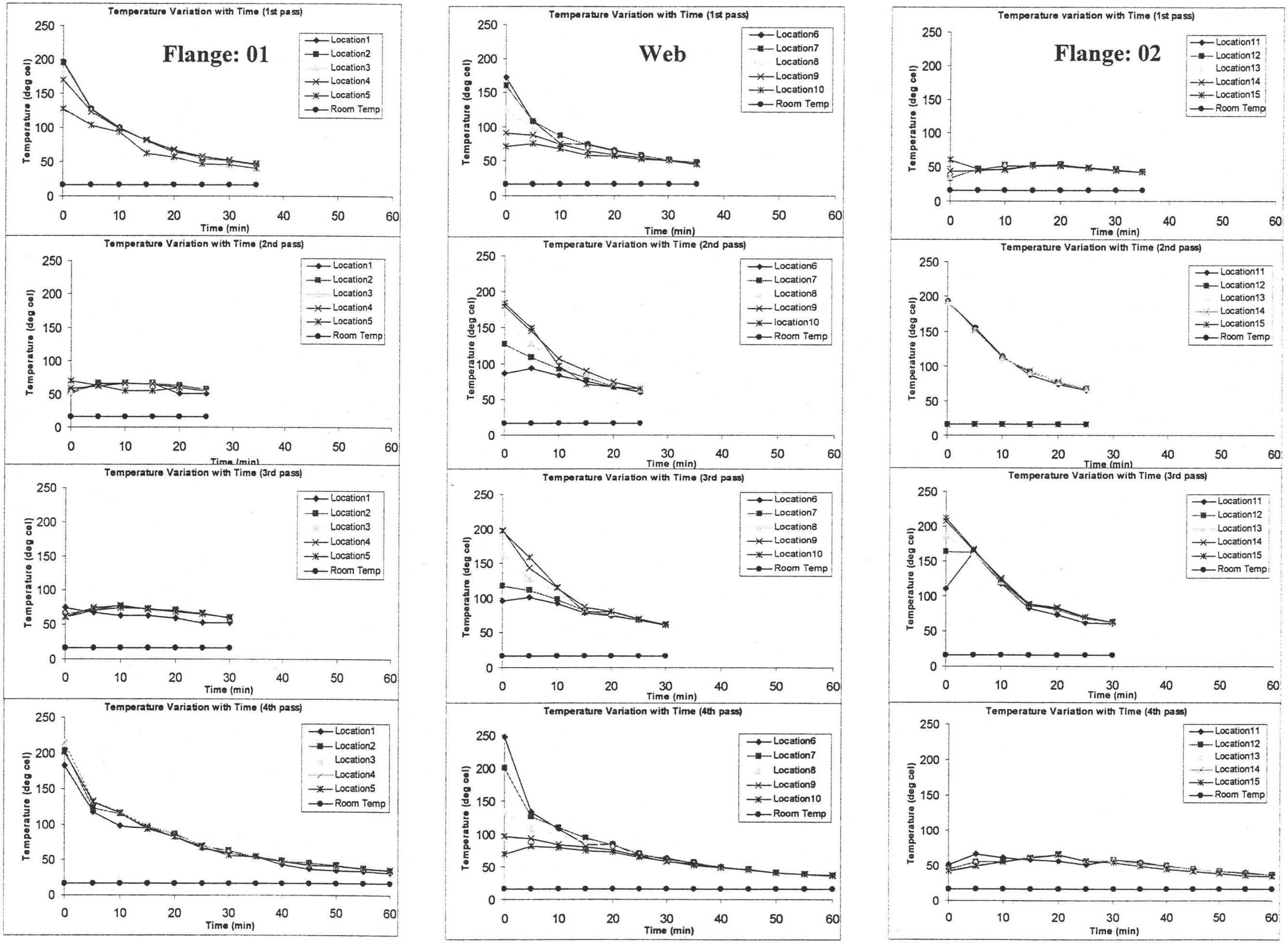

Figure 3.17: Temperature Profile Due to Welding (Column-04)

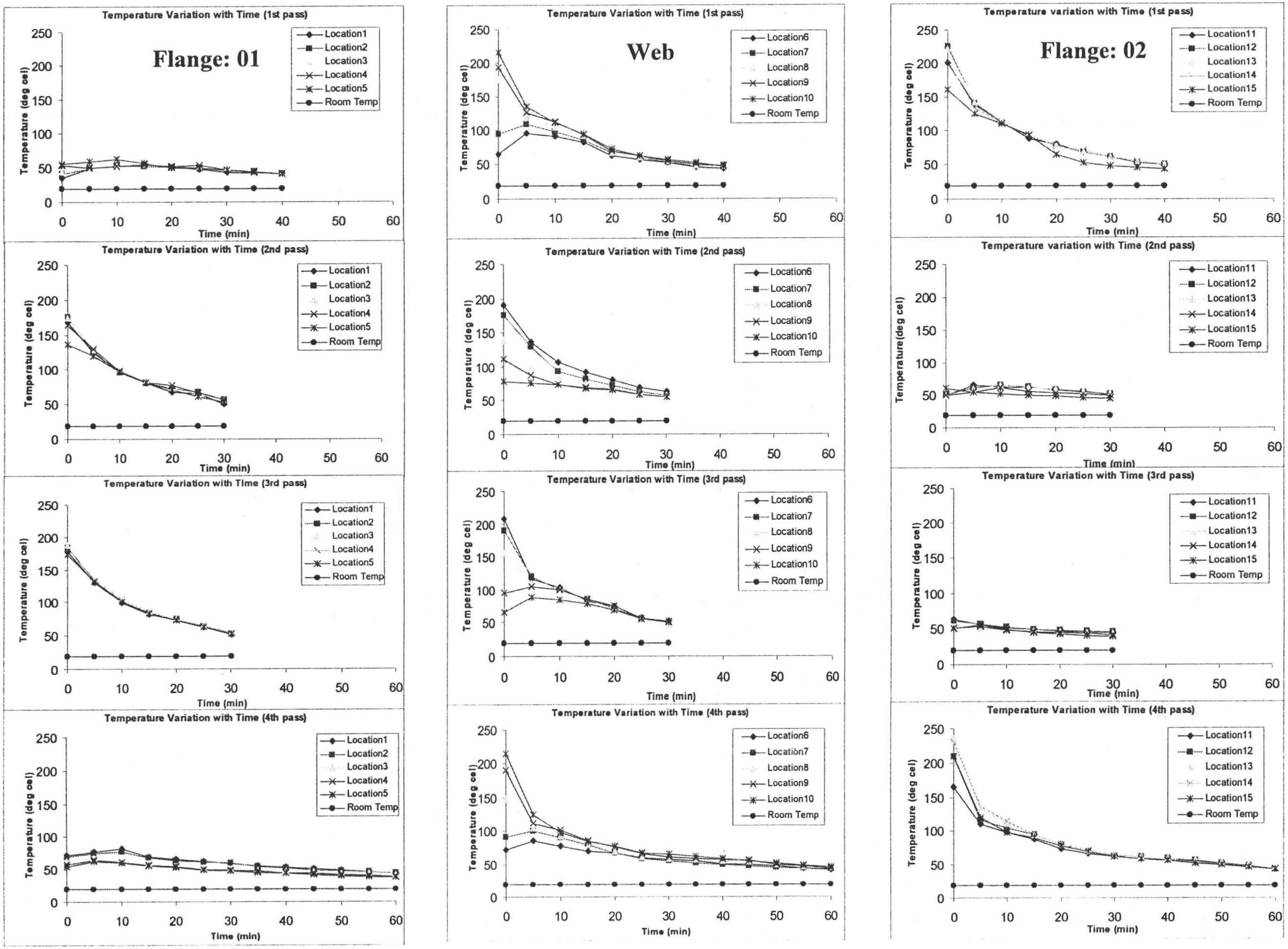

Figure 3.18: Temperature Profile Due to Welding (Column-05)

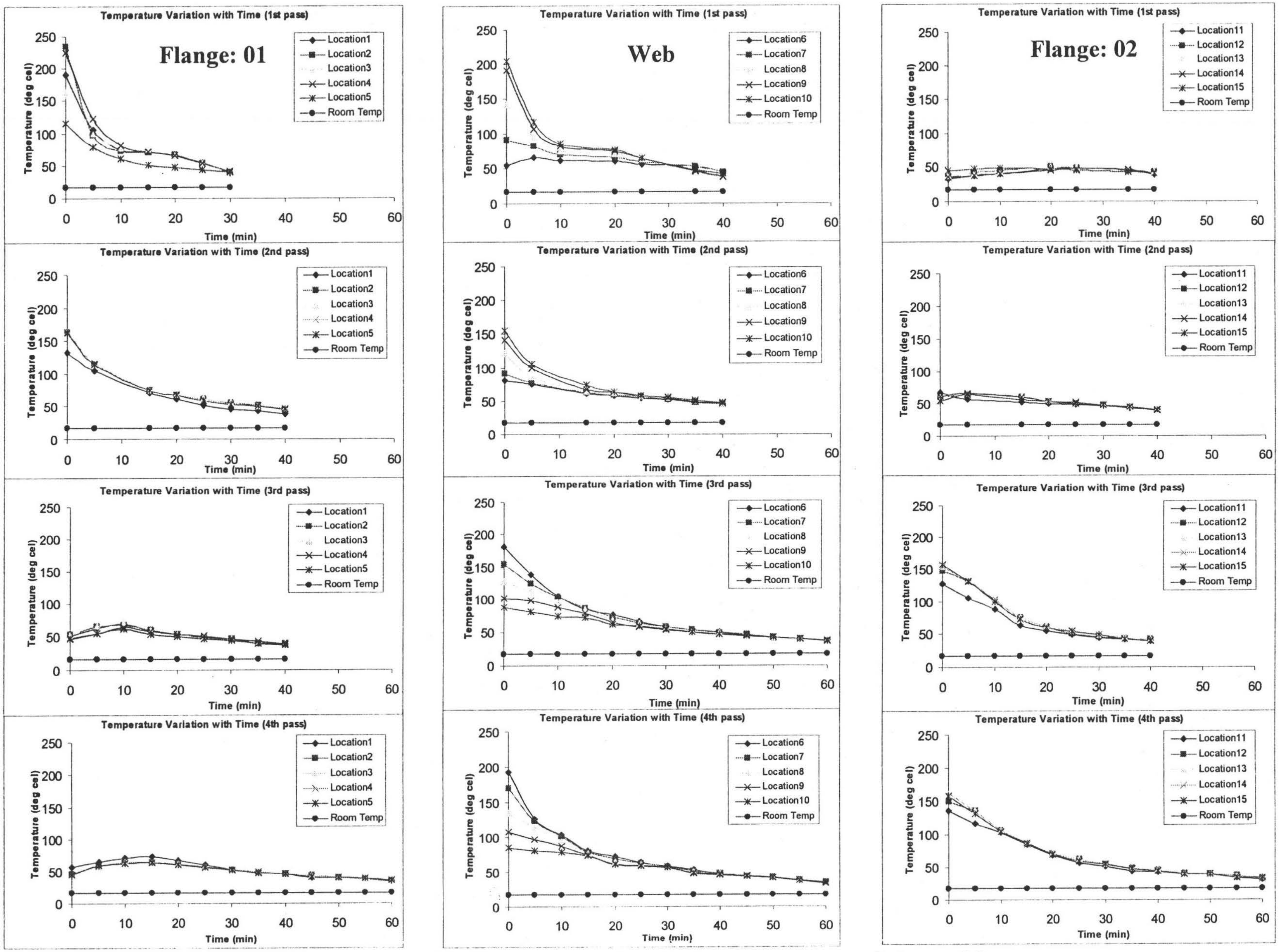

Figure 3.19: Temperature Profile Due to Welding (Column-06)

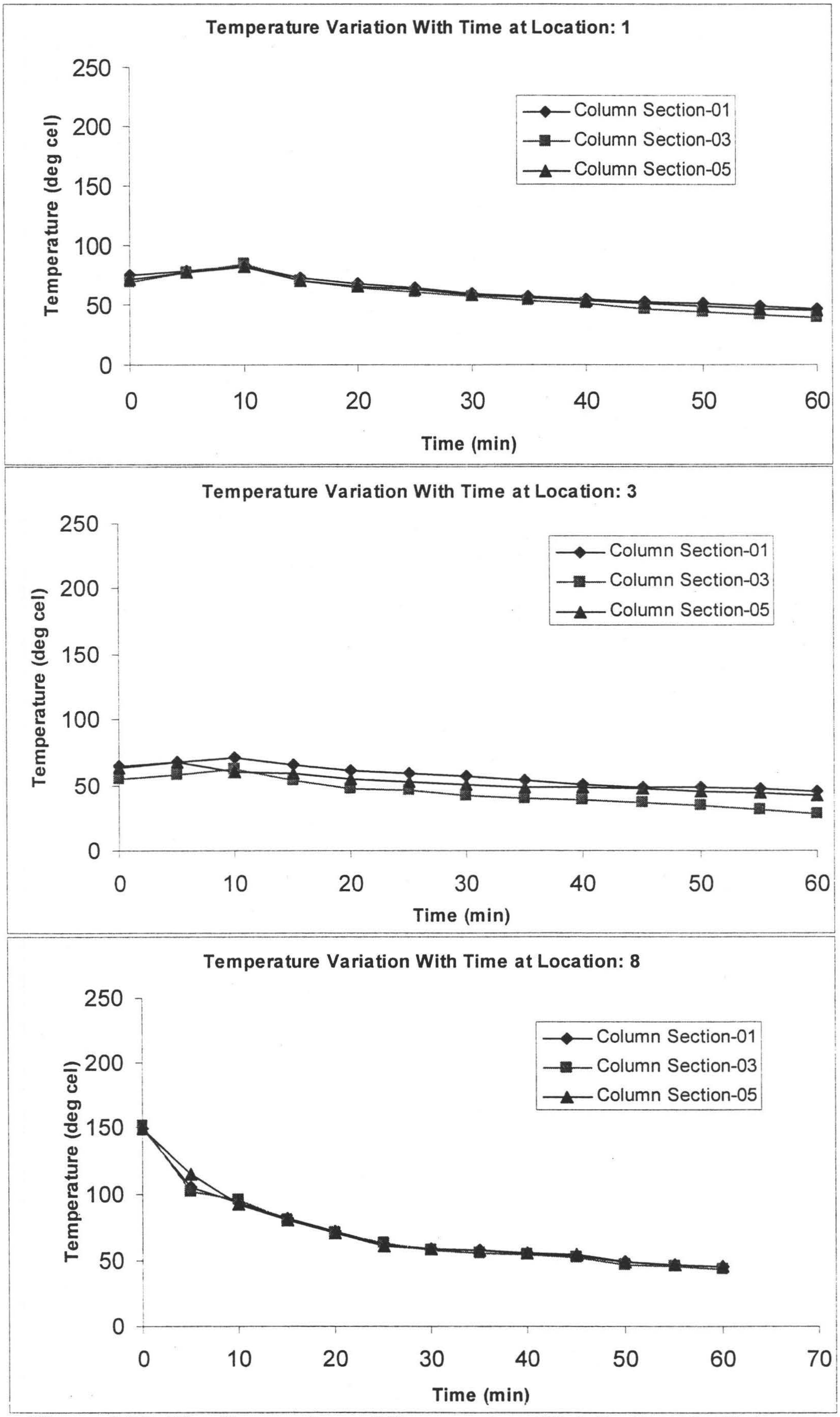

Figure 3.20: The Comparison of Temperature Distributions in Column Section-01, -03, and -05

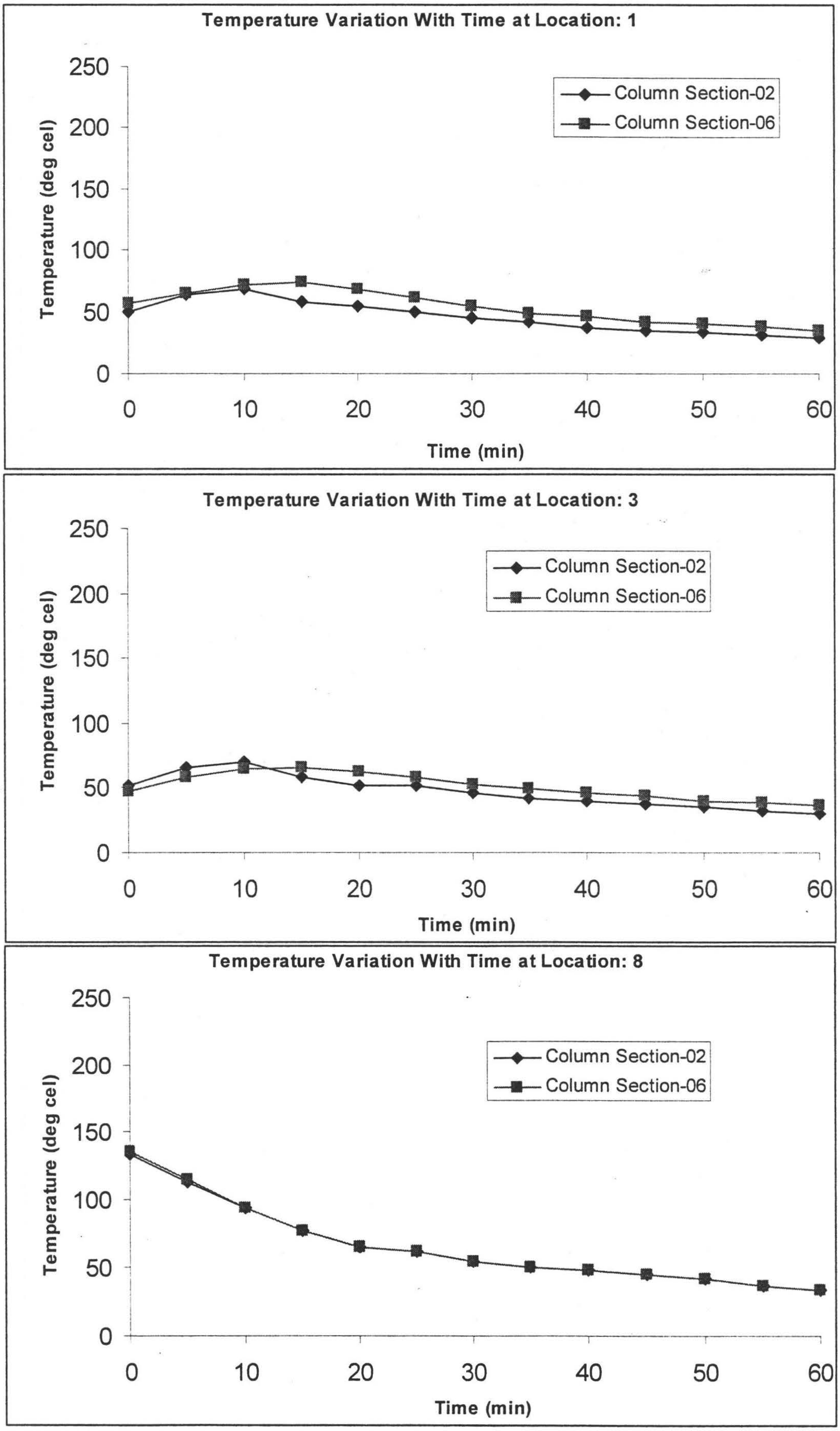

Figure 3.21: The Comparison of Temperature Distributions in Column Section-02 and -06

Chapter 4

GEOMETRICAL IMPERFECTIONS

4.1 Introduction

This chapter includes a general discussion on the influence of geometrical imperfections on the behavior of structural steel columns such as H-shaped sections, box-sections, etc., and a review of the previous research work in this area. It also discusses how such imperfections were taken into account in the development of column strength criteria; the SSRC (Structural Stability Research Council) curves, the ECCS (European Convention for Constructional Steel Work) curves, etc (Galmbos, 1998). Further, this chapter covers the general discussions associated with the limiting values of geometrical imperfections specified in the standard mill practice according to the Canadian CSA G40.20 (CISC, 2004) and the American ASTM A6 standards (ASTM, 2002). The procedures undertaken in this investigation to establish the geometrical imperfections associated with the initial virgin steel plates, the plate-strips after cutting, and the column sections will be explained in detail in this chapter.

This chapter presents the graphical interpretation of out-of plane imperfections present in the initial virgin steel plates and the imperfections measured after cutting of those plates. Also it provides the presentation of imperfections associated with each of the column sections measured in terms of sweep, camber, and sectional variations due to different fabrication techniques. The cross sectional variations of each of the column sections traced in this investigation will be provided. Finally, the values of maximum imperfections measured at critical locations along the column sections fabricated from plasma cut plates and flame cut plates will be tabulated herein for comparison purposes.

4.2 A General Review of the Geometrical Imperfections

4.2.1 Introduction

The geometrical imperfection of a column is an important factor that influences column strength. In general, the degree of geometrical imperfections to which a structural steel member would be exposed to is closely associated with the following factors;

Type of profile: I-shape, box shape, circular tube shape, square tube shape, solid round shape, T-shape, etc.

Fabrication Process: In general, the fabrication process involved in forming a steel section can be classified into three different stages such as *before assembly* - plasma cut, flame cut, laser cut, water-jet cut, shear cut, universal mill, *during assembly* - rolled, welded, cut-out forming, etc, and *after assembly* - as-delivered, annealed, cold straightened, etc.

Geometry: ordinary section, heavy section, cross-sectional dimensions. (For example, for the same welding conditions a wider heat affected zone is created in thinner plates than in thicker plates (Nagaraja Rao and Tall, 1961).

Yield Strength: Steel sections made from low strength steels are more susceptible to the geometrical imperfections during their fabrication process, whereas, the high strength steels are less susceptible to the associated geometrical imperfections during the fabrication process (Fukumoto and Itoh, 1983).

As this investigation focuses only on strength of welded built up members, the pronounced effect of different fabrication techniques on the strength of steel columns has been given the importance in this discussion.

There are different types of fabrication techniques used, today, in forming the steel sections. The different types of fabrication techniques deal with different amount of locally concentrated heat input. As a consequence of these different quantity of heat input, the degree of imperfections to which a section being exposed is considerably different. Therefore the presence of different degrees of imperfections influences the strength of a column section in different manner. For example, the general behavior of a column section, fabricated from flame cut plates is considerably different from that of a similar column section fabricated from universal mill plates (Bjorhovde et al, 1972). The reason why they behave differently is because both fabrication techniques result in different degrees of Heat-Affected-Zone (HAZ), which translate into residual stresses and geometric imperfections. The different quantity of heat input may alter the mechanical characteristics over the cross section. Moreover, the degree of imperfections depends on the rate of cooling during the fabrication process. Figure 4.1 explains the different stages of fabrication process associated with the fabrication technique by which the built up sections are generally formed.

The Effects of Cutting Methods on Geometrical Imperfections: Steel plates before welding are normally cut by means of any one of the cutting methods such as flame cut, plasma cut, laser cut, water-jet cut, shear cut, etc. Different cutting operation produces different amount of localized concentrated heat energy. As a result, the size of Heat-Affected-Zone associated with different cutting techniques varies significantly. Therefore, the translations of imperfections from these Heat-Affected-Zones are considerably different for each cutting methods.

The Effects of Welding on Geometrical Imperfections: Structural elements built up by welding undergo a variable thermal treatment, due to the heating of zones near the weld. The welding process creates not only significant locked-in stresses (residual stresses), but also creates out of flatness of sectional elements, out of squareness of the section, and out-of-straightness of the member, i.e., camber and sweep. The welding changes the material properties of the plate elements only in the vicinity of the weld, thus the in-homogeneous material characteristics becomes another factor influencing the strength of steel columns. The observations made during the welding process will be presented in section 4.3.

4.2.2 The Development of Column Theories Based on Geometrical Imperfections Only

In reality, all columns are not perfect because of the presence of imperfections. The imperfections associated with steel sections can be categorized as material imperfections (residual stresses and inhomogeneous material characteristics) and geometrical imperfections (primarily initial crookedness, sectional variations, etc). In early days, establishment of column strength curves, covering entire ranges of slenderness ratios focused mainly on the effects of imperfections such as initial out-of-straightness and load eccentricity. Thus, the secant curve, semi-empirical column curves such as the Perry-Robertson and Ranking-Gordon formulas, as well as empirical column curves such as the Johnson parabola and simplified straight-line approximations (Chen and Lui, 1987) were developed. However, the Secant and Perry-Robertson formulas had a great influence in developing the most recently accepted multiple column strength criteria such as CRC (Column Research Council), AISC ASD (Allowable Stress Design), AISC PD Curves (Plastic Design), SSRC Curves, etc (Chen and Lui, 1987). The derivation of theses formulas have been based on the following assumptions that,

(1) Plane section remains plane before and after deformation

(2) Deflection of the member is due to bending only (i.e., shear deformation is ignored).

(3) The material obeys Hooke's Law.

(4) The initial crookedness and the subsequent deformation when buckling are assumed as half sinusoidal form.

The Secant and Perry-Robertson formulas are, strictly speaking, valid only for very long or slender columns. Moreover, the failure criteria associated with those formulations have been defined such that the failure of a column section takes place when the maximum stress reaches the yield stress of the column material. So, the critical location of the column would be at the mid height, i.e., the maximum stress will occur in the mid-height of a column.

The final derivation of Secant formula is given as below,

$$F_{\max} = \frac{P}{A}\left(1 + \frac{ec}{r^2}\sec\left(\frac{\pi}{2}\sqrt{\frac{P}{P_e}} - 1\right)\right) \qquad (4.1)$$

In equation (4.1), P is compressive load, A is cross-sectional area of the member, e is load eccentricity measured from the centroid of the member, c is distance from neutral axis to extreme fiber, P_e is Euler buckling load, and r is radius of gyration corresponding to axis of buckling.

The Perry-Robertson formula is as below,

$$F_{\max} = \frac{P}{A}\left(1 + \frac{\delta_0 c}{r^2}\frac{1}{1 - \frac{P}{P_e}}\right) \tag{4.2}$$

In equation (4.2), P is compressive load, A is cross-section area, δ_0 is the maximum initial crookedness, c is distance from neutral axis to extreme fiber, r is radius of gyration corresponding to axis of buckling, and P_e is Euler buckling load.

Since most of the practical steel columns fall into the intermediate column range, the column behaves inelastically, i.e., some of the fibers across the cross-section of a column yield before buckling. The analytical predication of ultimate strength of such columns considering geometrical imperfections only will not give the actual or even reliable results. Therefore the analysis based on the combined effects of residual stresses and initial crookedness becomes more reliable and accurate in predicting the ultimate strength of such columns. The analyses that were made on predicting the strength of columns by previous researchers have incorporated the residual stress distributions and initial out-of-straightness. Hence, the studies have been done considering (a) the idealized residual stress distributions with the assumed values and shapes of the initial out-of-straightness, (b) the measured residual stress distributions with assumed initial out-of-straightness, and (c) the measured values of imperfections. In fact, the analysis based on measured initial out-of-straightness is relatively complicated since the true configuration of the initial-out-straightness of a column may be complicated.

4.2.3 The Limitations of Geometrical Imperfections

The magnitude of the maximum initial out-of-straightness (either camber or sweep) and permissible variations in sectional dimensions for different types of sections are limited by the structural steel delivery specifications according to CAN/CSA G40.20 (CISC, 2004) (in Canada) and ASTM A6 (ASTM, 2002) (in US). In general, the limitation for maximum permissible initial out-of-straightness is expressed as a fraction of the length of the member. According to CAN/CSA G40.20 (CISC, 2004), the maximum permissible variation in straightness for W-shape and welded columns having the length (L) of less than 14,000mm is specified as L/1,000≤ 10mm. For the columns having length of more than 14,000mm, the maximum permissible variation in straightness is specified as [10+ (L-14,000)/1,000] mm.

As an interest of analyzing the limitations for different types of structural shapes, this chapter discusses the limitations provided by the past researchers in this area. Galambos (1998) reviewed the work done by Bjorhovde (1972) in the area of analyzing the limitations of geometrical imperfections associated with various structural steel shapes. It was observed from the measurements made on the hot-rolled wide-flange shapes (W-shapes) that those sections tended to have values toward the maximum permissible, with an average of approximately L/1,500 (Bjorhovde, 1972). However, Dux and Kitipornchai (1981) provided a mean value of initial deflections of L/3,300 for wide-flange shapes having length varying from 6,000mm to 10,000mm. Thereafter, Essa and Kennedy (1993) provided a mean value of initial deflection L/2,000 for the wide-flange shapes having the same ranges of length.

It was observed from the measurements made on tubular members that those members commonly exhibited values significantly smaller than the specification limitations, with out-of-straightness on the order of L/3,000 to L/8,000, with an average of L/6,300 (Galambos, 1998). Furthermore, it was observed from the measurements made on the welded wide-flange shapes (WWF shapes) that those members exhibited small initial crookedness values, with a mean of approximately L/3,300 (Galambos, 1998). On the whole, it was rare to encounter columns with out-of-straightness larger than the maximum permitted. This was because the columns of having initial out-of-straightness more than the permitted values were cold straightened before shipment.

Even though the initial out-of-straightness of the most column sections were well within the maximum permitted values as specified in the mill practice based on either CAN/CSA G40.20 (CISC, 2004) or ASTM A6 (ASTM, 2002), in the development of column strength criteria such as the SSRC curves (Galambos, 1998) and the ECCS curves (Galambos, 1998), the maximum permissible values of initial out-of straightness were used in the development of strength criteria. This was done for several reasons, the primary one being that L/1,000 constituted the upper limit of what is acceptable for actually delivered members and thus, could be regarded as a conservative measure.

Moreover, Bjorhovde (1972) developed the column curves using the mean values of the initial out-of-straightness of L/1,470 in parallel with his development of the original SSRC curves. Because, it can rationally be argued that the mean crookedness should be utilized since mean characteristics were used for the other strength parameters. The mean value of initial crookedness was determined through statistical evaluations. Figure 4.2 shows the originally developed column strength curves using the maximum value of initial crookedness of L/1,000 and the curves developed for rational argument using the mean value of initial crookedness of L/1,470.

There were 112 column strength curves considered for a number of different column types in developing the SSRC column curves by Bjorhvode (1972). It was also analyzed the strength of such columns considering different values of initial out-of-straightens; L/500, L/1,000, and L/2,000 in his investigation. The results for the band of column strength curves are shown in Figure 4.3. The results of the studies on the maximum strength of columns emphasized the fact that the incorporation of the initial out-of-straightness into column strength was essential to form the basis for design criteria.

4.3 The Geometrical Imperfections

The geometrical imperfections in this investigation were established at various stages of the fabrication process. Firstly, the surface imperfections associated with the original plates were established. Secondly, the surface imperfections associated with the plate strips after cutting were established. Finally, the geometrical imperfections associated with the column sections to be tested were established in terms of sweep and camber. Also the sectional variations such as out- of- squareness of the section and out-of-flatness of sectional elements for each column sections were observed.

Geometric Imperfections in Plates: As this investigation was partly concerned with the establishment of geometrical imperfections in original plates having dimensions of (3960x710x9.5mm), the out-of-surface imperfections of plates (six plates) were established individually. As the first step of measurement for the out-of-surface imperfections, the steel plate was supported on a flat surface to ensure that the plate was not bent. The grid-lines along which the out-of-surface imperfections were to be measured were identified as shown in

Figure 2.3 (provided in Chapter 2). The spacing between the grid-lines marked in the longitudinal direction of the plate was 75mm. But, the grid-lines in the transverse direction were spaced at approximately 1000mm (see Figure 2.3). After establishing the grid-lines, a string attached to plum bobs was placed along the grid-line so that the plum bobs were hanging from the opposite edges of the plate. The out-of-surface imperfections along the grid-lines were measured using a flat ruler having the least count of 0.5mm. The ruler was held vertically as the measurements were taken. The measurements in the longitudinal direction of the plate were taken at every 305mm (12 inch) along the grid lines 1-1, a-a, 2-2, b-b, 3-3, c-c, and 4-4 (see the Figure 2.3). Also, the measurements were taken at every 100mm (4 inch) in the transverse direction along the grid lines A-A, B-B, and C-C (see the Figure 2.3).

Figures 4.4 and 4.5 show the mesh plot associated with the out-of-surface imperfection of each of the original plates used in this investigation. As a common observation from the measurements taken for all six plates, the out-of-surface imperfection was relatively high in the region roughly from 600mm to 1200mm and the region roughly from 3000mm to 3600mm along the longitudinal direction (see Figures 4.4 through and 4.9). Moreover, it was observed that the original plate-01, -03, -05, and -06 seemed to be almost flat in their middle region (roughly from 1500mm to 2500mm) with respect to the opposite edges in the longitudinal direction. But the plate-02 and -04 seemed to have relatively high out-of-surface deflections in the middle region (see Figures 4.7 and 4.8). Maximum out-of-surface imperfections measured in each plate are tabulated in Table 4.1. The maximum values are provided separately for the portions identified in the original plate as flange-01, flange-02, and the web (see Figure 2.2 provided in Chapter 2).

The maximum out-of-surface imperfections measured in plate-01,-03 and -05 were about 2.5mm, 1.5mm, and 3mm, respectively. However, the maximum out-of-surface imperfections of plate-02, -04, and -06 were 13mm, 13mm, and 7mm, respectively. Furthermore, from the measurement taken in the transverse direction it was observed that the plate-01, -03, and -05 were almost flat. However, the maximum imperfections measured in plate-02, -04, and -06 were approximately 2.5mm. It was also observed from the measurements taken in the transverse direction that the tendency of the maximum deflections was to occur in the middle region of each plate.

Geometric Imperfections in Plate Strips (After Cutting): The out-of-surface imperfections were measured on plate strips (3960x150x9.5mm) after they were cut into three pieces (two flange pieces and a web piece) from the original steel plate (3960x710x9.5mm). Two side plate strips were used as flanges and the middle piece was used as web to form the I-shaped section in this investigation. The out-of-surface imperfections of plate strips were measured in the same way followed in the original steel plates. However, the individual measurements along the edges of flange pieces and the web piece cut from the same plate were taken since the individual plate strips had different level of out-of-plane deflections along their edges. Note that the measurements in the transverse direction of the plate strips were not taken since there were no significant deflections observed in that direction of each plate strips. Figures 4.4 and 4.5 show the out-of-surface imperfections associated with the original steel plate and the plate strips by putting them closer to each other. Note that the average values of imperfections along the common edges of the flange pieces and the web piece were used to plot the representative mesh surface for plate strips herein.

Table 4.2 shows the maximum out-of-surface imperfections measured in plate strips, which were designated herein as Flange: 01, Web, and Flange: 02 cut from the same original plates. The maximum out-of-surface imperfections in plate strips cut from plate-01, -03, and -05 were 3mm, 2mm, and 3.5mm, respectively and also these plates were cut by plasma cutting in this investigation. The maximum out-of-surface imperfections measured in plate strips cut from plate-02, -04, and -06 were 17mm, 14mm, and 9.5mm, respectively and also these plates were cut by flame cutting. Moreover, the plate strips cut by flame cutting had relatively high change in out-of-surface imperfections than the plate strips cut by plasma cutting. Because, it was observed in this investigation, that the plate bent upwards to a certain height from the cutting bed and then came down as plate was cooling down during the flame cut operation. However, there were no such observations made during the plasma cut operation. The following can be reasons for these observations,

(1) High heat energy was delivered to the steel plate during the flame cut than that delivered during the plasma cut. Hence, it was evident that the striking temperature of flame cut was greater than that of plasma cut from the temperature measurements during each cutting operations.

(2) The flame cut operation was more suitable for thick plates (more than 13mm), because, high heat energy delivered from flame during cutting operation can create considerably larger Heat Affected Zone in thin plates than thick plates (Galambos, 1998)

It was observed from the measurements taken for out-of-surface imperfections in original plate and in plate strips that the general variation of imperfections in longitudinal direction seemed to occur almost in the same region. That is, as discussed earlier, the out-of-surface imperfection was relatively high in the region roughly from 600mm to 1200mm and the region roughly from 3000mm to 3600mm along the longitudinal direction of original plates and the plate strips after cutting. Moreover, as an overall observation, the out-of-surface imperfections after cutting were increased in plate strips after cutting when compared to the original plates.

<u>Geometric Imperfections in Column Sections</u>: As discussed earlier, there were twelve column specimens that were cut from the six initial column sections formed just after welding. The column imperfections in terms of sweep (deformation about minor axis) and camber (about major axis) were measured at certain intervals as provided with the graphical interpretation of sweep and camber for each column sections (see Figure 4.10). The sweep of a column was measured at three different locations over the cross-section of the column; top-flange, bottom-flange, and mid-web in this investigation. A string was placed along the edges of flanges as close loop, assuming the tip of the flanges in opposite direction as reference points when measuring sweep along the edges of flanges. The string was firmly held by a turn buckle. Then, the measurements were taken using flat ruler having the least count of 0.5mm in this investigation. The same procedure was followed in measuring camber of the column section. However, the string was close looped around the flange-web junction in measuring camber. The positions for measuring sweep and camber are shown in Figure 4.10. Figures 4.11 through 4.16 show the variation of sweep and camber in each of the column specimen.

Table 4.3 shows the maximum sweep and camber in welded built-up column sections fabricated from plasma cut plates and flame cut plates. As a general observations made form the variation of sweep and camber along the column sections used in this investigation, the

maximum values of sweep and camber seemed to occur in the vicinity of the mid length of specimens (see Figures 4.11 through 4.16). Moreover, the maximum sweep and camber of each column sections were compared with the CAN/CSA G40.20 (CISC, 2004) code limitations for permissible variations in straightness. The out-of-straightness of all the column sections were within the code limitations for the maximum permissible values of L/1,000≤10mm since all of the column sections tested in this investigation were having the initial length of less than 14,000mm (L≤14,000mm) .

The representative measures of sectional variations after forming the sections by gas metal arc welding are shown in Figure 4.17. These representative measures were taken from specimens obtained from initial column specimens for residual stress measurements in this investigation. The Figure 4.17 also shows how the sectional variations such as out-of-squareness and out-of flatness were formed in column sections to be tested in this investigation. The measurements of sectional variations associated with (a) plasma cut-gas metal arc welded columns (3-initial column section) and (b) flame cut-gas metal arc welded columns (3-initial column section) are provided in Table 4.4. This table provides the nominal depth which was calculated by adding the flange thicknesses (9.5mm for each top and bottom flange) to width of the web piece just after cutting and the measured depth (A) which was measured from the top flange surface to bottom flange surface along the middle line of the web (see Figure 4.17). Moreover, in this table, the nominal width of the flanges (top and bottom flange of a section) that were measured just after cutting and the measured width taken after forming the section are provided for each column section. The variations in nominal depth (A), width of flange (B), out-of-square (T+T'), out-of-parallel (C-D), and web off-centerline (E) was measured for each of the column sections as shown in Figure 4.18. These values were then compared with the permissible variations in sectional dimension as provided in CAN/CSA G40.20 (CISC, 2004) code limitations. Figure 4.14 shows the code limitations for sectional variations according to CAN/CSA G40.20 (CISC, 2004) standard. Table 4.5 provides the sectional variations of each column section comparing with the code limitations. From the comparison it was observed that, all the column sections satisfied the code limitation for variations in nominal depth (A), variations in width of flange (B) and variations in web off-centerline (E). The column sections designated herein as C2 and C6 (both of them were fabricated from flame cut plate strips) did not satisfy the code limitations for out-of-square (T+T') and out-of-parallel (C-D). However, all the other column sections satisfied the code limitations as specified in CAN/CSA G40.20 (CISC, 2004). Note that the above comparison and discussion were based on the representative values obtained at one location across the cross-section from each of the column specimens immediately after welding. In addition to this, it was observed that the cutting edge due to plasma cut was not perfectly square, but the cutting edge was slightly slanted with the vertical plane (see the Figure 4.17). However, the cutting edge of the flame cut was relatively square in shape (see the Figure 4.17).

Plate Designation	Surface in Which Imperfections Measured	Location		
		Flange:01	Web	Flange:02
01	Top Surface	2.5mm	2.5mm	2.5mm
02	Bottom Surface	13mm	11.5mm	11.5mm
03	Top Surface	1.5mm	1.5mm	1.5mm
04	Bottom Surface	12.5mm	13mm	13mm
05	Bottom Surface	2.5mm	3mm	2mm
06	Bottom Surface	6.5mm	6.5mm	7mm

Table 4.1: The Maximum Out-of-Surface Imperfections in Original Plate (Before Cutting)

Method of Cutting	Plate Designation	Surface in Which Imperfections Measured	Location		
			Flange:01	Web	Flange:02
Plasma	01	Top Surface	3mm	3mm	3.5mm
	03	Bottom Surface	2mm	1.5mm	2.5mm
	05	Top Surface	3.5mm	3mm	3mm
Flame	02	Bottom Surface	17mm	16mm	10mm
	04	Bottom Surface	14mm	12mm	7mm
	06	Bottom Surface	9.5mm	9.5mm	9mm

Table 4.2: The Maximum Out-of-Surface Imperfections in Plate Strips (After Cutting)

Column Designation		Column Length- L (mm)	Max Sweep (mm)	Max Camber (mm)
Plasma Cut	C1 (b)	700	0	0
	C1 (a)	2650	2	0.5
	C3 (b)	1214	1	0
	C3 (a)	2144	2	1
	C5 (b)	308	0	0
	C5 (a)	3077	3	0.5
Flame Cut	C2 (b)	696	0	0
	C2 (a)	2653	3	1
	C4 (b)	1210	0.5	0
	C4 (a)	2149	3	0.5
	C6 (b)	306	0	0
	C6 (a)	3081	4.5	1.5

Table 4.3: The Maximum Geometrical Imperfections in Columns

(a) - Denotes- intermediate column specimens

(b) - Denotes- short column specimens

(a) & (b) were obtained from the same initial column stock

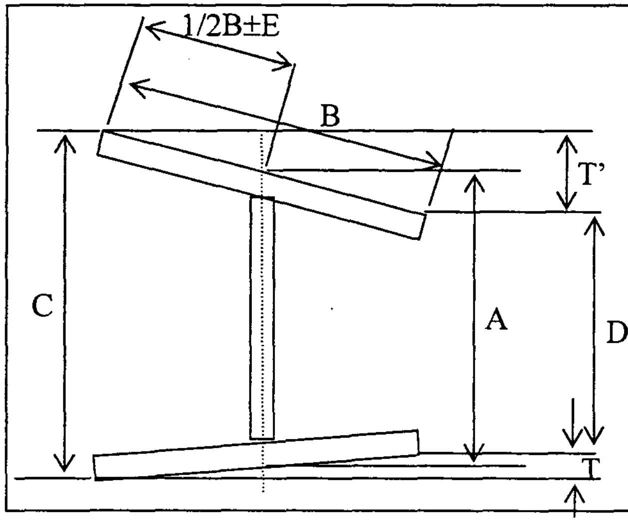

Nominal Depth = Web width + 2 X Flange thickness (Calculated)

Measured Depth = A

T.F - Top Flange

B.F - Bottom Flange

Method of Cutting	Column Designation	Nominal Depth (mm)	Measured Depth [A] (mm)	Nominal Width (mm)		Measured Width [B] (mm)		Out of Square [T+T'] (mm)	Out of Parallel [C-D] (mm)	Web off-Centerline [E] (mm)	
Plasma	C1	164	163	T.F	149	T.F	148	4	4	T.F	0
				B.F	151	B.F	148			B.F	±1
	C3	165	167	T.F	153	T.F	154	2	2	T.F	±2
				B.F	147	B.F	146			B.F	±1
	C5	165	166	T.F	147	T.F	146	5	5	T.F	0
				B.F	146	B.F	147			B.F	±0.5
Flame	C2	164	167	T.F	147	T.F	146	9	9	T.F	±1
				B.F	150	B.F	149			B.F	±0.5
	C4	167	171	T.F	147	T.F	145	1	1	T.F	±0.5
				B.F	148	B.F	150			B.F	±2
	C6	165	166	T.F	151	T.F	149	7	7	T.F	±3.5
				B.F	147	B.F	149			B.F	±0.5

Table 4.4: The Measurements of Sectional Variations in Column Sections

Method of Cutting	Column Designation	Depth [A]	Width of Flange		Out-of-Square [T+T'] (mm)	Out-of-Parallel [C-D] (mm)	Web off-Centerline [E] (mm)
Plasma	C1	1mm- under	T.F	1mm-under	Not over 6mm	Not over 5mm	Not over 5mm
			B.F	3mm-under			Not over 5mm
	C3	2mm-over	T.F	1mm-over	Not over 6mm	Not over 5mm	Not over 5mm
			B.F	1mm-under			Not over 5mm
	C5	1mm-over	T.F	1mm-under	Not over 6mm	Equal to 5mm	Not over 5mm
			B.F	1mm-over			Not over 5mm
Flame	C2	3mm-over	T.F	1mm-under	Over 6mm	Over 5mm	Not over 5mm
			B.F	1mm-under			Not over 5mm
	C4	4mm-over	T.F	2mm-under	Not over 6mm	Not over 5mm	Not over 5mm
			B.F	2mm-over			Not over 5mm
	C6	1mm-over	T.F	2mm-under	Over 6mm	Over 5mm	Not over 5mm
			B.F	2mm-over			Not over 5mm

Table 4.5: The Measurements of Sectional Variations in Column Sections

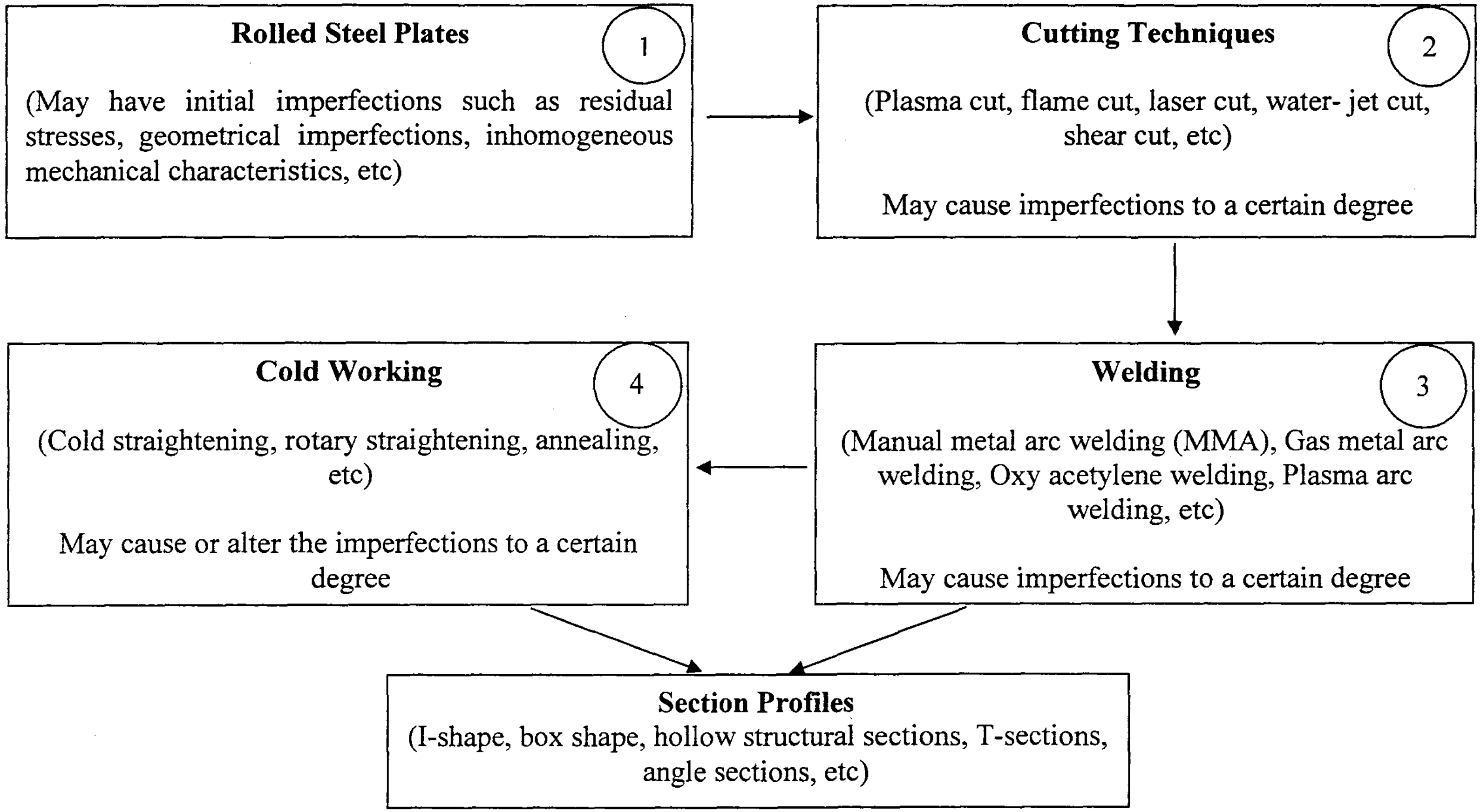

The steps associated with the fabrication process can be either;

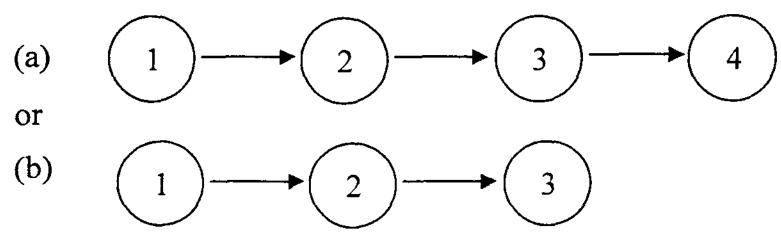

Figure 4.1: The Different Stages of Fabrication Process Associated with Welded Built-up Sections

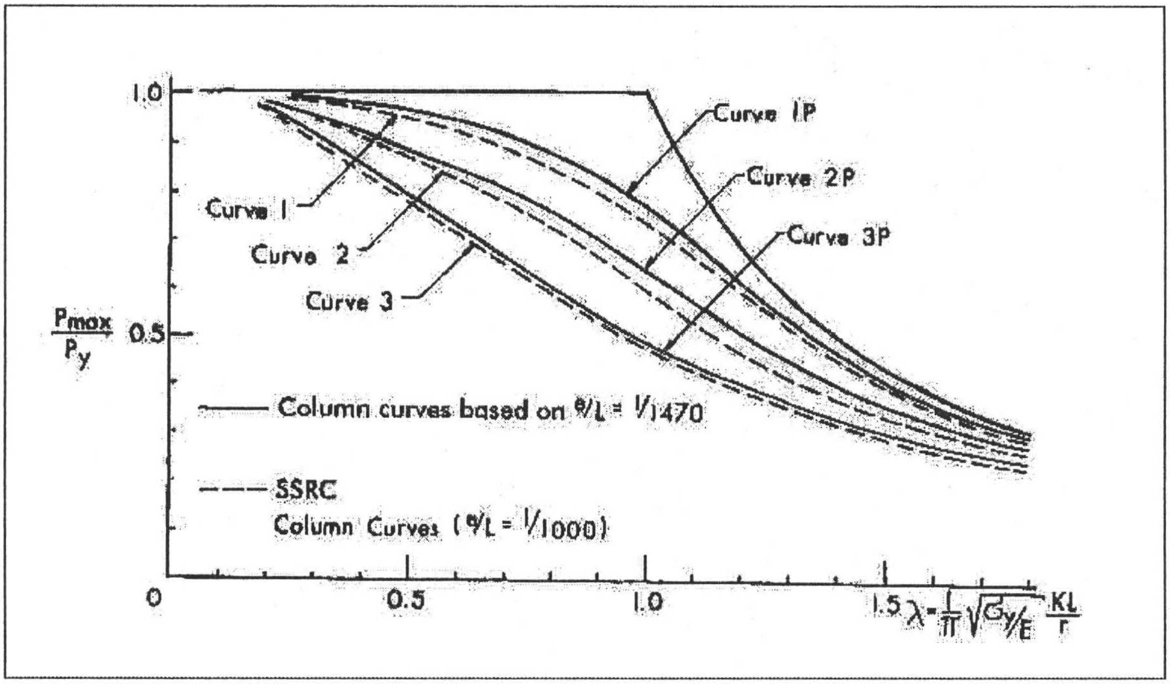

Figure 4.2: Comparison of Multiple Column Curves Developed on The Basis of Maximum Permissible (L/1000) and Mean (L/1470) Out-of-Straightness (Bjorhovde, 1972)

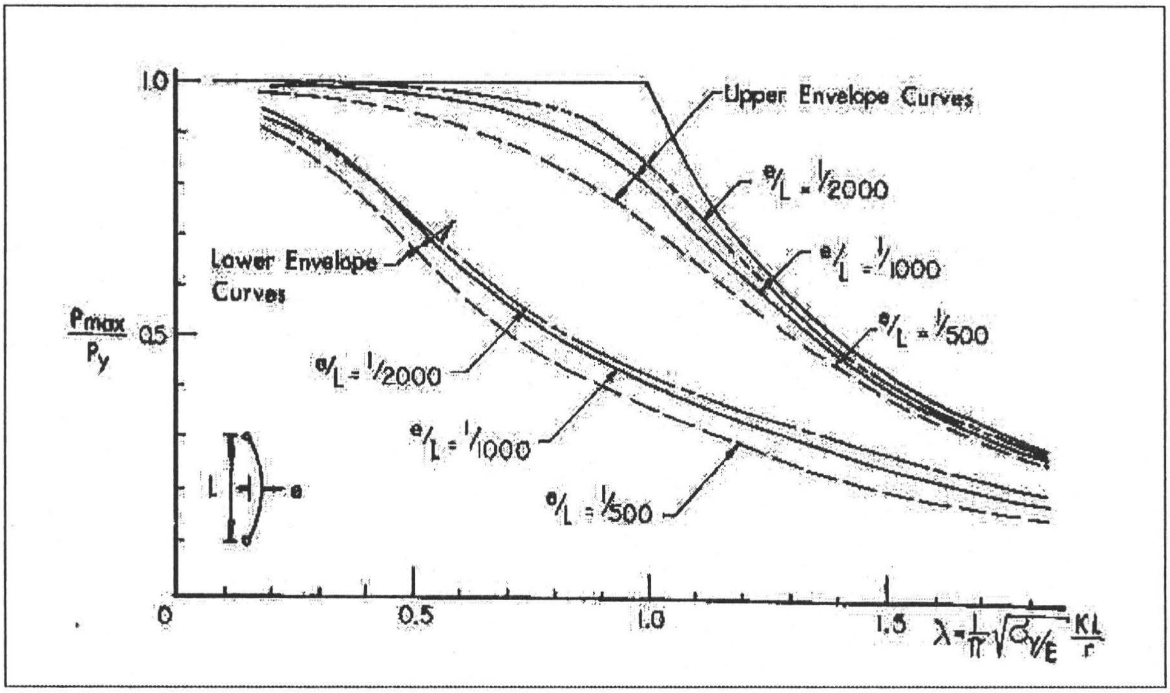

Figure 4.3: Column Curve Bands for 112 Columns Based on Initial Out-of-Straightness of L/500, L/1000, L/2000 (Bjorhovde, 1972)

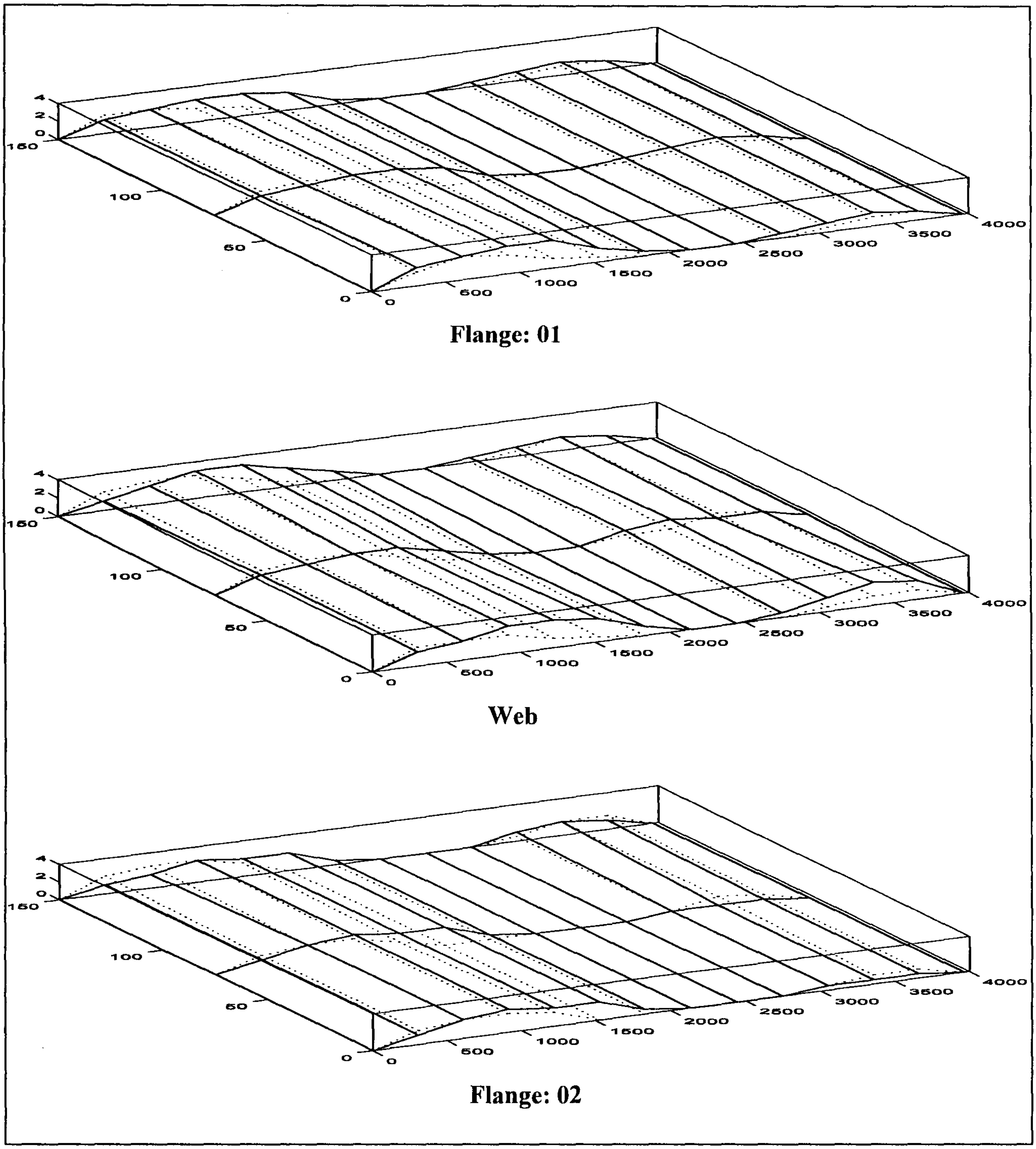

Figure 4.4: The Out-of-Surface Imperfections on Initial Plate-01 and on Plate Strips after Plasma Cutting

(---- Out-of-Surface Imperfections on Original Plate — Out-of-Surface Imperfections on Plate Strips (After cutting))

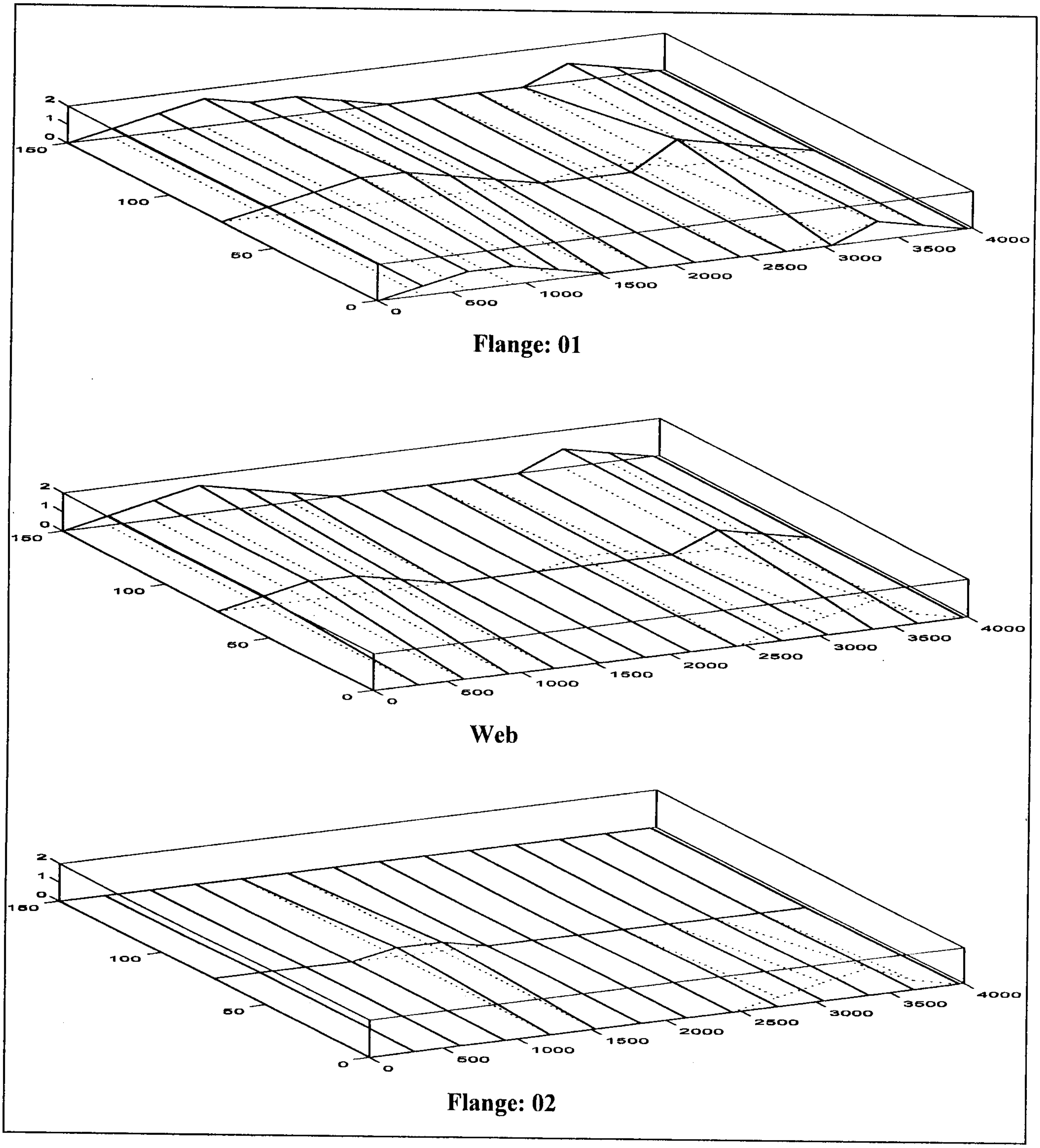

Figure 4.5: The Out-of-Surface Imperfections on Initial Plate-03 and on Plate Strips after Plasma Cutting

(---- Out-of-Surface Imperfections on Original Plate — Out-of-Surface Imperfections on Plate Strips (After cutting))

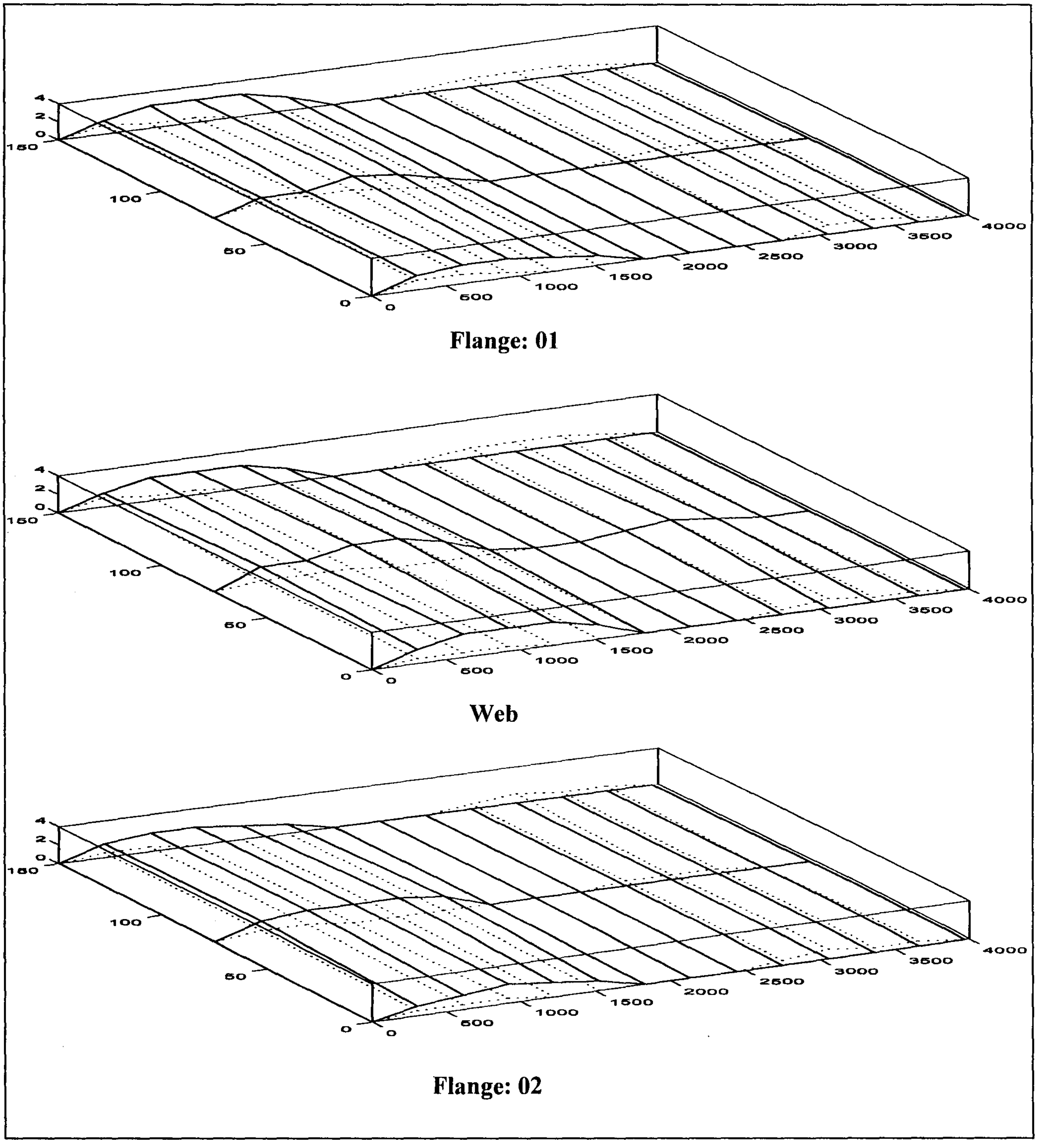

Figure 4.6: The Out-of-Surface Imperfections on Initial Plate-05 and on Plate Strips after Plasma Cutting

(---- Out-of-Surface Imperfections on Original   ▬ Out-of-Surface Imperfections on Plate Strips (After cutting))

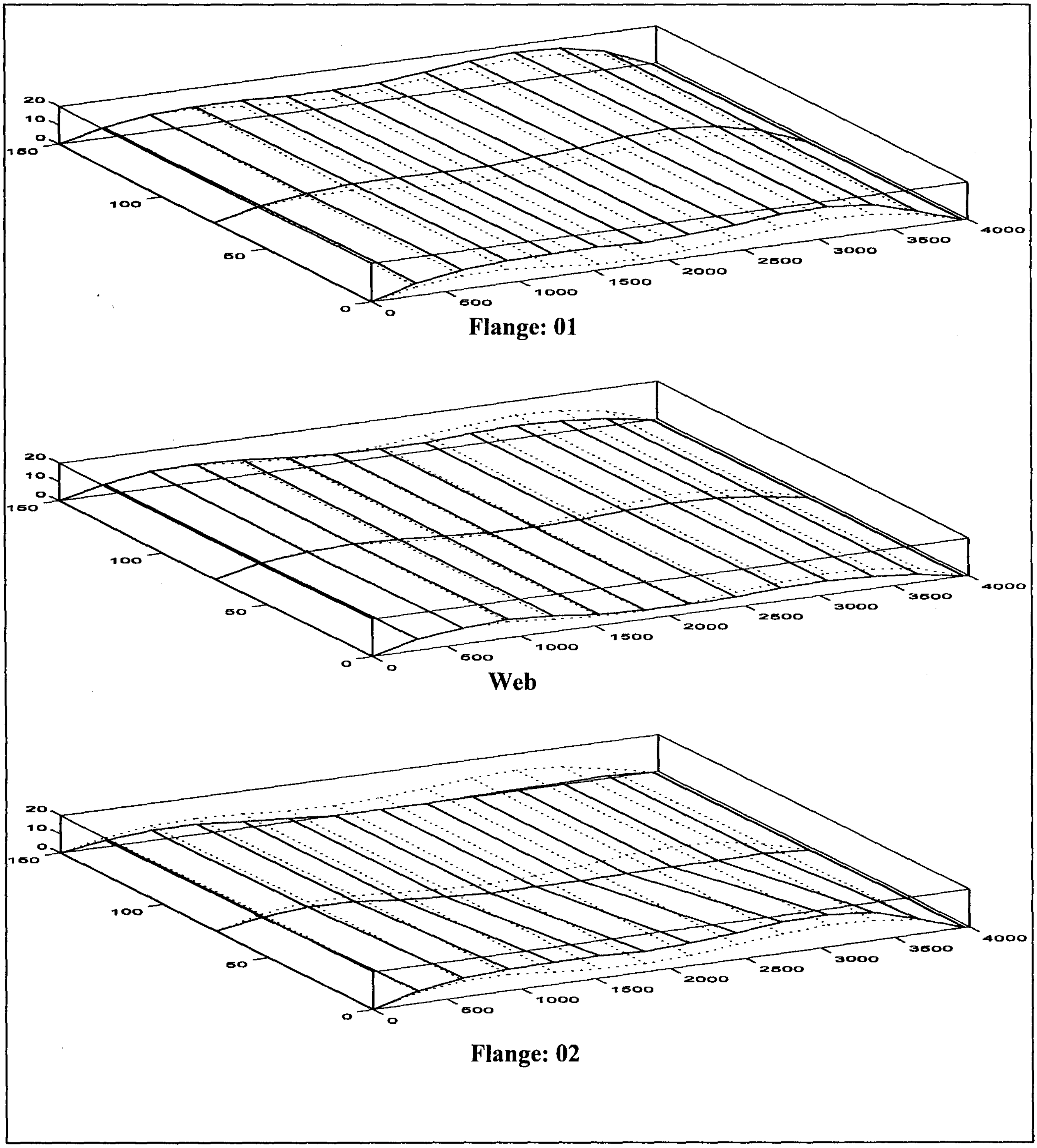

Figure 4.7: The Out-of-Surface Imperfections on Initial Plate-02 and on Plate Strips after Flame Cutting

(---- Out-of-Surface Imperfections on Original Plate —— Out-of-Surface Imperfections on Plate Strips (After cutting))

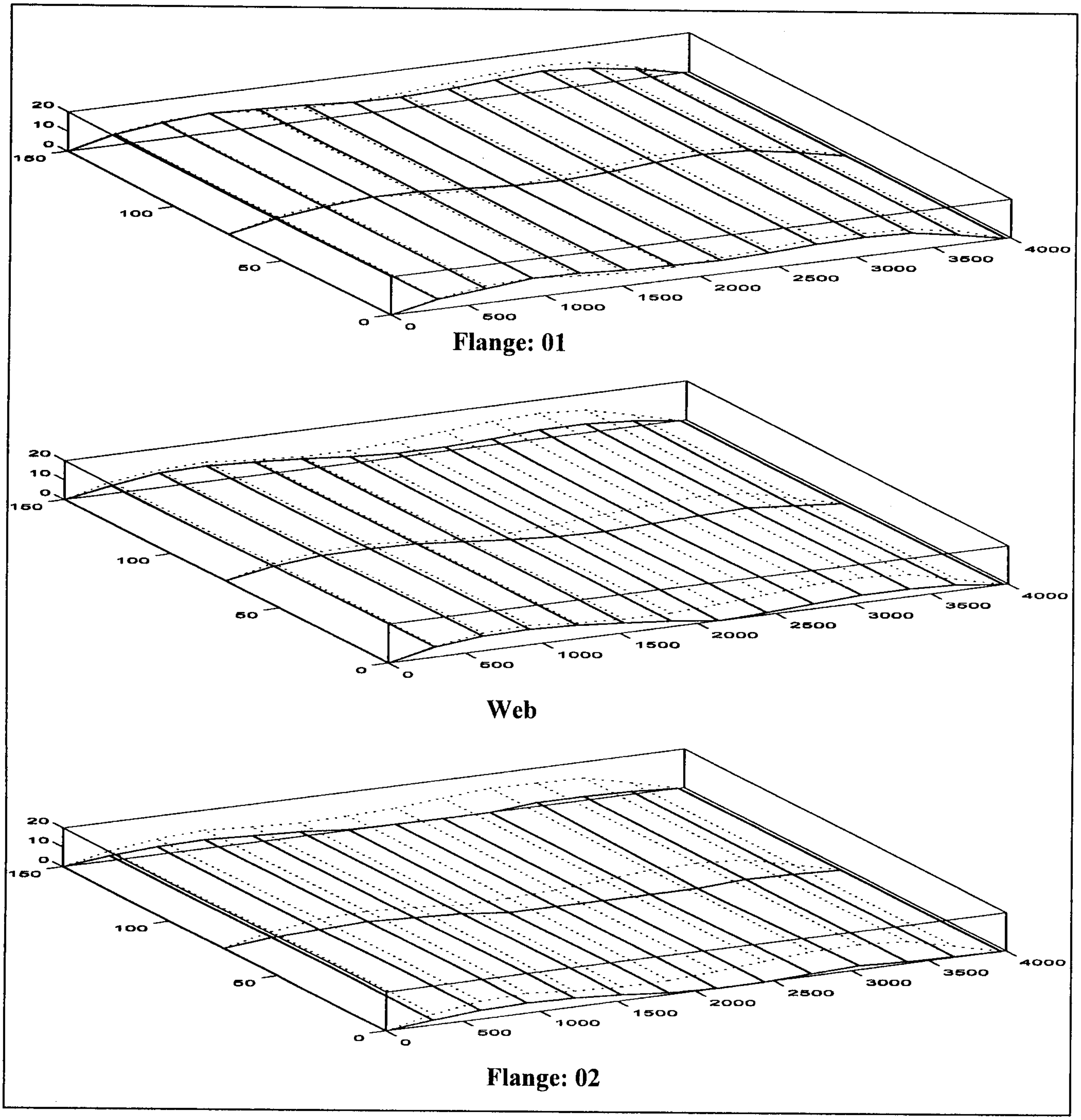

Figure 4.8: The Out-of-Surface Imperfections on Initial Plate-04 and on Plate Strips after Flame Cutting

(---- Out-of-Surface Imperfections on Original Plate — Out-of-Surface Imperfections on Plate Strips (After cutting))

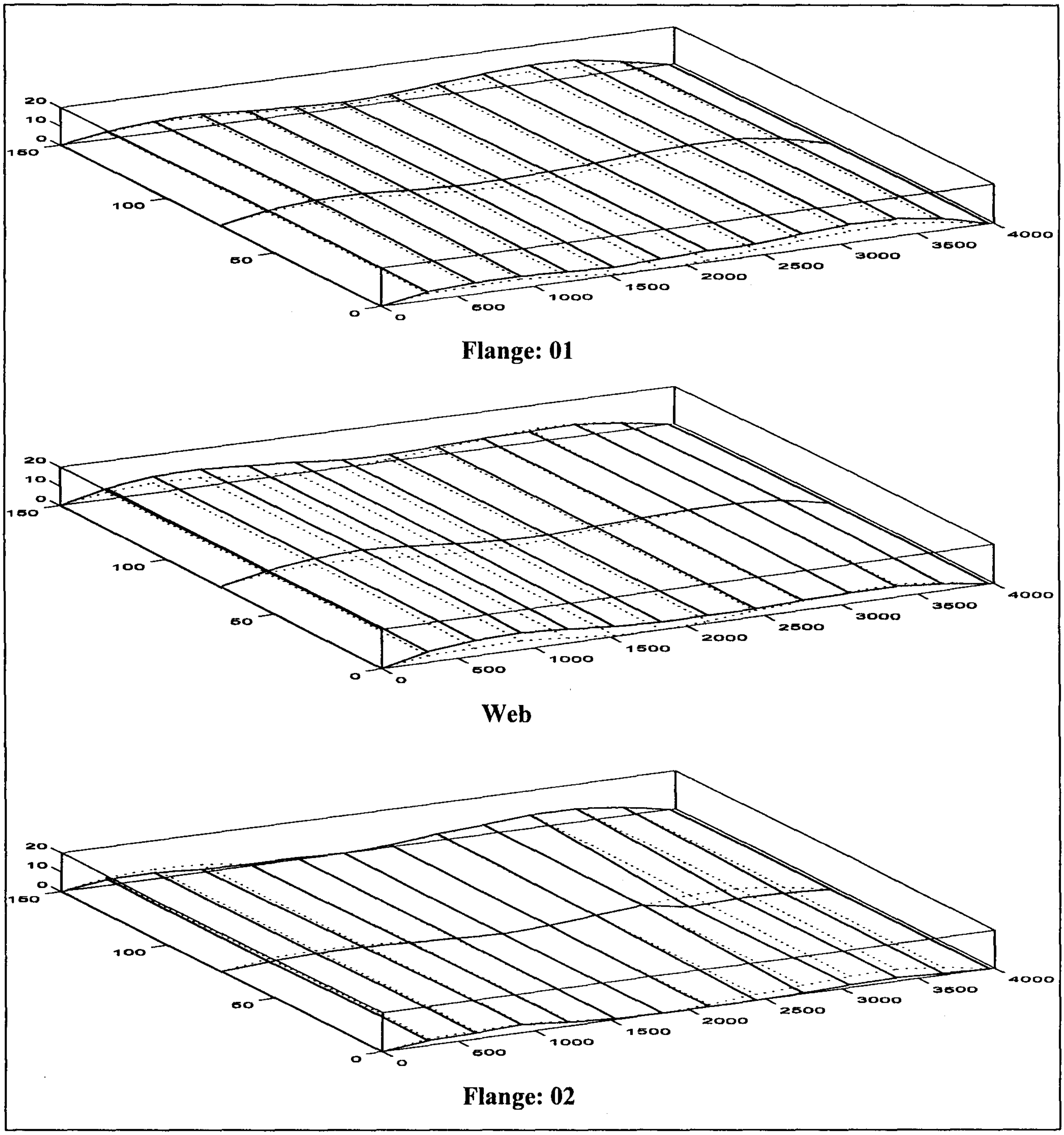

Figure 4.9: The Out-of-Surface Imperfections on Initial Plate-06 and Strips after Flame Cutting

(---- Out-of-Surface Imperfections on Original Plate — Out-of-Surface Imperfections on Plate Strips (After cutting))

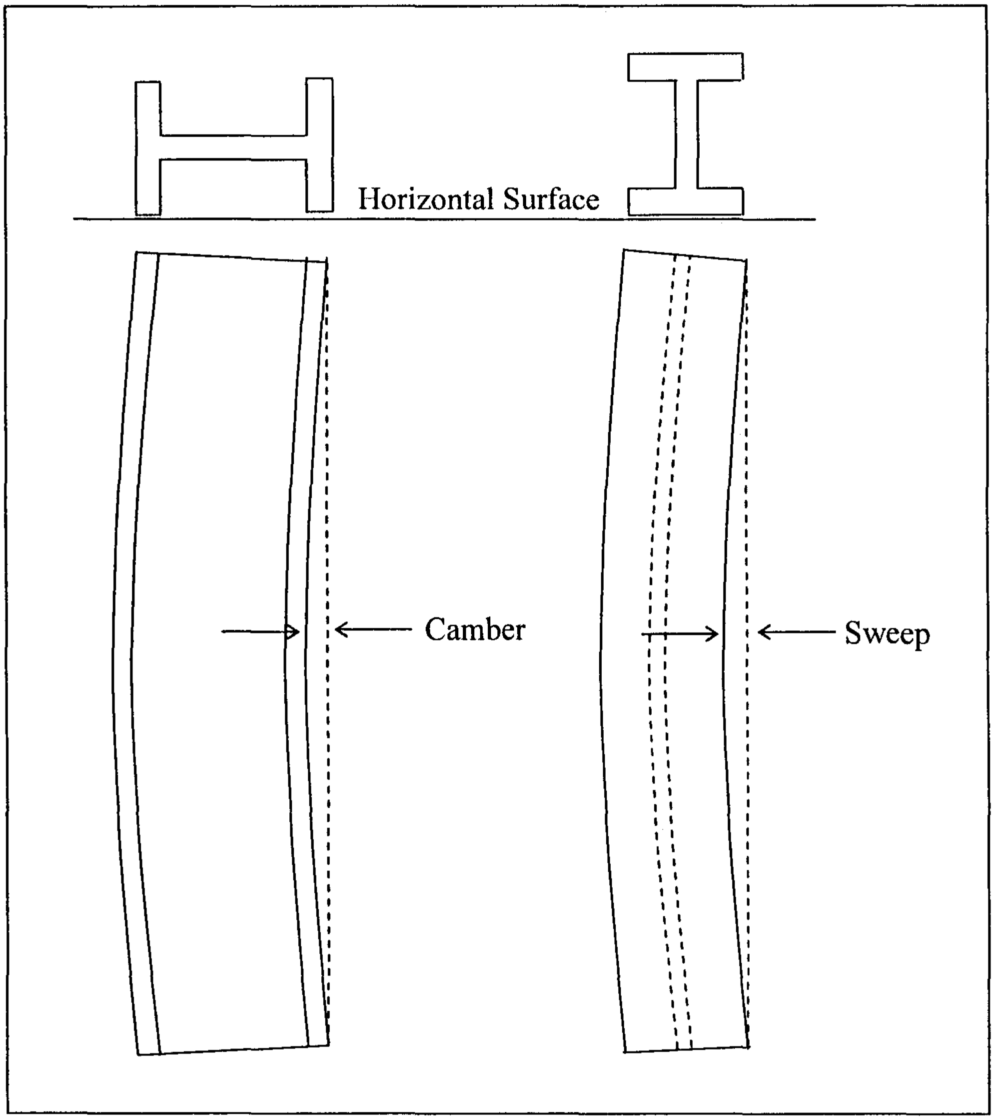

Figure 4.10: The Positions for Measuring Camber and Sweep

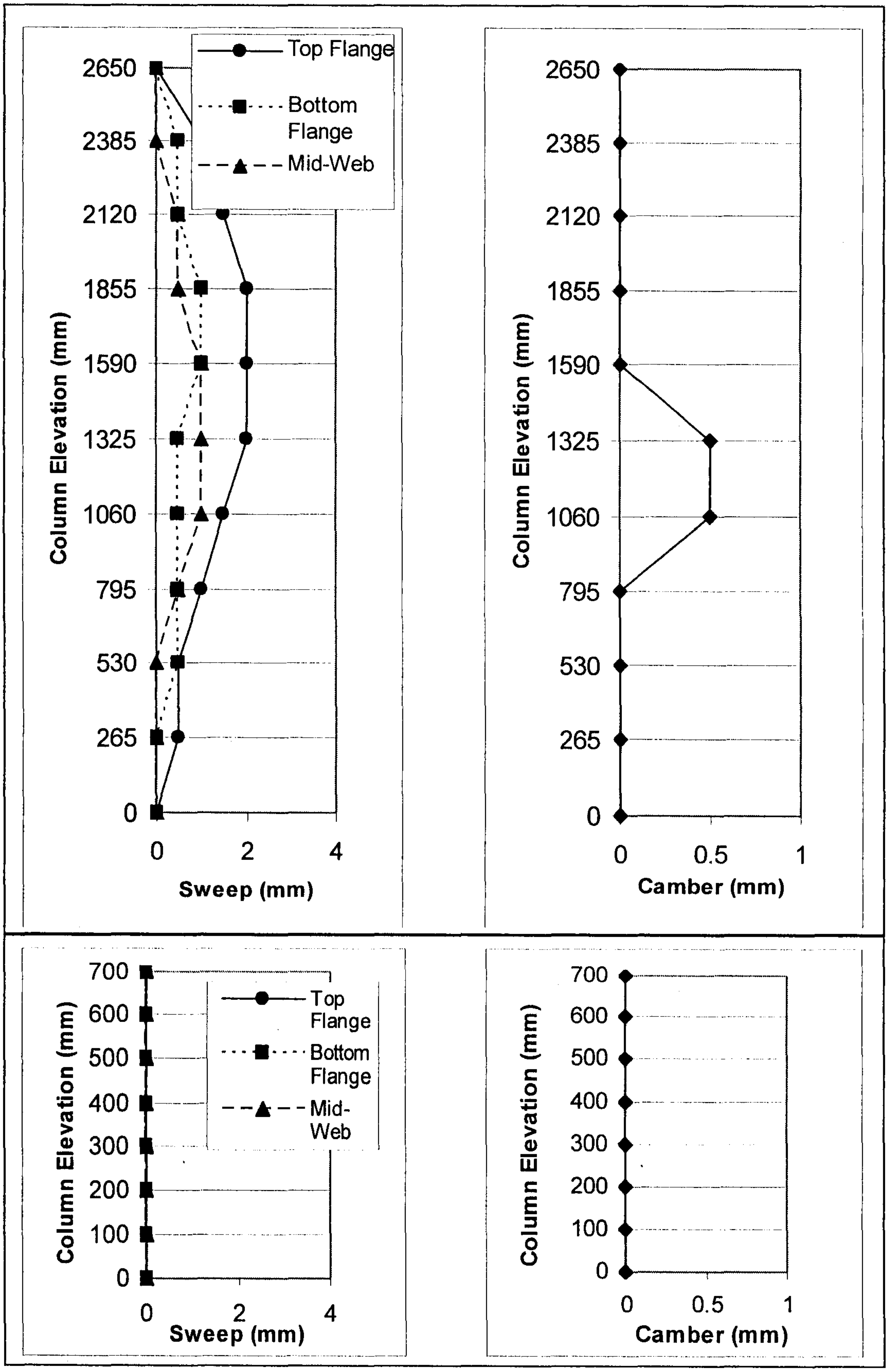

Figure 4.11: The Sweep and Camber of Long Column and Short Column from Plate-01

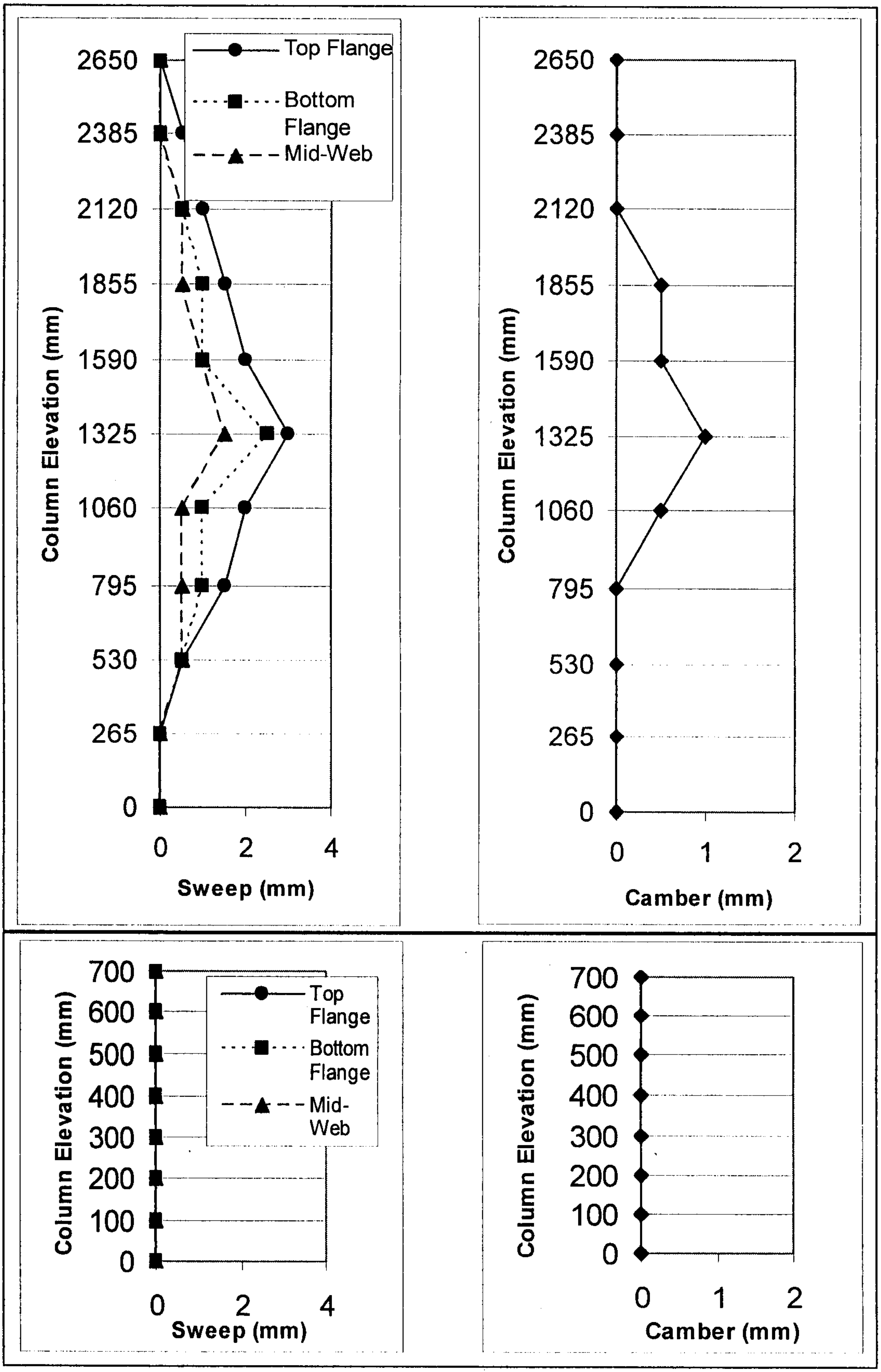

Figure 4.12: The Sweep and Camber of Long Column and Short Column from Plate-02

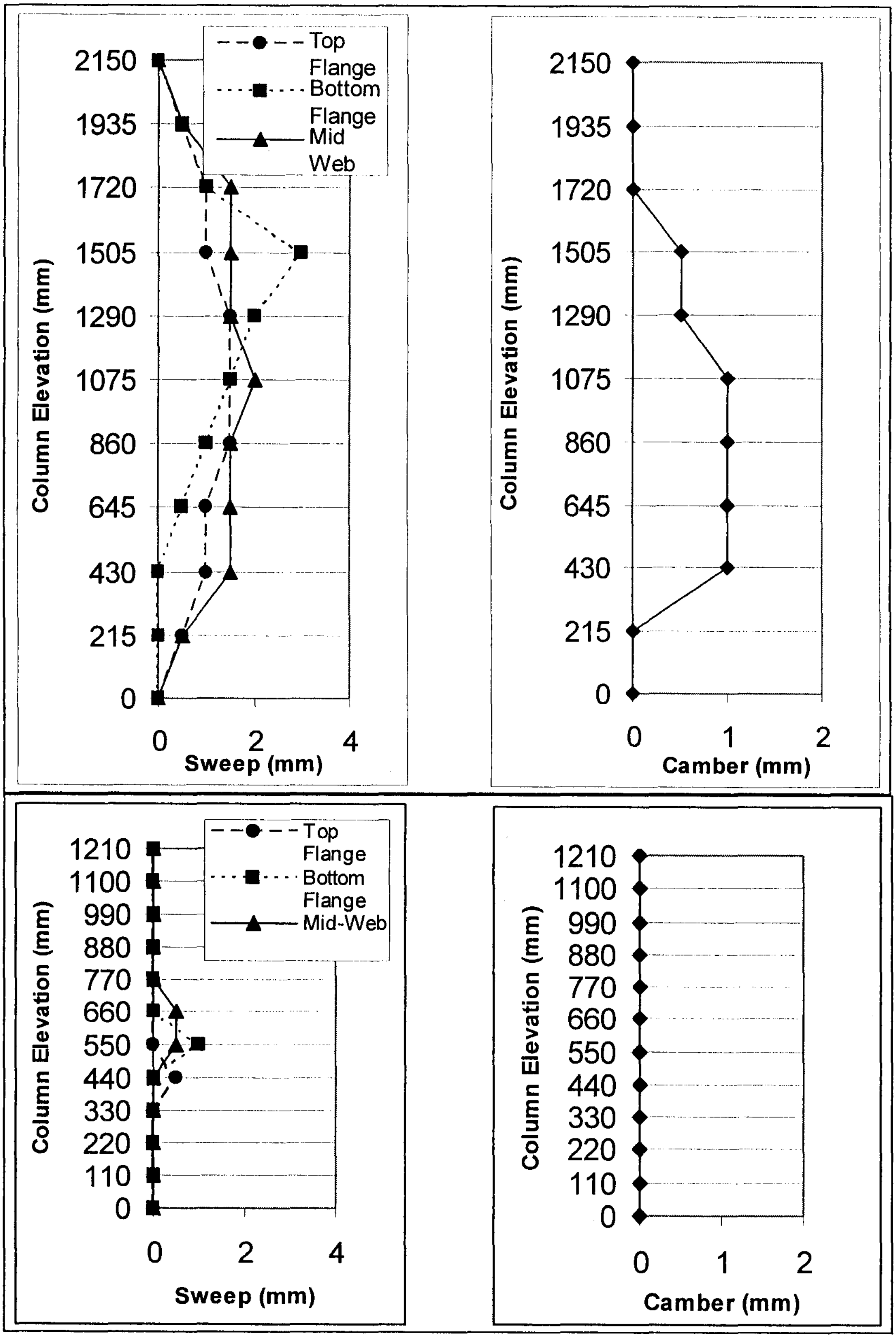

Figure 4.13: The Sweep and Camber of Long Column and Short Column from Plate-03

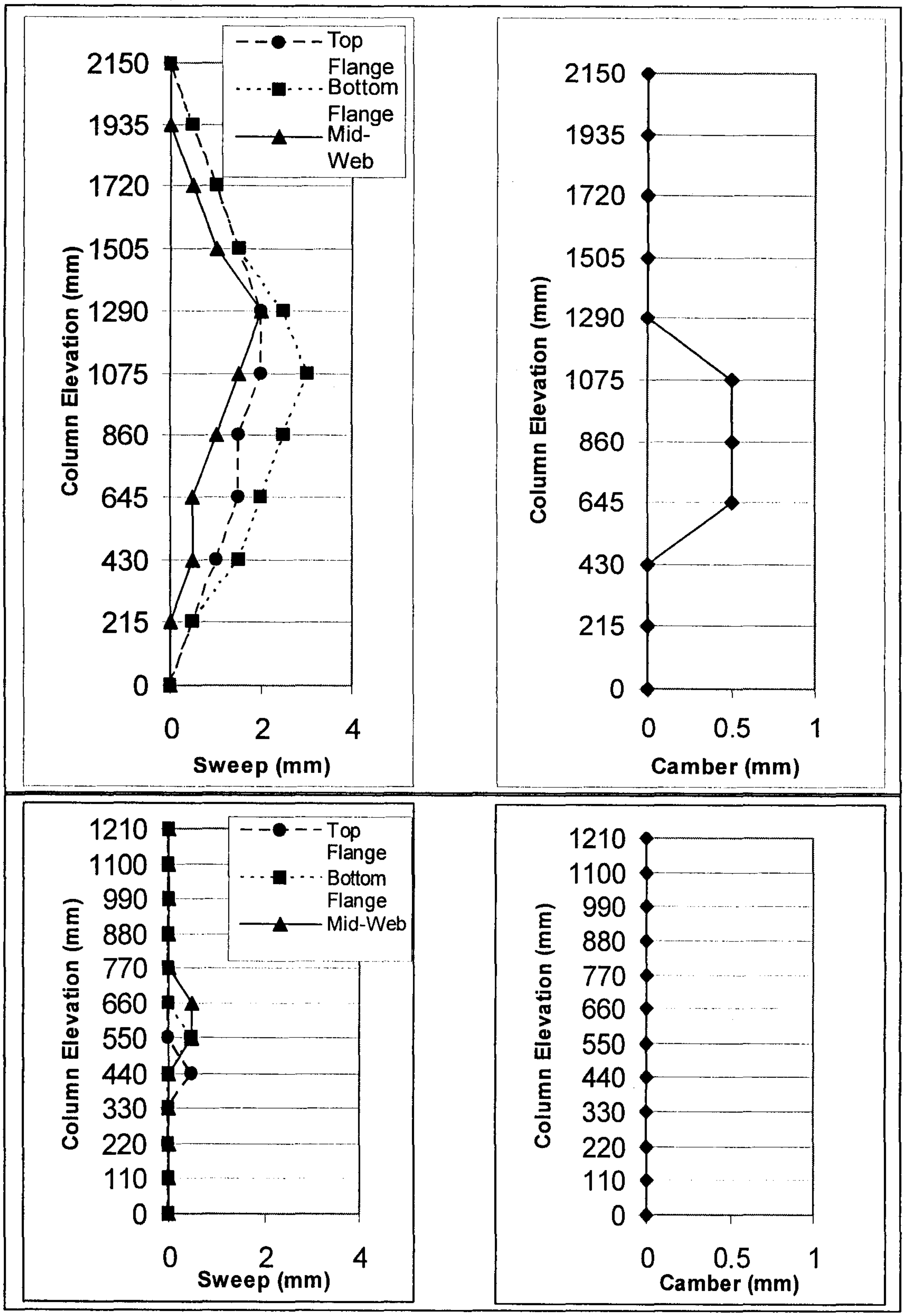

Figure 4.14: The Sweep and Camber of Long Column and Short Column from Plate-04

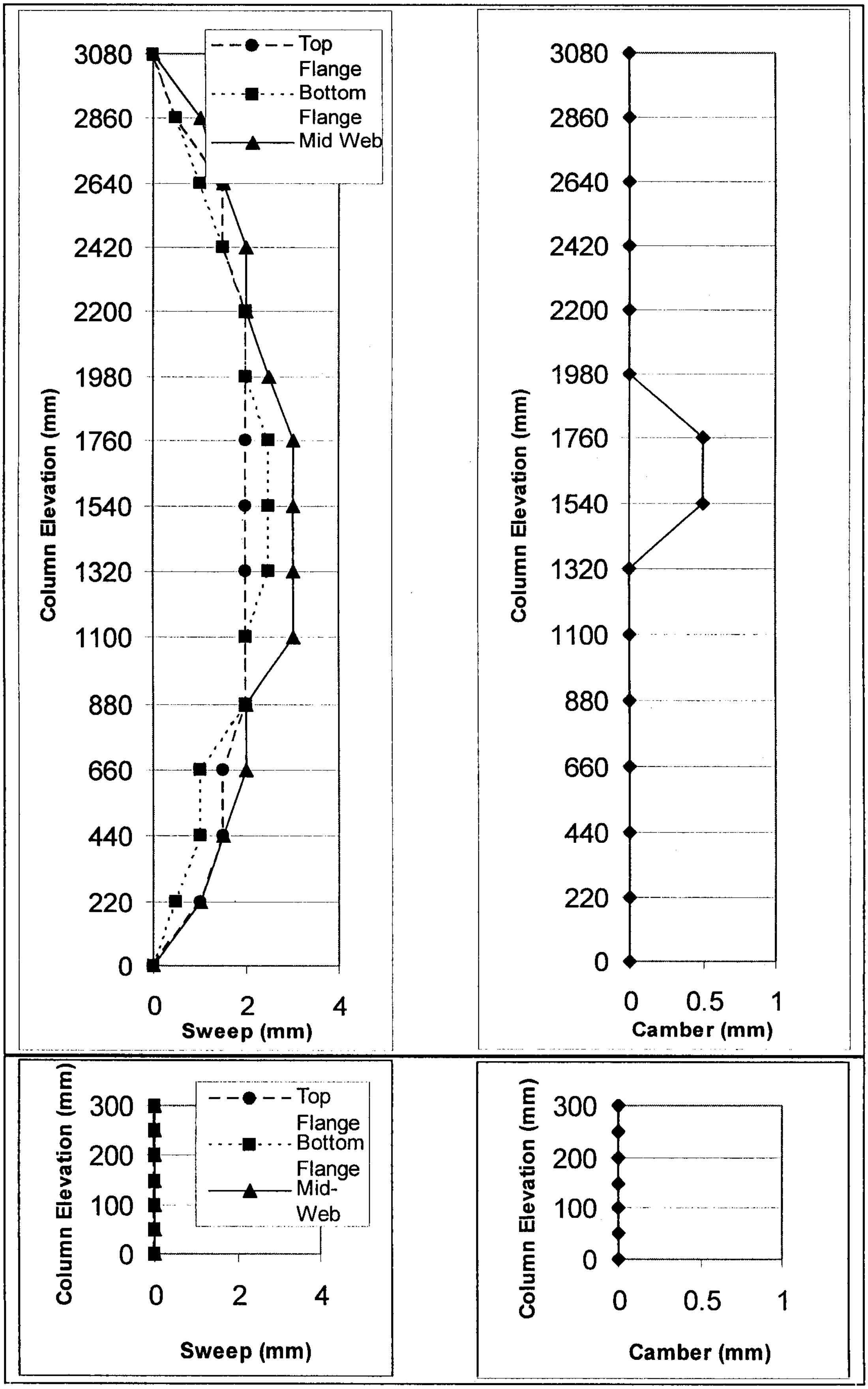

Figure 4.15: The Sweep and Camber of Long Column and Short Column from Plate-05

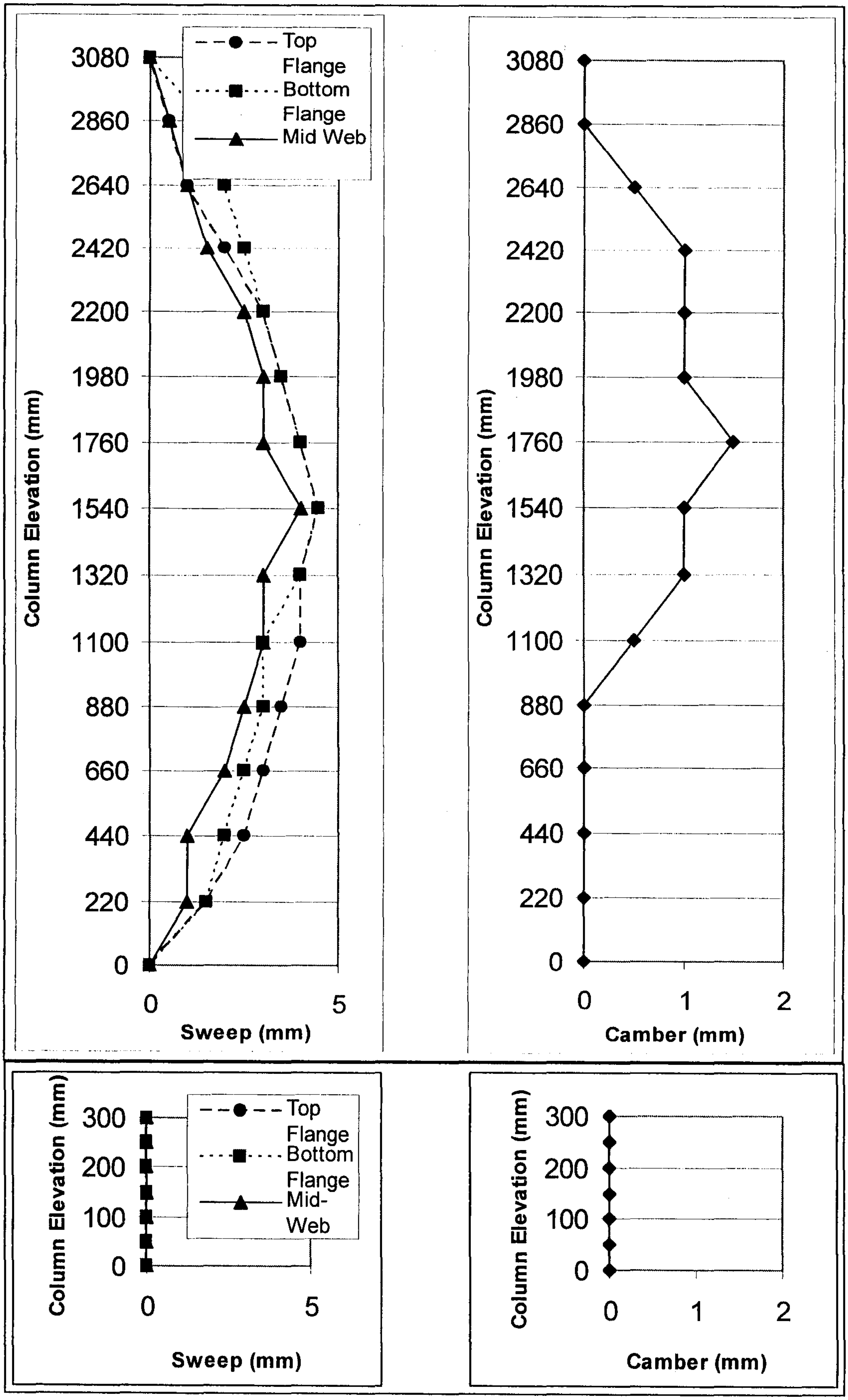

Figure 4.16: The Sweep and Camber of Long Column and Short Column from Plate-06

[A] Plasma Cut-Gas Metal Arc Welding Column | **[B] Flame Cut-Gas Metal Arc Welding Column**

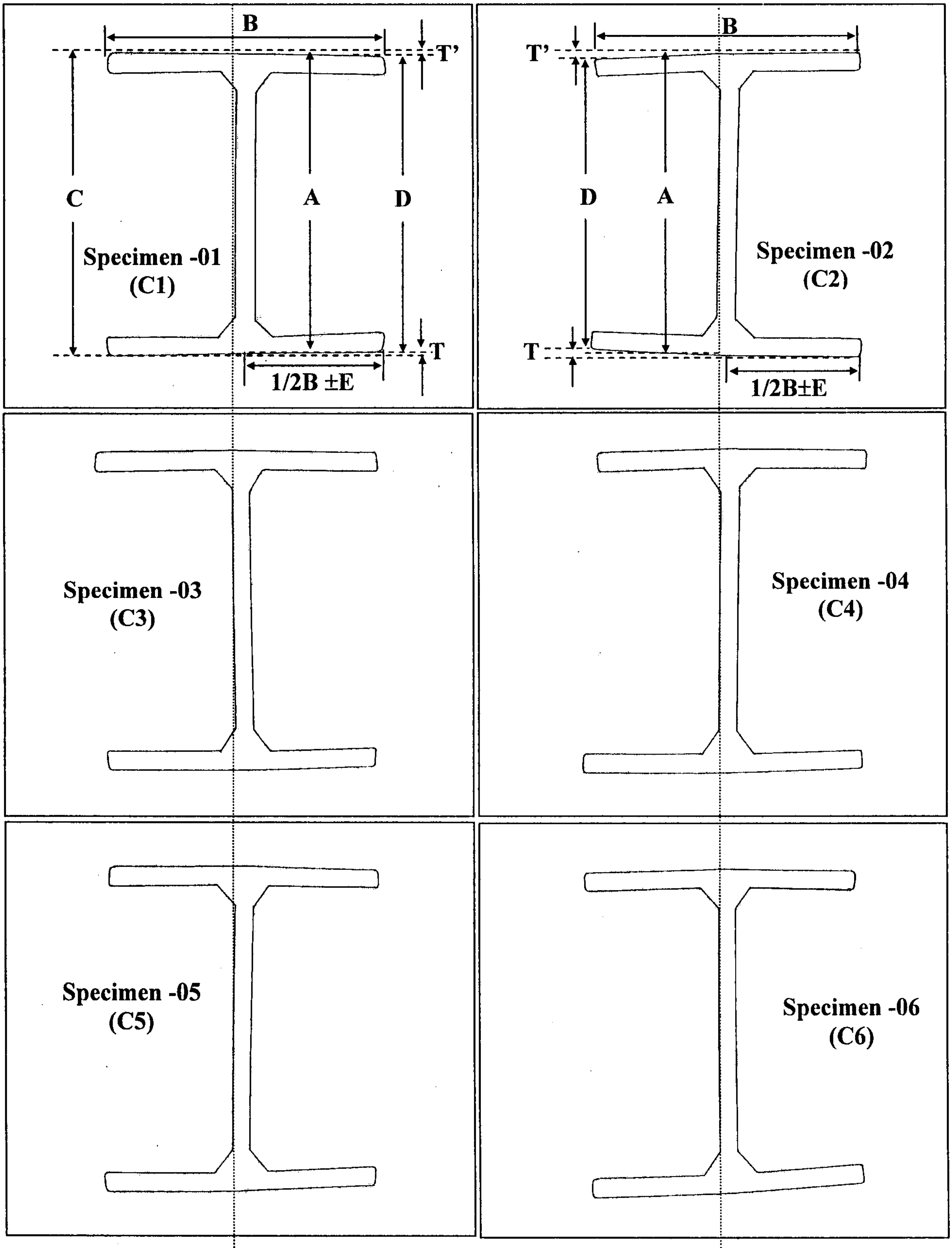

Figure 4.17: Typical Cross- Section Shapes of Column Specimens
(Obtained from One End of the Residual Stress Specimen)

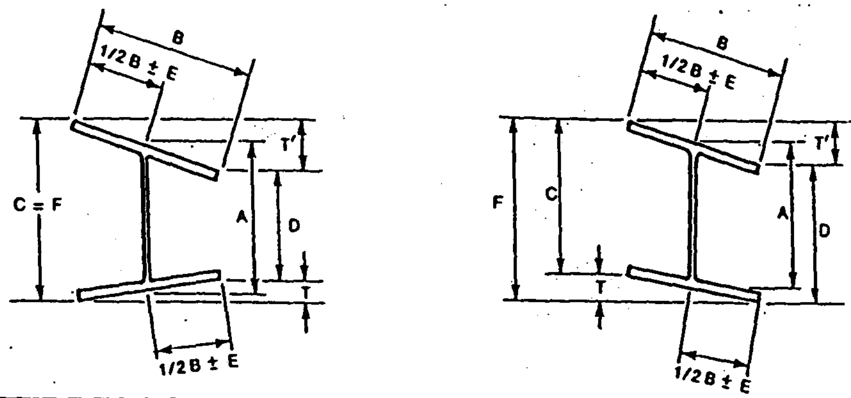

Nominal Depth, mm	Depth, A, mm		Width of flange, B, mm		Out-of-square T + T', mm	Out-of-parallel C–D, mm	Web off-centreline, E mm	Max. overall depth at any cross-section, F, mm
	Over	Under	Over	Under	Not over	Not over	Not over	Over nominal
300 and under*	4	3	6	5	6	5	5	6
Over 300	4	3	6	5	8	6	5	6

Figure 4.18: Permissible Variations in Sectional Dimensions of Wide-Flange Shapes (CISC Hand Book, 2004)

A is measure at the centerline of the web

B is the actual flange width and is measured parallel to the flange

F is measured parallel to the web

Chapter 5

RESIDUAL STRESSES

5.1 Introduction

Residual stresses can be defined as those stresses that remain in a material or body after manufacturing process in the absence of external forces or thermal gradients. In general, the formation of residual stresses in structural steel sections are mainly due to uneven cooling after rolling process and other fabrication processes such as cutting and welding operations. The magnitude and distribution of residual stresses vary depending upon the type of cross section, rolling temperature, cooling conditions, material properties, etc (Beedle and Tall, 1960). In most practical steel column sections, the presence of compressive residual stresses affects their load carrying capacity. The areas with compressive residual stresses in a column section will reach yield first, when an external compressive stress is applied. Yielded areas posses no stiffness, hence the section suffers a deterioration in stiffness, until the effective inertia is significantly reduced that buckling occurs. Therefore, the evaluation of residual stress distributions in column sections is a key factor in predicting the reliable value of the column strength based on analytical approaches.

This chapter describes various aspects of residual stresses in steel members and their measurement procedures. This chapter also provides the detailed description of pioneering tests that have been carried out in this investigation to (a) familiarize with the procedures associated with the "method of section" residual stress measurement technique (b) evaluate the applicability of the "method of section" technique and (c) to evaluate the appropriateness of the use of the "*Demec*" mechanical dial gauge. The procedures that have to be followed in the "method of section" residual stress measurement technique are explained in this chapter in detail. Finally this chapter concludes with the presentation, comparison, and discussion of the residual stress measurement results associated with steel members made using different fabrication techniques.

5.2 Residual Stress Measurement Methods

There exist a number of residual stress measurement techniques that are presently used in determining residual stresses present in different material such as metals, ceramics, plastics, polymers, ferromagnetic materials, and composite materials. Each of the methods has its own inherent advantages and disadvantages based on availability of the equipment, measurement speed, existence of standard procedure, the level of expertise required, portability, and cost. Hence, some of the methods are only applicable for a limited range of materials. The residual stress measurement methods can basically be divided into three categories depending upon the way they are used to measure the residual stresses. They are fully-destructive or destructive, semi- destructive or partial–destructive, and non-destructive methods. In the destructive and semi-destructive methods the residual stresses are determined from distortions caused by the removal of materials. The testing method is said to be semi-destructive when the amount of material removed is small compared to the initial volume of the specimen. In non-destructive method, no material distortion takes place.

<u>Hole-Drilling Method</u>: Hole-drilling is one of the most widely used semi-destructive techniques for measuring residual stresses. It is relatively simple, cheap, quick and versatile. Equipment can be laboratory based or portable, and the technique can be applicable to a wide

range of materials and components. The basic principle related to this method involves the introduction of a small hole into a component containing residual stresses and subsequent measurement of the locally relieved surface strains, assuming that the material is isotropic and linearly elastic. The state of stresses in any direction can easily be measured by using this technique. However, the technique suffers from limited strain sensitivity, potential errors and uncertainties related to the dimensions of the hole such as diameter, concentricity, profile depth, surface roughness, flatness and specimen preparation (Kandil et al., 2001).

Incremental hole-drilling improves the versatility of the technique and enables stress profiles and gradients to be measured. Since any residual stress relieved by the drilling process will adversely affect the results, it is important that suitable drilling method be chosen. Also the selection of suitable gauge type and size is very important in relation to the type of stress present. Figure 5.1 shows the typical arrangement of hole drilling apparatus and different types of strain rosettes currently used in this method. Strain gauge type A is the one most commonly used and recommended for general purpose measurements. Type B is useful where measurements need to be made near an obstacle or close to a fillet or radius. Type C uses six grids and it has been introduced recently to give improved strain sensitivity (ASTM, 2002).

<u>Curvature and Layer Removal</u>: The curvature and layer removal technique, which is referred to as a fully destructive technique, is often used for measuring the presence of residual stress in simple test-piece geometries. The method is generally quick and requires only simple calculations to relate the curvature to the residual stresses. When layers are removed from one side of a flat plate containing residual stresses the plate bends, due to unbalanced stresses. The

curvature depends on the original stress distribution present in the layer that has been removed and on the elastic properties of remainder of the plate. The distribution of stresses in the original plate can be deduced by measuring out a series of curvature measurements after successive layer removals.

The curvature of the specimen can be measured using a variety of methods including optical microscopy, laser scanning, strain gauges, or profilometry, depending on the resolution and range of the measuring instrument. Measurements are usually made in narrow strips to avoid multi-axial curvature and mechanical instability. Layer removal method is only applicable to plate samples. Stresses at or very near to the surface cannot be measured by this technique (Kandil et al., 2001).

Diffraction Based Methods:

(a) X-Ray diffraction: is one of the nondestructive methods available for measuring residual stresses. This method relies purely on the elastic deformation within a polycrystalline material to measure internal stresses in a material. The deformation causes changes in the spacing of the lattice planes from their stress free value to a new value that corresponds to the magnitude of the applied stress. This new spacing will be the same in any similar oriented planes with respect to the applied stress and the crystal lattice therefore effectively acts as a very small strain gauge. The measurement itself is relatively straightforward and equipment readily available. One of the major disadvantages with the X-ray diffraction method is the limitation imposed on the test piece size and geometry. The geometry has to be in such a way that an X-ray can both hit the measurement area and still be diffracted to the detector without hitting any obstructions. Surface roughness is also another concern with this technique. The speed of measurement depends on a number of factors including the type of material being examined, the X-ray source, and the degree of accuracy required (Kandil et al., 2001).

(b) Synchrotron: This method uses more advanced technology of X-ray diffraction method. Synchrotron or hard X-rays provide intensive beams of high energy X-rays and these X-rays have a higher depth penetration than conventional X-rays, typically around 50mm (2-inch) in aluminum. The increased penetration depth means that Synchrotron diffraction is capable of providing high spatial resolution with three dimensional maps of strain distribution to millimeter depths in engineered components. The measurement time is significantly less than that of conventional X-ray diffraction. The technique is based on laboratory tests and not widely available (Kandil et al., 2001).

(c) Neutron Diffraction: This measurement technique is almost same as the X-ray diffraction and Synchrotron methods. This method has capability of measuring stresses to high depth, 100mm (≈ 4-inch) in aluminum and 25mm (≈1-inch) in steel, with high spatial resolution. Also the Neutron diffraction can provide complete three dimensional strain maps of engineered components. This is achieved through translational and rotational movements of the component. This technique is more useful in validating the theoretical and numerical models for residual stress measurements since the technique has the capacity of collecting large amount of data, via position sensitive detectors, over the whole surface and depth, depending on the thickness of the sample. However, the availability of the technique is limited and relative cost is much higher compared to the other techniques, such as X-ray diffraction (Kandil et al., 2001).

Method of Section: This method is widely used in determining the residual stresses in structural steel shapes. This method is known as the destructive method, since the test specimen is totally sliced by sectioning. The "method of section" technique was firstly used in Fritz Laboratory, US, by Johnston and Luxion (1940). Using this method, the residual stress variation in longitudinal direction as well as the variation through thickness can be predicted. The variation of residual stresses through the thickness is usually not important in members having thickness of less than 25mm (1inch) and thus, the variation of residual stresses can reasonably be assumed as constant through the thickness of a member. However, this assumption is not valid for very thick members and cold-formed tubular members (SSRC Task Group, 1981).

The "method of section" technique has proven itself adequate, accurate and economical to obtain residual stress distributions in a steel member, if proper care is taken in the preparation of the specimen and the measurement procedure (Tebedge et al., 1973). The basic principle of the "method of section" is that the internal stresses are relieved by cutting the section into many longitudinal strips. A new state of equilibrium is formed after each cut during the cutting down process, since the residual stresses in the body are in equilibrium. Thus, the new state of equilibrium is directly associated with a change in the deformation state. The resulting strain is measured by employing either a mechanical dial gauge or strain gauge over the each strip. Subsequently the stresses are simply obtained by applying Hooke's law, since in general, the residual stresses present in structural steel members are within the elastic limit.

Moreover, the "method of section" technique is preferably applicable for measuring of residual stresses in the longitudinal direction, assuming that the transverse stresses are negligible and the cutting process itself produces no appreciable strains. Therefore this method is more suitable for measuring residual stresses in structural steel members. Because, the magnitude of the residual stresses as a result of thermal stresses during the fabrication process such as cutting plus welding and rolling (hot-rolled sections) operations are far greater in the longitudinal direction of a structural steel member than in any transverse direction (SSRC Task Group, 1981). Similarly, the magnitude of residual stresses as a result of cold-work stresses during cold-straightening process in rolled structural shapes and welded built-up shapes such as bent by gagging to remove camber or sweep or to introduce camber or sweep, rotary straightened process and etc is very high in longitudinal direction than in transverse direction (SSRC Task Group, 1981). As far as structural steel members are concerned, the residual stresses in longitudinal direction have a pronounced influence on the load carrying capacity of those members. For example, columns and plate structures built up by welding are severely influenced by these longitudinal residual stresses. Therefore, the technique so called "method of sectioning" is more appropriate to predict residual stresses in longitudinal direction in such members. Hence, this method is more cost effective and relatively straightforward procedures compared to other methods such as; Hole-Drilling, X-Ray diffraction, Neutron diffraction and etc.

The steps involved in the sectioning method are shown in Figure 5.2. In the first step, a specimen on which residual stress measurements are to be taken is cut from an original steel section. This step is called as "partial sectioning". In the second step called as "complete sectioning", slicing of flanges and web of the section are done by cutting. In the third step called as "slicing through thickness", the slicing through thickness is further done by cutting.

Note that the step related to "slicing through thickness" was not done in this investigation, since the thickness of flanges and web of the column sections were not relatively thick.

5.3 Residual Stress Measurements Using "Method of Section"

In this investigation, the technique called "method of section" was used to establish residual stress distributions. The residual stress measurements were taken on three W-shape steel columns, three plasma cut-welded H-shaped columns, and three flame cut-welded H-shaped columns. The residual stress measurements on W-shaped columns were done as three pioneering tests. Each of the pioneering tests in this investigation were done in order to come up with the more accurate specific procedure associated with the "method of section" technique, which was to be used in the subsequent residual stress measurements on other steel columns. The reasons why the "method of section" was chosen over the other measurement techniques in this investigation are given as follows,

1. As this investigation was concerned with establishing the strength of steel columns, the presence of residual stresses in longitudinal direction influences the strength of columns heavily than the presence of residual stresses in any other directions.
2. As discussed earlier, the magnitude of the residual stresses as a result of thermal stresses during cutting and welding operations is far greater in the longitudinal direction of a shape than in any transverse direction (SSRC Task Group, 1981).
3. The procedure associated with the "method of section" is very straight forward compared to other techniques such as hole-drilling and the diffraction methods.
4. The "method of section" technique is more cost effective than the other techniques.
5. No much skill workmanship is essentially needed in this method.

This chapter describes the general procedure for preparing a test piece for residual stress measurements using "method of section" technique. This chapter also provides the detailed description of each of the pioneering tests, the associated conclusions derived from these test, and the recommended procedures (specific procedure) for the "method of section" technique.

5.3.1 Pioneering Tests on W-shape Columns

General Preparation of a Test Piece: Firstly, the stock should be carefully examined for evidence of cold work prior to selecting the portion to be used for residual stress measurements. If the residual stresses due to thermal effects only are to be established, then the test piece should be cut from the portion of the original stock that does not have transverse cracks in the mill scale if any are present (Galambos, 1998). Such cracks are generally evidence that the member has been subjected to cold-straightening process, either by gagging or rotary straightening. Secondly, the length of the test piece for the subsequent residual stress measurements should be cut to a minimum length, equal to gauge length plus 50mm (2 inch). Thirdly, the location of the test piece along the original stock should be selected far enough from the ends to reduce end effects. Hence, a distance of 1.5 to 2 times the largest dimensions of the cross-section is preferred, though theoretically a ratio of 1.0 is sufficient. A gauge length of 250mm (10 inch) is recommended, because the larger the gauge length, the better the average strain will be obtained.

Finally, lines defining the longitudinal strips to be cut to release the lock-in strain (residual strain) during sectioning will be marked on the test piece. The number of longitudinal strips to be cut depends on the expected residual strain gradient and the needs of the investigation. After marking all grid lines, the gauge holes for the extensometer will be laid out. The test piece should be cold-sawed from the original stock at very low speed to avoid excessive vibrations and to reduce localized stresses that might occur due to the saw cut.

Pioneering Tests: There were three pioneering tests carried out in this investigation. As discussed earlier, each of the pioneering tests were done (a) to learn how the "method of section" is practically applied (b) to become familiar with the testing procedures associated with the residual stress measurements based on "method of section" technique and (c) to evaluate the appropriateness of the use of "*Demec*" dial gauge which was used throughout the tests in this investigation. For these purposes, three almost identical long I-shaped hot rolled sections having cross sectional dimensions of about 150x150mm (6x6 inch) were chosen. First, the original specimens were gently ground to remove rust appearing in the specimens, if any. Then, they were cut down at one of their ends by saw cut so that the lengths of the initial specimens were 1500mm.

(a) Pioneering Test-01: In the specimen for pioneering tets-01, a 305mm (12inch) length somewhere along the mid part of the specimen was selected as potential location for residual stress measurements. Because the previous studies have shown that the end effect can be eliminated by selecting the potential location for residual stress measurements far enough form the ends. A distance of 1.5 to 2.0 times the lateral dimension is recommended (Tebedge et al., 1973). However, the potential location for residual stress measurements in all pioneering tests was chosen somewhere in the mid-portion of specimens in this study. Then, grid lines were marked for sectioning the section for residual stress measurements. The locations of the gauge holes are shown in Figure 5.3. The width of each slice was selected to be about 13mm (1/2 inch). The gauge holes were, then centrally located using punch-fixture of 203mm (8 inch) length to reduce variation in gauge lengths. A series of gauge holes were laid out on the outer surface of flanges and on both sides of the web using manually operated hand-drill. The # 60 drill bit was used for drilling the gauge holes to a depth of about 3 to 5mm.

Some of the initial procedures, as described under "recommended procedure" in the next section, were followed before taking the initial readings. After taking the initial dial gauge readings, the test piece was separated from the original specimen, for which the sectioning was to be done for residual stress measurements. This cut was designated as "cut-01" in this investigation. As a point of interest, the gauge readings were taken at all locations after this first cut. No significant changes were observed, indicating that no significant residual strains were released during this first cut. Then, the web was separated from flanges for facilitating the sectioning process to be carried out in the next stage. This cut was designated as "cut-02" in this work. After this cut, the gauge readings were recorded and compared with the reading obtained after "cut-01". No significant changes in the readings were observed. However, slight differences were observed between the readings obtained after cut-01 and after cut-02. Finally, the sectioning was carried out by using a cold-saw cutting machine at very low speed in order to reduce the localized stresses that could be produced during the cutting operation itself. In this investigation, the final sectioning was designated as "cut-03". Eventually the gauge readings obtained from slices were recorded and thus the relieved strain corresponding to each of the slices was calculated.

(b) Pioneering Test-02: In the pioneering test-02, however, the residual stresses were measured with the mechanical dial gauge and electrical resistant strain gauge. The gauge length of electrical strain gauges used in this test was of 5mm. This test was done to confirm the applicability as well as reliability of the mechanical dial gauge, which was to be used throughout this research work to establish the residual stresses. This is why, in this test, the electrical resistant strain gauges were used for comparison purposes. Though the specimen preparation for second specimen was exactly same as that for the first specimen, additional care was taken in order to get a very smooth surface in the places where resistant gauges were to be attached. The Figure 5.3 also shows the locations of electrical-resistant strain gauges associated with the second specimen.

Based on the experiences gained from the first pioneering test, no intermediate readings after cut-01 and cut-02 were taken, but just observed for any significant variation, if any, from the data acquisition system which was used to pick up the readings that came out from the electrical resistant strain gauges. No significant variations in readings were observed after cut-01 and cut-02. The readings from the strain gauges were recorded in millivolts by the data acquisition system. Then, they were converted to strain using the relationship between strain and the input/output voltages for a "*quarter bridge circuit*". The readings, in this test too, were taken only on the outer surface of flanges, but on both sides of the web.

(c) Pioneering Tets-03: The initial procedure for a specimen preparation for the residual stress measurements was exactly same as that of specimen-01 and 02. However, in this test, a drill stand was used to hold the hand-held drill firmly as shown in Figure 5.4 Because, based on the experiences gained from the test-01 and 02, it was observed that the alignment of the gauge holes played a key role in the residual stress measurements. Therefore the drill-stand was subsequently selected to firmly hold the hand-held drilling machine to drill holes as close to normal to the surface as possible. Also, it was more convenient to drill holes through the thickness of flanges and the web. Note that the # 55 drill bit was used in this test.

In the pioneering test-03, sectioning was done by using water jet cut (see Figure 1.5) since the sectioning by cold-saw cutting was a more tedious operation, as observed from pioneering test-01 and 02. The heat generation during water jet cutting is less than the heat generation during the saw cutting. Thus, the localized stresses produced during cutting operation itself could be reduced. Moreover, the sectioning by water jet cutting was much faster than that by saw cutting. The results obtained from pioneering test-1, 2, and 3 are shown in Figure 5.5.

Conclusions Derived from the Pioneering Tests:

1. The residual stress measurements be preferably taken on both sides of flanges and the web.
2. The # 55 drill-bit was more compatible with the peg points of the "*Demec*" mechanical dial gauge used in this investigation.
3. The gauge holes had to be drilled as close to normal to the surface as possible, which was hard to achieve by manually operated hand-drill, without drill-stand.
4. The sequence of cutting had no influence on the final results.
5. From the pioneering test-02, it was confirmed that the mechanical dial gauge could be reliably used for subsequent residual stress measurements. This was ensured by comparing the results obtained from the electrical strain gauge readings and mechanical dial gauge readings.

6. Water jet cutting was selected as the cutting tool for sectioning welded built-up sections in this investigation.

5.3.2 Recommended Procedure

The procedure given herein as "recommended procedure" was basically derived from the observations and experiences gained through three pioneering test in this investigation. The same procedure was followed in the subsequent work associated with establishing residual stresses for the welded built-up column sections fabricated from plasma cut plates and flame cut plates in this investigation.

The Procedure Followed in This Investigation (Specific Procedures): After selecting the portion as a potential location for residual stress measurements along the column section, the grid lines were marked along the edges of each of the strips to be sectioned for relieving residual strains present in the column section. It was selected in this investigation that the width of each of the strips was to be about 13mm (1/2 inch). The centers of the gauge holes were located within the strip by using a punch fixture available with the "Demec" dial gauge kit. This was done to reduce variations in gauge lengths. Then a center punch was used to enlarge the holes marked by the punch fixture. These enlarged holes served to guide the drill bit during drilling operation.

Significant care was taken to prepare gauge holes, since the accuracy in the reading depends heavily upon the type of gauge holes. The #60 and #55 drill bits were used to drill gauge holes in the first two pioneering tests and the third pioneering test, respectively. However, #55 drill bit was selected in this investigation as an appropriate size of drill bit for subsequent work. Gauge holes were drilled using hand-drill machine connected to a drill-stand as shown in Figure 5.3 since it was preferable to drill holes as close to normal to the surface as possible for obtaining more reliable results. In the first two pioneering tests, gauge holes were laid out only on the outer surface of flanges, but on both sides of the web. The depth of the gauge holes were about 3 to 5mm.

Closer attention was given to the initial readings, since these cannot be duplicated after the specimen has been cut. Therefore some certain initial procedures were followed repeatedly in each of the tests before taking the initial readings as below:

1. Chamfering the gauge holes by using sharpening stone to remove burrs from the drilling operation.
2. Cleaning the gauge holes using compressed air blaster and then Alcohol and again air blaster.
3. Placing the standard bar and the reference bar on the specimen for about an hour to stabilize the temperature of the bars (standard bar and reference bar) and the specimen to almost the same condition.
4. Recording the temperature of working place just before taking initial measurements.
5. Taking dial gauge readings from the standard bar and the reference bar.
6. Taking five sets of measurements for each gauge length unless great variation persists, in which case making a new set of holes would be preferred.
7. Taking intermediate readings on the standard bar and the reference bar to make sure whether any temperature changes during the period of measurements.
8. Protecting the gauge holes from damage which may occur during moving, handling, sawing, etc.

Since the main source of error could result from temperature changes, the standard bar of the same material as the test member was used to eliminate the error due to temperature variations. In addition to that, measurements were performed in places, where the temperature was found to be fairly uniform in order to maintain experimental accuracy.

5.4 Residual Stresses in Welded Built-Up Sections

General Description

There were six identical columns of 3962mm (156 in) in length fabricated from six rolled steel plates obtained from the same production batch. Firstly, the web and flange pieces were cut to size from the original plates such that the final width was about 150mm. In this study, three columns were fabricated from flame cut plates and the other three were from plasma cut plates. The cut pieces from the same plate were finally welded together using gas metal arc welding procedure to form a H-shaped column. The columns numbered herein as C1, C3, and C5 were fabricated from plasma cut plates while the columns numbered as C2, C4, and C6 were fabricated from flame cut plates.

Before bringing the plates to fabrication shop for cutting, the plates were marked with grid lines and drilled holes using a hand-drill attached to the drill-press. Figure 2.2 in Chapter 2 shows the locations for residual stress measurements, stub column, and intermediate column as well as the locations for temperature measurements during cutting and welding operations. The # 55 drill bits were used to drill holes through the thickness of plates. Then, the procedure as described under "residual stress measurement procedures" was carried out step by step and finally the initial set of readings was recorded. Also the standard bar readings, reference bar readings, and temperature of working area were recorded for corrections associated with temperature changes. Figure 5.6 shows the specimens for residual stress measurements. Figure 5.7 shows slices for final residual stress measurements after sectioning was done by water jet cutting.

Procedure and Accuracy of Measurements

The "*Demec*" mechanical extensometer with the least count of 1.01×10^{-5} strain was used throughout this experimental work. In this investigation, dial gauge readings were continuously taken as the plates were going through the various stages of fabrication process. Firstly, the gauge readings were taken on the original plate (*stage: 01*). Secondly, the dial gauge readings were taken after the original plate was cut to size as flanges and the web by plasma cut and flame cut (*stage: 02*). Thirdly, the gauge readings were carefully taken after the H-shaped section was formed by Gas Metal Arc Welding (GMAW) process (*stage: 03*). Fourthly, a 305mm (12 inch) specimen in which the final sectioning was to be made for the residual stress measurements was cut by cold-sawing from the long column section and then the gauge readings were monitored (this cut was named as cut-01 in this research work). As a part of the observations, the change of the readings monitored after cut-01 was compared with the readings obtained in stage: 03 to see whether any significant changes occurred. There were no significant changes observed at this point. Then, the flanges and the web of the specimen were separated from each other before performing the final sectioning (this cut was named as cut-02 in this research work). This was done to facilitate the sectioning process easy. The gauge readings were monitored at this stage too (after separating the flanges from the web). However, no significant changes of gauge readings observed at this stage when comparing with the readings obtained in stage: 03. Thus, it could be concluded that relatively no significant strain was released through this separation. Finally, the sectioning was done by water jet cutting and the readings from the each slice were carefully recorded (*stage: 0*). Every time before taking the dial gauge reading, the cleaning procedure as mentioned previously in this chapter, was performed.

In the sectioning method the main sources of error can be as a result of temperature changes (Tebedge et al., 1973). This is because the mechanical dial gauge is very sensitive to temperature changes. However, temperature changes during readings may be practically eliminated by using a reference bar of the same material as the test member. In this investigation, temperature of the working place was measured whenever the dial gauge readings were taken in each of the stages. It was observed that the temperature of the working place was consistent. However, the reference bar reading was noted every time before taking the dial gauge measurements using the '*Demec*'extensometer. It was also noted that the gauge readings obtained from the reference bar were relatively consistent, and thus it could further be evidenced that the temperature variation of the working place was not significant in this investigation. The reference bar was placed on the test member for at least one hour ahead of time to stabilize the temperature of reference bar to that of test member (keeping the same environment for the reference bar and the test member). This was done because the response of the test member and the reference bar may not be identical for the same variation of room temperature. The reference bar responds fairly closely to the actual variation, while a big specimen responds with less fluctuation and with considerable time lag (Tebedge et al., 1973). The gauge readings from a standard bar were also noted intermittently to ensure the mechanism of the extensometer with the dial system worked properly throughout the measurements.

Furthermore, the experimental errors can arise from some additional factors, such as curvature of strips sliced at regions of high stress gradients, effects of lost motion when the motion is in the opposite direction, and whenever the axes of the drilled hole and the conical gauge point do not coincide. However, the curvature correction does not have significant influence on relatively thick slices (Galambos, 1998). The other errors may be minimized by taking more readings for each gauge length (Tebedge et al., 1973). Therefore, in this study five readings were taken for each gauge length. In case, if the gauge readings were not in the acceptable range for any of the gauge lengths, a new set of gauge holes would be laid out until the readings were reasonably steady.

5.4.1 Presentation of Residual Stress Results

As discussed earlier, the residual stress distributions in welded H-shape column sections were established by use of "method of section" technique in this investigation. In this method, stresses are simply calculated using Hooke's law. That is, the residual stress at a particular location is calculated from measured strain which is multiplied by the elastic modulus (E). In this investigation the elastic modulus of 200 GPa was used since this value can reasonably be assumed to represent the average value for the entire cross section of a column section. For clear understanding, the different stages of residual stress measurements associated with different stages of fabrication process are defined as follows,

Stage (0):- Defined as the dial gauge measurements taken after final slicing (used as reference value for calculating residual stresses in column section, plate strips after cutting, and the original plate)

Stage (1):- Defined as the dial gauge measurements taken from initial plates

Stage (2):- Defined as the dial gauge measurements taken from plate strips (after cutting)

Stage (3):- Defined as the dial gauge measurements taken from column sections (after welding)

The released residual strains associated with a column section were calculated by considering the differences of dial gauge readings between stage (3) and stage (0) and then, the differences were multiplied by elastic modulus (E) of 200 GPa. The released residual strains associated with the plate strips (after cutting) were calculated by considering the differences of dial gauge readings between stage (2) and stage (0). Similarly, the released residual strains associated with the original plate were calculated by considering the differences of dial gauge readings between stage (1) and stage (0).

The residual stress measurements were taken on both faces of plate, plate strips (after cutting as well as the flanges and web of column sections (after welding). However, only outer surface measurements were taken at the flange-web junctions of a column section. It was, because unable to reach the gauge hole which was located on the inner-surface of the flange besides the flange-web junction in this investigation.

Figures 5.8 through 5.13 show the residual stress distributions measured on both faces of flanges and the web of six column specimens. The general variation of residual stress distributions measured on inner and outer surfaces of flanges of each column specimen seemed to be within a reasonable fashion. Therefore, it can be concluded that the residual stresses at the flange-web junction measured on the outer flanges would be a reasonable representation of residual stresses at those locations, even though only one measurement was taken.

The residual stresses associated with welded H-columns fabricated from plasma cut plate strips are presented graphically as shown in Figures 5.14 through 5.16. The residual stresses associated with welded H-columns fabricated from flame cut plate strips are as shown in Figures 5.17 through 5.19. It was noticed that for both sections fabricated from plasma cut plate strips and flame cut plate strips, the residual stresses had the same general distributions, i.e., the regions of tensile or compressive residual stress occurred near the same locations. The maximum averaged values of tensile and compressive residual stresses measured at flange tips, web-flange junction, somewhere along the web and flanges are given in Table 5.1. The main difference observed between these two shapes was in the magnitude of the residual stresses at the flange tips. Moreover, the web portion of all specimens seemed to have tensile residual stresses. The maximum tensile residual stresses observed in the web of all specimens were to occur near to the flange-web junction.

(a) Residual Stresses in Column Sections

<u>Plasma Cut Steel Column Sections</u>:

Column Section- 01: Figure 5.8 shows the variation of residual stress distributions over the cross-section of column section-01. The magnitudes of residual stresses shown herein are for both faces (inner and outer faces) of flanges and the web of the H-shaped sections, except at the flange-web junctions. From the Figure 5.8, it can be observed that the high intensity of tensile residual stresses was observed in the vicinity of flange tips and the flange-web junctions. Considering all the outer flange tips, the largest tensile residual stress was about 90MPa. Similarly, considering all the inner flange tips, the largest residual stress was about 88MPa. The middle portion of the flanges seemed to have approximately uniform compressive residual stresses. Considering all the outer flange-middle portion, the largest compressive residual stress was about 130MPa, whereas it was about 140MPa considering all the inner flange-middle portion. Moreover, the largest tensile residual stress of about 143MPa was measured, considering all the flange-web junctions.

Column Section- 03: Figure 5.9 shows the variation of residual stress distributions over the cross-section of column section-03. The high intensity of tensile residual stresses was observed in the vicinity of flange tips and the flange-web junctions. The largest tensile residual stress was about 76MPa, considering all the outer flange tips, whereas it was about 86MPa, considering all the inner flange tips. The largest compressive residual stress was about 150MPa, considering all the outer flange-middle portions, whereas it was about 120MPa, considering all the inner flange-middle portions. Moreover, the largest tensile residual stress of about 152MPa was measured in the vicinity of the flange-web junctions, considering all the flange-web junctions.

Column Section- 05: Figure 5.10 shows the variation of residual stress distributions over the cross-section of column section-05. The high intensity of tensile residual stresses was observed in the vicinity of flange tips and the flange-web junctions. The largest tensile residual stress was about 104MPa, considering all the outer flange tips, whereas it was about 92MPa, considering all the inner flange tips. The largest compressive residual stress was about 133MPa, considering all the outer flange-middle portions, whereas it was about 141MPa, considering all the inner flange-middle portions. The largest tensile residual stress of about 135MPa was measured in the vicinity of the flange-web junctions, considering all the flange-web junctions. It was noted in specimen-05 that the residual stress measurement taken from the inner Flange: 01 at location 9 was ignored since that value was unreasonable.

Flame Cut Steel Column Sections:

Column Section- 02: Figure 5.11 shows the variation of residual stress distributions over the cross-section of column section-02. The high intensity of tensile residual stresses was observed in the vicinity of flange tips and the flange-web junctions. The largest tensile residual stress was about 172MPa, whereas it was about 169MPa, considering all the outer and inner flange tips, respectively. The largest compressive residual stress was about 165MPa, considering all the outer flange-middle portions, whereas it was about 141MPa, considering all the inner flange-middle portions. The largest tensile residual stress of about 139MPa was measured, considering all the flange-web junctions.

Column Section- 04: Figure 5.12 shows the variation of residual stress distributions over the cross-section of column section-04. The high intensity of tensile residual stresses was observed in the vicinity of flange tips and the flange-web junctions. The largest tensile residual stress was about 104MPa and 92MPa, considering all the outer flange tips and inner flange tips, respectively. The largest compressive residual stress was about 133MPa and 141MPa, considering all the outer flange-middle portions and inner flange-middle portions, respectively. The largest tensile residual stress of about 135MPa was measured, considering all the flange-web junctions.

Column Section- 06: Figure 5.13 shows the variation of residual stress distributions over the cross-section of column section-06. The largest tensile residual stress was about 130MPa, considering all the outer flange tips, whereas it was about 143MPa, considering all the inner flange tips. The largest compressive residual stress was about 155MPa and 137MPa, considering all the outer flange-middle portions and inner flange middle portions, respectively. The largest tensile residual stress was about 155MPa, considering all the flange-web junctions.

(b) *Residual Stresses in Plate Strips (After Cutting)*

As discussed earlier, three plate strips having the dimensions of 3960mm long, 150mm wide, and 9.5 mm thick were cut from the original steel plate having the dimensions of 3960mm long, 710mm wide, and 9.5mm thick. The plates designated herein, as plate-01, -03 and 05 were cut by plasma cutting. The plates designated herein, as plate-02, -04 and 06 were cut by flame cutting. As a continuous part of this investigation, the gauge hole measurements on each plate strips were taken. Before taking the gauge hole measurements, the procedures described under "recommended procedure", which is given in this chapter was followed. As discussed earlier, the residual stresses associated with plate strips were calculated based on the readings obtained in stage (2) and stage (0) in this investigation. The influence of plasma cutting and flame cutting operation in creating the residual stresses during the fabrication of structural steel columns in this investigation are shown in Figures 5.14 through 5.19. As a general observation, the high intensity of tensile residual stresses was formed near to the cutting edges. Moreover, the residual stresses in the middle region of each plate strips seemed to have compressive residual stresses, except at some locations.

<u>Plate Strips Cut by Plasma Cutting</u>

Plate-01: Figure 5.14 shows the average residual stress variation in each plate strips after cutting. The maximum tensile and compressive residual stresses measured in the plate strip named as Flange: 01 in this investigation, were 69MPa and 57MPa, respectively. However, in the plate strip named as Flange: 02, the maximum tensile and compressive residual stresses were 67MPa and 62MPa, respectively. In the plate strip used as Web in this investigation, the maximum values of compressive and tensile residual stresses were 63MPa and 62MPa, respectively.

Plate-03: Figure 5.15 shows the average residual stress variation in each plate strips after cutting. The maximum tensile and compressive residual stresses measured in the plate strip named as Flange: 01 were 73MPa and 58MPa, respectively. However, in the plate strip named as Flange: 02, the maximum tensile and compressive residual stresses were 65MPa and 60MPa, respectively. In the plate strip used as Web, the maximum values of compressive and tensile residual stresses were 61MPa and 53MPa, respectively.

Plate-05: Figure 5.16 shows the average residual stress variation in each plate strips after cutting. The maximum tensile and compressive residual stresses measured in the plate strip named as Flange: 01 were 79MPa and 53MPa, respectively. However, in the plate strip named as Flange: 02, the maximum tensile and compressive residual stresses were 50MPa and 47MPa, respectively. In the plate strip used as Web in this investigation, the maximum values of compressive and tensile residual stresses were 68MPa and 39MPa, respectively.

Plate Strips Cut by Flame Cutting

Plate-02: Figure 5.17 shows the average residual stress variation in each plate strips after cutting. The maximum tensile and compressive residual stresses measured in the plate strip named as Flange: 01 were 137MPa and 65MPa, respectively. However, in the plate strip named as Flange: 02, the maximum tensile and compressive residual stresses were 154MPa and 68MPa, respectively. In the plate strip used as Web, the maximum values of compressive and tensile residual stresses were 124MPa and 55MPa, respectively.

Plate-04: Figure 5.18 shows the average residual stress variation in each plate strips after cutting. The maximum tensile and compressive residual stresses measured in the plate strip named as Flange: 01 were 137MPa and 55MPa, respectively. However, in the plate strip named as Flange: 02, the maximum tensile and compressive residual stresses were 120MPa and 68MPa, respectively. In the plate strip used as Web, the maximum values of compressive and tensile residual stresses were 69MPa and 44MPa, respectively.

Plate-06: Figure 5.19 shows the average residual stress variation in each plate strips after cutting. The maximum tensile and compressive residual stresses measured in the plate strip named as Flange: 01 were 126MPa and 121MPa, respectively. However, in the plate strip named as Flange: 02, the maximum tensile and compressive residual stresses were 123MPa and 42MPa, respectively. In the plate strip used as Web, the maximum values of compressive and tensile residual stresses were 97MPa and 70MPa, respectively.

(c) *Residual Stresses in Initial Plate*

The residual stresses associated with initial steel plate (3960mmx710mmx9.5mm) was calculated using the gauge readings obtained in stage (1) and stage (0) in this investigation. Also, the Figures 5.14 through 5.19 show the residual stress variation associated with initial steel plates. The maximum compressive residual stresses measured in plate-01, -03, -05 were 48MPa, 49MPa, and 50MPa, respectively. There were no tensile residual stresses observed in all these three plates. Similarly, the maximum compressive residual stresses measured in plate-02, -04, -06 were 50MPa, 46MPa, and 57MPa, respectively. The maximum tensile residual stresses measured in plate-02 and plate-06 were 28MPa and 19MPa, respectively. However, no tensile residual stress region was observed in plate-04.

On the whole, the observations derived from the residual stress measurements can be given as follows:

1. The residual stresses were almost invariant along the sections made by the same fabrication technique
2. The residual stresses due to cutting operation were heavily influenced closer to cutting edges.
3. Tensile residual stresses were obtained at the flange tips, the flange-web junctions, and the web portions for both sections made from plasma cut plates and flame cut plates. This was because the high heat input was delivered to the edges of flanges during cutting operation. Also, at the juncture of the flange and the web, the effect of the welds on the section was clearly evident in the higher tensile residual stress due to the delivery of high heat input during the welding operation.
4. The measured tensile residual stresses at the flange-web junction was almost the same for the plasma cut columns and the flame cut columns, as the high heat input from welding overrides the heat input from different cutting operations
5. The residual stress distributions in the web portion of plasma cut sections and flame cut sections were almost identical and hence, the manner of preparing the edge of the plate strip used as the web, had little effect on the residual stress distributions. This was because, the web was nearly unaffected by cutting operation since the high localized heat input from the welding operation overrides the cutting effects at the edges of web piece.

6. In most of the locations for residual stress measurements, the stress variation through the thickness was relatively small.

Theoretically, the residual stresses are assumed to be self-equilibrating stresses, i.e., the internal stresses are balanced in a component. Tensile residual stresses are counter balanced by compressive residual stresses. Thus, the resultant reactions as a result of residual stresses must satisfy the following conditions in any structural shape.

1. The total algebraic sum of axial stresses over a cross section is zero
2. The resultant bending moment about major axis is zero
3. The resultant bending moment about minor axis is zero

Table 5.2 shows the calculated resultant axial load, bending moment about major axis, and bending moment about minor axis of each section as a result of respective unbalanced residual stress distributions. The resultant unbalanced reactions were calculated assuming the width and thickness of each slice was approximately 13mm (1/2 inch) and 9.5mm (3/8 inch), respectively. As high as 42kN of resultant axial load was calculated from the column specimen-06 in this investigation. Thus, the maximum axial stress due to the axial load of 42kN can be calculated as 9.6MPa, since the cross sectional area of the column section was approximately 4366mm^2. This unbalanced tensile axial stress was less than 10% of the maximum averaged residual stresses measured at the important locations of the column specimen-06. Similarly, the unbalanced resultant axial stresses were compared with the maximum averaged residual stresses measured at important locations of the respective column specimens. It was observed that the influence of unbalanced axial stresses was less than 10% of the averaged maximum residual stresses measured in this investigation. Therefore, it can reasonably be presumed that the overall influence of the axial stresses due to unbalanced axial loads was considerably insignificant. Moreover, the calculated maximum bending moment about major axis was approximately 1kNm in column specimen-03. The maximum bending moment about minor axis was approximately 0.9kNm in column specimen-05.

However, in practice, the residual stresses measured over a section won't meet the conditions, stating that the residual stresses are in equilibrium. This is because; the section on which the residual stresses are to be measured may not be perfect considering various reasons. The primary reasons can be given as to why the residual stresses didn't satisfy the above three condition in this investigation are as follows;

1. The material property over a cross section may be inhomogeneous, i.e., the yield strength and elastic modulus of the section may vary over the cross section. Cutting and welding operations are basically involved with high heat energy. Thus, such operations change the material properties of plate elements of the H- shaped section in the vicinity of the cut-edge and the welded portions.
2. The internal stresses are not balanced as a result of deformations of a section on which the measurements were to be made. The deformations can be in the form of either out-of-plane or in-plane deformations of plate elements of the section (flanges and web)
3. The sectioning process itself can alter the residual stress distribution to a certain degree by generating localized stresses.
4. The accuracy of the measurement procedure associated with the "method of section" may have certain limitations such as different readings for different vertical alignment of the extensometer, different reading for different alignment of gauge holes, etc.

5. The number of longitudinal strips to be cut depends on the variation of residual stresses. Steep gradients in residual stresses, for example, would require closer spacing for longitudinal cuttings (Tebedge et al., 1973). Therefore, the number of cuts made in this investigation may not be sufficient.

Column Designation		Locations			
		Flange Tip (Max)	Mid Flange (Max)	Web (Max)	(*)Flange-Web Junction (Max)
Plasma Cut	C1	σ_{rt} =80MPa	σ_{rc} =122MPa	σ_{rt} =98MPa	σ_{rt} =143MPa
	C3	σ_{rt} =85MPa	σ_{rc} =133MPa	σ_{rt} =97MPa	σ_{rt} =152MPa
	C5	σ_{rt} =98MPa	σ_{rc} =123MPa	σ_{rt} =94MPa	σ_{rt} =135MPa
Flame Cut	C2	σ_{rt} =168MPa	σ_{rc} =135MPa	σ_{rt} =111MPa	σ_{rt} =139MPa
	C4	σ_{rt} =139MPa	σ_{rc} =129MPa	σ_{rt} =91MPa	σ_{rt} =137MPa
	C6	σ_{rt} =132MPa	σ_{rc} =132MPa	σ_{rt} =107MPa	σ_{rt} =155MPa

Table 5.1: The Maximum Measured Residual Stresses at Important Locations

(*) No averaged values used at flange-web junction

Column Designation		Reactions		
		Axial Load (kN)	Bending Moment (kNm)	
			Major Axis	Minor Axis
Plasma Cut	C1	27	0.27	0.27
	C3	36	1.13	0.20
	C5	29	0.36	0.93
Flame Cut	C2	34	0.32	0.60
	C4	26	0.45	0.34
	C6	42	0.73	0.04

Table 5.2: Unbalanced Reactions Due to Residual Stress Distributions

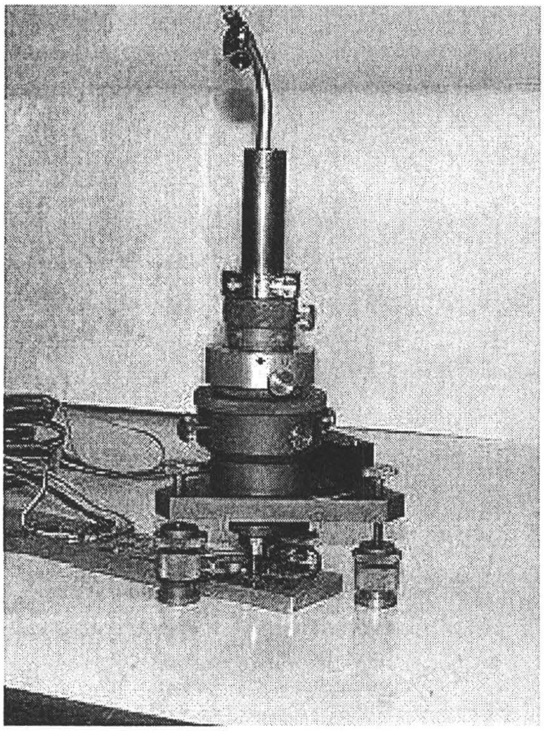

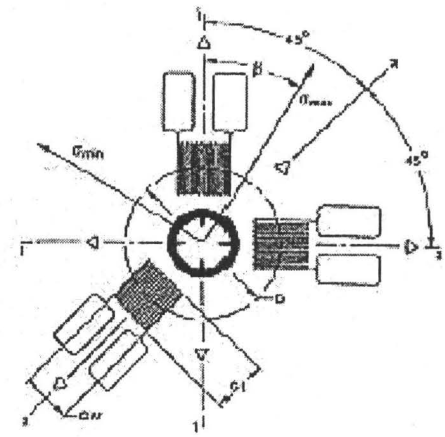

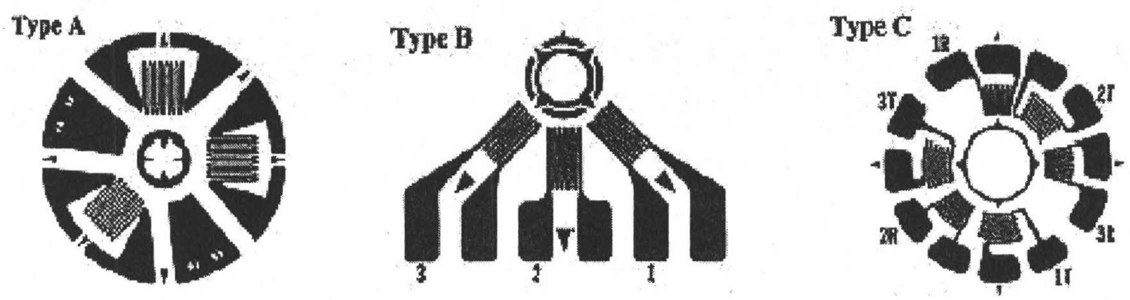

Figure 5.1: Typical Hole Drilling Apparatus and Different Types of Rosettes Used in this Method

("*Determining Residual Stresses by the Hole-Drilling Strain Gauge Method*" ASTM Standard E837)

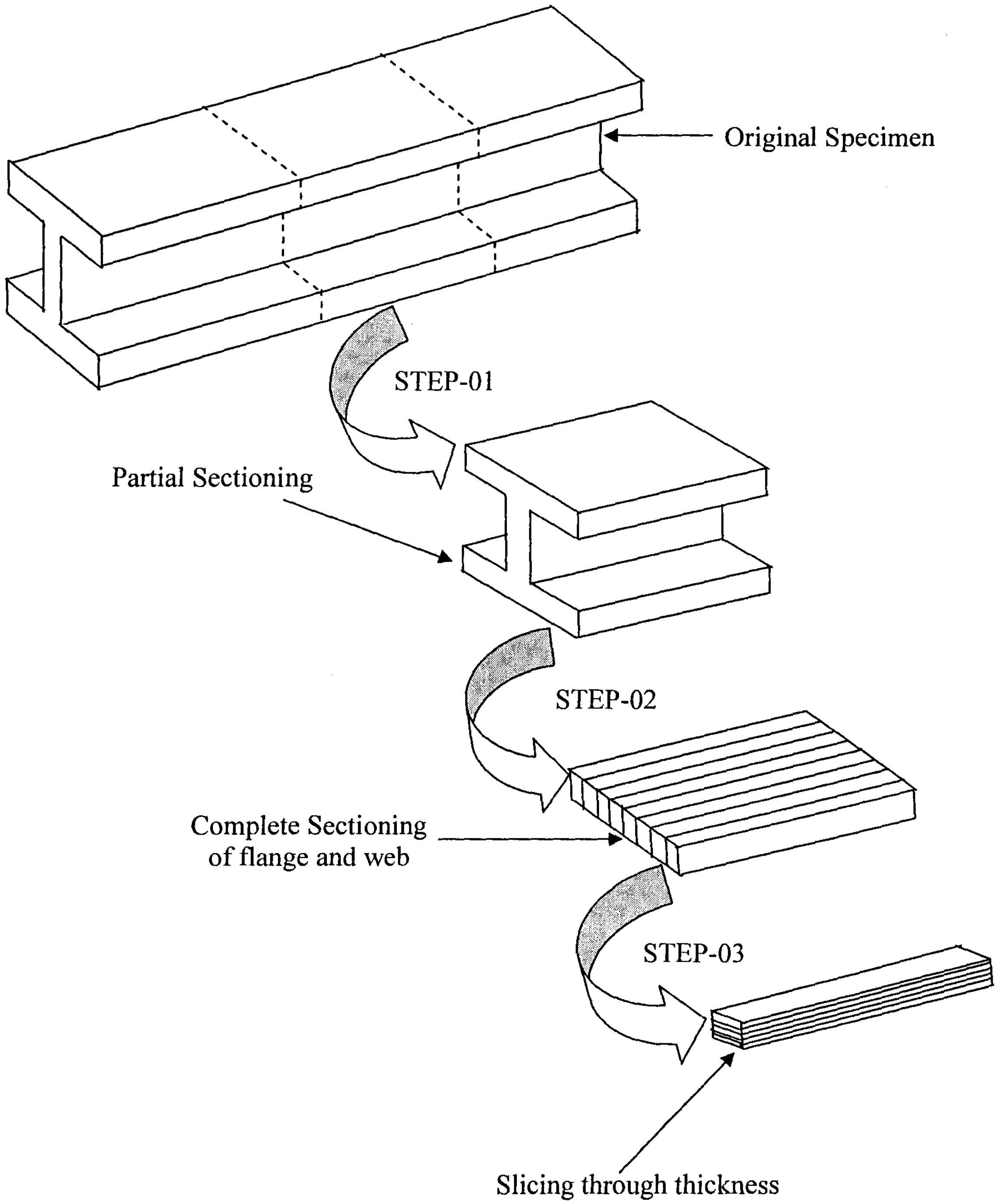

Figure 5.2: The Steps Involved in "Method of Section"

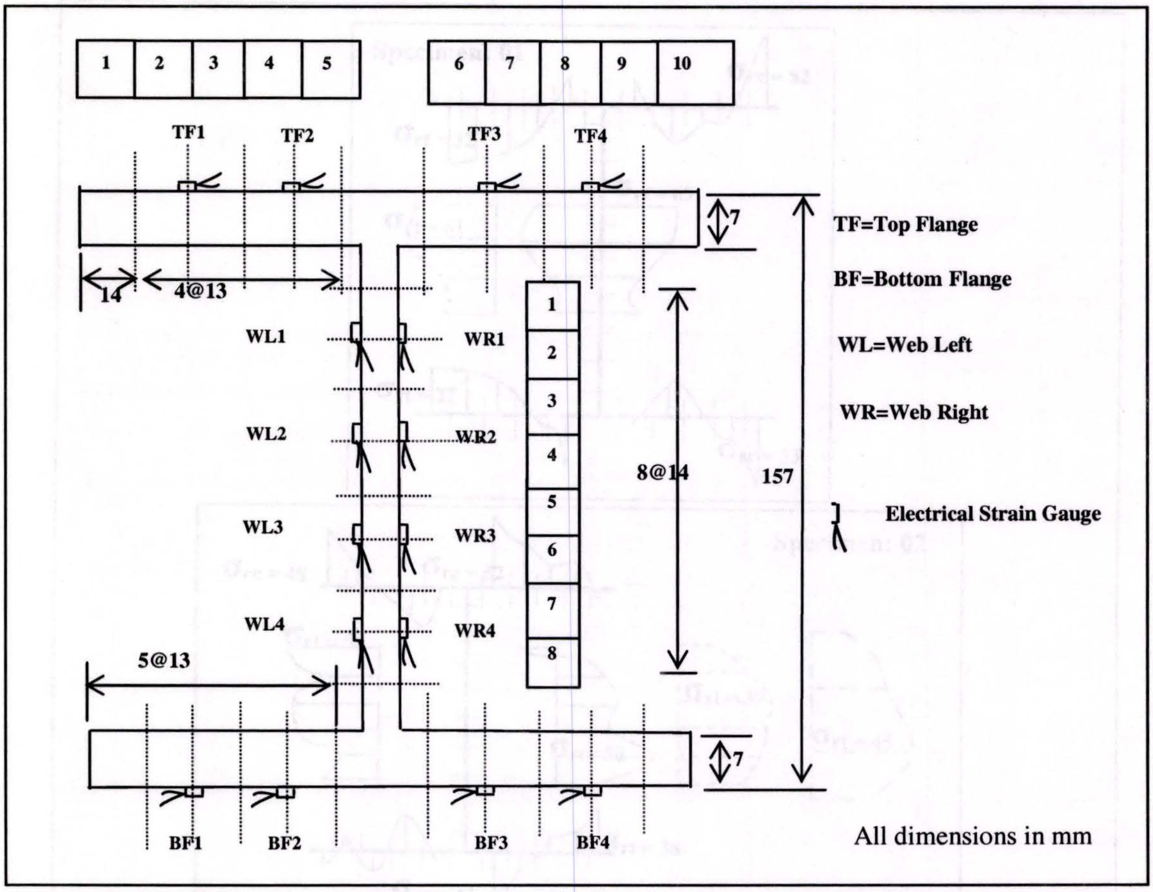

Figure 5.3: The Cross-Section Showing the Locations of Gauge Holes and Electrical Strain Gauge

Figure 5.4: Gage Hole Drilling Assembly

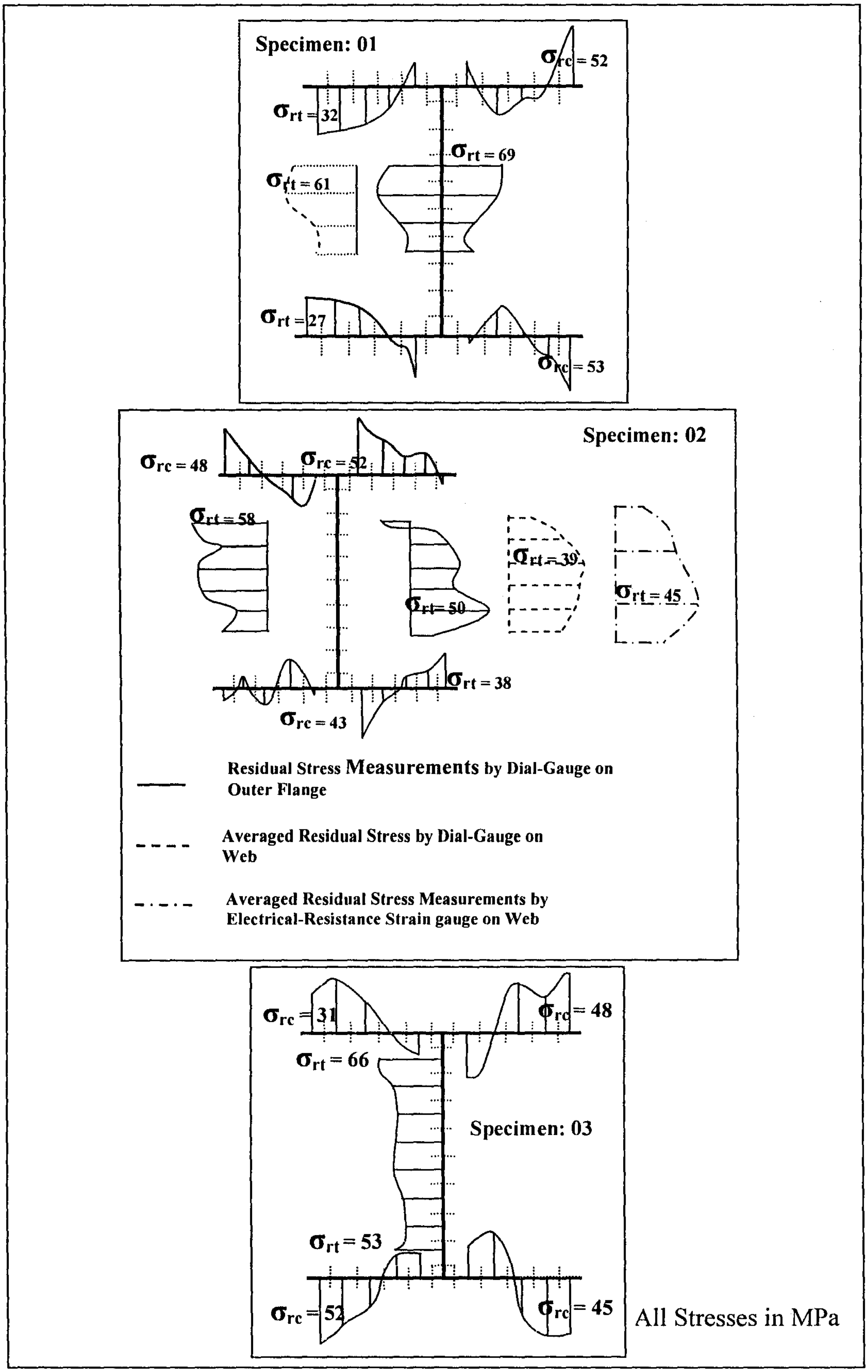

Figure 5.5: The Residual Stress Distribution Obtained from Pioneering Tests

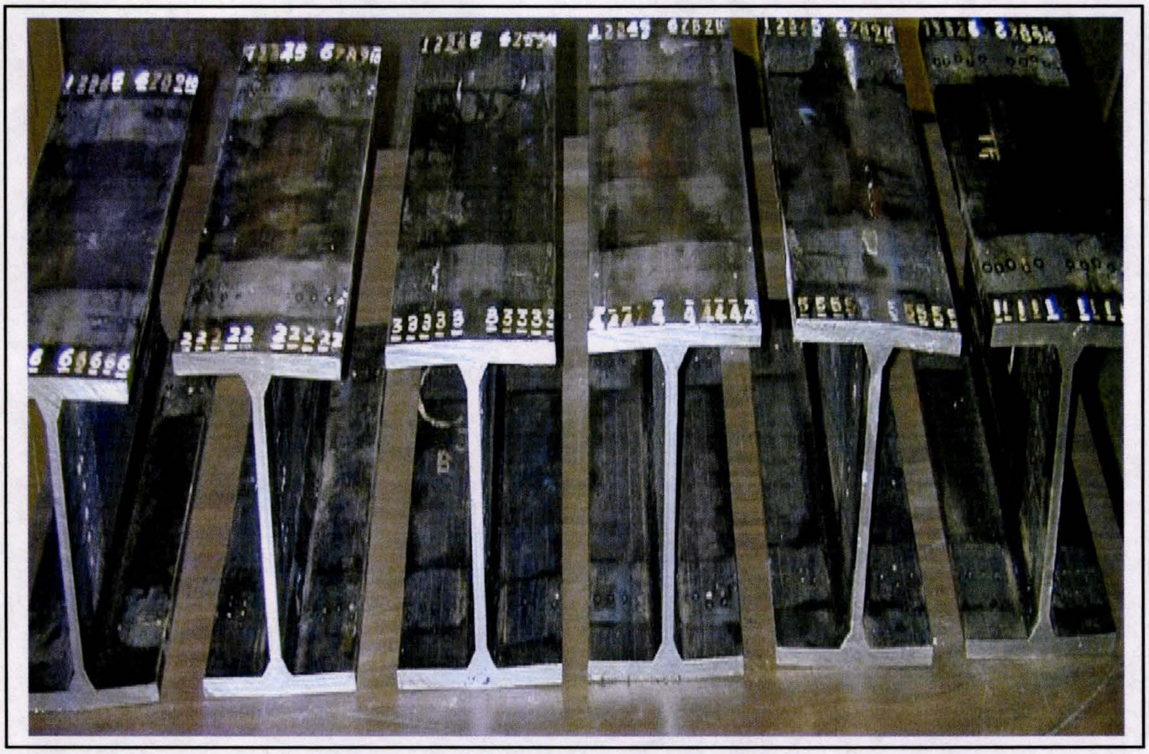

Figure 5.6: Specimens for Residual Stress Measurements

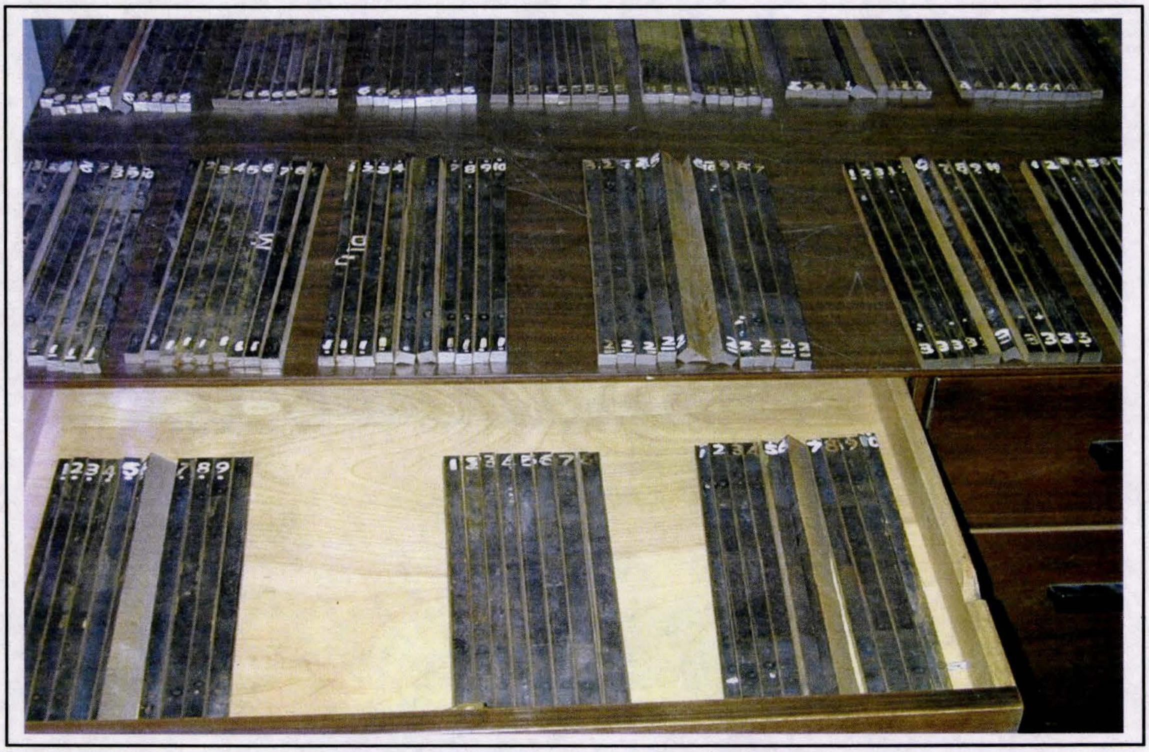

Figure 5.7: Slices after Sectioning by Water Jet Cutting

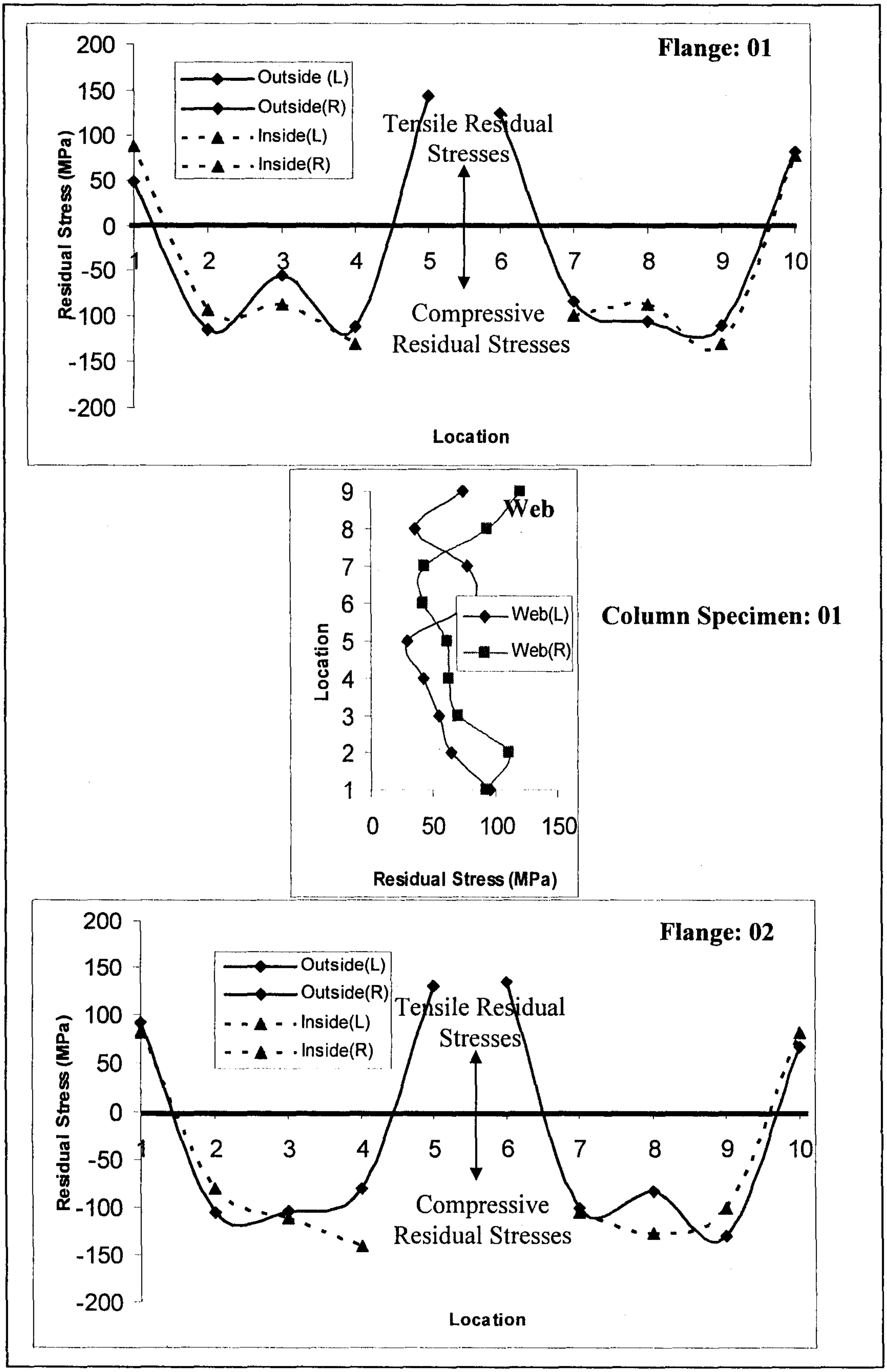

Figure 5.8: The Residual Stress Distribution of Column Spcimen-01 (Plasma Cut and Gas Metal Arc Welding Process)

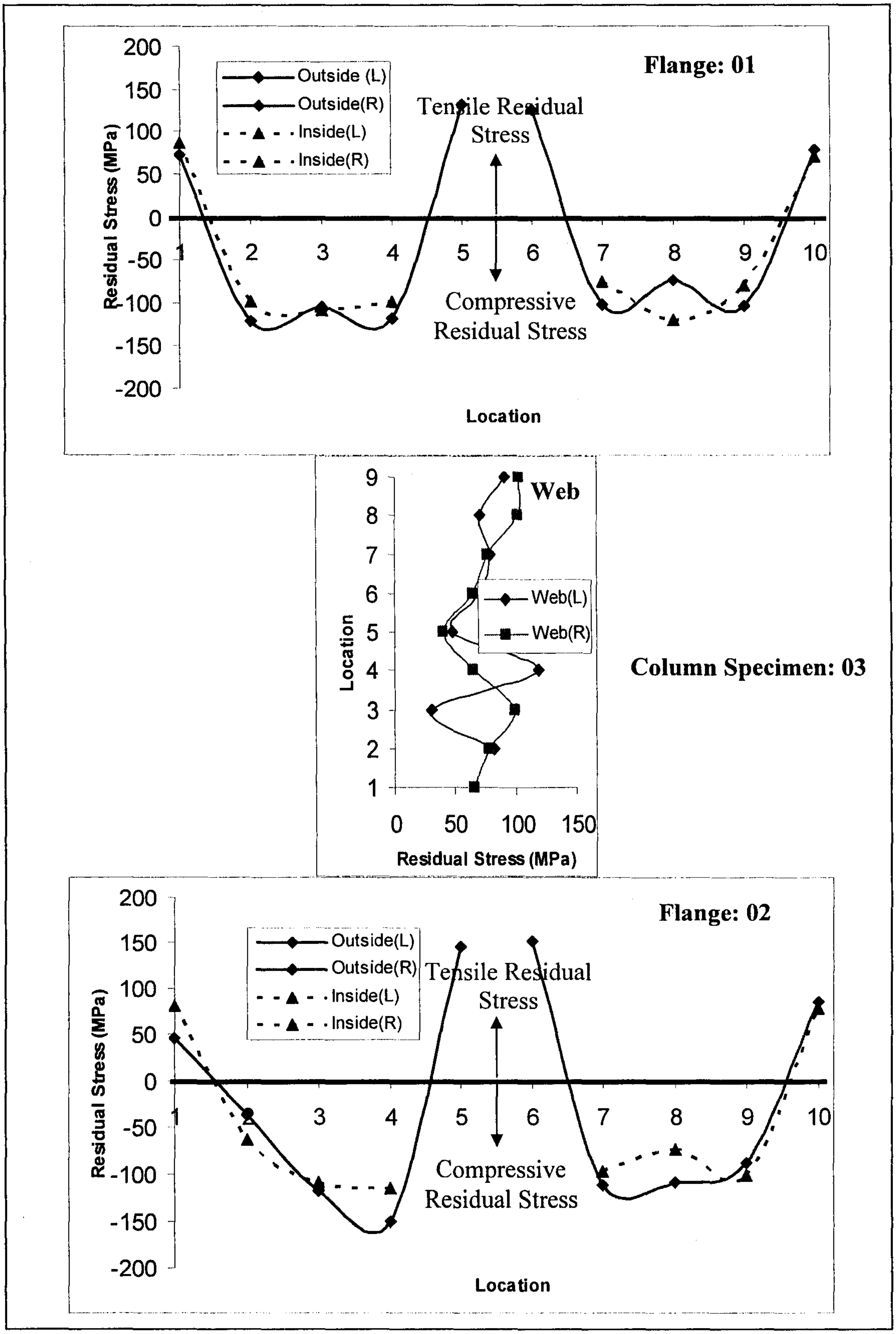

Figure 5.9: The Residual Stress Distribution of Column Spcimen-03 (Plasma Cut and Gas Metal Arc Welding Process)

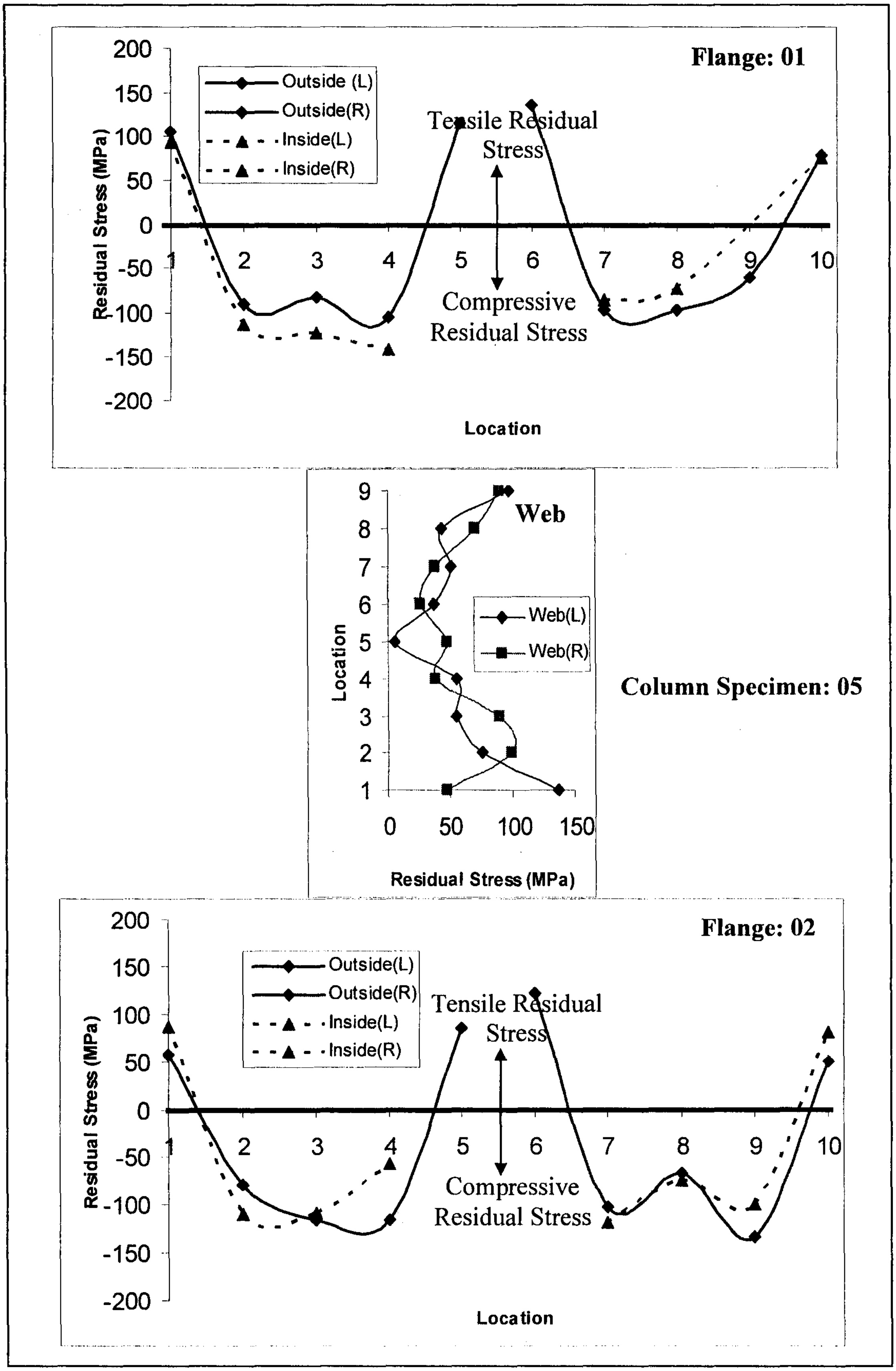

Figure 5.10: The Residual Stress Distribution of Column Spcimen-05 (Plasma Cut and Gas Metal Arc Welding Process)

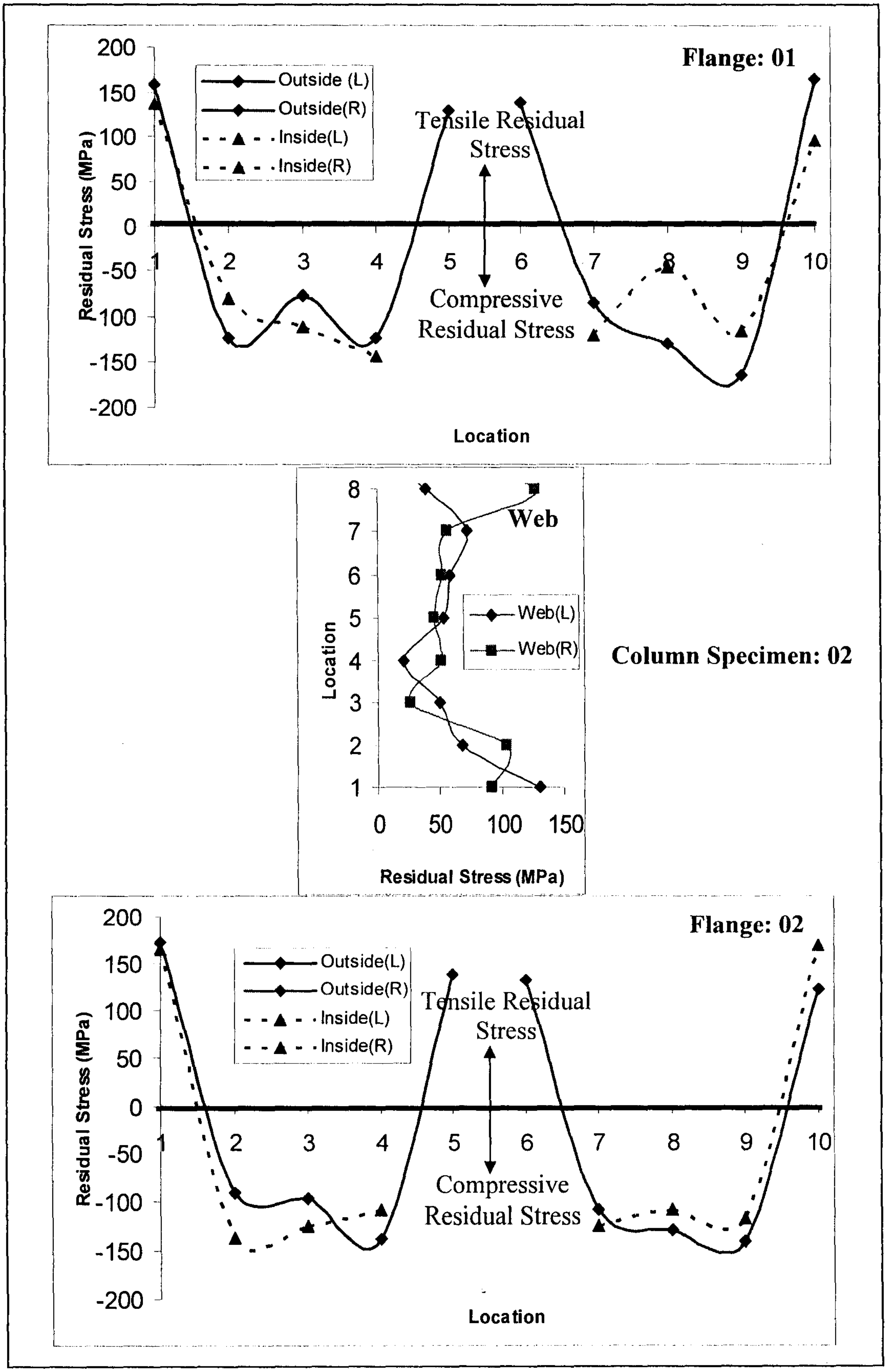

Figure 5.11: The Residual Stress Distribution of Column Spcimen-02 (Flame Cut and Gas Metal Arc Welding Process)

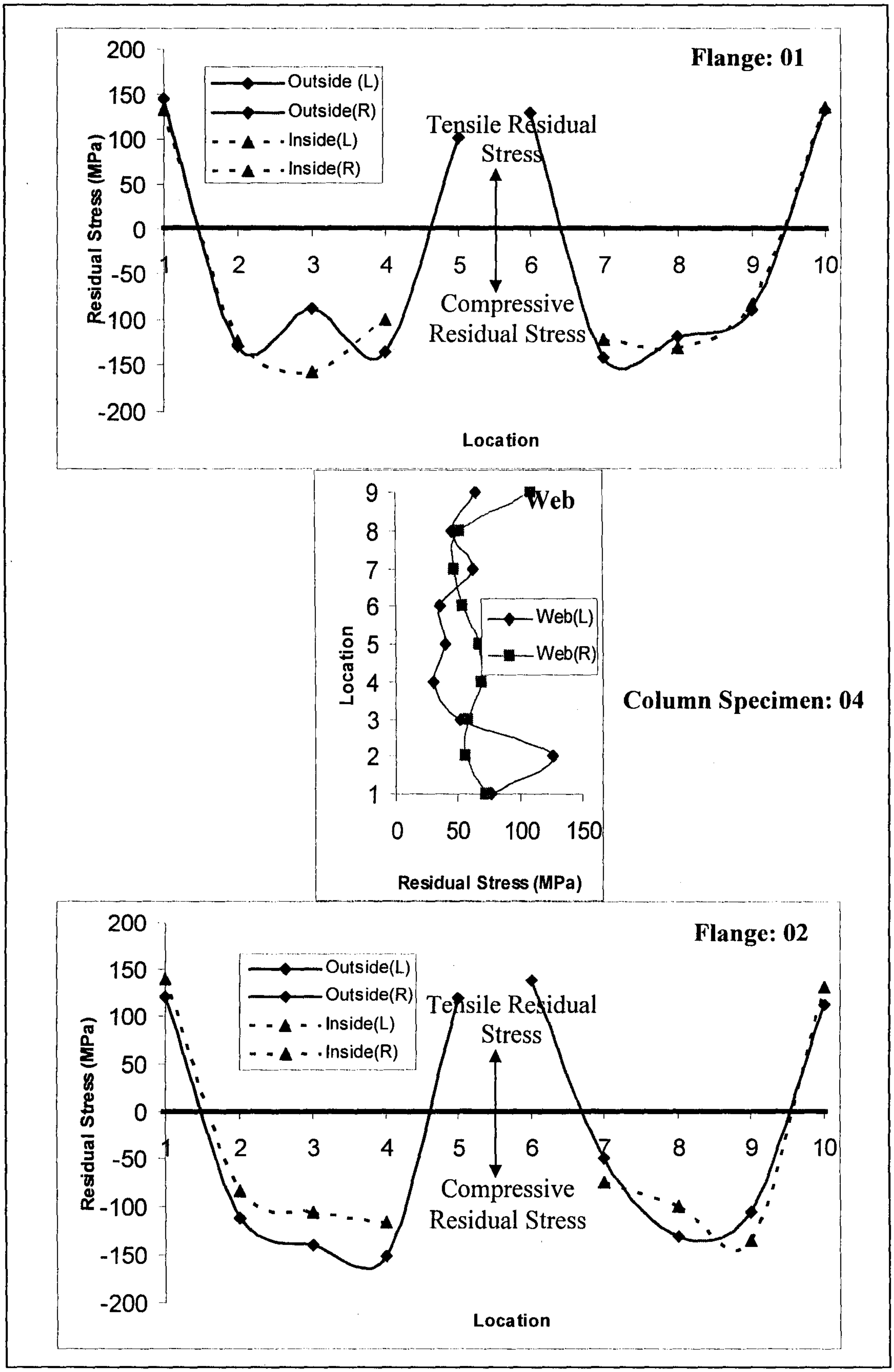

Figure 5.12: The Residual Stress Distribution of Column Spcimen-04 (Flame Cut and Gas Metal Arc Welding Process)

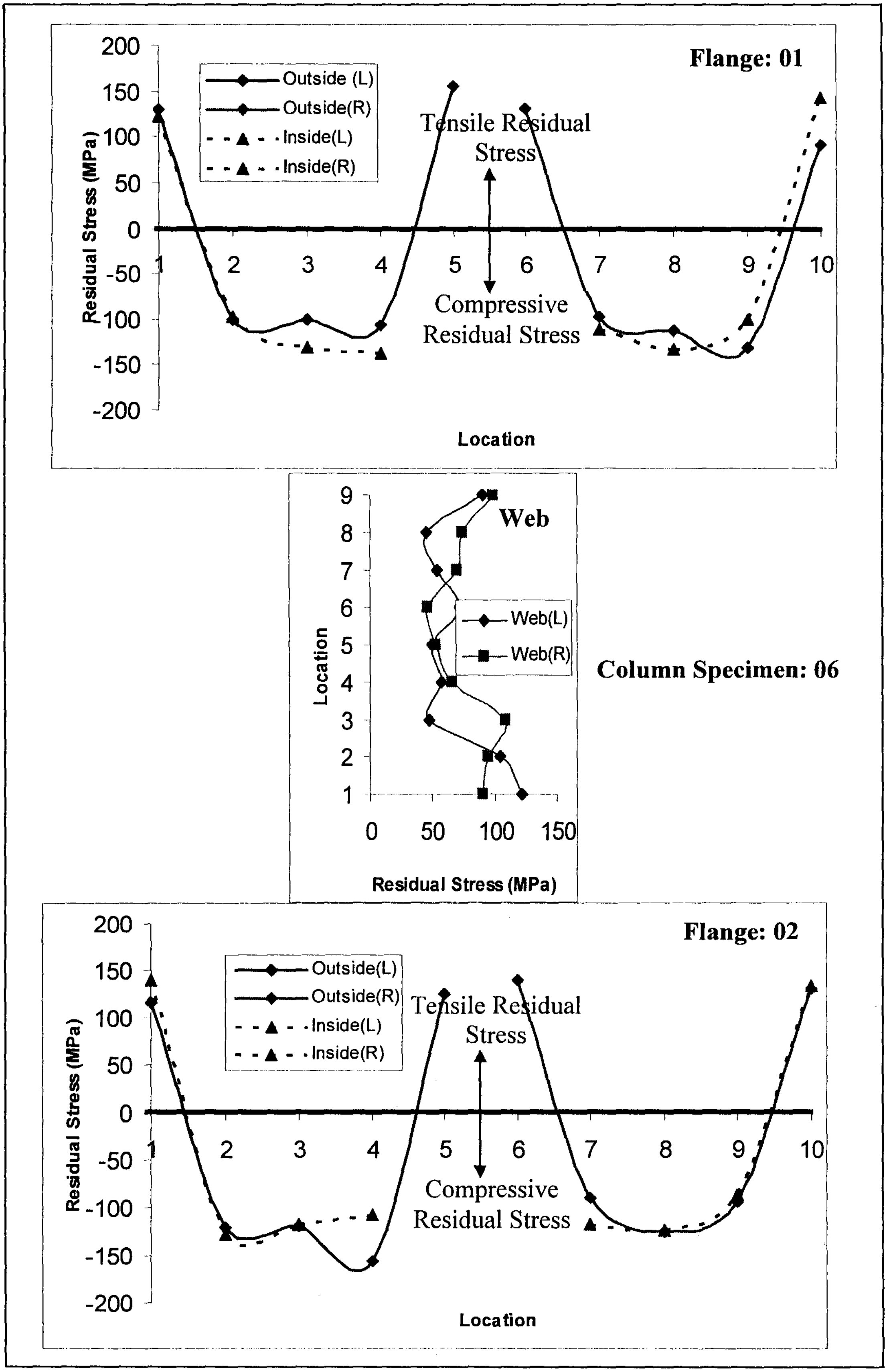

Figure 5.13: The Residual Stress Distribution of Column Spcimen-06 (Flame Cut and Gas Metal Arc Welding Process)

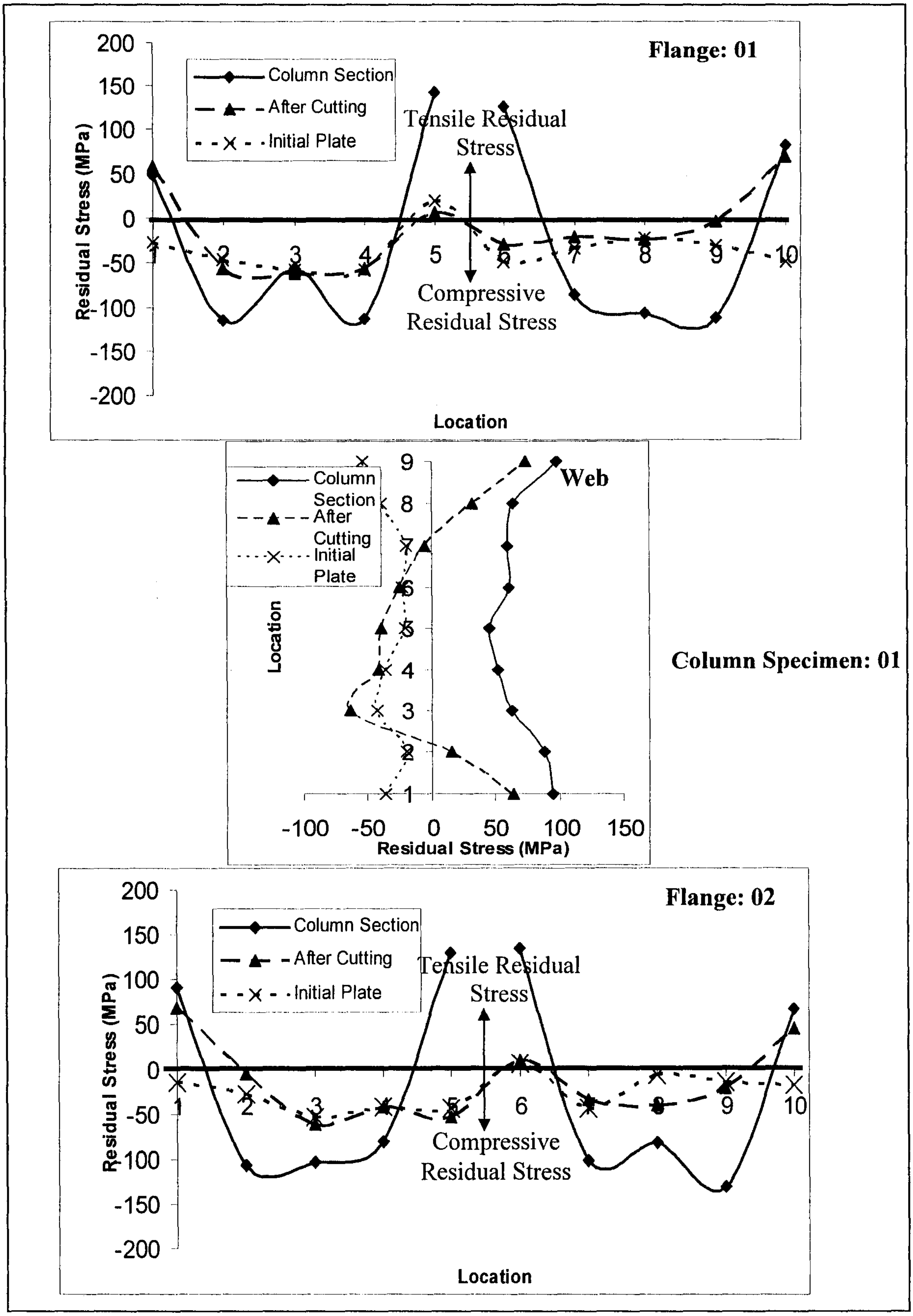

Figure 5.14: The Residual Stress Distribution of Initial Plate, Plate Strips after Plasma Cutting, and Column Section-01 after Welding

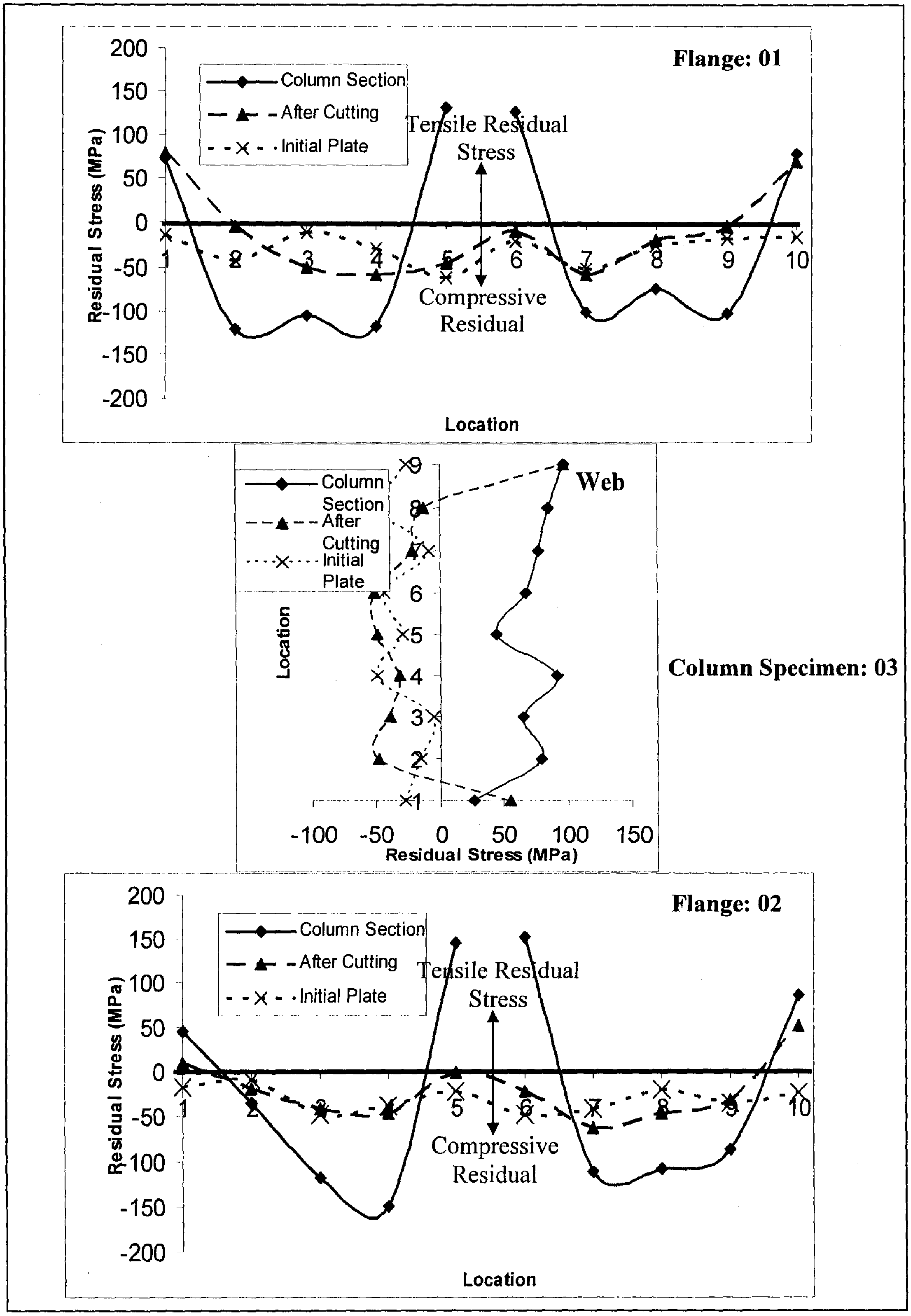

Figure 5.15: The Residual Stress Distribution of Initial Plate, Plate Strips after Plasma Cutting, and Column Section-03 after Welding

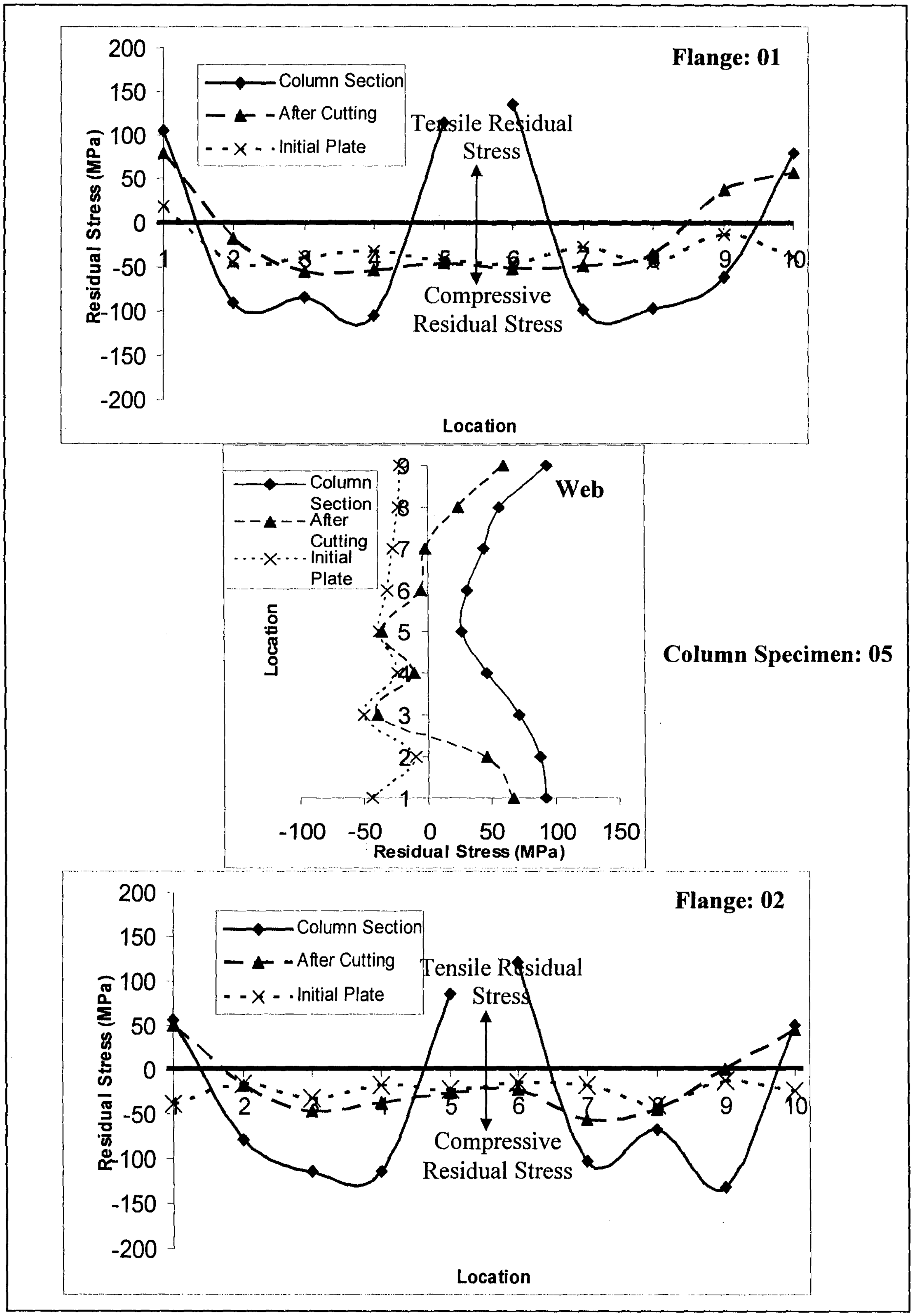

Figure 5.16: The Residual Stress Distribution of Initial Plate, Plate Strips after Flame Cutting, and Column Section-05 after Welding

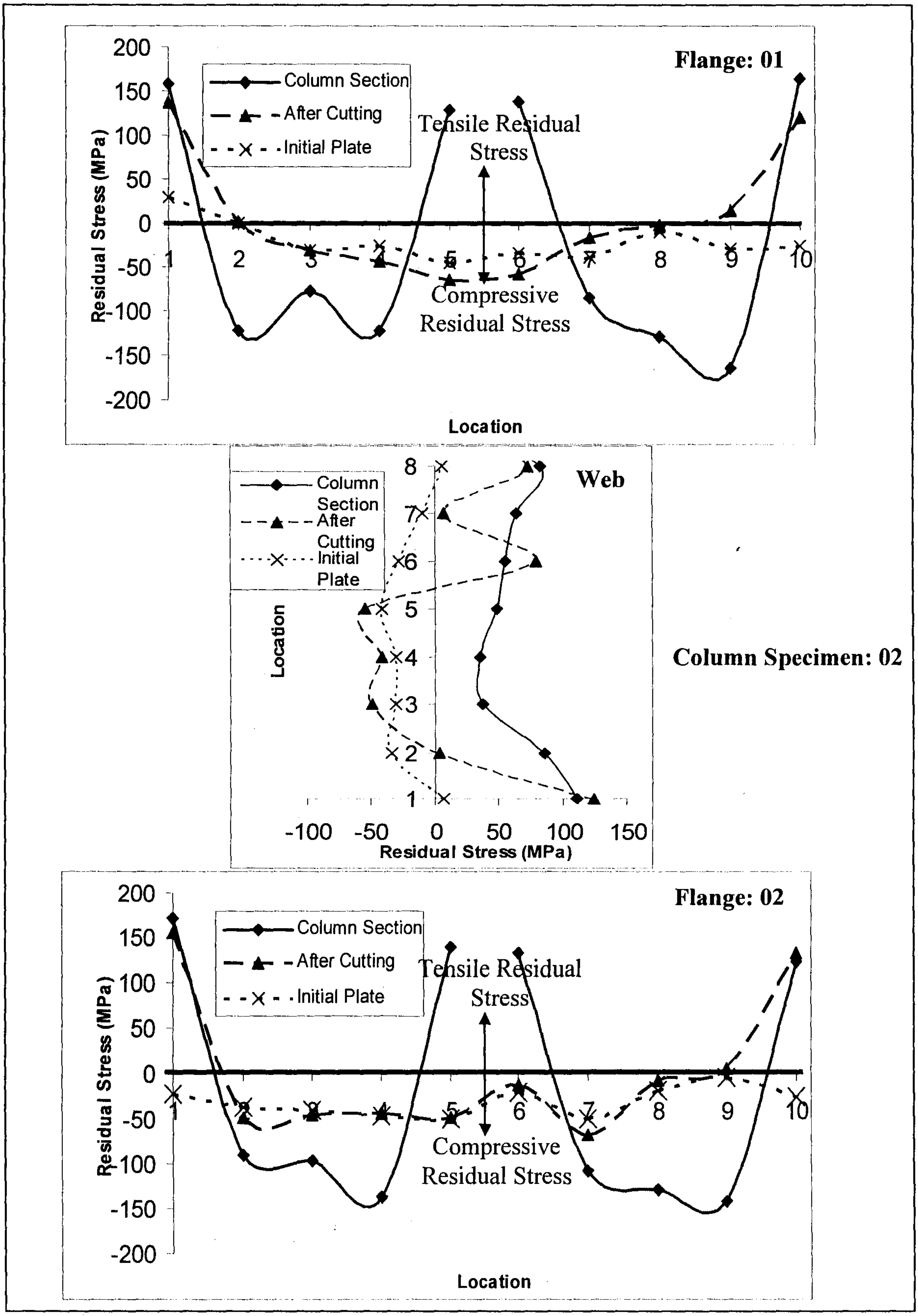

Figure 5.17: The Residual Stress Distribution of Initial Plate, Plate Strips after Flame Cutting, and Column Section-02 after Welding

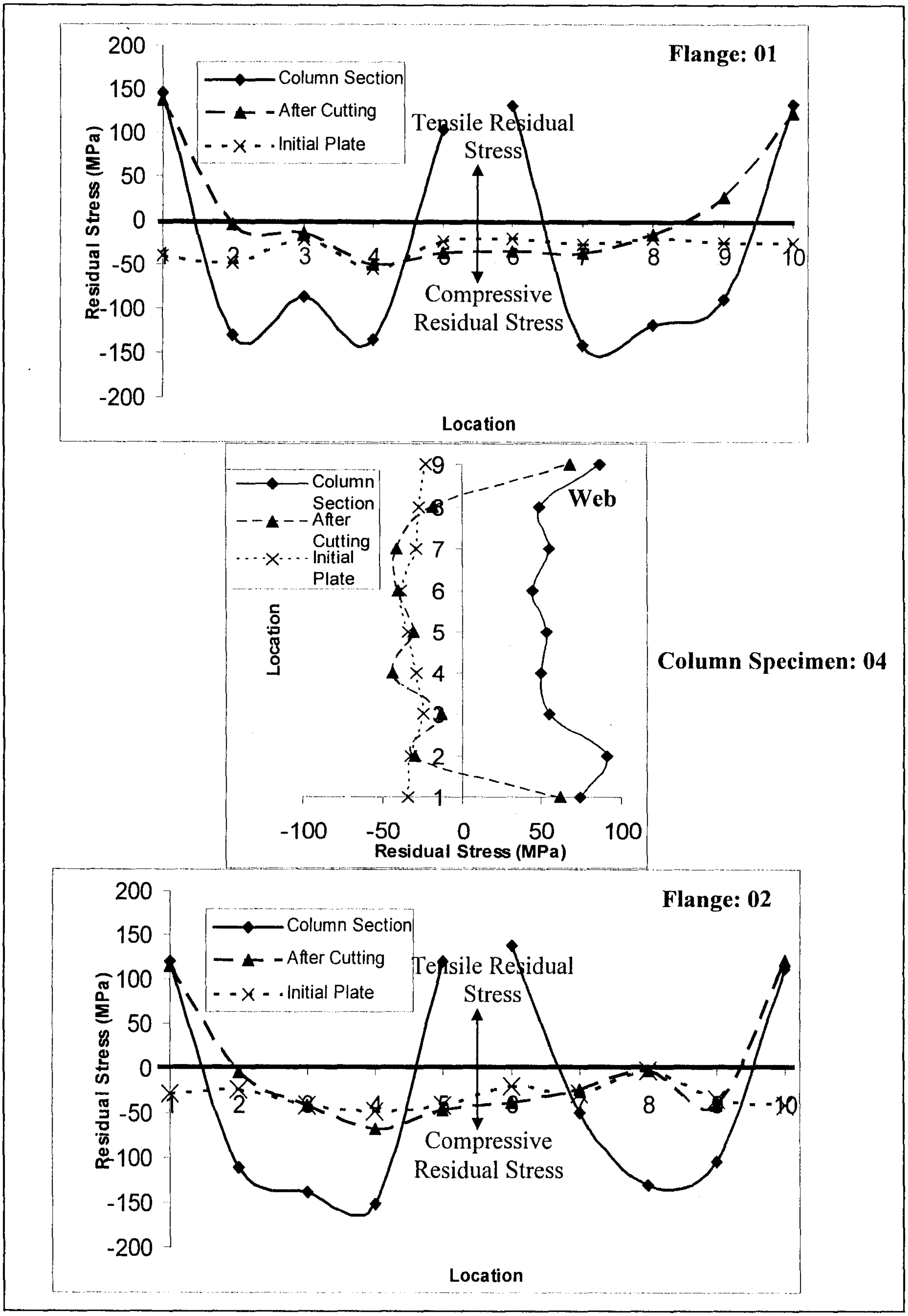

Figure 5.18: The Residual Stress Distribution of Initial Plate, Plate Strips after Flame Cutting, and Column Section-04 after Welding

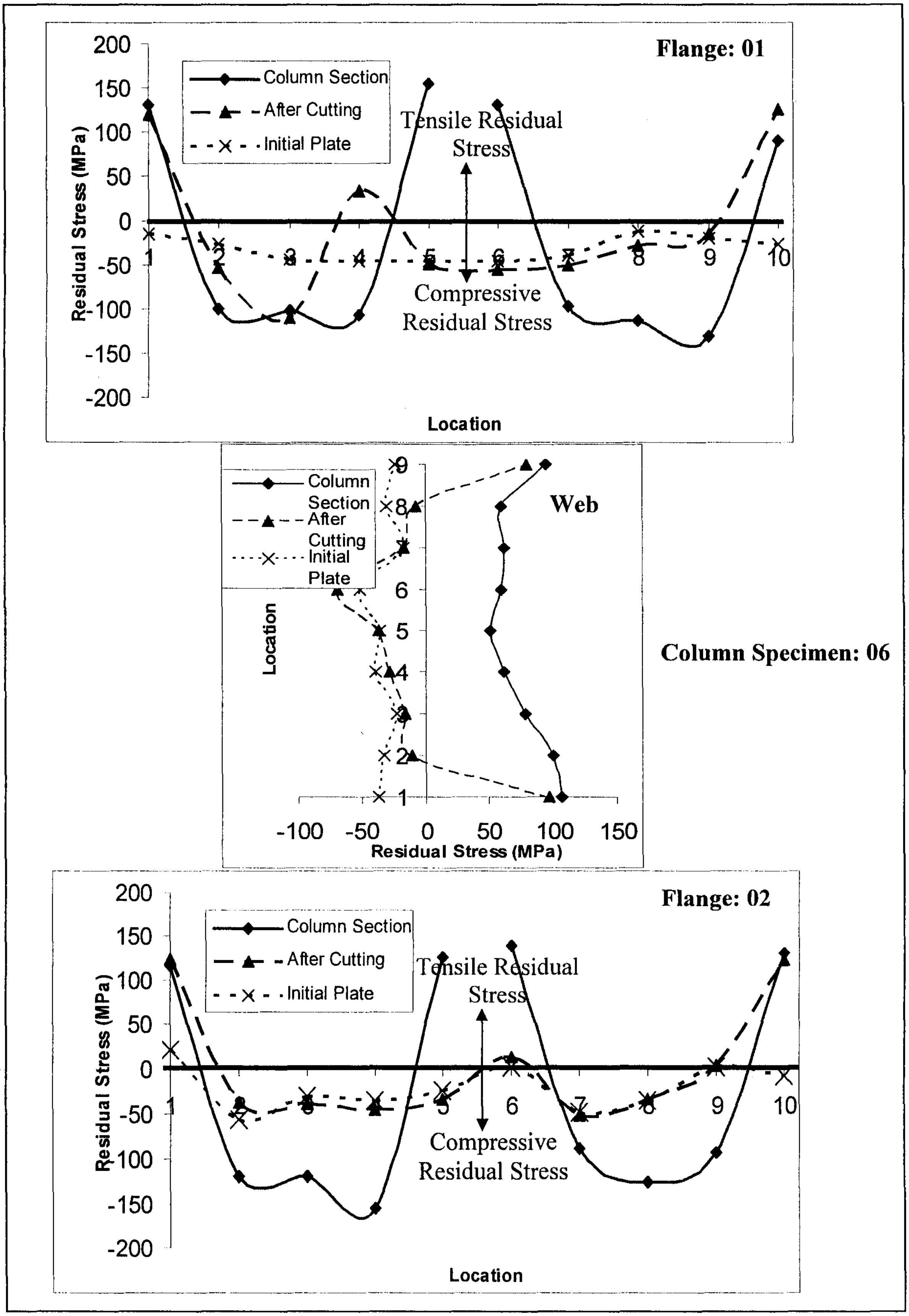

Figure 5.19: The Residual Stress Distribution of Initial Plate, Plate Strips after Flame Cutting, and Column Section-06 after Welding

Chapter 6

EXPERIMENTAL STUDY OF COLUMN STRENGTH

6.1 Introduction

In practice, most of the common shapes of steel columns are bi-axially symmetric. These sections include rolled or fabricated I-shapes, rectangular boxes, solid and hollow round shapes. When such sections buckle they buckle in the pure flexural mode. However, other shapes such as angles and channel sections may be subjected to flexural-torsional buckling when subjected to axial loads. In general, such sections are usually not used as structural columns in practice. In some instances, if the elements of a section (flanges and webs) are thin and slender, then the individual elements may locally buckle at considerably low loads. This type of failure mode, in general is referred to as "local buckling failure" mode. Local buckling doesn't essentially mean failure of member, since the members may have substantial post buckling strength.

The local buckling failure in either rolled column sections or built-up column sections can easily be precluded by limiting the slenderness of component plates. According to the CAN/CSA-S16-01 standard (CSA, 2004), the sections can be classified as class: 1, 2, 3 or 4, and the associated definitions for each of the classes are given in Clause 11.1.1. As far as axially loaded columns are concerned, they need not to strain harden or re-distribute loads, and thus Class: 3 limits will be sufficient for such columns. The Class: 4 sections can be analyzed and designed using North American Specification for the Design of Cold-Formed Steel Structural Members, CSA-S136-01 (CSA, 2004).

Flexural buckling of columns can be divided into three regions of slenderness and the associated failure modes. The columns having lowest slenderness fail by yielding in compression. The strength of theses stub column sections is function of cross-sectional area, compressive yield stress, and strain hardening. Columns in the intermediate range of slenderness have strengths dependent on number of additional variables, including slenderness, initial straightness, tensile yield stress, elastic modulus, moment of inertia, residual stresses, and end conditions. Columns with larger slenderness fail by elastic buckling. This buckling is governed by the factors such as; slenderness, end condition, initial straightness, elastic modulus, and moment of inertia of the axes of buckling. The variation of strength of columns with their increasing effective length can be qualitatively represented as shown in Figure 6.1

In this study, welded built-up columns fabricated from plasma cut plates and flame cut plates were considered in order to predict their ultimate strength. The non-dimensional slenderness values (λ) of columns tested, herein were considered ranging from 0.2 to 1.3. All of the column tests were performed allowing for minor-axis buckling only. The axial shortening, mid-height out-of-plane deflections and column end rotations will be observed for increasing axial loads. The ultimate strength of columns fabricated from plasma cut and flame cut will be compared and presented in this chapter. This chapter will include discussions on the test results and comparisons with the current column strength curves based on CAN/CSA-S16-01 (CSA, 2004). Moreover, this chapter includes a general discussion of the development of column strength curves and review of previous research. This chapter also provides a summary of the work done towards establishing the mechanical characteristics of steel plates used in forming the column sections in this investigation.

6.2 The Development of Column Strength Curves

The first empirical equation for column curve was presented by Musschenbreok, in 1729 in the form, $P=k(bd^2/ L^2)$, where P is column strength, k is an empirical factor, b and d are the width and depth of a rectangular section, and L is length of the column. Due to the development of the differential and the integral calculus in the second half of the seventeenth century, the formulations of many natural phenomena, such as column buckling, were further developed. In 1744, Euler was the first to realize that buckling of column could be a concern of stability of columns in reality, and thus it could be a potentially dangerous failure mode. The original buckling load determined by Euler (1744) was for a column with one end built in and the other free, in the form, $P=C\pi^2/4L^2$, where P is the buckling strength and C is the "absolute elasticity", depending merely upon the elastic properties of the material. Euler's investigation (1744) was primarily based on purely elastic phenomenon of buckling. Thus, this theory covers only buckling situations where compressive stresses are below the elastic limit, acting uniformly over a complete cross section. However, elastic instability of columns, in reality, occurs only with very slender columns.

In 1889, Engesser presented his original tangent modulus theory, in which he used a variable modulus of elasticity to further improve the prediction of buckling behavior of columns than that predicted by Euler's theory. He assumed a modulus of elasticity that is tangent to the non-linear stress strain curve. Also, he assumed no strain reversal to occur as the member changes from straight to bent form. Finally he derived a similar formula as Euler with the change of using the tangent modulus (E_t) instead of the modulus of elasticity (E). However, Engesser's modified formulae for column buckling behavior provided lower loads than the actual capacities of columns obtained from full scale lab tests. Thus, he further modified his theory to work with a combined value known as combined modulus theory. In this theory, he assumed that the stress increase is proportional to the tangent modulus (E_t) in loading fibers, whereas the stress relieved in unloading fibers is proportional to elastic modulus (E). However, this adjustment using a combined or reduced modulus theory provided higher buckling values than the experiments.

Shanely (1947) explained the tangent modulus concept by using a simple model to show that an initially straight column will buckle at the tangent modulus load and then continue to bend with an increasing axial load. Therefore, based on Shanely's explanation, the tangent modulus theory predicts lower bound of buckling load of a real column, while the reduced modulus predicts the upper bound. The actual inelastic buckling load of a perfect column may lie anywhere between the lower and upper bound.

However, in practice the application of these theories in predicting column strength will not give reliable results since the imperfections associated with a real column influence the strength of such columns considerably. Moreover, most of the practical steel columns are within the intermediate slenderness values, and thus the strength of such columns depends upon various factors such as residual stress distributions, the shape and the magnitude of the initial out-of-straightness, cross-sectional dimensions, material properties,etc. Because of these variabilities present in a real column, a wider scatter of column strength, mostly in the intermediate range, was observed by the past researchers from their full scale lab tests. Subsequently, the adoption of multiple column curves obtained through deterministic and probabilistic approaches became more popular and the concept has been widely accepted and practiced throughout the world. The development of different column curves proposed by different researchers in this area at different time will be explained in the following section.

6.2.1 The Development of Multiple Column Strength Curves

The concept of multiple column curves for the design of steel compression members has been accepted as desirable both in North America and in Europe (Michael Rotter, 1982). The reason for increased use of the multiple column curve concept has been that it is hard to develop rational, representative, and sufficiently reliable column strength criteria covering all ranges of columns having different shapes, steel grades, manufacturing methods, etc. The development of multiple column strength curves was achieved by subdividing the band, which was obtained considering various types of columns with wide range of variabilities into groups of curves with a mean or similar curve for each group.

The extensive research on development of multiple column curves had been continuously undertaken from the late 1950s to the early 1980s. In 1959 the German Standard DIN 4114 (Galambos, 1998) introduced a special curve for tubes and another curve for all other shapes. Finally, the work under the auspices of the European Convention for Constructional Steelwork (ECCS) (Galambos, 1998) resulted in recommended design application and code adoption in several countries. The present column design criterion, Eurocode 3 (ECCS, 1992) which is being adopted by some European countries is the slightly modified version of the ECCS curves.

The widely accepted both ECCS and SSRC multiple column curves were obtained numerically by computer simulations using deterministic and probabilistic approaches with experimentally obtained geometrical imperfections, residual stresses, and yield stresses. In 1974, The SSRC Curve 2 was used as the basic column strength criterion by The Canadian Standard Association. Then, in 1984, the SSRC Curve 1 was used for heat-treated tubes by the same association. In 1994, the CSA assigned welded wide-flange (WWF) columns made from flame-cut plate to SSRC curve 1 (Chernenko and Kennedy, 1991).

Before the development of the SSRC column strength curves, the CRC (former name of the SSRC) column curve (1960) had been generally accepted and used as the basis for steel column design formula in North America and elsewhere (AISC, 1979). The development of column strength curve; CRC curve, AISC Allowable Stress Design Curve, AISC Plastic Design Curve, and then the SSRC Multiple Column Design Curves are described below.

Column Research Council Curve (CRC)

The CRC Curve was developed based on idealized I-shaped columns (neglecting the effect of web portion) with linear and parabolic residual stress distributions and test results obtained from a number of small and medium size hot-rolled, wide-flange shapes of mild structural steel. The CRC has recommended that the column strength curve in the inelastic buckling range be a parabola of the form.

$$F_{cr} = F_y - B\left(\frac{KL}{r}\right)^2 \qquad \text{Where,} \qquad B = \frac{F_y^2}{4\pi^2 E} \tag{6.1}$$

In equation (6.1), F_{cr} and F_y denote the critical buckling stress and yield stress, respectively. K is effective length factor, L is length of a member, r is radius of gyration, and E is elastic modulus. The column strength curve in the elastic range is represented by the Euler formula. Moreover, in the development of the curve, the maximum value of compressive residual stress present in hot-rolled wide-flange shapes is assumed to be 0.5 times the material yield stress (F_y). Nevertheless, the value is more conservative for hot-rolled sections which usually experience the maximum compressive stress in the range of $0.3F_y$. Therefore the demarcation point between elastic range and inelastic range is at $F_{cr} = 0.5F_y$ as shown in Figure 6.2.

There are a number of semi-empirical formulas for buckling in columns in the intermediate length range. One of theses is the Johnson formula. The Johnson formula is the equation of a parabola with the following characteristics. For a graph of stress versus slenderness ratio, the parabola has its vertex at the value of the yield stress on the y-axis. Additionally, the parabola is tangent to the Euler curve at a value of the slenderness ratio, such that the corresponding stress is one-half of the yield stress as seen in Figure 6.2. Thus, the Johnson's formula (equivalent to equation 6.1) was applied in development of CRC curve within the inelastic range. The inelastic range according to Johnson's parabola is between non-dimensional slenderness parameter (λ) of zero and C_c as shown in Figure 6.2

AISC Allowable Stress Design Curve (ASD Curve)

ASD curve was originally derived from the CRC curve. To obtain this curve, the CRC curve is divided by variable factor of safety for the different range of columns. In the inelastic range, a factor of safety (F.S) as given in equation (6.2) is used. However, in the elastic range, a constant factor of safety of 23/12 is used. The factor of safety is chosen in such a way to take into account of the adverse effects of the load eccentricity and geometrical imperfections that are inevitable in practical columns to develop this curve.

$$F.S = \frac{5}{3} + \frac{3}{8}\left(\frac{\lambda}{\sqrt{2}}\right) - \frac{1}{8}\left(\frac{\lambda}{\sqrt{2}}\right)^3 \quad \text{Where,} \quad \lambda = \frac{KL}{r}\sqrt{\frac{F_y}{\pi^2 E}} \tag{6.2}$$

In equation (6.2), λ is defined as non-dimensional slenderness value. Further, the λ is defined in terms of effective length factor K, Length L, radius of gyration r, yield strength F_y and elastic modulus E.

AISC Plastic Design Curve

The Allowable Stress Design curve and the Plastic design curve are originally developed from CRC curve by applying a different factor of safety. The intention of using these factors of safety is to account for the effect of geometric imperfections on strength of columns, since the CRC curve was developed based on the assumption that the column is perfectly straight. However, the effect of residual stresses on the strength of steel columns has been considered in developing CRC curve. The AISC Plastic Design Curve is obtained from AISC Allowable Stress Design curve by multiplying it by a factor of 1.7. In plastic design only the inelastic regime of the curve is used due to the slenderness requirement.

AISC Load and Resistance Factor Design Curve (LRFD)

The LRFD curve is provided by only one curve as shown in equation 6.3 below to represent column strength for the whole range of possible column strengths. The curve is developed based on assumptions that the column has small end restraints. For example, an effective length factor K=0.96 for pinned end, initial crookedness of a column is sinusoidal in shape with the mid-height maximum imperfection of L/1500 and no load eccentricity is expected.

$$\frac{P}{P_y} = \begin{cases} \exp[-0.419\,\lambda^2] & \lambda \leq 1.5 \\ 0.887\,\lambda^{-2} & \lambda > 1.5 \end{cases} \qquad (6.3)$$

In equation (6.3), an axial load is denoted as P and an axial load capacity of a cross-section is denoted as P_y.

SSRC Multiple Column Strength Curves

Galambos (1998) reviewed in his book about the investigation on estabilsing column strength by past researchres; Jacquet (1970); Bjorhovde (1972a), Sherman (1976) ;Birkemoe (1977a); Kato (1977b); Bjorhovde and Birkemoe (1979); Fukumoto et al., (1983); Bjorhovde (1988b). From the extensive investigation on column strength by Bjorhovde (1972), experimentally and analytically, covering the full practical range ofshapes, steel grades, and manufacturing methods, he observed the wide variation in column strength. The partial study on strength of columns by other researchers; Jacquet (1970); Sherman (1976) ;Birkemoe (1977a); Kato (1977b); Bjorhovde and Birkemoe (1979); Fukumoto et al., (1983); Bjorhovde (1988) confirmed the wide variability in column strength. Based on the computer model developed for a geometrically imperfect column with an initial out-of-straightness at mid-height as L/1000, assuming the variation of imperfection as half sinusoidal, and with actual measured residual stress values, a set of 112 column strength curves were generated for column member having different sizes, shapes and lengths. These shapes specially incorporated the major shapes of rolled and welded shapes from light to heavy dimensions of generally used columns. There are three curves known as SSRC column strength curves 1, 2, and 3 available for columns with different shapes and sizes, different steel grades, different axes of bending, as well as columns made up of different fabrication techniques. The SSRC curve 1, 2, and 3 are shown in Figure 6.3. The SSRC curve 1 and curve 2 are used in

CAN/CSA-S16-01 standard (CSA, 2004; Loov, 1995) with one mathematical formulation as shown in equation 6.4 below.

$$P_u = P_y (1 + \lambda^{2n})^{-1/n} \tag{6.4}$$

In equation (6.4), P_u denotes the ultimate load a column can sustain before failure, P_y denotes the cross sectional capacity at yield strength of the column section, λ is non-dimensional slenderness ratio, and n is defined as follows,

Where n = 2.24 for WWF shapes with flange edges flame-cut produced in accordance with CSA Standard G40.20 and hollow structural sections manufactured according to CSA Standard G40.20, Class H (hot- formed or cold- formed stress-relieved) (SSRC Curve 1)

n = 1.34 for W shapes of Group 1, 2, and 3 of Table 1 of CSA Standard G40.20, fabricated I-shapes, fabricated box shapes, and hollow structural sections manufactured according to CSA Standard G40.20,Class C(cold-formed non-stress-relieved) (SSRC Curve 2)

The AISC Allowable Stress Design Curve, AISC Plastic Design Curve, AISC Load Resistant Factor Design Curve, SSRC Multiple Column Curves, and the CRC Curve are drawn to scale for comparison purposes as shown in Figure 6.3.

ECCS Multiple Column Curves

The ECCS (European Convention for Constructional Steel Work) multiple column strength curves also were developed considering various types of most practical column shapes and sizes as well as considering different axes of buckling and the sections manufactured form different fabrication process. Moreover, the development was based on the assumed initial out-of-straightness as half sinusoidal with the maximum permissible amplitude of L/1000 at mid height and the actual measured residual stress distributions. Figure 6.4 shows the ECCS multiple column curves.

6.3 Test Specimens

As discussed earlier, H-shape column sections in this investigation were fabricated from steel plates having original dimensions of 3960mm long 710mm wide and 9.5mm thick. The specified yield strength of these steel plates was 350MPa. The plate elements for the flanges and the web of each column sections were cut by plasma cutting and flame cutting. There were six plates used in this investigation to fabricate the column sections. Each of the plate was designated herein as Plate: 1, 2, 3, 4, 5, and 6. The plates designated as 1, 3, and 5 were cut by plasma cutting, while the plates designated as 2, 4, and 6 were cut by flame cutting. Therefore, the column sections formed just after welding were named accordingly. For example, a column section formed just after welding of plate strips from plate: 1 was named as column: 1 (C1). The resulting column was about 3960 mm long. This column was cut into residual stress specimen, long column, and a short column. The long and short column sections obtained from the initial column: 1 (C1) was named as C1 (a) and C1 (b), respectively in this investigation. In similar manner, the other column specimens obtained from other initial column stocks (just after welding) were named accordingly.

As most practical steel columns fall into intermediate slenderness range, this investigation focused on establishing strength of such intermediate columns. The non-dimensional ratios ranging from 0.2 to 1.3 were considered. Moreover, only one column test was done for each of the slenderness values. The length of column sections were selected such that the length of sections fabricated by plasma cut-gas metal arc welding process and flame cut-gas metal arc welding process were to be almost same. This was done to compare the strength of both sections under similar testing conditions (pinned end allowing rotation about minor axis for all column section). However, the theoretically calculated values of non-dimensional slenderness ratios were slightly different since the actual values of elastic modulus, yield strength, radius of gyrations were slightly different from plate to plate and column section to column section.

To ensure proper contact with the roller support and thus to eliminate the eccentricity effects, the column was welded with the square base plates having thickness of 6.25mm (1/4 inch) on either ends. Before welding the base plates with the column ends, the base plates were set parallel to each other and then the column was positioned center and perpendicular to the base plates.

Table 6.1 provides the designation of each individual column sections and the respective sectional dimensions in terms of length (L), cross sectional area (A), second moment of area (I_{yy}), and radius of gyration about minor axis (r_y). The mechanical properties in terms of yield strength (F_y) and elastic modulus (E) obtained from tensile coupon test are also given in this table. The experimental evaluation of mechanical properties of the steel grade associated with the virgin steel plates used to fabricate column sections was performed by standard tensile coupon tests. In general, the important mechanical characteristics of specific steel grade such as yield strength, ultimate strength, and final elongation over a certain length under tension are provided by the steel supplier with a mill certificate. However, it is essential to perform an experimental evaluation on the specific steel grade to have better knowledge and understanding of the material behavior of that steel grade. The testing procedures associated with the standard tensile coupon tests followed in this investigation and the test results are provided in Appendix A. Moreover, the non-dimensional values calculated based on actual information are provided in the Table 6.1 for each column sections to be tested in this investigation.

Table 6.2 provides the design values calculated for each of the sections in accordance with CAN/CSA-S16-01 (CSA, 2004) code equation. For example, the design strength of a column specimen 1(a) was calculated as 878kN. This value was calculated based on measured effective length (L) 2790mm, measured cross sectional area (A) of 4360mm^2, radius of gyration (r_y) of 34.85mm, experimentally obtained yield strength (F_y) of 370MPa, experimentally obtained elastic modulus (E) of 202GPa, and the factor n of 1.34 for fabricated I-shape sections according to CAN/CSA-S16-01 standard (CSA, 2004). This table also provides the experimentally obtained ultimate strength of each column sections in this investigation. The percent of differences in column strength were calculated between code values and experimental values of plasma cut columns, code values and experimental values of flame cut columns, and between experimental values of flame cut columns and plasma cut columns. Discussions and comparison of column strength obtained experimentally for both plasma cut and flame cut sections will be made in the next section in this chapter.

6.4 Experimental Setup and Test Procedure

The objective of this investigation is to establish the strength of plasma cut-gas metal arc welded H-shape column sections having the sectional dimension of 150mm width and 170 mm overall depth. The strength of flame cut-gas metal arc welded column sections also was established. This was done to compare the strength of plasma cut column sections with the flame cut column sections. In order to achieve this objective, the column sections made from both cutting techniques were selected at equal lengths and the test was done under similar conditions, i.e, the same boundary condition, loading system, etc were used in this investigation. The following section describes how the test set-up was made and why this set-up was used, and associated measurements taken in this test procedure to establish the strength of columns.

Overall setup

Figure 6.5 shows the overall setup used for all the column tests carried out in this investigation. In this setup, two supporting columns acting as a reaction frame were bolted tightly to test lab strong floor. The actual column tests were carried out within this reaction frame consisting of two columns (see the Figure 6.5). There were two plates known as top supporting plate and bottom supporting plate used in this setup (see Figures 6.5 and 6.6). The column to be tested was positioned within these two plates. The top supporting plate was attached to two channel sections which were securely connected to supporting columns (reaction frame). The movement of the column to be tested at its top end was prevented by this top supporting plate. In order to facilitate the rotation about minor axis of the column specimen, roller box arrangement as shown in the Figure 6.5 was positioned between the top supporting plate and top end of a column specimen. Similar arrangement was done at the bottom end of the column specimen. The bottom supporting plate was placed symmetrically on top of two load cells as shown in Figure 6.6. Furthermore, this plate was vertically movable, i.e., it would move in both upward and downward direction as load was applied to a column specimen. The setup is known as closed loop experimental setup since the external movement of the reaction frame is relatively insignificant.

In this experimental setup, two load cells having capacity of 1600kN each were used to obtain the total reaction applied to the column. The two load cells were placed on top of two loading jacks, which were symmetrically placed with respect to the supporting columns and rested on the rigid floor. These loading jacks were double-acting loading cylinders, which can be controlled as a displacement loading jack. The two loading jacks were manually controlled by a pair of hydraulic pumps connected through the pairs of hoses to each of the loading jacks separately.

As an important step to make sure that the whole experimental setup was good to see and applicable throughout the testing procedure, the strength calculations based on shear check and bearing check for supporting columns, supporting plates, channel sections and bolts (A490) were carried out. Moreover, the associated deformations of the reaction frames, supporting plates, and supporting channel sections were also calculated based on maximum expected ultimate load. Thus, it was found that the strength and the deformations were satisfactory and within the acceptable range to withstand the maximum expected load of 2200kN, which was cross section (4400mm^2) times the ultimate strength of 500MPa obtained from the coupon tensile test. This load could be expected to transfer from the short columns to be tested in this investigation.

Centrally loaded columns may have different end conditions, ranging, theoretically, from full restraint (fixed) to zero restrained (pinned), with respect to end rotation and warping. Most of the columns tests carried out by past researchers have been associated with pinned-end condition for a number of reasons. Under the pinned-end conditions the critical cross section is located near the mid-height of the column. Thus, it makes the cross section of interest remote from the boundary and therefore, little influenced by end effects (Galambos, 1998). For the same effective slenderness ratio, the pinned-end condition requires the use of only half the column length used for the fixed-end condition. Furthermore, the reasons for why the end fixture as shown in Figure 6.6 was chosen in this investigation were to (1) prevent warping of the column specimen to be tested, (2) prevent twisting during the test, and (3) ensure the column specimen to buckle only about minor axis during the test.

Measurement of Displacements

In this testing arrangement, a total of 13 linear voltage displacement transducers (*LVDTs*) were used to measure displacements. As seen in Figure 6.6, four LVDTs (LVDT: 10, 11, 12 and 13) were placed under the bottom supporting plate to measure the movement of the plate when applying the load. Due to the use of two loading jacks with separate control, there was a possibility that the loading cylinders could be raised unevenly and thus might be causing an eccentric loading on the columns. To ensure that the bottom plate was raised evenly so that a uniform compressive load was applied, two LVDTs were placed on either side of an each of the loading cylinders symmetrically. One LVDT (LVDT: 9) was placed at the top supporting plate to measure the movements of the top supporting plate. This was done because there might be a possible slippage of the bolts in the initial stages of loading. One LVDT (LVDT: 8) was placed in one of the mid flanges of the column to see whether there was any movement in the transverse direction. The other seven LVDTs (LVDT: 1, 2, 3, 4, 5, 6, and 7) were placed along the mid web (see the Figure 6.6). In the seven LVDTs placed along the mid web, one of them (LVDT: 4) was placed in the mid-height of the column and other two (LVDT: 3 and 5) were placed at quarter points of the column. Also, a pair of LVDTs was placed roughly at 50mm interval at the top (LVDT: 1 and 2) and bottom (LVDT: 6 and 7) ends of the column along the mid web in order to measure the rotation of both ends during the test (see the Figure 6.6).

Column Alignment

Aligning the specimen within the testing setup is the most important step in the column testing procedure, prior to loading. Commonly two approaches have been used to align centrally loaded columns by past researchers (Galambos, 1998). In the first approach the column is aligned under load so that the axial stresses are essentially uniform over the mid-height and the quarter-point cross sections. In the second approach the column alignment is carefully done geometrically, but no special effort is made to secure a uniform stress distribution over the critical cross-section. In this investigation, the second approach of aligning the columns geometrically was followed, because this approach is generally considered to be simpler and quicker. Also this approach is most cost effective. In addition to these, the first approach may not be applicable for longer columns since the geometrical imperfections of those columns are significant and thus onset of bending stresses would come into play. In addition, columns in actual construction are aligned geometrically than using axial stress values.

The alignment of the column was carried out within the test setup by observing the averaged displacement values from the two LVDTs (LVDT: 10 &11 with loading jack:1 and LVDT: 12& 13 with loading jack: 2) placed with each of the loading jacks under the bottom plate and the associated readings obtained from two load cells. The column position within the setup was adjusted such that for averaged displacement values and the respective load cell readings were to be almost equal. Also the level bar and plumb-bob were used to make sure the column was leveled. During the alignment procedure, a load well within the proportional limit of each column was applied.

Data Acquisition System

The computer software called "DATA LOGGER" was used to acquire the data from the experimental work. The voltage signals received from the LVDTs and the load cells were transferred by this acquisition system as displacements in millimeter (mm) and loads in kilo-Newton (kN), respectively. This conversion was done by multiplying each signal input by a corresponding calibration factor. The real time display for axial load versus axial deformation was observed during the test which provided the most real situation of the whole test performance as well as monitoring of the whole test. The test data were scanned at an interval of every one second for real time display on the screen.

Test Procedure and Measurements

A pioneering test on a 300W column having non-dimensional slenderness ratio of about 0.5 was carried out in order to become familiar with the testing procedures and to make sure of the applicability of the test setup. The column was carefully aligned within the test setup as explained in the previous sections. Before adjusting the initial values of LVDTs, a load was applied to the column specimen. The load was well within the proportional limit. The load was brought back to zero and then the LVDTs were adjusted for their initial values.

This procedure is necessary because the LVDTs began to realize the loading and be adjusted themselves. The experimental ultimate load of this stub column was 1120kN.

In this investigation, axial load versus corresponding axial deformation, axial load versus corresponding mid-height out-of-plane (transverse) deflection were the most important measurements. However, it was also desirable to measure the deflections at quarter points, rotations at the ends of a column and transverse movement of a column during buckling. Moreover, the overall axial shortening was calculated based on the bottom plate movement with respect to the top plate movement (relative movement) in this investigation. Because, it was observed from readings of the LVDT (LVDT: 9) connected to top supporting plate that slippage of top supporting plate took place during initial stages of loading.

After the column was aligned and the initial values of LVDTs were set to zero, the bottom supporting plate was raised evenly by applying hydraulic pressure to both loading jacks. Both loading jacks were raised at the same incremental displacement simultaneously. The load was applied slowly since the loading jacks took some time to settle down to a steady state and thus to provide sufficient time to allow stress to distribute within the steel cross-section as well as along the length of the specimen. The incremental displacement, or the axial deformation of the specimen, was controlled by monitoring the real time display of the relative displacements between the top and bottom supporting plates. The load-displacement curve began to drop down, after the ultimate load and thus the failure of the column either by flexural buckling or by cross-sectional yielding was reached. During the time the test was performed, the LVDTs were intermittently touched smoothly by hand to ensure that they worked properly.

6.5 Experimental Observations

The behavior of the test specimens under load was determined with the aid of measurements of lateral deflections at mid-height as well as at quarter points along the minor principal direction about which the rotation was allowed (minor axis buckling), rotations at the ends, and the column shortening in the axial direction. The maximum load attained by each column was compared with the design value obtained based on the Canadian Standard (CAN/CSA-S16-01) code equation (CSA, 2004). The experimentally obtained yield strength, and elastic modulus of the individual plates, from which the respective columns were made, were used in the calculation of design value. Moreover, in design calculations, the actual sectional dimensions were used for calculating the radius of gyration of individual column specimens to be tested in this investigation. The Figure 6.7 shows the column specimens having different non-dimensional slenderness ratios after failure. The observations made during the test and after the test for the column specimens in this research work are categorized as below for clear understanding;

(a) Plasma Cut Columns

1. The Column of $\lambda = 1.28$
2. The Column of $\lambda = 1.09$
3. The Column of $\lambda = 0.86$
4. The Column of $\lambda = 0.51$
5. The Column of $\lambda = 0.33$
6. The Column of $\lambda = 0.18$

(b) Flame Cut Columns

1. The Column of $\lambda = 1.29$

2. The Column of $\lambda = 1.18$

3. The Column of $\lambda = 0.90$

4. The Column of $\lambda = 0.53$

5. The Column of $\lambda = 0.35$

6. The Column of $\lambda = 0.18$

Long Columns: (*Defined herein as $\lambda \geq 1$*)

Plasma Cut Column ($\lambda = 1.28$) – [specimen: C5 (a)]

In the column specimen designated herein as C5 (a), it was observed that the failure was accompanied by the flexural buckling. No local buckling was observed in the specimen during the entire test. The behavior of the column specimen is as shown in Figure 6.8. It could be seen that the load versus axial deformation curve was almost linear until the column specimen reached its ultimate load. After the maximum or the ultimate load the curve was no longer linear. Moreover, the load suddenly dropped down for sometime as soon as the maximum load was reached and thereafter the load gradually dropped down with the increased axial displacement. However, the load versus mid height deformation was gradually increasing until the failure load was reached and then the load started dropping down gradually with the increasing displacement. Similar behavior was observed for the load versus displacement at quarter points (as seen in the Figures 6.8(d)) and the load versus rotations at the ends of the column (as seen in the Figures 6.8(b)). It was observed that the movement of the column specimen in the transverse direction was negligible during the test. The maximum value obtained for this column specimen through the lab test was 633kN, whereas the design value of this column according to CAN/CSA-S16-01 standard was 703kN. Therefore the actual tests value is about 90% of the calculated design value.

Flame Cut Column (λ = 1.29) – [specimen: C6 (a)]

The column designated as C6 (a) in this investigation also failed by the flexural buckling. No local buckling was observed during the entire test. The behavior of the column specimen is as shown in Figure 6.9. The load versus overall axial deformation of this column was almost linear up to about 200kN and then the rate of change of loading with increasing axial displacement was slightly lower than the initial rate up to the loading of about 250kN and then again the load increased gradually with the increasing axial displacement as shown in Figure 6.9(a). The reason for such behavior of axial load versus overall axial shortening can be explained as below:

(1) The axial shortening of the column doesn't belong to the component of pure axial shortening of the column; rather this depends on how the column deflects laterally.

(2) The initial out-of- straightens about minor axis (sweep) of this column C6 (a) was relatively larger than that of column C5 (a) (see Table 4.3).

(3) It was commonly observed in this investigation during each of the column tests that the behavior of axial load versus overall axial displacement was heavily dependent upon the rate of applied loading. Hence, even though the load was applied at very slow rate during the tests in this investigation, it was very hard to maintain the consistency for each individual test since the load was applied manually.

The maximum load attained by this column was 539kN. The calculated design value for this column based on CAN/CSA-S16-01 was 744kN (Table: 6.2). Therefore the experimentally obtained value is 73% of the calculated design value. Note that the design values were calculated based on actual yield strength, elastic modulus, and cross sectional dimensions of respective column sections.

Plasma Cut Column (λ = 1.09) – [specimen: C1 (a)]

The column designated herein as 1(a) failed by the flexural buckling and no local buckling was observed during the entire test. The general behavior of the column is as shown in Figures 6.10(a) through (d). The behavior of axial load versus overall shortening of the column was almost same as the behavior of the column C6 (a). The maximum load attained by this column was 720kN. The calculated design value based on CAN/CSA-S16-01 was 878kN. Therefore the actual test value is about 82% of the design value.

Flame Cut Column (λ = 1.18) – [specimen: C2 (a)]

The column designated herein as C2 (a) also failed by flexural buckling and no local buckling was observed during the entire test. The general behavior of the column is as shown in Figures 6.11(a) through (d). The behavior of axial load versus overall shortening of the column was linear until the column reached its maximum capacity. The maximum load attained by this column was 647kN. The calculated design value based on CAN/CSA-S16-01 was 864kN. Therefore the actual test value is about 75% of the design value.

Short Columns: *(Defined herein as, $1.0 \geq \lambda \geq 0.5$)*

Plasma Cut Column (λ = 0.86) – [specimen: C3 (a)]

The column designated herein as C3 (a) failed by the flexural buckling and no local buckling was observed during the entire test. The general behavior of the column is as shown in Figures 6.12 (a) through (d). The behavior of axial load versus overall shortening of the column was almost same as the behavior of the columns 6(a) and C1 (a). The axial Load versus overall axial shortening was linear up to the load of about 225kN and then the rate of change of load with increasing axial deformation was slightly lower than the initial variation and then again the variation of load versus overall axial shortening was almost same as the initial variation. The maximum load attained by this column was 752kN and the calculated design value of this column was 1040kN. Therefore the actual test value is 72% of the calculate design value based on CAN/CSA-S16-01.

Flame Cut Column (λ = 0.90) – [specimen: C4 (a)]

The column designated herein as C4 (a) also failed by flexural buckling and no local buckling was observed during the entire test. The general behavior of the column is as shown in Figures 6.13(a) through (d). The behavior of axial load versus overall shortening of the column was linear until the column reached its maximum capacity. The maximum load attained by this column was 812kN. The calculated design value based on CAN/CSA-S16-01 was 1040kN. Therefore the actual test value is about 78% of the design value.

Plasma Cut Column (λ = 0.51) – [specimen: C3 (b)]

The column having non-dimensional slenderness value of 0.5 was designated as C3 (b) in this investigation. The failure of this column was accompanied by flexural buckling as seen in Figure 7. The maximum load attained by this column was 1308kN and the calculated design value based on CAN/CSA-S16-01 was 1370kN. Therefore the actual test value is almost 95% of the design value. The behavior of the column is as shown in Figures 6.14(a) through (d). Moreover, it was observed that the local buckling of the flange plate element occurred just after the attainment of the maximum load with increasing lateral defection of the column.

Flame Cut Column (λ = 0.53) – [specimen: C4 (b)]

The column having non-dimensional slenderness value of 0.54 was designated as C4 (b) in this investigation. The failure of this column was accompanied by flexural buckling. The maximum load attained by this column was 1364kN and the calculated design value based on CAN/CSA-S16-01 was 1408kN. Therefore the actual test value is almost 97% of the design value. The behavior of the column is as shown in Figures 6.15(a) through (d). Moreover, it was observed that the local buckling of the flange plate element occurred just after the attainment of the maximum load with increasing lateral defection of the column.

Stub Column: *(Defined herein as λ< 0.5)*

Plasma Cut Column (λ = 0.33) – [specimen: C1 (b)]

The column having non-dimensional slenderness value of 0.3 was designated as C1 (b) in this investigation. The failure of this column was accompanied by combination of flexural buckling and cross-sectional yielding as seen in Figure 6.7.The maximum load attained by this column was 1532kN and the calculated design value based on CAN/CSA-S16-01 was 1563kN. Therefore the actual test value is almost 100% of the design value. The behavior of the column is as shown in Figures 6.16(a) through (d). Unfortunately, the behavior of column having non-dimensional value of 0.2, designated herein as C5 (b) was not able to obtain due to the failure of the supporting end plate during the test.

Flame Cut Column (λ = 0.35) – [specimen: C2 (b)]

The column having non-dimensional slenderness value of 0.35 was designated as C2 (b) in this investigation. The failure of this column was accompanied by the combination of flexural buckling and cross-sectional yielding .The maximum load attained by this column was 1533kN and the calculated design value based on CAN/CSA-S16-01 was 1668kN. Therefore the actual test value is 92% of the design value. The behavior of the column is as shown in Figures 6.17(a) through (d).

Plasma Cut Column (λ = 0.18) – [specimen: C5 (b)]

The column having non-dimensional slenderness value of 0.2 was designated as C5 (b) in this investigation. Unfortunately, the test on this specimen was not totally carried out since the failure of the bottom end plate during the test. The test was stopped at an axial loading of about 1545kN. Figure 6.18 shows the behavior of the column specimen until the test was stopped.

Flame Cut Column (λ = 0.18) – [specime: C6 (b)]

The column having non-dimensional slenderness value of 0.2 was designated as C6 (b) in this investigation. The failure of this column was accompanied mainly by cross-sectional yielding. However, it was observed during the test that this very short column was slight bent about the minor axis. This bending may be as a result of the small eccentricity in the loading arrangement. The maximum load attained by this column was 1710kN and the calculated design value based on CAN/CSA-S16-01 was 1687kN. Therefore the actual test value is almost 100% of the design value. The behavior of the column is as shown in Figures 6.19 (a) through (d).

6.6 The Comparison and Discussion of Test Results

Figure 6.20 shows the ultimate load of plasma cut-gas metal arc welded columns obtained experimentally in this investigation. The variation of strength with the length of columns according to CAN/CSA-S16-01 standard is also shown in this figure. Figure 6.21 shows the ultimate load of flame cut-gas metal arc welded columns. The design values calculated in accordance with the CAN/CSA-S16-01 standard for these columns are also shown in the same figure. The overall behavior of the columns fabricated by the two different fabrication techniques such as plasma cut-gas metal arc welding process and flame cut-metal gas arc welding process (plasma and flame) were relatively identical. However, the column sections having non-dimensional slenderness values of more than 1 fabricated from flame-cut plates seemed to have lower strength than that of plasma-cut columns. This may be due to fact that the presence of relatively high initial out-of-straightness about the minor axis of the flame-cut columns tends to reduce the ultimate load carrying capacity of these columns in this investigation. On the other hand, for the sections having non-dimensional slenderness values of less than 1, the flame cut columns seemed to carry relatively higher loads than that of plasma cut columns in this investigation. This may be due to the fact that the presence of relatively high tensile residual stresses at flange tips results in delayed loss of stiffness as weak axis inelastic buckling occurs. Subsequently, there could be increase in load carrying capacity.

Moreover, for the column sections having non-dimensional slenderness values of more than 0.9 in this investigation, there was no local buckling failure mode observed during the test. The failure was purely accompanied by the flexural buckling only for these sections since the possibility of torsional effects were prevented by the test setup itself in this investigation. However, for the short column sections ($\lambda \leq 0.5$), the local buckling was observed after the member reached its ultimate load. The determination of load at which the local buckling takes place was out of objective of this investigation, thus only visual inspection was made during the tests.

Method of Fabrication	Column Designation	Length (L) (mm)	I_{yy} (mm^4)	Area (A) (mm^2)	r_y (mm)	F_y (MPa)	E (GPa)	λ
Plasma-Cut Columns	C5 (a)	3217	$5.022 x 10^6$	4342	34.01	362	200	1.28
	C1 (a)	2790	$5.303 x 10^6$	4366	34.85	370	202	1.09
	C3 (a)	2284	$5.396 x 10^6$	4415	34.96	347	203	0.86
	C3 (b)	1354	$5.396 x 10^6$	4415	34.96	347	203	0.51
	C1 (b)	840	$5.303 x 10^6$	4366	34.85	370	202	0.33
	C5 (b)	448	$5.022 x 10^6$	4342	34.01	362	200	0.18
Flame-Cut Columns	C6 (a)	3221	$5.266 x 10^6$	4366	34.73	389	203	1.29
	C2 (a)	2793	$4.941 x 10^6$	4377	33.60	398	200	1.18
	C4 (a)	2289	$5.042 x 10^6$	4326	34.14	369	206	0.90
	C4 (b)	1350	$5.042 x 10^6$	4326	34.14	369	206	0.53
	C2 (b)	836	$4.941 x 10^6$	4377	33.60	398	200	0.35
	C6 (b)	446	$5.266 x 10^6$	4366	34.73	389	203	0.18

Table 6.1: The Calculated Sectional Properties of Column Sections

Plasma Cut Columns				% difference Between Flame cut Column and Plasma Cut Column	Flame Cut Columns			
Column Identific -ation / Slenderness	Code value (Based on CAN/CSA S16-01) (kN)	Experimental Value (kN)	% difference Between Code Value and Experimental Value		Column Identific -ation / Slenderness	Code value (Based on CAN/CSA S16-01) (kN)	Experimental Value (kN)	% difference Between Code Value and Experimental Value
C5 (a) / $\lambda = 1.28$	703	633	-9.9	+17.4	C6 (a) / $\lambda = 1.29$	744	539	-27.5
C1 (a) / $\lambda = 1.09$	878	720	-18.0	+11.3	C2 (a) / $\lambda = 1.18$	864	647	-25.1
C3 (a) / $\lambda = 0.86$	1044	752	-28.0	-7.4	C4 (a) / $\lambda = 0.90$	1040	812	-21.9
C3 (b) / $\lambda = 0.51$	1370	1308	-4.5	-4.1	C4 (b) / $\lambda = 0.53$	1408	1364	-3.1
C1 (b) / $\lambda = 0.33$	1563	1532	-2.0	0.0	C2 (b) / $\lambda = 0.35$	1668	1533	-8.1
C5 (b) / $\lambda = 0.18$	1561	N/A	N/A	N/A	C6 (b) / $\lambda = 0.18$	1687	1710	+1.4

Table 6.2: The Strength of Column Sections

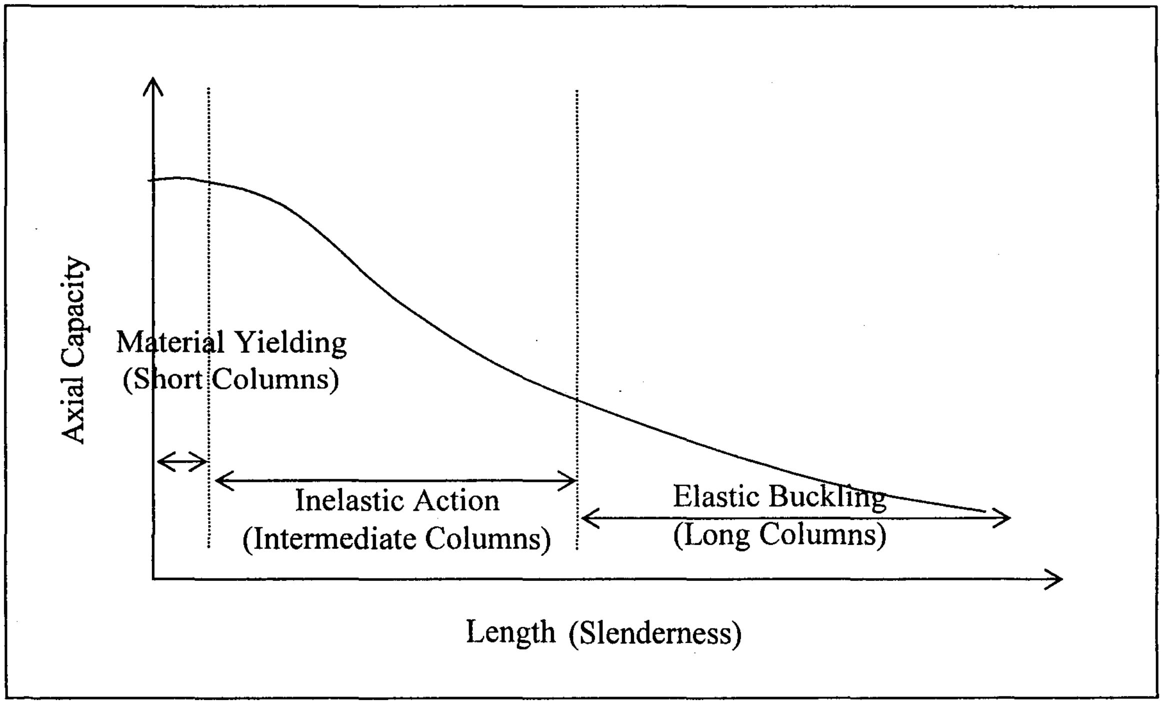

Figure 6.1: Strength of Steel Columns

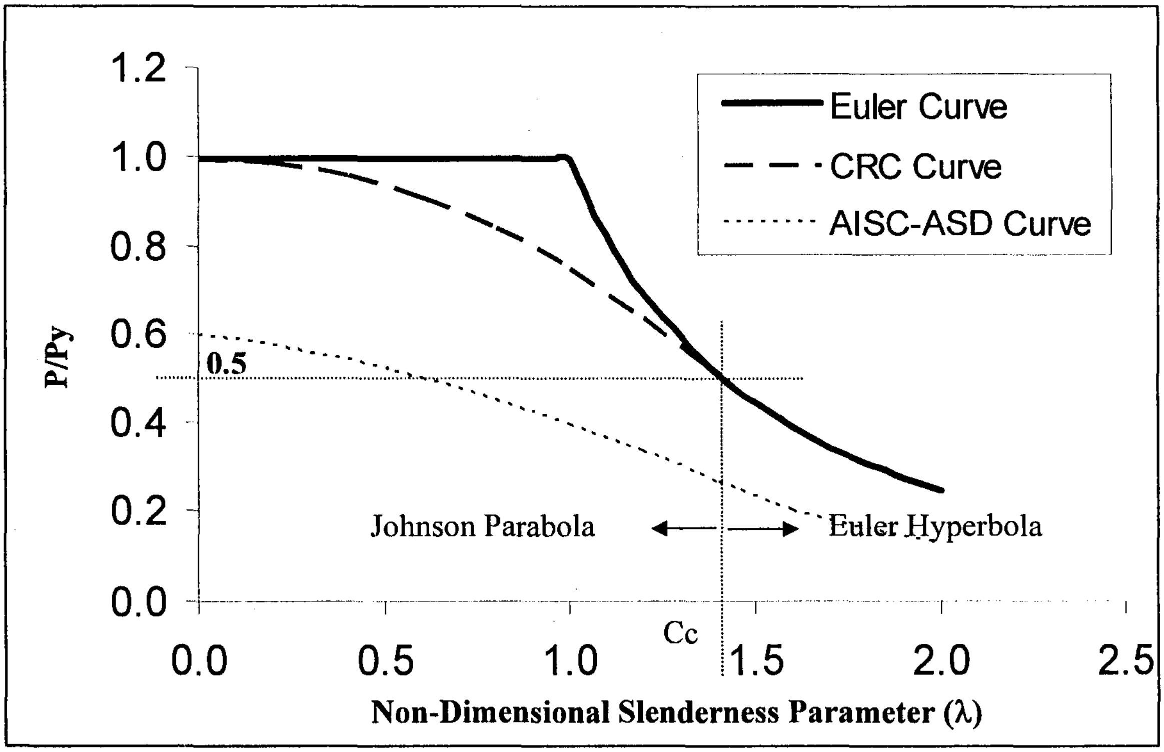

Figure 6.2: Column Curves (Euler, Theoretical CRC, and AISC)

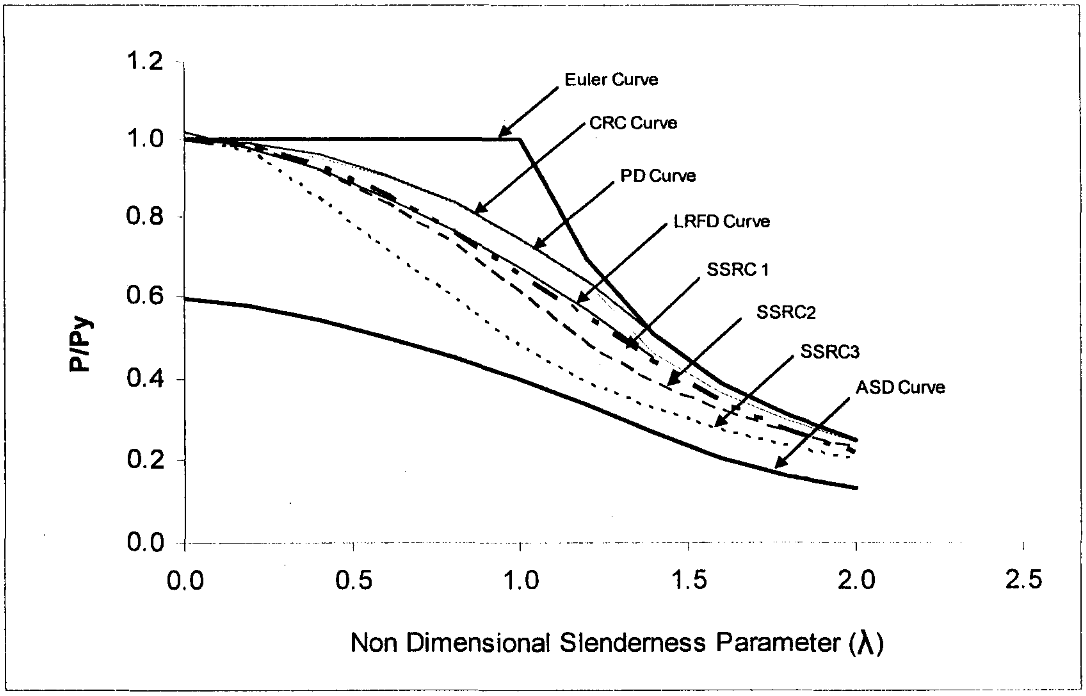

Figure 6.3: The Column Curves

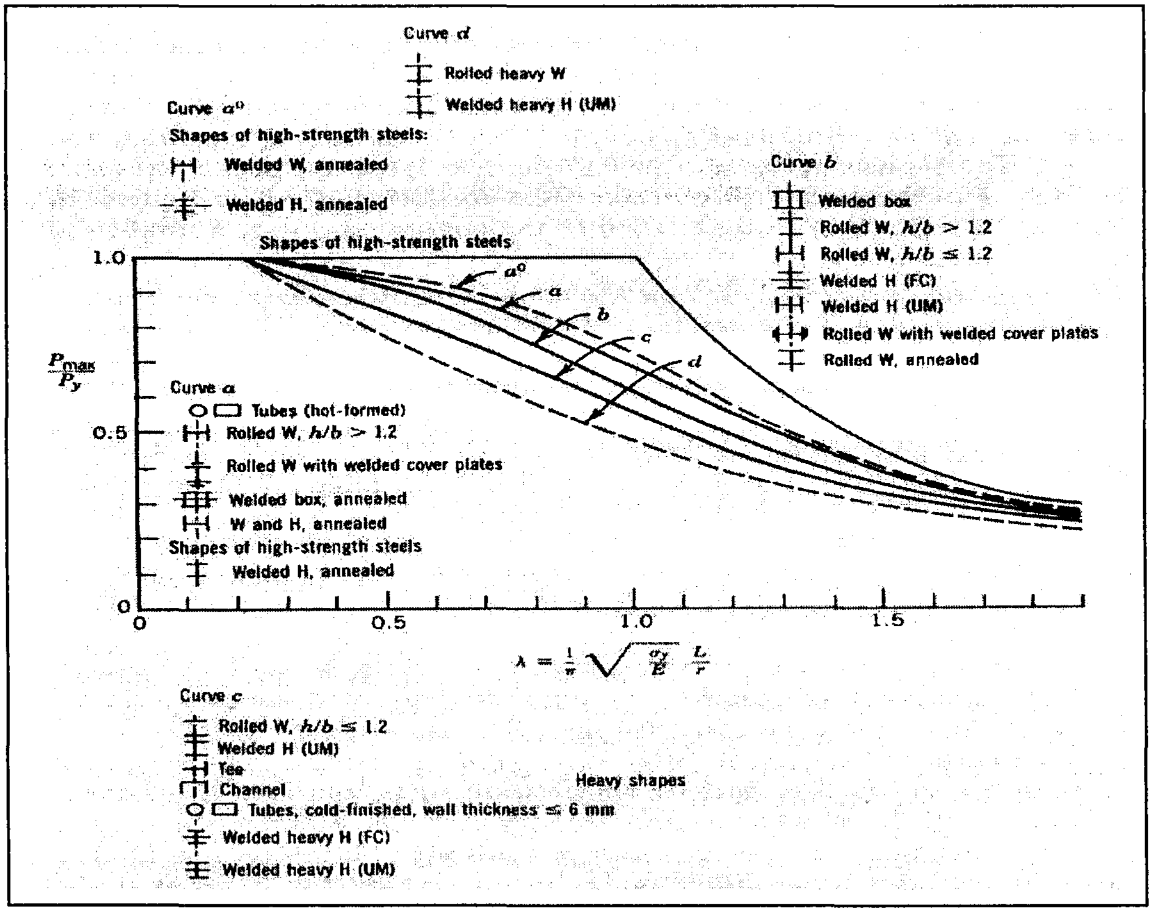

Figure 6.4: The ECCS Column Curves (Galambos, 1998)

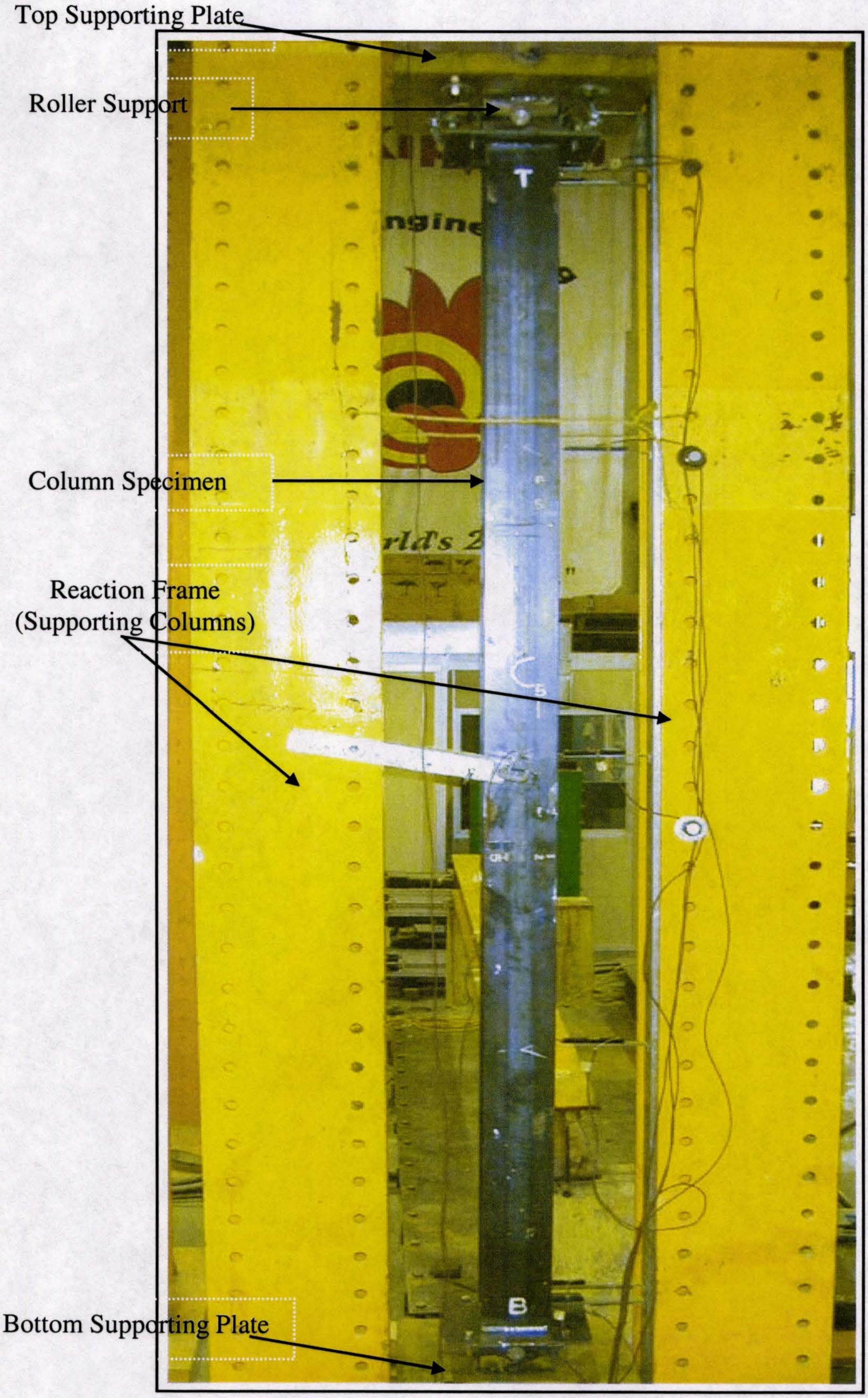

Figure 6.5: The Experimental Setup for Axially Loaded Column Tests

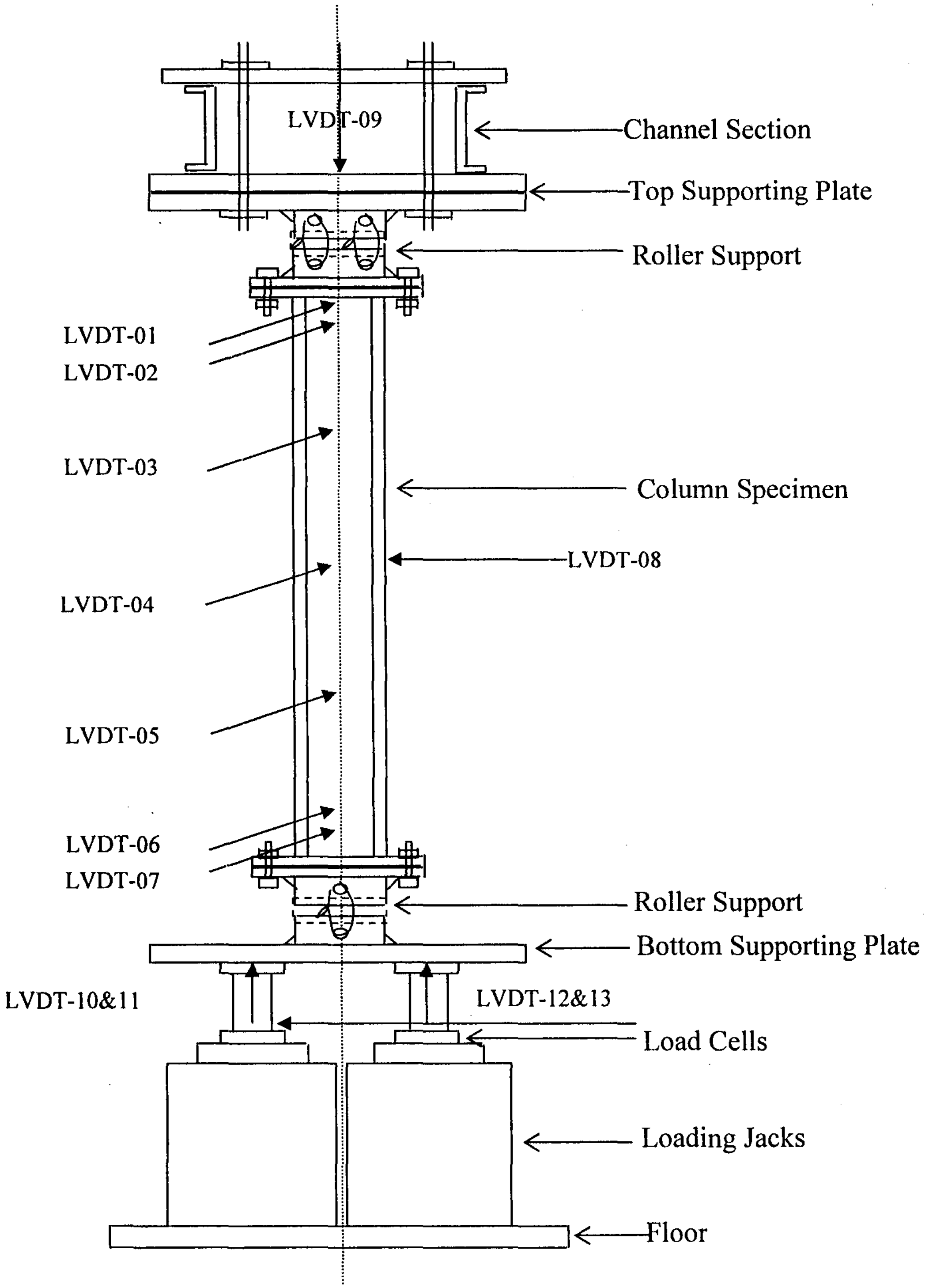

Figure 6.6: The Placement of LVDTs

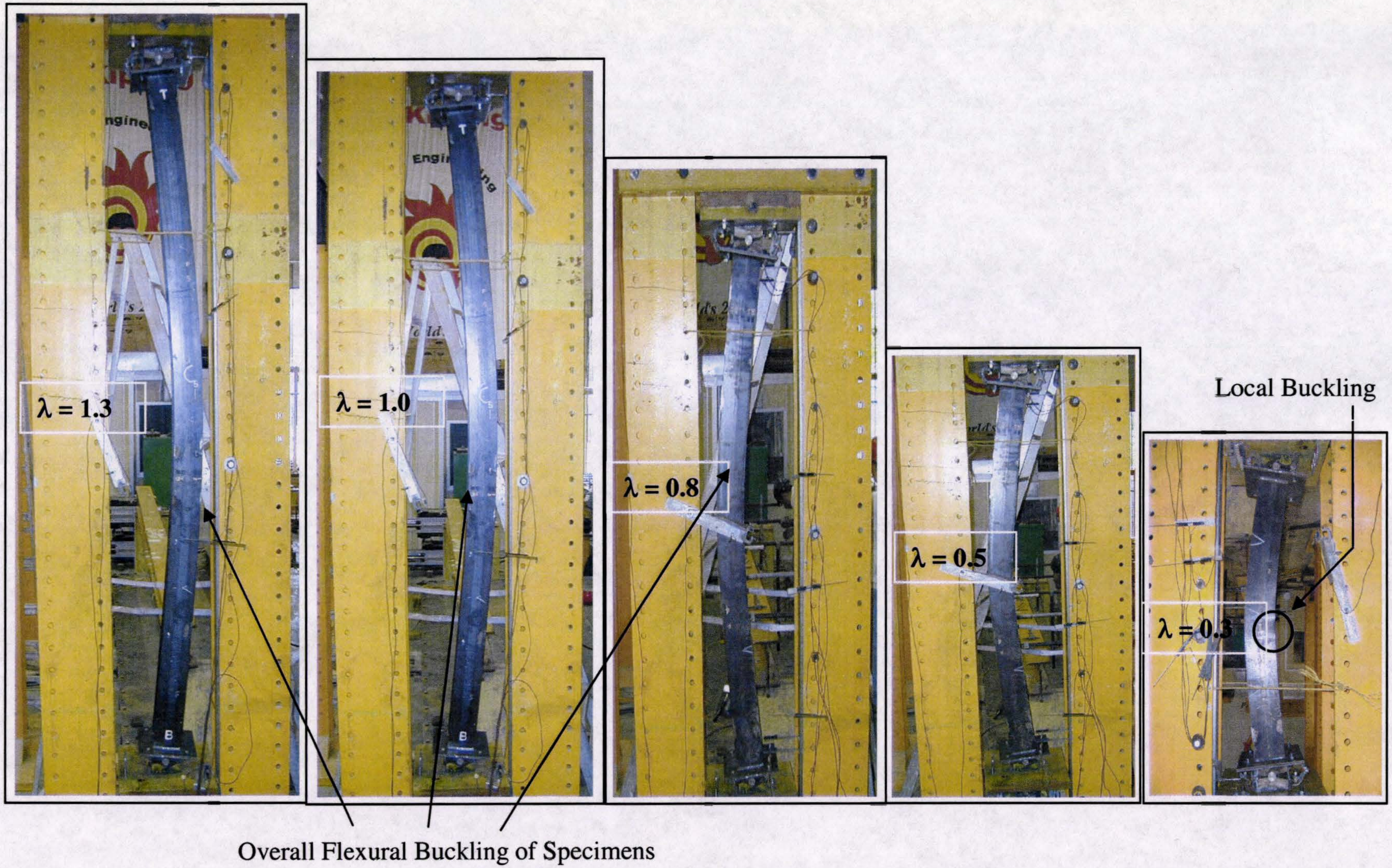

Figure 6.7: The Column Specimens after Failure

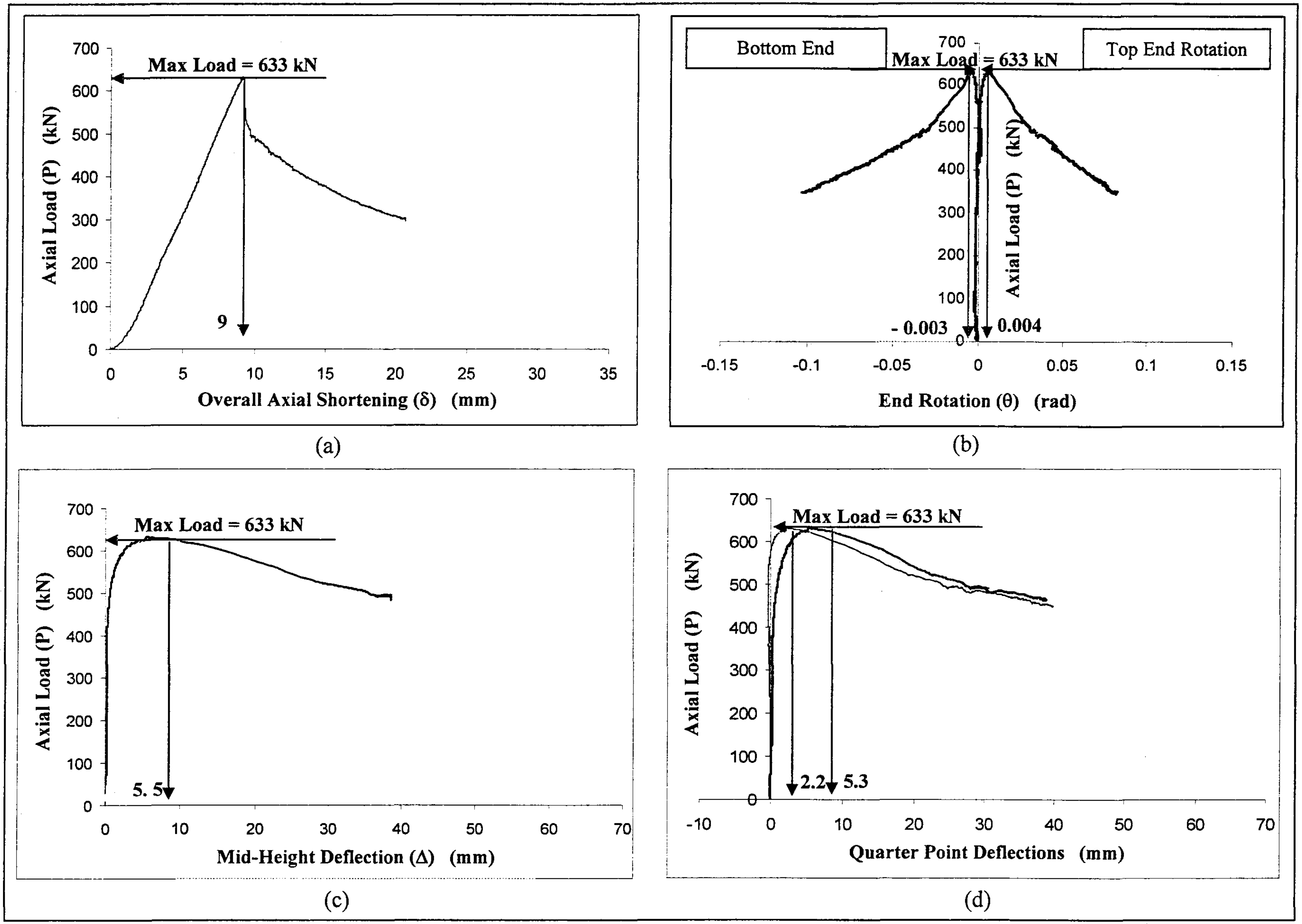

Figure 6.8: The Behavior of Plasma Cut Column 'C5 (a)' Having Non Dimensional Ratio of 1.28

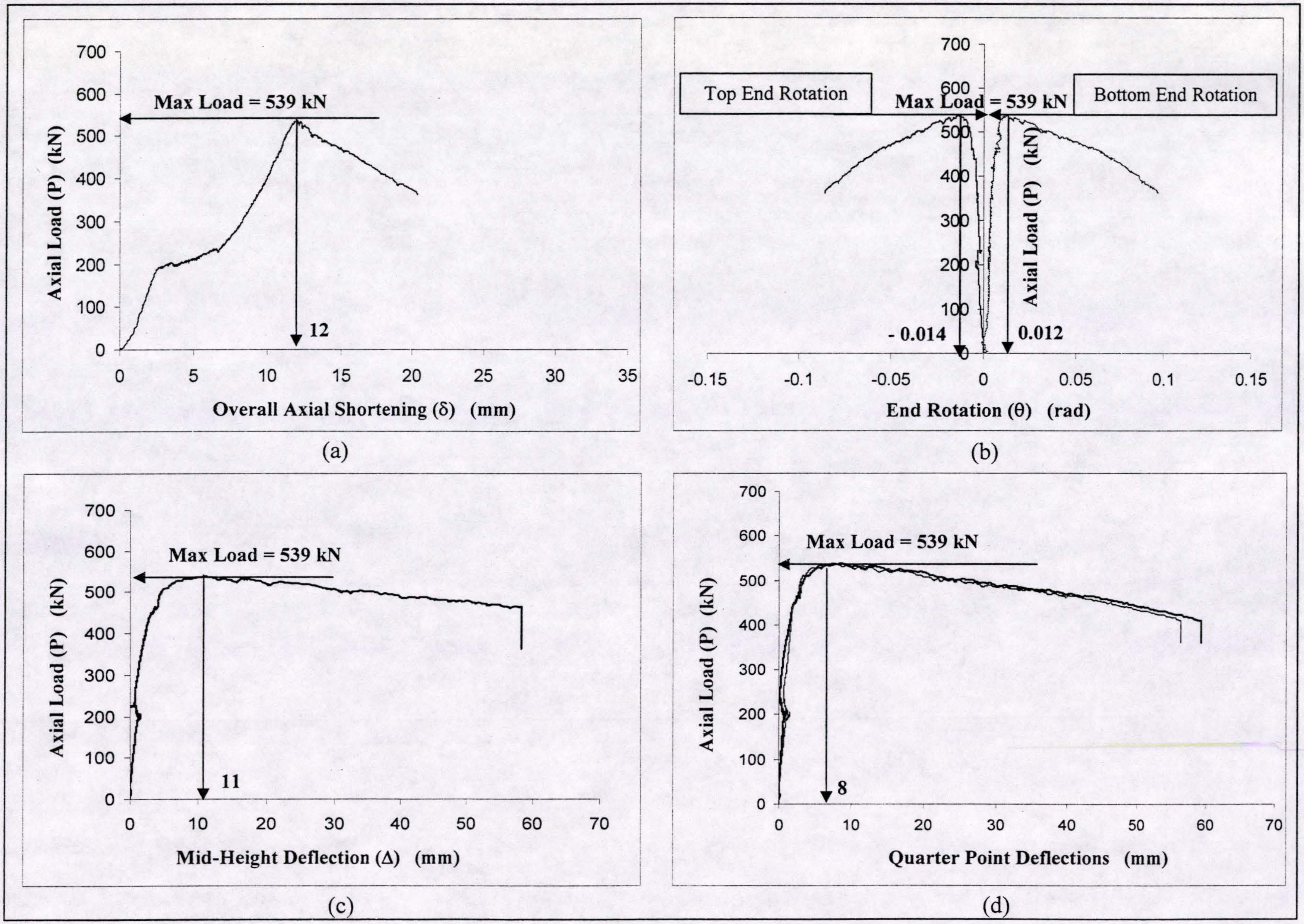

Figure 6.9: The Behavior of Flame Cut Column 'C6 (a)' Having Non Dimensional Ratio of 1.29

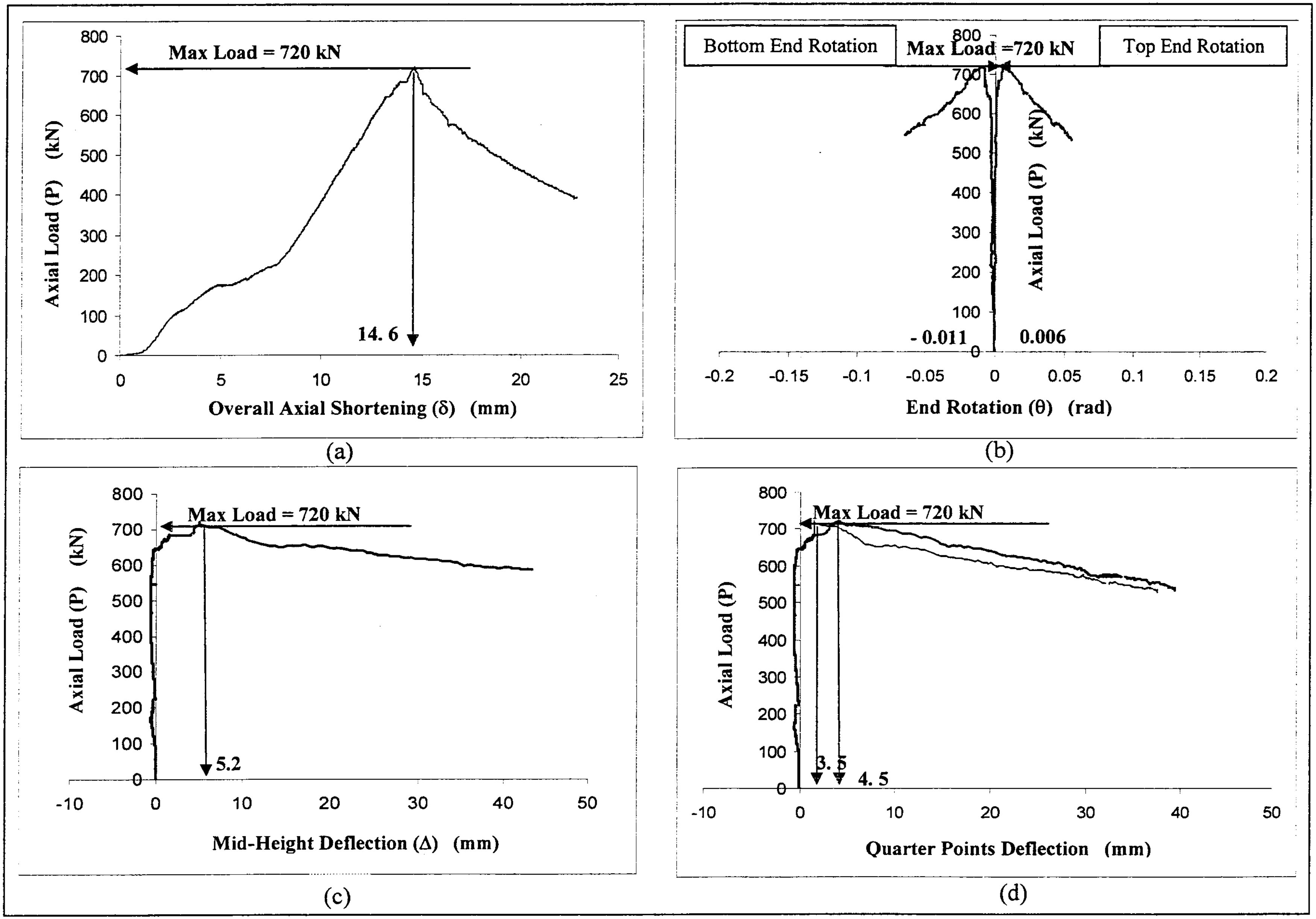

Figure 6.10: The Behavior of Plasma Cut Column 'C1 (a)' Having Non Dimensional Ratio of 1.09

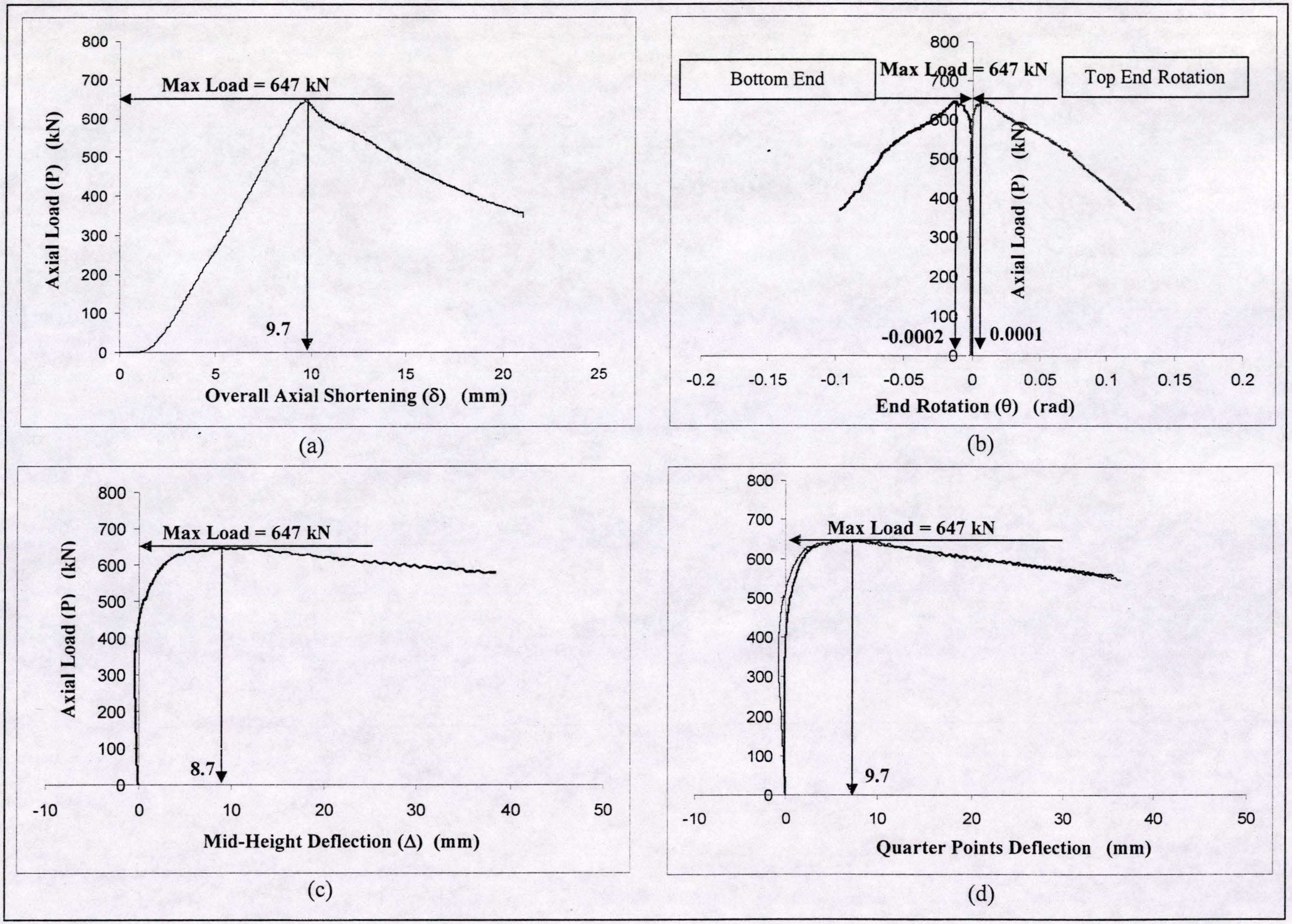

Figure 6.11: The Behavior of Flame Cut Column 'C2 (a)' Having Non Dimensional Ratio of 1.18

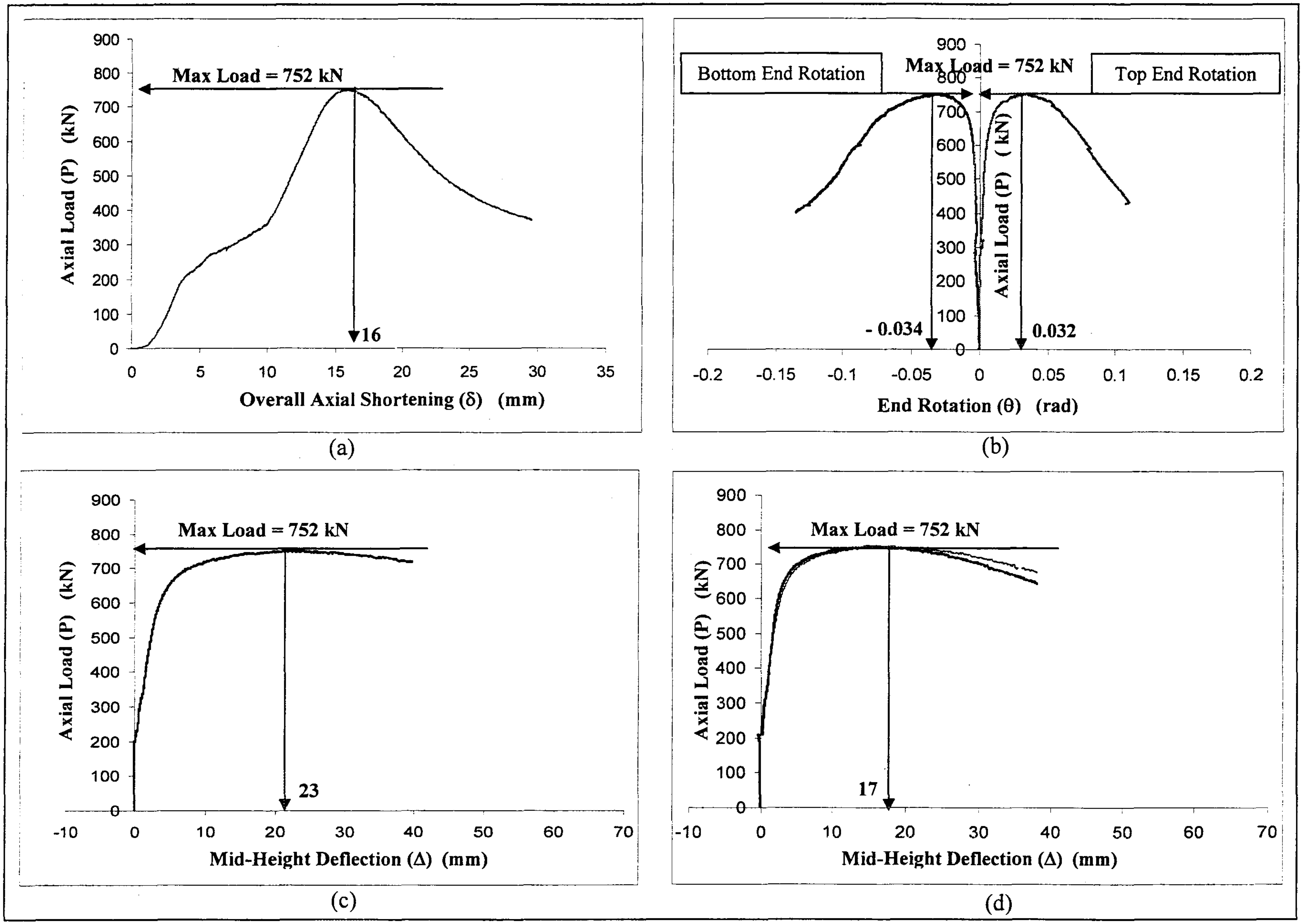

Figure 6.12: The Behavior of Plasma Cut Column 'C3 (a)' Having Non Dimensional Ratio of 0.86

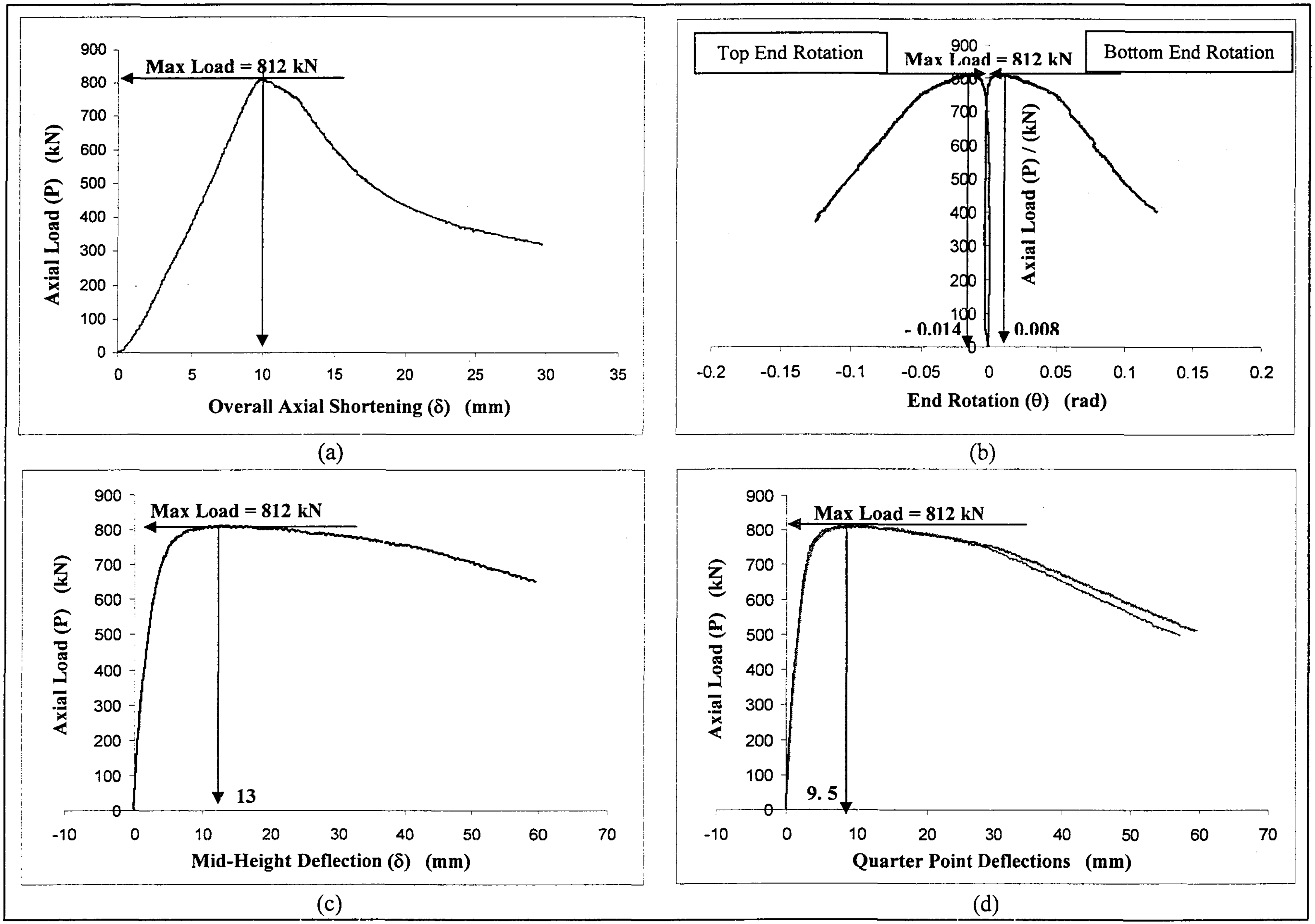

Figure 6.13: The Behavior of Flame Cut Column 'C4 (a)' Having Non Dimensional Ratio of 0.90

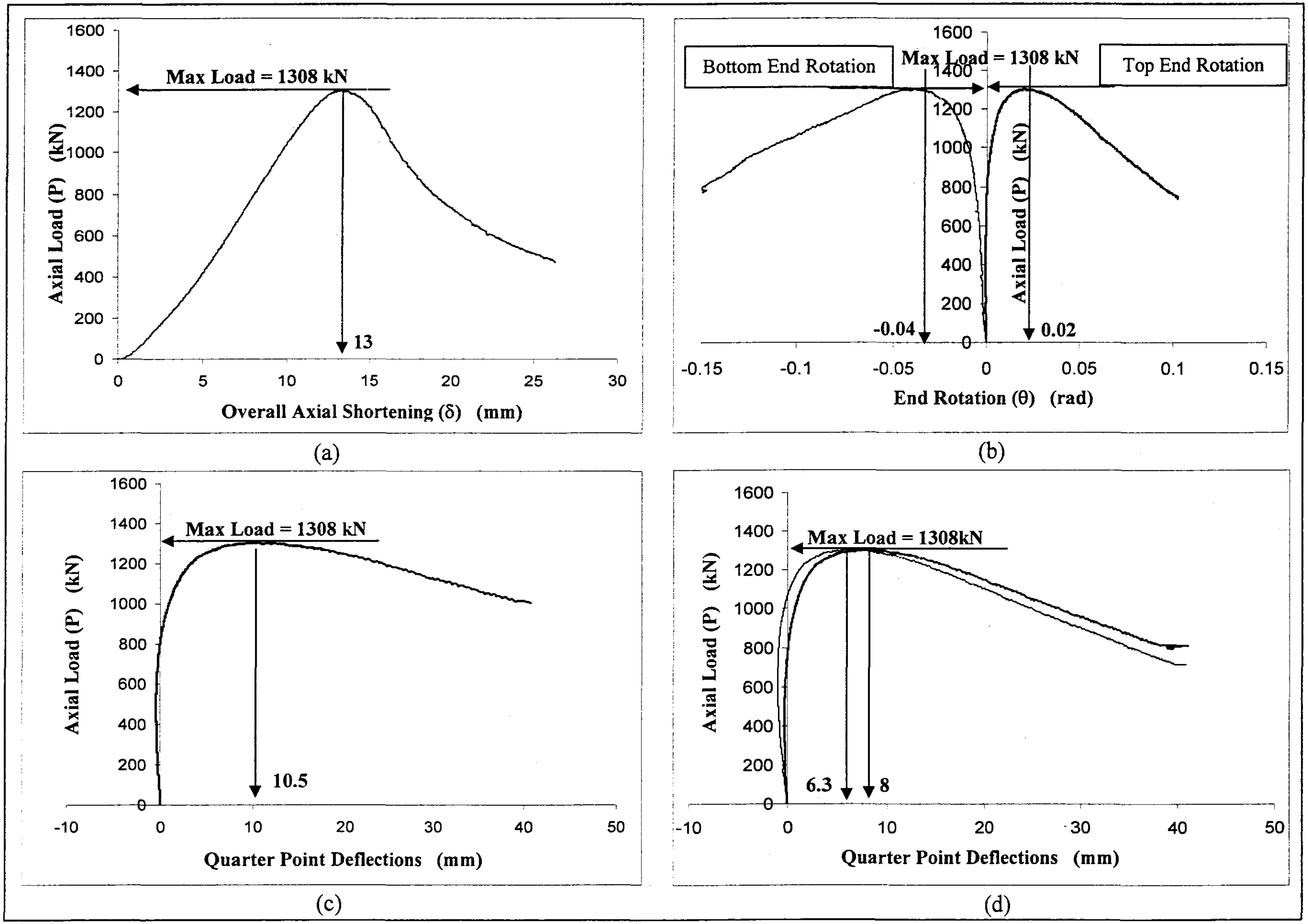

Figure 6.14: The Behavior of Plasma Cut Column 'C3 (b)' Having Non Dimensional Ratio of 0. 51

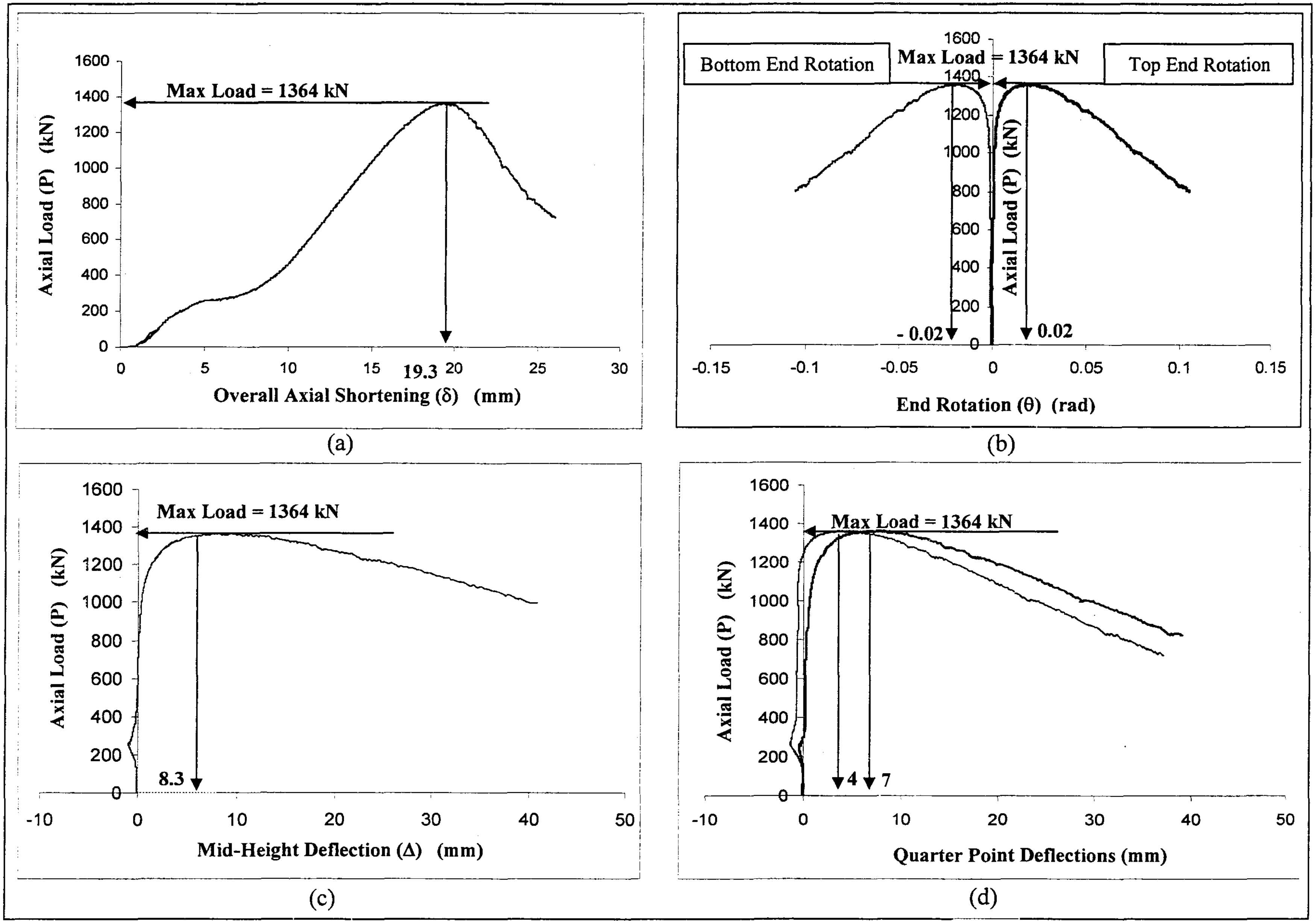

Figure 6.15: The Behavior of Flame Cut Column 'C4 (b)' Having Non Dimensional Ratio of 0. 54

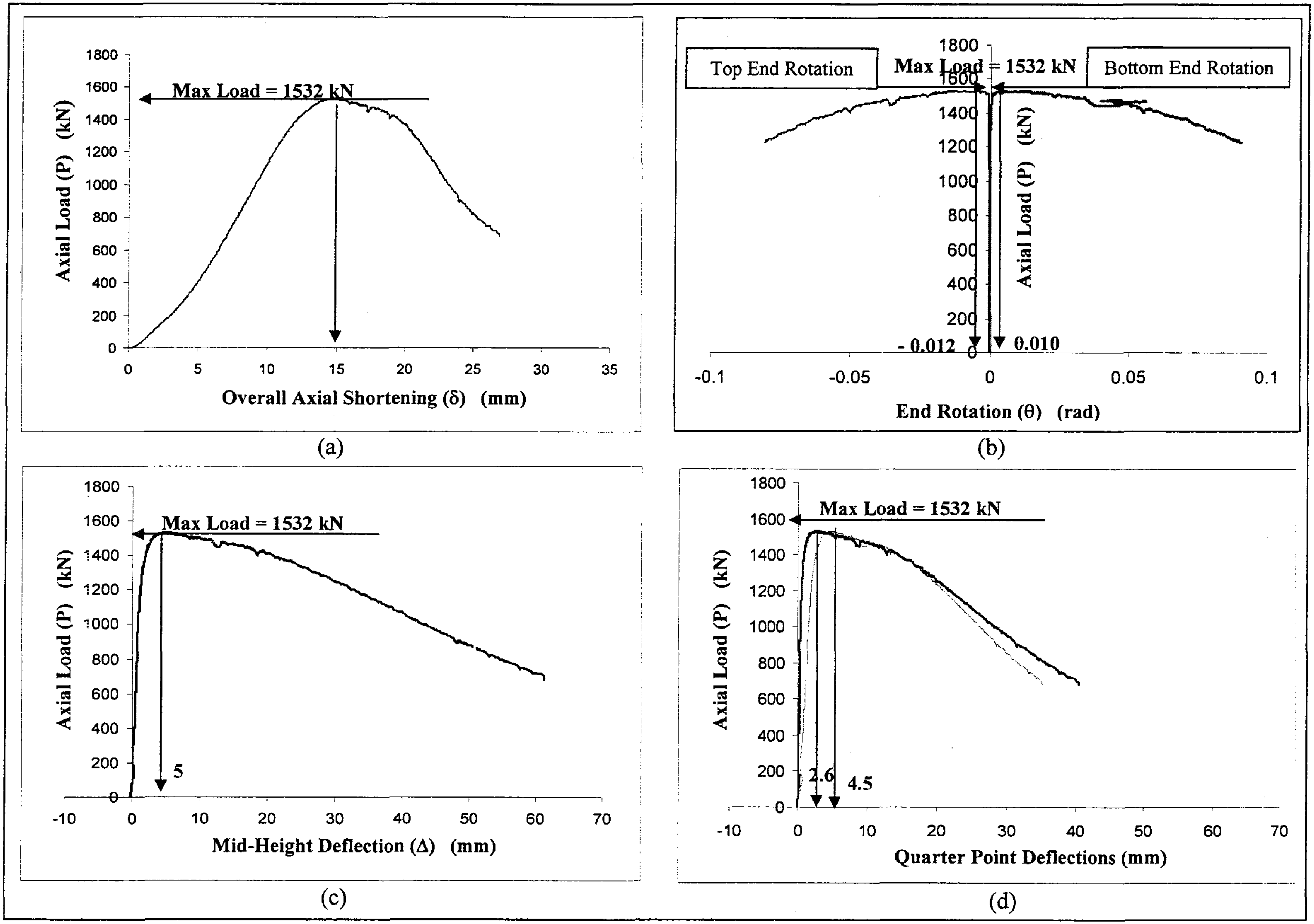

Figure 6.16: The Behavior of Plasma Cut Column 'C1 (b)' Having Non Dimensional Ratio of 0. 33

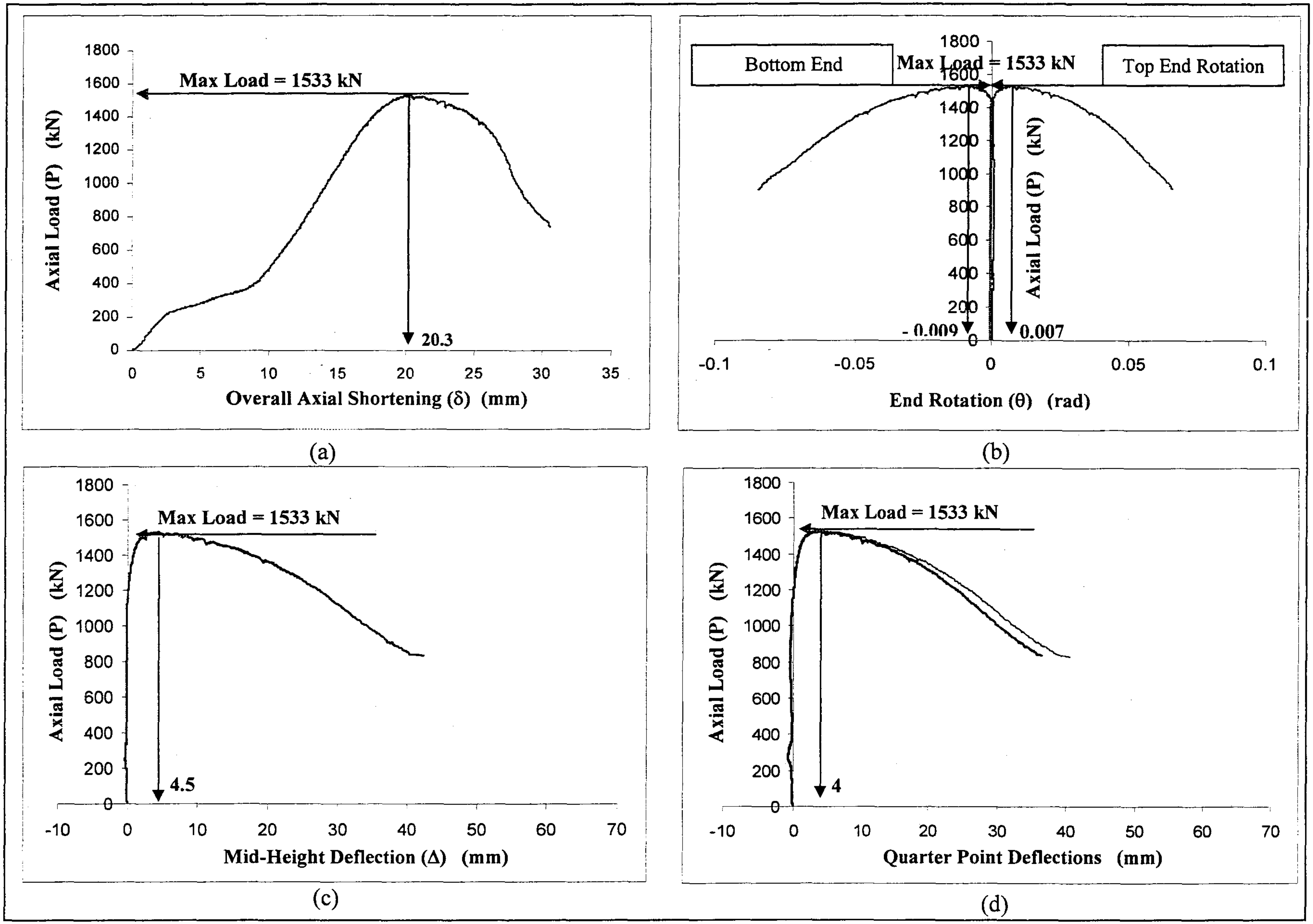

Figure 6.17: The Behavior of Flame Cut Column 'C2 (b)' Having Non Dimensional Ratio of 0. 35

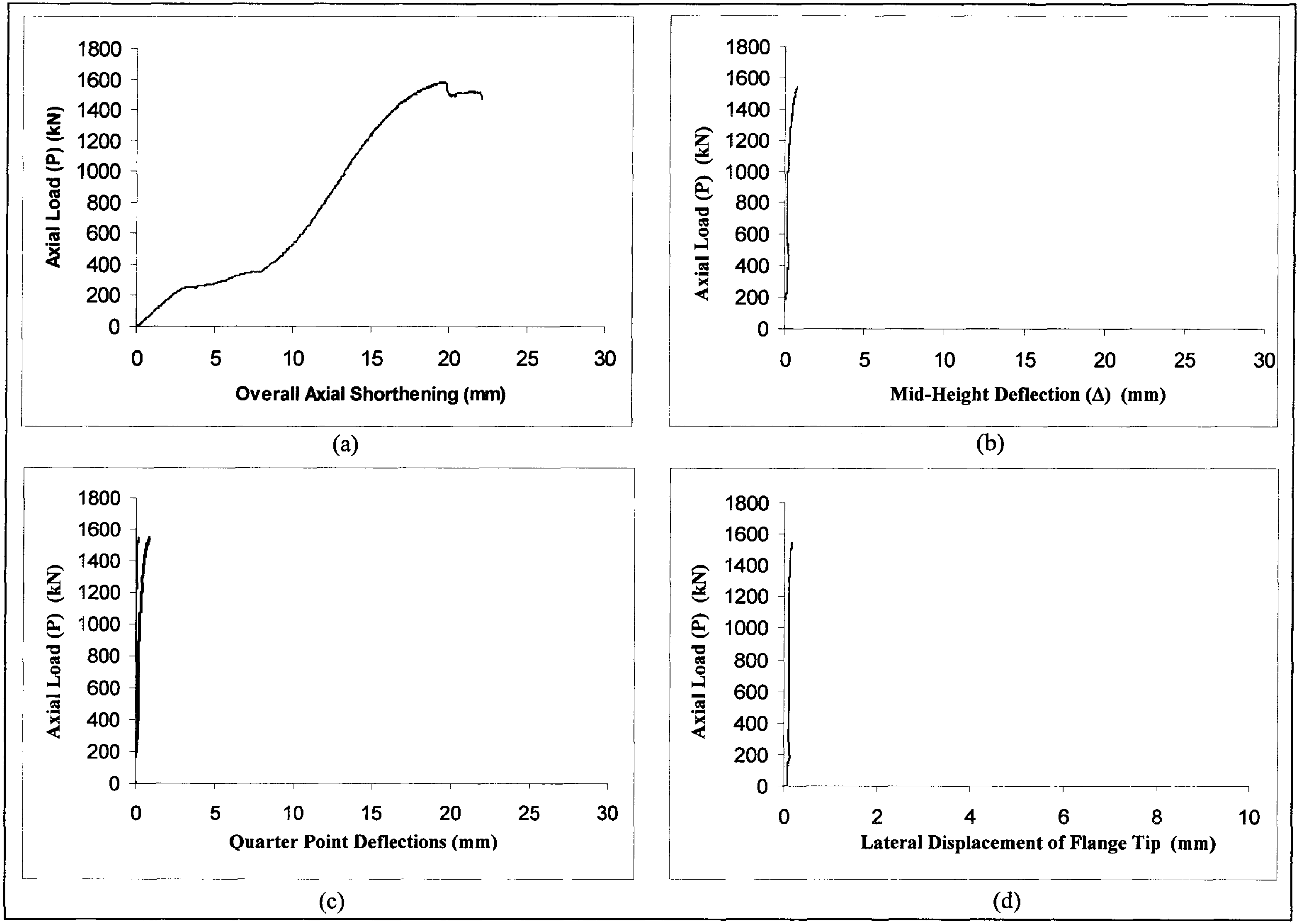

(a)

(b)

(c)

(d)

Figure 6.18: The Behavior of Plasma Cut Column 'C5 (b)' Having Non Dimensional Slenderness Ratio of 0. 18

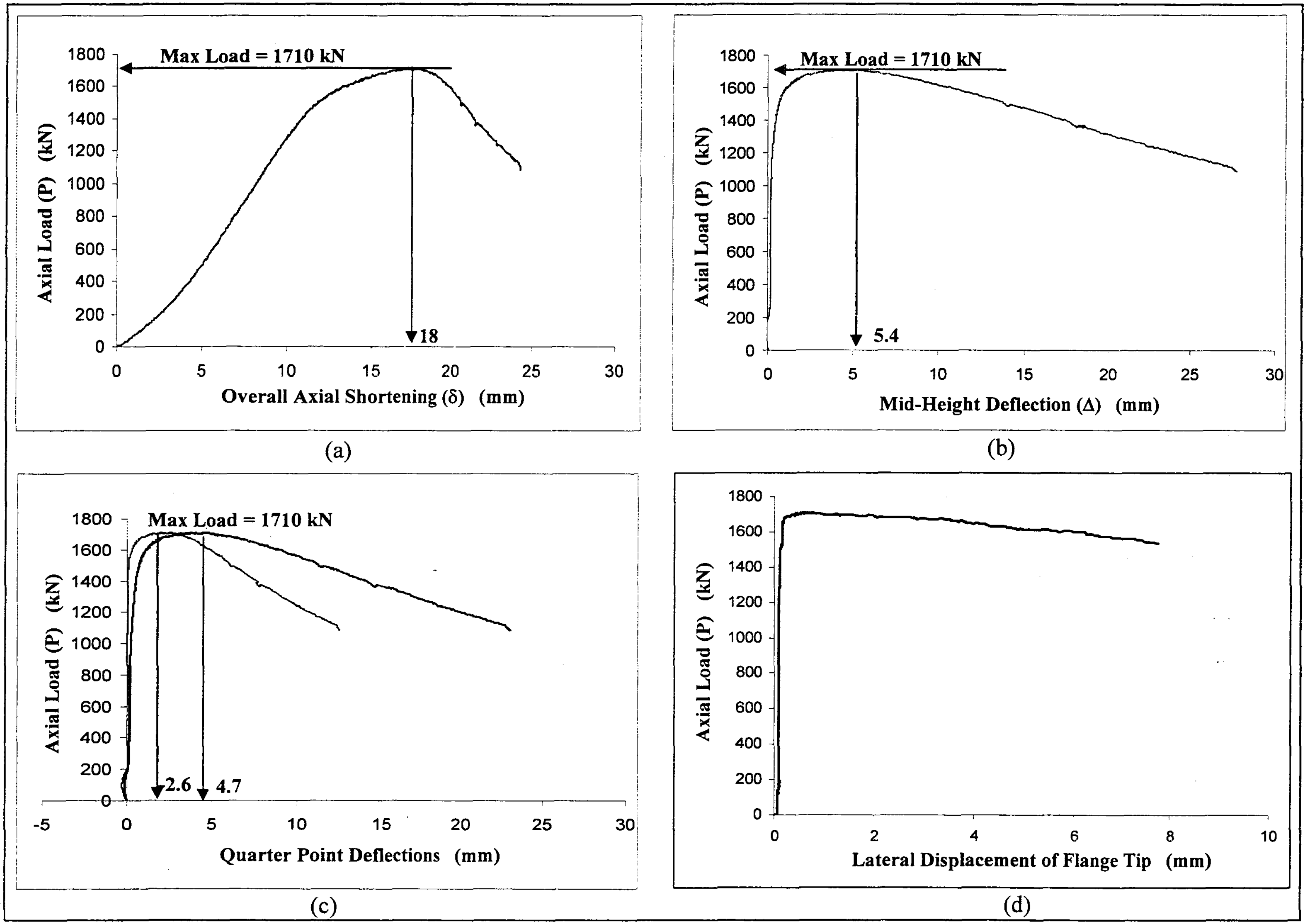

Figure 6.19: The Behavior of Flame Cut Column 'C6 (b)' Having Non Dimensional Slenderness Ratio of 0.18

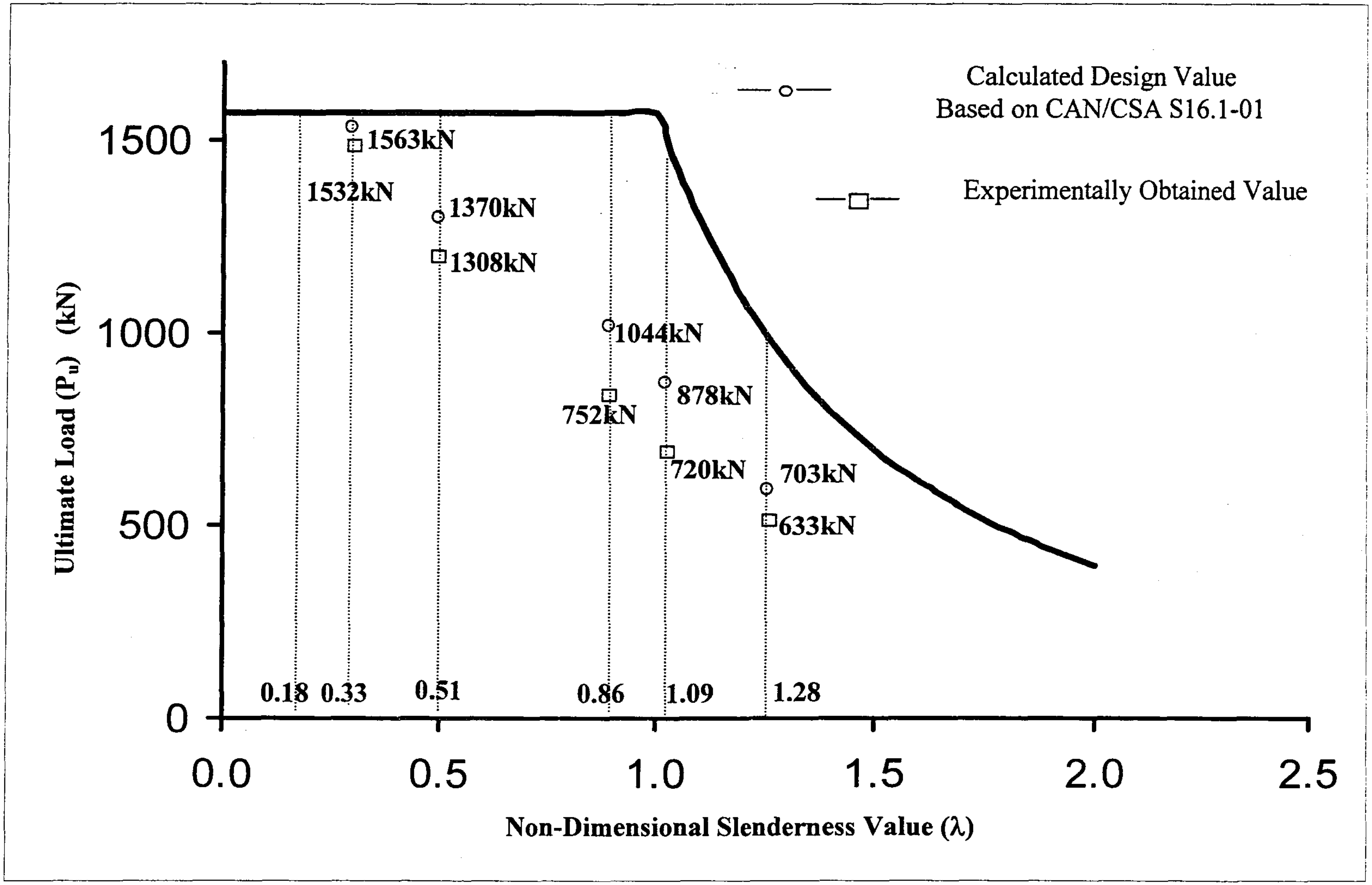

Figure 6.20: The Strength of Plasma-Cut Welded Columns (Pinned End Column Test Allowing for Minor Axis Rotation)

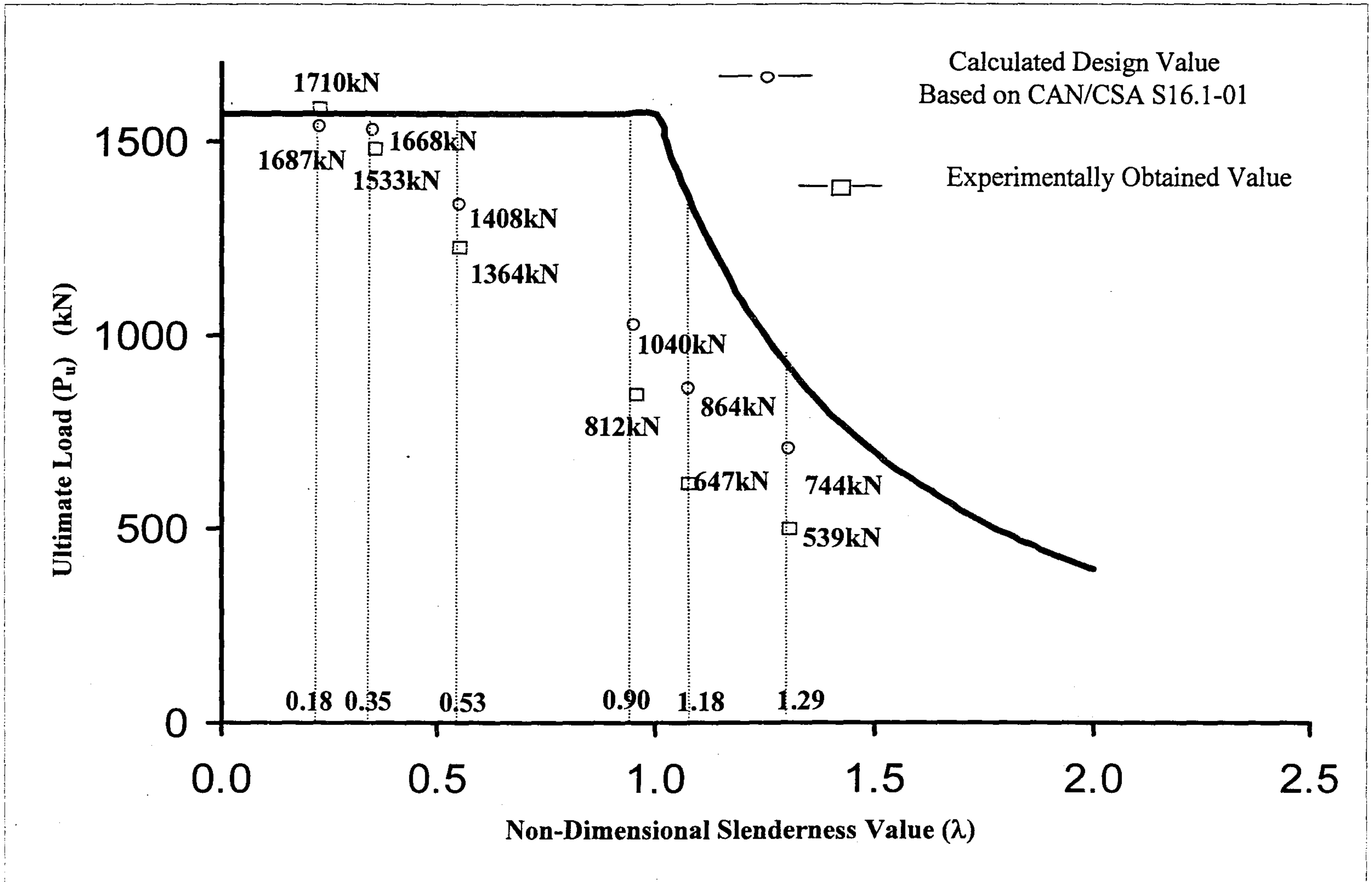

Figure 6.21: The Strength of Flame-Cut Welded Columns (Pinned End Column Test Allowing for Minor Axis Rotation)

Chapter 7

SUMMARY, CONCLUSIONS, AND RECOMMENDATIONS

7.1 Introduction

A large percentage of structural steel columns manufactured today are made up of welded built-up columns from rolled steel plates. The rolled steel plates are first cut to required size to provide the basic elements for desired built-up shapes. The tendency of applying the modern cutting techniques such as plasma, laser, and water-jet cutting have increasingly been utilized in steel fabrication and construction industries. Because these cutting techniques have more advantages over the other traditional cutting techniques (saw cutting, flame cutting, etc) considering the factors such as cutting speed, tight tolerance, bevel control, etc.

However, the true behavior of structural steel columns fabricated by these cutting techniques has not been fully or even partially identified yet. Because, most of the research work carried out by previous researchers in this area has been focused only on flame cut columns, universal mill plate columns, and rolled shapes. Therefore this investigation mainly has focused on the effects of plasma cutting with gas metal arc welding process on strength of steel columns. Also, in this investigation the strength of flame cut columns were established for comparing the strength of plasma cut columns. Moreover, this investigation has focused on ensuring whether the available code equations for establishing the column strength based on CAN/CSA-S16-01 (CSA, 2004) would be applicable for columns fabricated from plasma cut columns.

Due to lack of data on the geometrical imperfections and residual stress patterns on welded built up steel columns fabricated from rolled plates cut by the modern cutting techniques, the steel designers are more concerned with the current code [CAN/CSA-S16-01, Clause 13.3.1] (CSA, 2004) equations to such columns. Therefore, it was decided herein to focus on establishing the residual stresses and geometrical imperfections associated with each of the column sections. In this investigation, twelve pin ended column tests were carried out and the particular attention is given to columns with medium size I-shape cross section. Moreover, temperature profiles during the fabrication process (cutting and welding) were measured for future work related to prediction of analytical residual stress distribution models.

7.2 Summary

There were twelve pin ended column tests allowing minor axis buckling carried out in the testing set-up specially made for this research work (see the Figure 6.5). The test set-up was made as a closed-loop testing facility. The displacement control method was used for entire column tests. There were four LVDTs placed under the bottom plate which was movable (see the Figure 6.6) to make sure the movement of the plate was to be even when applying load. Moreover, one LVDT was placed at the top plate which was fixed to obtain the relative overall axial deformations. The important measurements such as over all axial deformations, mid-height deflections, and rotations at both ends of the column were taken in this investigation.

The measurements of residual stresses were made on six column stocks in which three of them were fabricated by plasma cutting plus gas metal arc welding process and other three were fabricated by flame cutting plus gas metal arc welding. The potential location for residual stress measurements were selected such that the end effects were to be minimal. Thus, the specimens for residual stress measurements were cut down between the two columns specimens obtained from the same column stock in this investigation (see the Figure 2.6). The "method of section" technique was used for entire residual stress measurements in this investigation. Slicing of the specimens was performed with water jet cutting operation. The "*Demec*" mechanical extensor meter was used to measure stress released during sectioning process in this investigation.

Moreover, the geometrical imperfections were established at different stages of fabrication process. The out-of-plane imperfections associated with the virgin steel plates were first established and then, the effects of cutting process on the out-of-plane imperfection of the plate elements were established. Also, the imperfections in terms of sweep, camber, and out of squareness of the column sections were established. As part of the scientific documentation, the standard tensile coupons obtained from each of the virgin steel plates were tested. The results relevant to the important material properties were obtained from the graphical interpretation of the test results.

As part of this investigation the temperature measurements due to different fabrication processes such as cutting and welding were taken. The temperature variation with time was plotted for the observations made during cutting process and welding process. The measurements were taken at five locations marked across the flanges and web portions (see Figure 2.1). For measuring the striking temperatures of cutting processes (plasma cutting and flame cutting) and welding process, the infrared pyrometer (Model #: OS3707) having the measurements range of 250°C to 2000°C was used. The Infrared Thermometer (Model #:

OS542) having the measurements range of -20°C to 500°C was used for the rest of temperature measurements were to be taken at certain time intervals in this investigation.

7.3 Conclusions

This study was primarily concerned with the effects of plasma cutting on strength of steel columns. The tests conducted during this investigation included columns built-up by welding from plasma cut and flame cut plates having yield strength of 350MPa. The columns having slenderness values falling into the intermediate range have been chosen for this study. Because this column range covers the range of most practical steel columns used in construction works. The columns of 'I' shape sections are of particular interest in this research work. The sizes of the column sections were selected so that the web and the flange slenderness were to be within the range of class-1 sections as specified in CAN/CSA-S16-01 (CSA, 2004) Standard. In particular, the main objective of this study was to predict the available strength of H-shaped built-up column sections fabricated from plasma cut steel plates and flame cut plates experimentally. The tests on predicting strength of flame cut columns were performed in the interest of comparing the influence of different cutting techniques on strength of steel columns as well.

As described in this research work, the following problems were investigated experimentally- the magnitude and distribution of residual stresses of welded built-up columns made from plasma cut plates and flame cut plates, the variation of geometrical imperfections due to the different edge preparation and welding procedure, and the prediction of temperature profiles during the cutting and welding operations. Based on the results of the studies made in this investigation, the following conclusions can generally be derived considering residual stress measurements, geometrical imperfections, and strength of columns.

Residual Stresses:

1. The general variation of residual stress distributions of sections fabricated from plasma cut plates and flame cut plates is the same
2. The variation of residual stress distribution at different locations of column sections was not appreciable. This might be true for the column sections made from the virgin plates obtained from same production batch.
3. The flame cut column sections had relatively high tensile residual stresses at their flange tips than that of plasma cut columns.
4. The intensity of residual stresses at the flange-web junction was approximately the same for both sections (plasma and flame cut section)
5. The variation of residual stresses through the thickness at most of the locations was not appreciable. However, the measurements of residual stresses at both faces of sections would provide the more reliable results for entire locations where the residual stresses are intended to be measured.

Geometrical Imperfections:

1. The occurrence of maximum out-of-crookedness in terms of sweep and camber was observed in the vicinity of mid length of column sections in this investigation.
2. In general, the overall imperfections due to flame cutting was higher than that due to plasma cutting

3. The out of flatness and the out-of-squareness were due to welding operation which was used to form H-shape sections.

Strength of Columns

1. The strength of flame cut columns having slenderness ratio of more than 1.0 was lower than that of similar plasma cut columns. Further, it was observed that the initial out-of-crookedness of flame cut column was higher than that of plasma cut column for slenderness ratio of more than 1.0 in this investigation. Therefore, it can be concluded that for relatively longer columns ($\lambda \geq 1.0$), the initial out-of-crookedness possibly play a key role in determining the load carrying capacity of such columns.
2. The strength of flame cut columns having slenderness ratio less than 1.0 was higher than that of similar plasma cut columns. Thus, it can be concluded that possibly the influence of residual stress distribution in relatively shorter columns ($\lambda \leq 1.0$) play a key role in determining the ultimate load carrying capacity of such columns. Moreover, this is evident by the fact that the flame cut columns have relatively high favorable residual stress distribution than that presents in plasma cut column sections.
3. As a whole it was generally observed that the strength of columns obtained by experimental investigation in this study was lower than the design values calculated according to present Canadian Standard Column Design Curve (CAN/CSA-S16-01). However, these observations may not be applicable for sections with different sizes and cross-sectional shapes. Therefore, it can be concluded that a considerable number of lab tests and analytical studies have to be done on the wide range of column sections which are fabricated by the modern cutting techniques to get clear

understanding of the behavior of such column sections and to make clear discussion on whether the current column design curve still needs to be improved for those column section.

4. From this study, it can be concluded that the different fabrication techniques of a column section result in different degree of column strength. Therefore, the influences of the fabrication techniques are clearly evidenced by this investigation.

7.4 Recommendations for Future Study

The following points are recommended to investigate the strength of columns fabricated using modern cutting techniques (plasma, laser, water-jet, etc) in the future experimental and analytical studies.

1. Consideration of various sizes and shapes of column section to derive a general column design curve or curves in future experimental studies.
2. More analytical studies based on actual/idealized models for residual stress distributions, initial out-of-straightness, and material characteristics can be incorporated to establish column strengths. Thus, the analytically obtained strength values can be compared with experimentally obtained values to validate the analytical studies.
3. The prediction of analytical models for residual stress distributions can be determined from the temperature profiles obtained during cutting and welding operations. However, it is essential to know how the elastic properties of steel vary with temperature for the step by step procedure associated with predictions of analytical models for residual stress distributions.

4. Experimental studies on column sections fabricated from laser cutting and water-jet cutting can be performed in the future studies. Moreover, the residual stress distributions and geometrical imperfections can be experimentally established for those column sections.
5. The study on establishing the strength of columns in the future can be extended to different steel grades.

REFERENCES

Adams, P.F., Krentz, H.A., & Kulak, G.L., (1979), Limit State Design in Structural Steel, 2nd Edition, Canadian Institute of Steel Construction, Canada.

Allen, H.G., Bulson, P.S., (1980), Background to Buckling, McGraw-Hill Book Company (UK) Limited, England.

ASTM Standard E837, (2002), Standard Test Method for Determining Residual Stresses by the Hole-Drilling Strain Gage Method, pp. 681-696.

ASTM Standards A370-02, (2002), Standard Test Methods and Definitions for Mechanical Testing of Steel Products, American Society for Testing and Materials, pp. 106-141.

Ballio, G., & Mazzolani, F.M., (1983), Theory and Design of Steel Structures, London, N.Y, Chapman & Hall.

Batteman, R.L., & Johnston, B.G., (1967), Behavior and Maximum Strengtb of Metal columns, Journal of Structural Division, Vol.93, No.ST2, pp. 205-230.

Beedle, L.S., & Tall, L., (1960), Basic Column Strength, Journal of the Structural Division, Vol.86, No. ST7, pp. 137-173

Bjorhovde, R., Brozzetti, J., Alpsten, G. A., & Tall, L., (1972), Residual Stresses in Thick Welded Plates, Welding Journal., Vol. 51, No. 8,pp. 392-405.

Brockenbrough, R.L., & Merritt, F.S., (1999), Structural Steel Designer's Handbook, 3rd Edition, by McGraw Hill N.Y, USA

Chen, W.F., & Lui, E.M., (1987), Structural Stability (Theory and Implementation), by Elsevier Science Publishing Co., Inc, England.

Chernenko, D.E., & Kennedy, D.J.L., (1991), An Analysis of the Performance of Welded Wide Flange Columns, Canadian Journal of Civil Engineers, Vol.18, pp.537-555.

CISC (2004), Handbook of Steel Construction, Canadian Institute of Steel Construction, Willowadale, Ontario, Canada

CSA (2004), North American Specification for the Design of Cold-Formed Steel Structural Members S-136-01, Canadian Standard Association, Ontario, Canada

Estuar, F. R., & Tall, L., (1963), Experimental Investigation of Welded Built-Up Columns, Welding Journal, Vol. 42, pp. 164-176.

Galambos, T.V., (1998), Guide to Stability Design Criteria for Metal Structures, 5th Edition, by John Wiley & Sons, Inc, N.Y, USA.

Hall, D.H., (1981), Proposed Steel Column Strength Criteria, Journal of the Structural Division, Vol. 107, No. St 4.

Hancock, G.J., (1981), Interaction Buckling in I-Section Columns, Journal of the Structural Division, Vol. 107, No. ST1. pp. 165-178.

Kandil, F.A., Lord, J.D., Fry, T.A., & Grant. P.V., (2001), A Review of Residual Stress Measurement Methods – A Guide to Technique Selection.

McFalls, R.K., & Tall, L., (1969), A Study of Welded Columns Manufactured from Flame Cut Plates, Welding Journal, Vol.48, pp. 141-153

Nagaraja Rao, N.R., & Tall, L., (1961), Residual Stresses in Welded Plates, Welding Journal, and Vol. 43, pp. 468-480.

Osgood, W.R., & Marshall, H., (1938), The Column Strength of Two Extruded Aluminum-Alloy H-section (Report# 656-National Advisory Committee for Aeronautics), pp. 289-312.

Rajan, S.D., (2000), Introduction to Structural Analysis & Design, John Wiley & Sons, Inc, USA.

Rasmussen, K.J.R., & Hancock, G.J., (1995), Tests of High Strength Steel Columns, Journal of Constructional Steel Research, 34, pp. 27-52.

Simith, D.J., Bouchard, P.J., & George, D., (2000), Measurement & Prediction of Residual Stresses in Thick Section Steel Welds, Journal of Strain Analysis, Vol. 35, N0.4, pp. 2 287-305.

Stewart, J., (1995), Local Buckling Behavior of W Shapes Steel Section, M.Eng Theses, McMaster University, Hamilton, On, Canada.

Stiemer, S.F., (2000), Design of Compression Members.doc, pp. 1-14, (Last Accessed: 2/16/2003)

Tall, L., (1964), Structural Steel Design, 2nd Edition, The Ronald Press Company, USA.

Tebedge, N., Alpsten, G., & Tall, L., (1973), Residual Stress Measurement by the Sectioning Method, Experimental mechanics, pp. 88-96.

Tesko Laser Division, (2003), (http:// www.teskolaser.com) (Last Accessed: 02/08/2003)

Trahair, N.S., (1997), The Behavior and Design of Steel Structures, John Wiley & Sons, N.Y, USA.

Wilson, W.M., & Hao, C.C., (1945), Residual Stresses in Welded Structures, Engineering Experiment Station, University of Illinois, USA, Bulletin Series No. 361, pp. 1-49.

Yuan, B., (1997), Local Buckling of High Strength Steel W-Shaped Sections, M.Eng Thesis, McMaster University, Hamilton, On, Canada.

Zuccarello, B., (1999), Optimal Calculation Steps for the Evaluation of Residual Stress by the Incremental Hole-Drilling Method, Experimental Mechanics, Vol. 39, No.2, pp. 17-124.

Appendix A

Tensile Coupon Test

The Mechanical properties of the steel plates used in this investigation were established through tension coupon tests. Two tension coupons were considered for each plate. Therefore, a total of twelve coupons were tested since six steel plates were used for the fabrication of columns in this investigation. The tension coupon testing procedures used in this study were in accordance with the specifications and recommendations provided by American Society for Testing Material Standards A370-02 (ASTM, 2002).

A.1 Testing Procedure

The tension coupons tested herein were cut along the same direction as the plates cut for fabrication of welded W-shaped sections. The associated dimensions for a standard coupon according to the ASTM standard are shown in Figure A.1. It can be observed in this figure that the gage length used to calculate the elongated strain is to be 200mm (8inch) with the standard width of the specimen set at 40mm (1.5inch). Prior to testing, the width and thickness of each coupons at three different locations along the section over which the extensometers were placed, were carefully measured. Such measurements were made within a tolerance of 1/100 of a millimeter and the average reading of the width and thickness of each coupon were recorded for calculation purposes.

All tensile coupon tests were carried out by using the Tinius Olsen Machine with an axial load capacity set at 600kN. The placement of a specimen in the testing machine is as shown in Figure A.2. Prior to applying the axial tensile load onto a tensile coupon, the coupon specimen was aligned vertically and located almost in the center position with respect to the pulling jaws available within the machine's loading platforms (see Figure A.2). This step was carefully done to avoid any eccentricity in load application with respect to the coupon. The coupon was then gripped on the machine by applying a load well within the elastic limit to ensure that the coupon was perfectly gripped in the pulling jaws and no possible slip would take place during the test, especially at the initial loading stages. Then it was unloaded to the axial tensile load of approximately 2 kN required to grip the coupon steadily. At this point the coupon was ready to be loaded for the tensile test.

In this testing procedure, there were two extensometers, working with a linear voltage displacement transducer (LVDT), placed on either side of the specimen. One is a longer extensometer with a gage length of 200mm (8inch) and elongation capacity of 75mm. The purpose of using this type of extensometer was to acquire data to study the overall behavior of a coupon until it fails due to necking and subsequent rupture. The other one is relatively smaller extensometer with a gage length of 50mm (2inch) and less capacity than the longer one. However, the smaller one was more accurate with high sensitivity in detecting elongation. Also the smaller extensometer was used to collect data in the elastic range only, since it has less measuring capacity. Therefore, this extensometer was removed shortly after yielding had taken place in each tensile specimen. The purpose of using this type of extensometer was to achieve more refined small-strain accuracy in the elastic range and thus to determine more precise value of Young's modulus (E).

The outputs from each of the extensometers were in volts, which were directly received by a data acquisition system and a computer. These voltages were multiplied by the corresponding calibration factors to convert them into elongations and then recorded by the computer. The load level was also continuously monitored by the reading voltage output from the testing machine. All data were recorded in two-second intervals. A real time display was observed during the test to visualize how the stress-strain relationship of a specimen varies, monitor the loading rate, and finally to observe the overall performance of the test.

In the elastic rage, the loading rate was set at 0.25mm (0.010in) per minute in order to gather as much data points as possible. In the inelastic range, the specimen was loaded at a rate of 0.89mm (0.035in) per minute until the test was completed. Even though the loading rates were somewhat lower than that specified by ASTM (2002) Standards, they represented better static behavior of the tensile coupon (Stewart, 1995). All tensile coupons were loaded until rupture. Figure A.3 shows the failed specimens. It was observed that, in all the tensile coupons, the failure occurred within the gage length of large extensometer.

A.2 Observation and Test Results

The resulting stress-strain relationships of tensile coupons obtained from each of the plates are shown in Figure A.4-1 through A.4-6. The stress values were calculated based on applied load divided by the initial cross-sectional area. The strains were calculated as associated elongation divided by initial gage length of extensometer. The results obtained from the small extensometer with the gage length of about 50mm (2 in) were used to calculate modulus of elasticity (E), yield strength (F_y), yield strain (ε_y) and the proportional limit (F_{pl}). Since the stress-strain relationship of all tensile coupons had no sharp yield point, the yield strength was obtained using 0.2% offset method with the initial assumed slope E of 200GPa. The proportional limit, herein was determined based on the use of a strain offset of $1\text{x}10^{-5}$ with the initial assumed slope E of 200GPa.

The stress-strain relations obtained from the large extensometer with the gage length of 200mm were used to predict the ultimate strength, corresponding ultimate strain, strain at rupture, and percent of area reduction at rupture. Table A.1 shows the results obtained from each of the tensile coupons. In this table, the important mechanical properties such as yield stress, yield strain, ultimate stress, ultimate strain, elastic modulus, the ratio between ultimate strength and yield strength, and the ratio between ultimate strain and yield strain are provided. Table A.2 shows the minimum specified mechanical properties of steel plates as provided in the mill report. Table A.3 shows the percent of chemical composition for the steel plates having different heat ID.

Figure A.4-1 shows the tensile coupon test results obtained from the 1st plate which was designated herein as plate-01. There were two sample coupons from the plate-01 tested. The stress-strain relationship in Figure A.4-1 exhibits no sharp yielding point and no well defined yield plateaus. The results obtained from the coupon specimen-1(a) showed that the yield and ultimate stresses were 374MPa and 467MPa, respectively. However, the results obtained from the specimen-1(b) showed that the yield and ultimate stresses were of 372MPa and 466MPa, respectively. Moreover, it could be observed from the Figure A.4-1 that the behavior of stress-strain variation of both specimens seemed to be closely identical to each other.

Figure A.4-2 shows the stress-strain relationships of coupon specimens obtained from plate-02. The results obtained from the specimen-2(a) showed that the yield and ultimate stresses were of 400MPa and 472MPa, respectively. The yield and ultimate stresses obtained from the specimen-2(b) were 395MPa and 470MPa, respectively. Hence from the Figure A.5, it could be concluded that both specimens behaved in most identical manner.

Figure A.4-3 shows the stress-strain relationships for coupon specimen-3(a) and 3(b) obtained from the third plate which was designated herein as plate-03. The general stress-strain behavior of the specimens was similar to the specimens obtained from the plate-01 and plate-02. However the yield stress of these specimens were slightly lower than that obtained form the other coupons. The yield and ultimate stresses of specimen 3(a) and 3(b) were 345MPa and 462MPa as well as 348MPa and 464MPa, respectively.

Figure A.4-4 shows the stress-strain relationships of coupons obtained from plate-04. The general stress-strain behavior of these specimens was almost identical to other coupon specimens. However, it was observed that the initial slope of stress-strain relationship for these specimens were higher than that of other coupon specimens. The results obtained from specimen-4(a) showed that the yield and ultimate stresses were 371MPa and 436MPa, respectively. The yield and ultimate stresses for specimen-4(b) were 366MPa and 462MPa, respectively.

Figure A.4-5 shows the stress-strain behavior of coupons specimens obtained form plate-05. The results obtained from specimen-5(a) showed that the yield and ultimate stresses were 371MPa and 463MPa, respectively. The results obtained from specimen-5(b) showed that the yield and ultimate stresses were 370MPa and 463MPa. The general stress-strain variations of these specimens were similar to other coupon specimens. However, it was observed that the $\varepsilon u/\varepsilon y$ ratio for these specimens was slightly higher than that of other specimens.

Figure A.4-6 shows the stress-strain behavior of coupon specimens obtained from plate-06. The yield and ultimate stresses obtained from specimen-6(a) were 385MPa and 467MPa, respectively while the yield and ultimate stresses obtained from specimen-6(b) were 392MPa and 468MPa, respectively. Also the general stress-strain behavior was same as the behavior of other coupons tested in this investigation. Moreover, it was generally observed that the ultimate stresses of all the coupons were between 460MPa and 475MPa while the yield stresses of all the coupons were between 345MPa and 400MPa.

Although the results obtained from the coupons cut from the same original plate were almost identical to each other, in the elastic range, their behavior exhibited slight deviations especially beyond the elastic limits. These deviations may be attributed to factors such as material imperfections, presence of residual stresses, variations in degree of cold work, variation in dislocation density, etc. Figure A.5 shows the stress-strain behavior of sample coupons obtained from the initial steel plates (6-plates).

As a point of interest to ensure whether the plates were from same production batch, the experimentally obtained yield and ultimate stresses were compared with those stresses provided in the mill certificate. From the comparison, it can be concluded that all plates used in this research work were having same heat ID (W3H676) as shaded in Table 3.2 i.e., from the same production batch (heat ID usually refers the production batch).

Plate (Steel Grade 350W)	Mechanical Properties							
	F_y (MPa)	ε_y	F_{pl} (MPa)	F_u (MPa)	ε_u	F_u/F_y	$\varepsilon_u/\varepsilon_y$	E (GPa)
1(a)	374	0.0039	256	467	0.1827	1.25	46.85	202
1(b)	372	0.0039	262	466	0.1518	1.25	38.92	202
2(a)	400	0.0040	262	472	0.1448	1.18	36.19	203
2(b)	395	0.0040	242	470	0.2035	1.19	50.88	202
3(a)	345	0.0037	230	462	0.1680	1.34	45.41	203
3(b)	348	0.0037	242	464	0.1754	1.33	47.4	203
4(a)	371	0.0039	232	464	0.1821	1.25	46.69	205
4(b)	366	0.0038	246	462	0.2178	1.26	57.32	208
5(a)	371	0.0039	266	463	0.2081	1.25	53.36	200
5(b)	370	0.0039	252	463	0.2295	1.25	58.85	200
6(a)	385	0.0039	252	467	0.1833	1.21	47.00	202
6(b)	392	0.0040	248	468	0.1889	1.19	47.23	205

Table A.1: Mechanical Properties Obtained from Coupon Tests

Heat ID	Piece ID	Mill Certificate Results For Yield Strength (MPa)	Mill Certificate Results for Ultimate Strength (MPa)	Elongation % of	
				2in	8in
W3H676	0897	360	496	30	N/A
		386	462	30	N/A
W3H676	0911	338	475	35	N/A
		360	448	33	N/A
W3J651	0574	353	489	32	N/A
		400	510	31	N/A
W3J648	0534	360	482	34	N/A
		400	510	29	N/A

Table A.2: The Mill Specified Values for Yield Strength and Ultimate Strength of Plates form Different Heat ID

Heat ID	Chemical Composition														
	C	Mn	P	S	Si	Al	Cu	Ni	Cr	Mo	Cb	V	Ti	B	N
[redacted]															
W3J651	0.150	0.830	0.013	0.004	0.030	0.025	0.320	0.210	0.180	0.050	0.002	0.007	0.032	0.000	0.009
W3J648	0.160	0.850	0.013	0.005	0.020	0.024	0.300	0.160	0.140	0.030	0.002	0.007	0.032	0.000	0.009

Table A.3: The Percentage of Chemical Composition of Steel Plates from Different Heat ID's

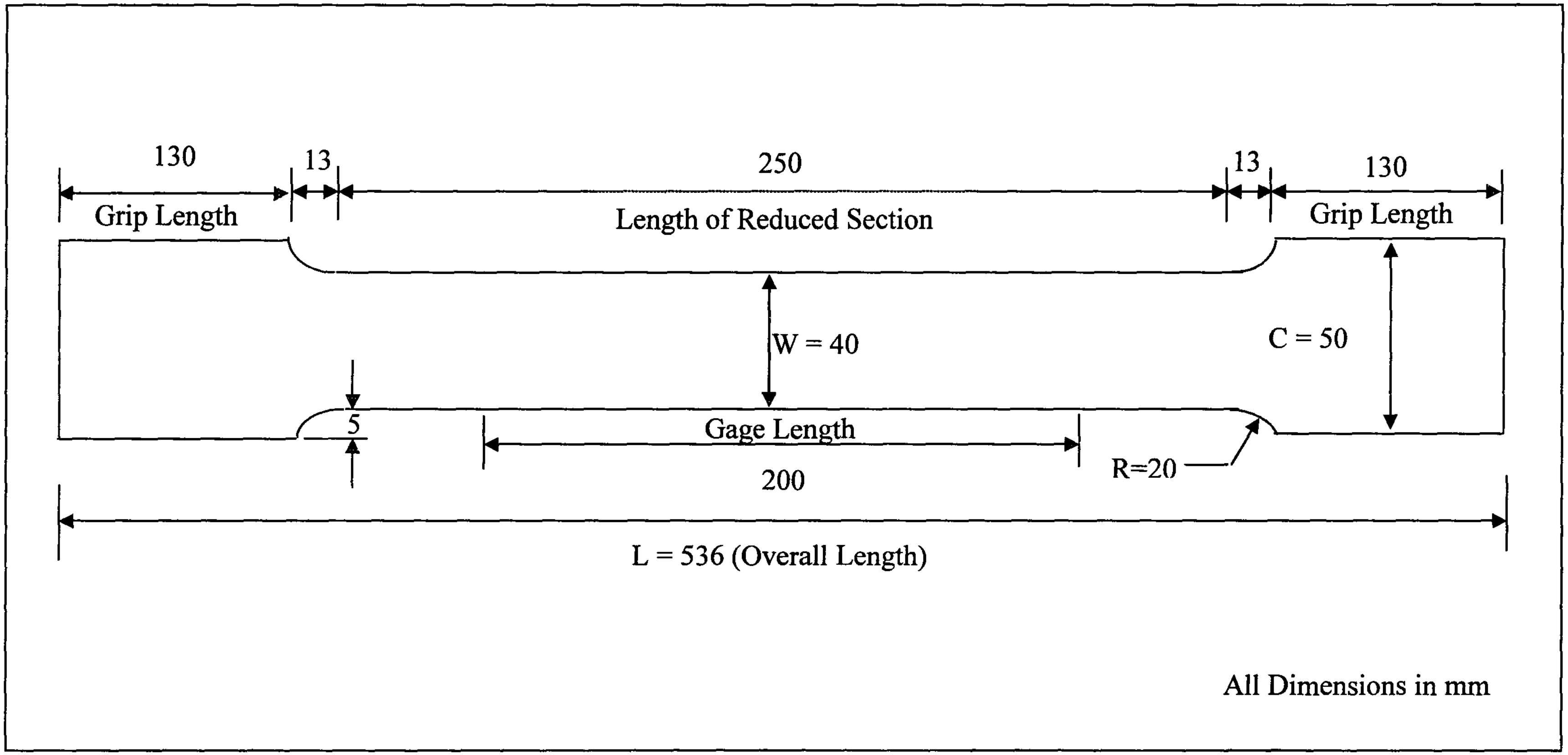

Figure A.1: The Dimensions of a Tension Coupon

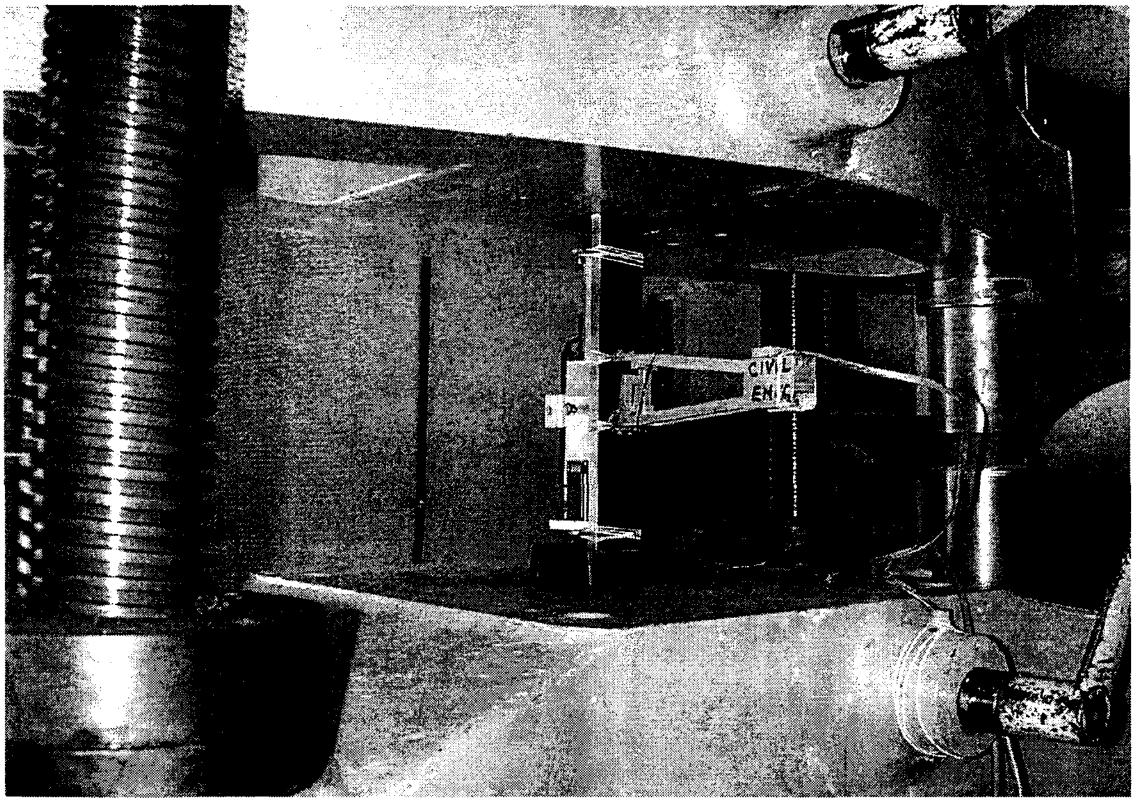

Figure A.2: Experimental Setup for Tensile Test

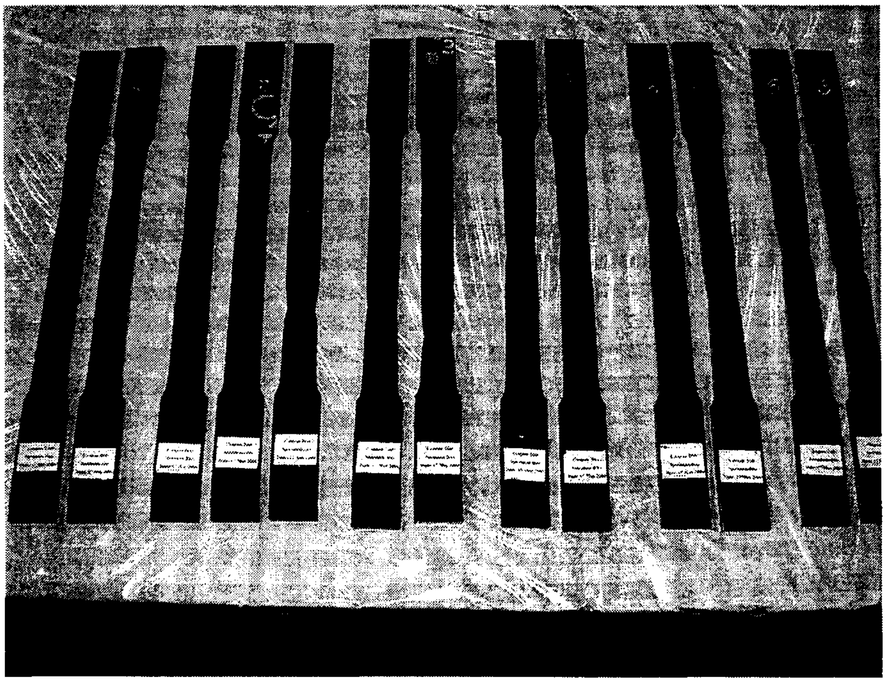

Figure A.3: The Specimens after Failure

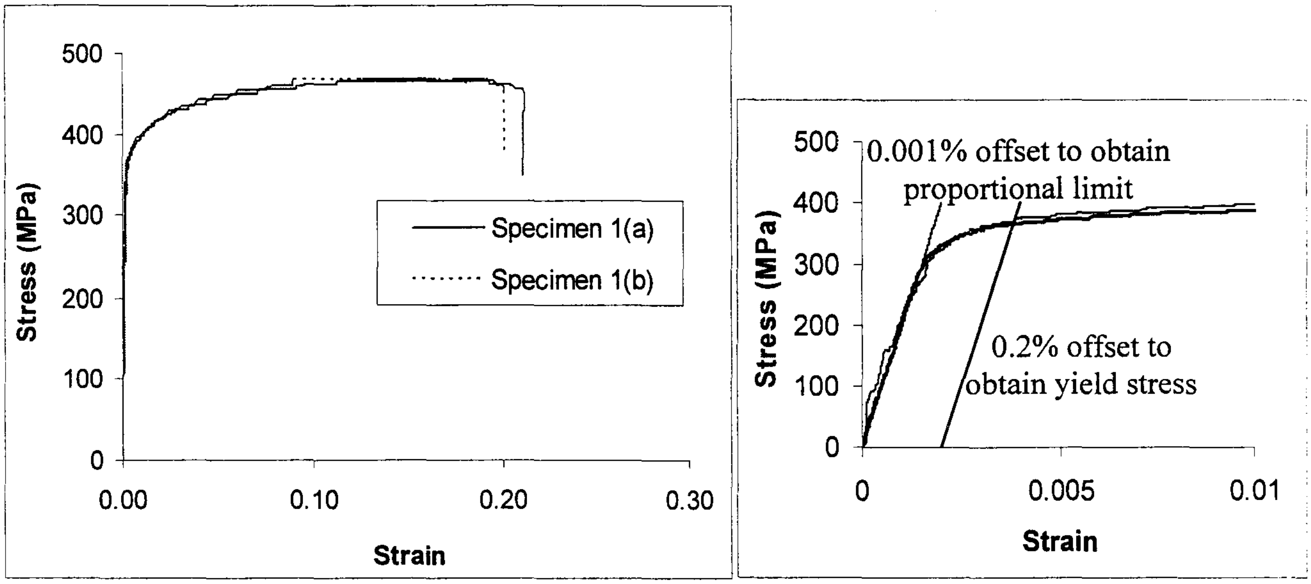

Figure A.4-1: Stress-Strain Relationship of Coupons Obtained from Plate-01

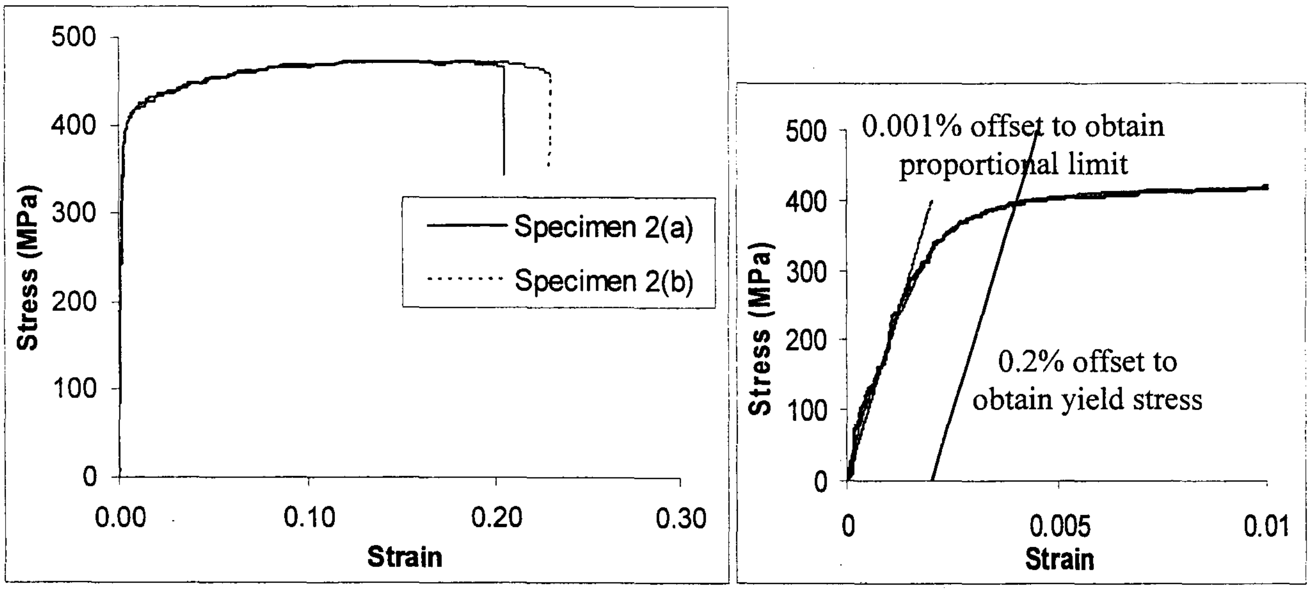

Figure A.4-2: Stress-Strain Relationship of Coupons Obtained from Plate-02

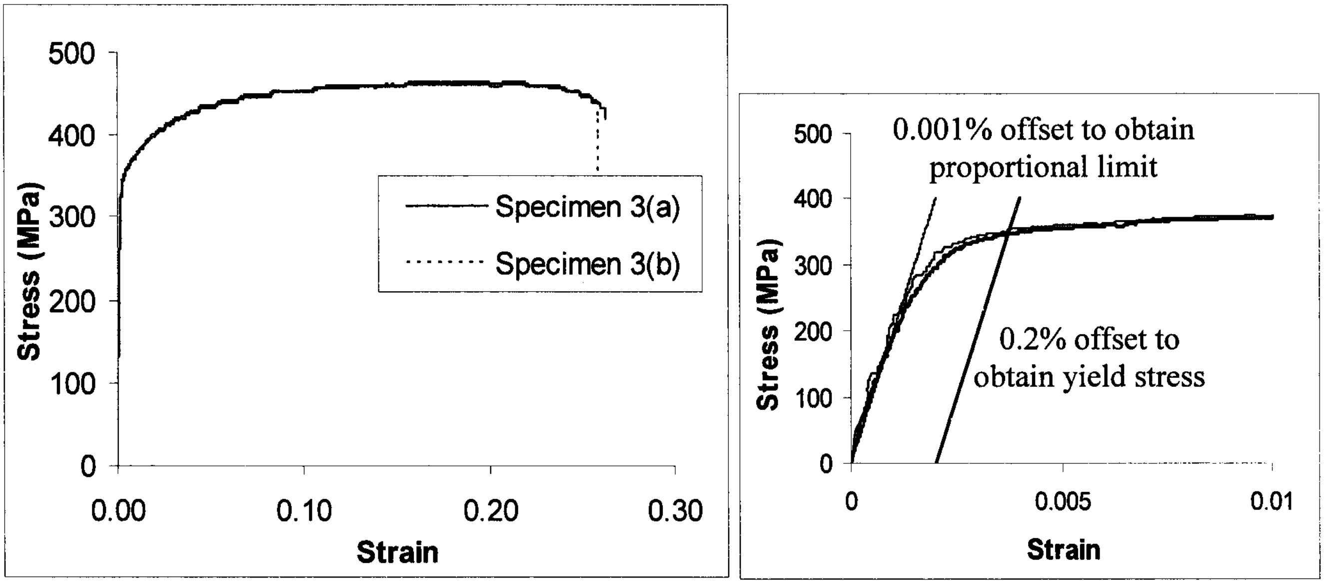

Figure A.4-3: Stress-Strain Relationship of Coupons Obtained from Plate-03

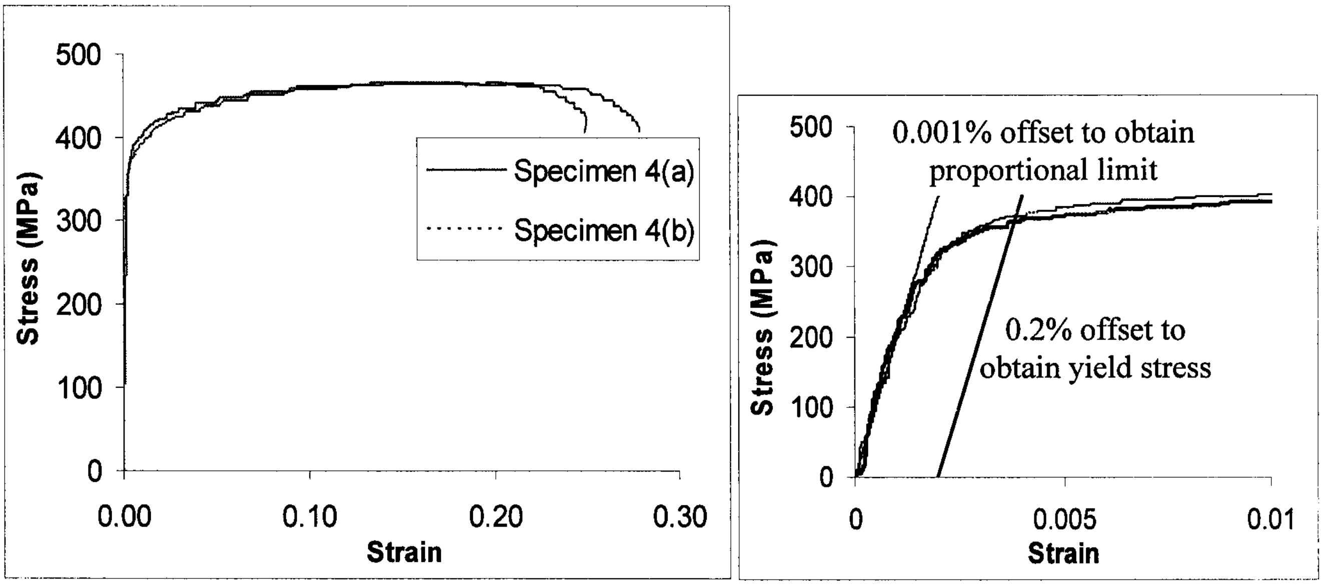

Figure A.4-4: Stress-Strain Relationship of Coupons Obtained from Plate-04

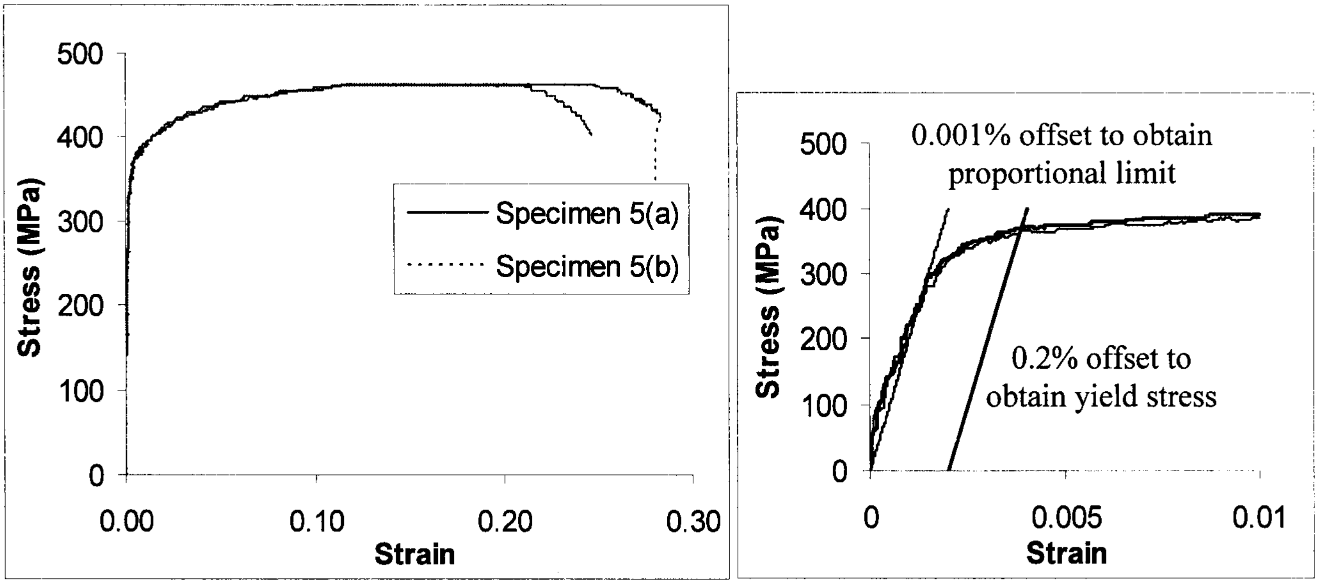

Figure A.4-5: Stress-Strain Relationship of Coupons Obtained from Plate-05

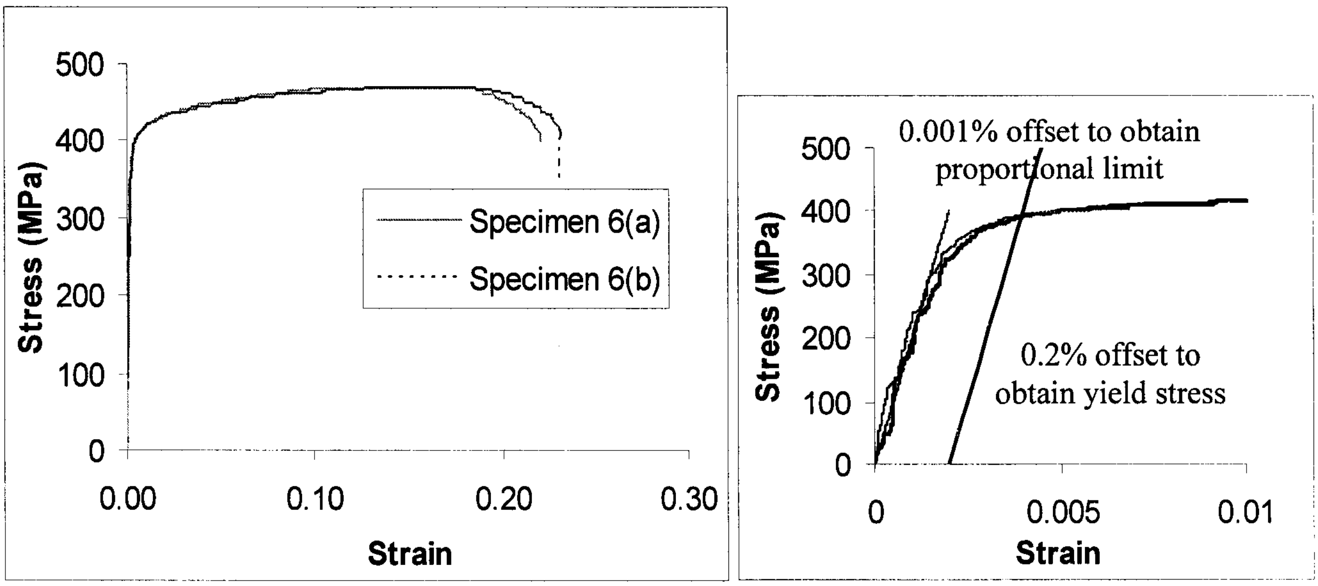

Figure A.4-6: Stress-Strain Relationship of Coupons Obtained from Plate-06

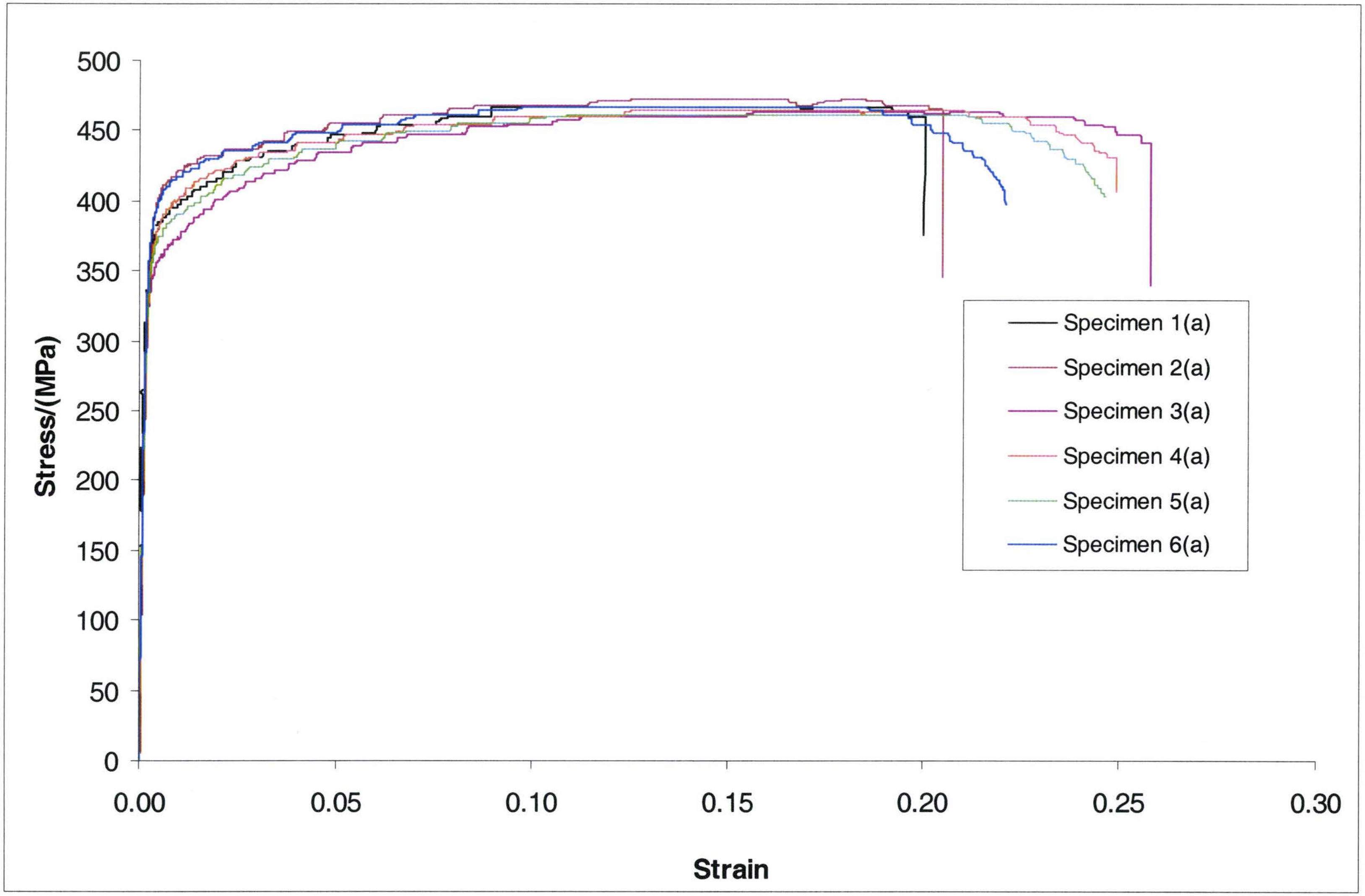

Figure A.5: The Comparison of Stress-Strain Relationship of Coupons Obtained from Each of the Original Plates